

**Deciphering mechanisms shaping
Natural Killer cell responses to
Trypanosoma cruzi-infected dermal fibroblasts**

Dissertation with the aim of achieving a doctoral degree
at the Faculty of Mathematics, Informatics and Natural Sciences

Department of Biology
University of Hamburg

submitted by
Jessica Monika Barton

Hamburg, Mai 2022

Diese Arbeit wurde in der Laborgruppe von PD Dr. Thomas Jacobs am Bernhard-Nocht-Institut für Tropenmedizin angefertigt.

1. Gutachter: Prof. Dr. Tim-Wolf Gilberger
Zentrum für strukturelle Systembiologie CSSB
c/o Deutsches Elektronen-Synchrotron DESY
2. Gutachter: PD Dr. Thomas Jacobs
Bernhard-Nocht-Institut für Tropenmedizin
Protozoen-Immunologie

Tag der Disputation: 15.08.2022

Vorsitzende der Prüfungskommission: Prof. Dr. Julia Kehr

Mitglieder der Prüfungskommission: Prof. Dr. Julia Kehr
Prof. Dr. Tim-Wolf Gilberger
PD Dr. Thomas Jacobs
Prof. Dr. Marcus Altfeld
Prof. Dr. Esther Schnettler

Eidesstattliche Versicherung

Hiermit erkläre ich an Eides statt, dass ich die vorliegende Dissertationsschrift selbst verfasst und keine anderen als die angegebenen Quellen und Hilfsmittel benutzt habe.

Hamburg, den 10.05.2022

Ort und Datum

A handwritten signature in blue ink, appearing to read 'J. Barken', is written above a horizontal line.

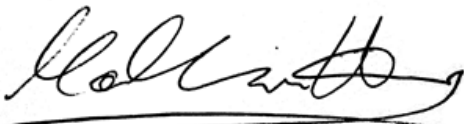
Unterschrift

Nachweis der Korrektheit der Sprache

Hiermit bestätige ich, Madeleine Hamley, geb. 02.10.1991 in London, dass die vorliegende Dissertation „Deciphering mechanisms shaping NK cell responses to *Trypanosoma cruzi*-infected dermal fibroblasts“ sprachlich korrekt ist.

Hamburg, den 29.04.2022

Ort und Datum



Unterschrift

Danksagung

Zuallererst möchte ich mich bei PD Dr. Thomas Jacobs für das spannende Projekt, die wunderbare Betreuung und die anregenden Diskussionen bedanken. Ganz besonders dankbar bin ich dabei für die Möglichkeit, stets meine eigenen Ideen umsetzen und daran wachsen zu dürfen.

Darüber hinaus danke ich Prof. Dr. Tim-Wolf Gilberger herzlich für die Bereitschaft diese Arbeit zu begutachten.

Ebenfalls ein großer Dank geht an Prof. Dr. Marcus Altfeld, Dr. Christian Körner und Dr. Annika Niehrs für die tolle Betreuung, uneingeschränkte Unterstützung und Inspirationen rund um das Thema NK-Zellen.

Dr. Jessica Rauch und Dr. Mathias Riehn danke ich vielmals für ihr stets offenes Ohr und ihre bedingungslose Hilfsbereitschaft.

Ich danke allen meinen Kollegen der Abteilung Protozoen-Immunologie für das grandiose Arbeitsklima und die unvergessliche, wundervolle Zeit. Ganz besonders möchte ich mich dabei bei Ulricke Richardt und Vivien Alders für Ihre grenzenlose Unterstützung im Labor bedanken. Bei meinen Chagas-Mädels Rosa Grote-Galvez und Cari Lehman möchte ich mich von ganzem Herzen für unsere Unterstützung im Labor, aber auch die unzähligen Gespräche bedanken, die mich stets inspiriert haben und mir geholfen haben, die kompliziertesten Probleme zu entwirren.

Außerdem möchte ich mich vielmals bei allen Blutspendern bedanken, ohne deren Beitrag diese Arbeit niemals möglich gewesen wäre.

Zuletzt möchte ich meiner Mutter, meiner Oma und meinen Freunden meinen Dank für ihre langjährige und nie endende Unterstützung aussprechen, ohne die ich es niemals bis zu diesem Punkt geschafft hätte. Ein besonderer Dank gilt meinem Partner Etienne Bartels für seinen beispiellosen Beistand, der mir auch in schwierigen Zeiten die Kraft gegeben hat, weiterzumachen und meine Ziele zu erreichen.

Vielen Dank für Alles!

Abbreviations

AF	Alexa Fluor
ADCC	Antibody-dependent cellular cytotoxicity
aKIR	Activating KIR
APC	Allophycocyanin
BNITM	Bernhard Nocht Institute for Tropical Medicine
bp	Base pairs
BSA	Bovine serum albumin
BTLA	B and T lymphocyte attenuator
BUV	Brilliant Ultraviolet
BV	Brilliant Violet
β ₂ m	β ₂ microglobulin
CD	Cluster of differentiation
CRISPR	Clustered regulatory interspaced short palindromic repeats
CTL	Cytotoxic T lymphocytes
Cy7	Cyanine7
DAP12	DNAX-activating protein 12
DAPI	4',6-Diamidin-2-phenylindol
DC	Dendritic cell
ddH ₂ O	Double-distilled water
DEG	Differentially expressed gene
DISC	Death inducing-signaling complex
DMEM	Dulbecco's Modified Eagle's Medium
DMSO	Dimethyl sulfoxide
DNA	Deoxyribonucleic acid
DNAM-1	DNAX accessory molecule 1
dNTP	Deoxyribonucleic triphosphate
DPBS	Dulbecco's Phosphate Buffered Saline
dpi	Days post infection
DTT	Dithiothreitol
EDTA	Ethylenediaminetetraacetic acid
ELISA	Enzyme-linked immuno-sorbent assay
E:T	Effector to target
FACS	Flow Activated Cell Sorting
FasL	Fas ligand
F-bottom	Flat-bottom
Fc	Fragment crystallizable region
FCS	Fetal calf serum
FDR	False discovery rate
FITC	Fluorescein
FMO	Fluorescence minus one
FSC	Forward scatter
GPI	Glycosylphosphatidylinositol
GTP	Guanosine 5'-Triphosphate
HA	Hemagglutinin
HCMV	Human cytomegalovirus
HDF	Primary human dermal fibroblasts
HDR	Homology directed repair
HEPES	2-(4-(2-Hydroxyethyl)-1-piperazinyl)-ethanesulfonic acid

His	Histidine
HIV	Human immunodeficiency virus
HLA-I	Human leukocyte antigen class I
hr	Human recombinant
HRP	Horse reddish peroxidase
HSPG	Heparan sulfate peptidoglycan
HSV	Herpes simplex virus
hpi	Hours post infection
HVEM	Herpesvirus entry mediator
IAA	Iodoacetamide
ICAM-1	Intercellular adhesion molecule 1
IFIT	Interferon-induced protein with tetratricopeptide repeats
IFITM	Interferon-induced transmembrane protein
IFN	Interferon
IgG	Immunoglobulin G
iKIR	Inhibitory KIR
IL	Interleukin
ILC	Innate lymphoid cell
inf.	infected
ISG	IFN-stimulated genes
ITAM	Immunoreceptor tyrosine-based activation motif
ITIM	Immunoreceptor tyrosine-based inhibition motif
ITT	Immunoreceptor tyrosine tail
JAK	Janus kinase
kb	Kilobase
KO	Knockout
KIR	Killer cell immunoglobulin-like receptor
L	Long
LAMP	Lysosomal associated membrane glycoproteins
LFA-1	Lymphocyte function associated antigen 1;
MCMV	Murine cytomegalovirus
MCP-1	Monocyte chemoattractant protein-1
MEM	Minimal Essential Medium
MFI	Mean Fluorescence Intensity
mg	Milligram
MHC-I/-II	Major histocompatibility complex class I/II
MICA/B	MHC class I chain-related protein A/B
min	Minute
µg	Microgram
µl	Microlitre
ml	Millilitre
MCP-1	monocyte chemoattractant protein-1
MOI	Multiplicity of infection
MX1/MX2	Interferon-induced GTP-binding protein 1/2
NCR	Natural cytotoxicity receptor
ng	Nanogram
NHEJ	Non-homologous end joining
NK cell	Natural Killer cell
NKT cell	Natural Killer T cell
OD	Optical density

PAMPs	Pathogen-associated molecular patterns
PBMCs	Peripheral blood mononuclear cells
PC	Principle component
PCA	Principle component analysis
PCR	Polymerase chain reaction
PE	Phycoerythrin
PFA	Paraformaldehyde
PfEMP-1	<i>Plasmodium falciparum</i> erythrocyte membrane protein 1
PMA	Phorbol myristate acetate
RNA	ribonucleic acid
PPR	Pattern recognition receptor
PVR	Poliovirus receptor
PVRIG	Poliovirus receptor related immunoglobulin domain containing
R	Receptor
rcf	Relative centrifugal force
RFP	Red fluorescent protein
RNP	Ribonucleoprotein
RPKM	Reads per kilobase of transcript per Million mapped reads
RPMI	Roswell Park Memorial Institute Medium
RT	Room temperature
S	Short
sec	Second
sgRNA	Single guide RNA
SN	Supernatant
spp.	Several species
SSC	Sideward scatter
STAT	Signal transducer and activator of transcription
TAP	Transporter associated with antigen processing
TAPBP	TAP binding protein
<i>T. cruzi</i>	<i>Trypanosoma cruzi</i>
T _H cell	T helper cell
TIGIT	T cell immunoreceptor with immunoglobulin and ITIM domains
TIM-3	T cell immunoglobulin and mucin-domain containing 3
TLR	Toll-like receptor
TMB	3,3',5,5'-Tetramethylbenzidin
TNF	Tumor necrosis factor
TRAIL	Tumor necrosis factor-related apoptosis-inducing ligand
UK	United Kingdom
USA	United States of America
ULPB1-6	UL16 binding protein 1-6
v/v	Volume per volume
WHO	World Health Organization
w/o	Without
WT	Wildtype
w/v	Weight per volume
YXXM	Tyrosine-x-x-methionine

List of figures

Figure 1.1: Developmental progression and functionally analogous subsets of human and murine NK cells.....	2
Figure 1.2: Recognition of tumorous or infected cells by NK cells	5
Figure 1.3: Selected human NK cell receptors, their ligands, and the effect of the interaction on the NK cell response	7
Figure 1.4: <i>T. cruzi</i> life cycle.....	15
Figure 4.1: Coculture of human NK cells and <i>T. cruzi</i> -infected primary human dermal fibroblasts (HDF) results in NK cell degranulation	55
Figure 4.2: Transcriptome analysis reveals comparable transcriptional changes of HDFs and BJ fibroblasts in response to <i>T. cruzi</i> infection	57
Figure 4.3: Coculture of human NK cells and <i>T. cruzi</i> -infected BJ fibroblasts induces NK cell degranulation	58
Figure 4.4: Expression of the classical MHC-I molecules HLA-A,B,C is slightly increased on the BJ fibroblast surface in the course of <i>T. cruzi</i> infection	59
Figure 4.5: BJ fibroblasts show increased presence of vimentin on their cell surface in the course of <i>T. cruzi</i> infection	60
Figure 4.6: Binding of NKp46 to fibroblasts is increased after <i>T. cruzi</i> infection.....	62
Figure 4.7: Engagement of NKp46 in the context of <i>T. cruzi</i> -infected BJ fibroblasts is dependent on cell-cell contact	63
Figure 4.8: NKp46 blockade reduces NK cell response to fibroblasts	66
Figure 4.9: Transcriptome analysis reveals increased HVEM expression in BJ fibroblasts and HDF in response to <i>T. cruzi</i> infection	67
Figure 4.10: Expression of HVEM is increased on the BJ fibroblast surface in the course of <i>T. cruzi</i> infection.....	68
Figure 4.11: Binding of CD160 is increased after <i>T. cruzi</i> infection	69
Figure 4.12: CD160 blockade reduces NK cell response to fibroblasts	71
Figure 4.13: NK cells are stimulated by soluble cellular factors released by <i>T. cruzi</i> -infected fibroblasts	73
Figure 4.14: Transcriptome analysis of BJ fibroblasts and HDF reveals induction of IFN signaling in response to <i>T. cruzi</i> infection	75
Figure 4.15: Proteome analysis of BJ fibroblasts confirms the induction of IFN signaling in response to <i>T. cruzi</i> infection	77
Figure 4.16: Type I IFN IFN- β and type III IFN IFN- λ 1 and IFN- λ 2/3 are secreted by BJ fibroblasts after <i>T. cruzi</i> infection	78
Figure 4.17: IFN- β secreted by <i>T. cruzi</i> -infected BJ fibroblasts contributes to increased NK cell activation.....	79
Figure 4.18: Transcriptome analysis confirms increased HLA-C expression in BJ fibroblasts and HDF in response to <i>T. cruzi</i> infection	81
Figure 4.19: Expression of HLA-C is increased on the surface of BJ fibroblasts during the course of <i>T. cruzi</i> infection	81
Figure 4.20: Increased HLA-C expression is mediated by soluble factors released by <i>T. cruzi</i> -infected BJ fibroblasts	82
Figure 4.21: IFN- β secreted by <i>T. cruzi</i> -infected BJ fibroblasts contributes to increase of MHC-I molecules such as HLA-C.....	83
Figure 4.22: Binding of KIR2DL1 and KIR2DL2 to BJ fibroblasts is increased after <i>T. cruzi</i> infection.....	85
Figure 4.23: Generation of HLA-C KO BJ fibroblasts using CRISPR/Cas9 technology	86
Figure 4.24: Successful HLA-C KO was confirmed by missing or strongly reduced binding of KIR2DL1 and KIR2DL2 to the selected HLA-C KO BJ fibroblast clone	87
Figure 4.25: HLA-C expressed on BJ fibroblasts reduces NK cell response during coculture	90
Figure 4.26: Despite the dual effect of IFN- β on the NK cell response to <i>T. cruzi</i> -infected BJ fibroblasts, the stimulatory effect tends to be predominant	93
Figure 4.27: Dermal fibroblasts exhibit increased nectin-2 expression in response to <i>T. cruzi</i> infection	94
Figure 4.28: Dermal fibroblasts show increased HLA-E expression in response to <i>T. cruzi</i> infection	96

List of tables

Table 1.1: KIRs, their identified ligands and the effect of the interaction on the NK cell response.....	9
Table 2.1: Laboratory equipment.....	21
Table 2.2: Glass and consumables.....	22
Table 2.3: Chemicals and reagents.....	23
Table 2.4: Buffers and solutions.....	24
Table 2.5: Cell culture media.....	25
Table 2.8: Fluorochrome-labeled Antibodies.....	27
Table 2.9: Blocking/ neutralizing antibodies and isotype controls.....	28
Table 2.10: Immune sera.....	28
Table 2.11: Recombinant constructs.....	28
Table 2.12: Primary cells.....	28
Table 2.13: Eukaryotic cell lines.....	29
Table 2.14: Parasites.....	30
Table 2.15: Kits.....	30
Table 2.16: Software and web-based tools.....	31

Table of content

1	Introduction	1
1.1	Natural Killer cells	1
1.1.1	Phenotype	1
1.1.2	Effector functions	3
1.1.3	Regulation of NK cell activity	4
1.1.4	NK cell receptors and their ligands	6
1.1.4.1	Killer cell immunoglobulin-like receptors and their MHC-I ligands	7
1.1.4.2	Natural Killer Group 2 receptors and their cellular ligands	9
1.1.4.3	Natural cytotoxicity receptors and their cellular or pathogen-encoded ligands	10
1.1.4.4	CD160 and its ligand HVEM	11
1.1.4.5	TIGIT, PVRIG and DNAM-1 and their ligand nectin-2	12
1.1.4.6	Cytokine receptors	12
1.2	<i>Trypanosoma cruzi</i> and Chagas disease	14
1.2.1	Morphology and life cycle	14
1.2.2	Epidemiology	16
1.2.3	Pathogenesis	16
1.2.4	Treatment and prevention	17
1.2.5	Immune response against <i>T. cruzi</i>	17
1.3	Aim of the study	20
2	Materials	21
2.1	Laboratory equipment	21
2.2	Glass and consumables	22
2.3	Chemicals and reagents	23
2.4	Buffers and solutions	24
2.5	Cell culture media	25
2.6	Oligonucleotide primers	26
2.7	Plasmids	27
2.8	Antibodies, immune sera and recombinant constructs	27
2.9	Primary cells	28
2.10	Eukaryotic cell lines	29
2.11	Parasites	30
2.12	Kits	30
2.13	Software and web-based tools	31
3	Methods	32
3.1	Cell culture	32
3.2	Cultivation of <i>T. cruzi</i> parasites <i>in vitro</i>	32
3.3	Cell counting	33
3.4	<i>T. cruzi</i> <i>in vitro</i> infection	33

3.5	Immunofluorescence microscopy.....	34
3.6	Flow cytometry	34
3.7	Flow cytometric bead-based immunoassay - LEGENDplex™	35
3.8	ELISA (enzyme-linked immuno-sorbent assay)	35
3.9	Expression analysis of NK cell receptor ligands on fibroblasts	36
3.9.1	Neutralization of IFN-β in fibroblasts supernatants	36
3.10	Receptor-Fc/recombinant receptor binding assay	37
3.11	Reporter cell assay	37
3.11.1	Stimulation by coculture with fibroblasts	38
3.11.2	Stimulation by supernatant from fibroblasts	38
3.12	Isolation of NK cells from whole blood.....	39
3.13	NK cell stimulation by <i>T. cruzi</i> -infected fibroblasts	39
3.13.1	Degranulation assay after coculture	39
3.13.2	Degranulation assay after stimulation by supernatants	40
3.13.3	Analysis of secreted NK cell effector molecules during coculture	41
3.14	Interruption of regulatory interactions	42
3.14.1	Blockade of NKp46 and CD160 on NK cells	42
3.14.2	HLA-C KO in fibroblasts	42
3.14.2.1	Generation of HLA-C KO fibroblasts via CRISPR/Cas9 technology	42
3.14.2.2	Selection of an HLA-C KO single-cell clone.....	43
3.14.2.3	Use in coculture experiments	45
3.14.3	Neutralization of IFN-β in the supernatant	45
3.15	HLA-C and KIR genotyping	46
3.15.1	DNA Isolation	46
3.15.2	HLA-C typing by polymerase chain reaction (PCR)	46
3.15.3	KIR genotyping PCR	47
3.15.4	Agarose gel electrophoresis	48
3.16	Transcriptomic analysis	49
3.16.1	Total RNA isolation.....	49
3.16.2	Determination of RNA Integrity Number (RIN)	49
3.16.3	RNA sequencing library preparation and next-generation sequencing (NGS)	50
3.16.4	Transcriptome data analysis	50
3.17	Proteomic analysis.....	51
3.17.1	Sample processing and liquid chromatography tandem mass spectrometry (LC-MS/MS).....	51
3.17.2	Proteome data evaluation	52
3.18	Statistical analysis.....	52

4	Results	53
4.1	Activation of human NK cells by <i>T. cruzi</i> -infected dermal fibroblasts	53
4.2	Implementation of BJ fibroblasts as a model for dermal <i>T. cruzi</i> infection and related NK cell activation	56
4.3	<i>T. cruzi</i> -infected fibroblasts exhibit no reduction of MHC-I expression	58
4.4	NK cell response to <i>T. cruzi</i> -infected fibroblasts is facilitated by the engagement of NKp46	60
4.4.1	Increased presence of <i>csVimentin</i> on fibroblasts in response to <i>T. cruzi</i> infection	60
4.4.2	Increased binding of NKp46 to <i>T. cruzi</i> -infected fibroblasts	61
4.4.3	NKp46 blockade reduces NK cell response to fibroblasts	64
4.5	NK cell response to <i>T. cruzi</i> -infected fibroblasts is promoted by the engagement of CD160	67
4.5.1	Increased expression of the CD160 ligand HVEM on fibroblasts in response to <i>T. cruzi</i> infection	67
4.5.2	Increased binding of CD160 to <i>T. cruzi</i> -infected fibroblasts	68
4.5.3	CD160 blockade reduces NK cell response to fibroblasts	69
4.6	Interferons secreted by <i>T. cruzi</i> -infected fibroblasts support NK cell effector function	72
4.6.1	NK cell degranulation is promoted by soluble cellular factors released by <i>T. cruzi</i> -infected fibroblasts	72
4.6.2	Fibroblasts secrete interferons in response to <i>T. cruzi</i> infection	74
4.6.3	IFN- β secreted by <i>T. cruzi</i> -infected fibroblasts contributes to increased NK cell activation	79
4.7	NK cell response against <i>T. cruzi</i> -infected fibroblasts is inhibited by the engagement of KIR2DL molecules	80
4.7.1	Increased expression of the KIR ligand HLA-C on fibroblasts in response to <i>T. cruzi</i> infection	80
4.7.2	Increased HLA-C expression is mediated by soluble factors like IFN- β released by <i>T. cruzi</i> -infected fibroblasts	82
4.7.3	Increased binding of KIR2DL1 and KIR2DL2 to <i>T. cruzi</i> -infected fibroblasts	84
4.7.4	Generation of HLA-C KO BJ fibroblasts	85
4.7.5	HLA-C expressed on fibroblasts reduces the NK cell response during coculture	88
4.7.6	Stimulatory effect of IFN- β on NK cell response tends to be predominant	91
4.8	Nectin-2 and HLA-E are further potential modulators of the NK cell response against <i>T. cruzi</i> -infected fibroblasts	93
5	Discussion	97
5.1	NK cell stimulation by <i>in vitro</i> coculture with <i>T. cruzi</i> -infected dermal fibroblasts	98
5.2	Cell-cell contact-dependent NK cell activation by <i>T. cruzi</i> -infected fibroblasts	101
5.2.1	NK cell activation by <i>T. cruzi</i> -infected fibroblasts is not mediated by reduction of inhibitory signals	101
5.2.2	NK cell activation by <i>T. cruzi</i> -infected fibroblasts is facilitated by the engagement of NKp46	102
5.2.3	NK cell activation by <i>T. cruzi</i> -infected fibroblasts is facilitated by the engagement of CD160	105
5.3	Dual effect of IFN- β released by <i>T. cruzi</i> -infected fibroblasts on NK cell activity	107
5.3.1	NK cells are stimulated directly by IFN- β	107
5.3.2	IFN- β dampens the NK cell response by promoting MHC-I expression on target cells	110
5.4	Cell-cell contact-dependent dampening of the NK cell response against <i>T. cruzi</i> -infected fibroblasts by HLA-C corresponding inhibitory KIRs	112

5.4.1	<i>T. cruzi</i> infection enhances HLA-C expression on dermal fibroblasts and the binding of corresponding KIRs	112
5.4.2	Infection-induced HLA-C dampens the NK cell response in most individuals	115
5.5	Further potential modulators of NK cell responses against <i>T. cruzi</i> -infected fibroblasts	118
6	Future Perspectives	120
7	Abstract	122
8	Zusammenfassung	124
9	Literature	126

1 Introduction

1.1 Natural Killer cells

As a part of the innate immune system, Natural Killer cells (NK cells) play an important role in the early response to infections. They were first described in 1975 and defined by their ability to kill target cells without prior priming [1]. In the context of infection, NK cells control the pathogen load before the T cell-mediated immune response kicks in [2]. Although NK cells are best known for the defense against virus-infected cells, they also participate in combating intracellular bacteria such as *Mycobacterium tuberculosis* [3] and protozoan parasites like *Leishmania major* [4] or *Trypanosoma cruzi* (*T. cruzi*), as described in detail in section 1.2.5.

1.1.1 Phenotype

NK cells are characterized by a large and granular shape, and represent another subtype of lymphocytes in addition to B cells and T cells. They comprise approximately 5 – 15% of circulating lymphocytes and feature many phenotypic and functional parallels to CD8⁺ T cells [5], [6].

Human NK cells are distinguished by the presence of the surface marker CD56 with simultaneous absence of the surface marker CD3 [7]. Based on the CD56 expression level, two phenotypically and functionally different groups can be distinguished (figure 1.1). CD56^{bright} NK cells, that exhibit a high CD56 expression intensity, account for approximately 10% of peripheral NK cells and express little or no CD16 on the cell surface [8]. They feature high proliferation and migration but low cytotoxic capacity and primarily specialize in the production of cytokines [8]–[10]. Furthermore, CD56^{bright} NK cells are precursors of CD56^{dim} NK cells [11], which show a low CD56 expression intensity and comprise approximately 90% of peripheral NK cells. They express CD16 at high levels, which mediates their antibody-dependent cellular cytotoxicity (ADCC) [8]. This process is described more precisely in section 1.1.2. CD56^{dim} NK cells exhibit primary cytotoxic effector functions but also show the ability to produce cytokines [8], [12].

Murine NK cells differ from human ones regarding their receptor composition. In contrast to human NK cells, they do not express CD56. Instead, they can generally be distinguished by the presence of the surface marker NK1.1 and the absence of CD3 (figure 1.1). Moreover, CD11b⁺

CD27⁻ NK cells represent the functional analogue to human CD56^{bright} NK cells. They are the precursors of CD11b⁻ CD27⁺ NK cells, which are the functional analogue to human CD56^{dim} NK cells [13], [14]. In addition, there are other differences in the occurrence and expression intensity of other receptors. For instance, the human killer cell immunoglobulin-like receptors (KIRs) and the murine Ly49 receptors have analog functions, as described in section 1.1.4.1, but belong to different protein families and interact with other major histocompatibility complex class I (MHC-I) ligands [15].

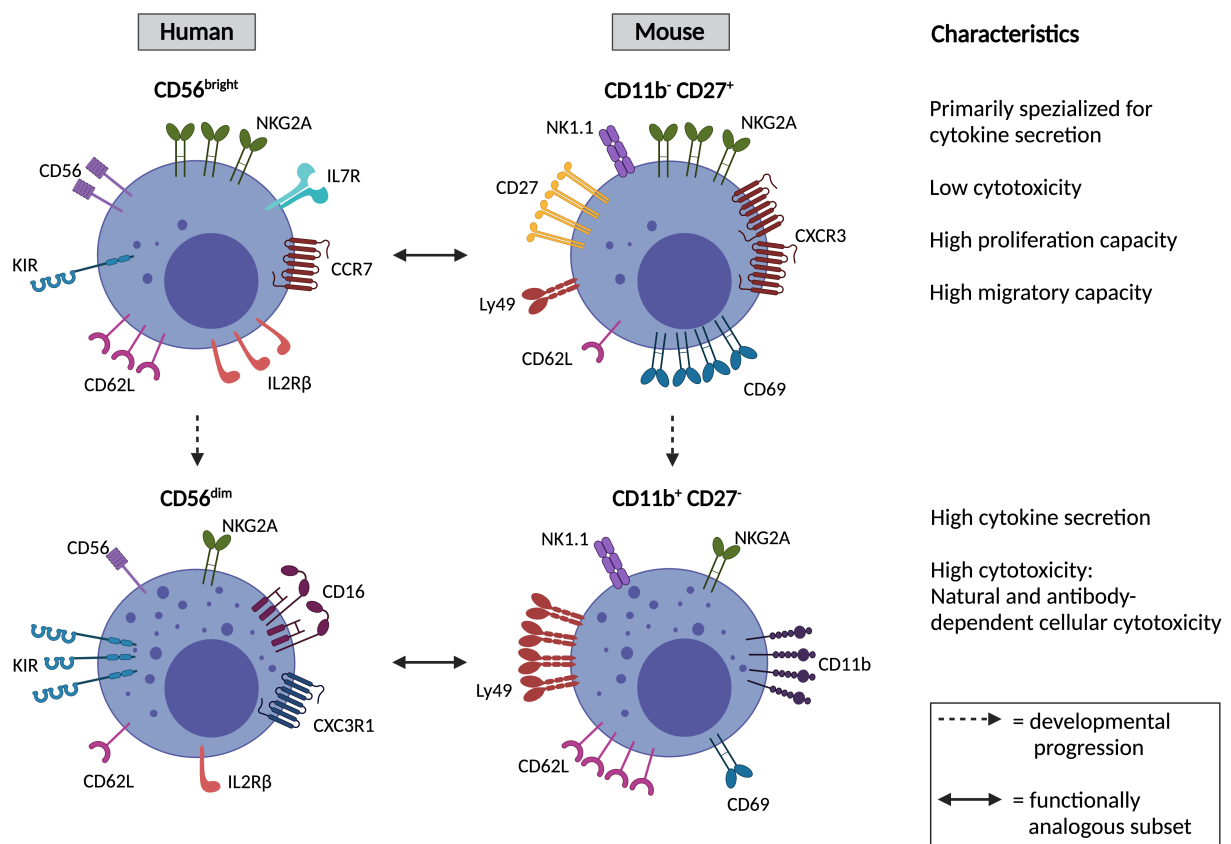


Figure 1.1: Developmental progression and functionally analogous subsets of human and murine NK cells. The immature human CD56^{bright} NK cells and the functionally analogous murine CD11b⁻ CD27⁺ NK cells are characterized by proliferation and migration but low cytotoxic capacity and are primary specialized for cytokine production. Mature human CD56^{dim} NK cells and analogous murine CD11b⁺ CD27⁻ NK cells feature abilities for high cytokine production, natural and antibody-dependent cellular cytotoxicity. Modified from Goyos *et al.*, 2019 [13]; Bald *et al.*, 2020 [14] and Cao *et al.*, 2020 [9]. Created with Biorender.com.

1.1.2 Effector functions

NK cells are named for their cytotoxic effector function that can be mediated either by the secretion of cytolytic granules or via death receptor-mediated pathways.

In response to NK cell activation, cytolytic granules containing perforin, granzysin and different granzymes are recruited to the site of the immunological synapse, leading to subsequent granule secretion. Perforin polymerizes to a circular polymer at the target cell membrane, resulting in a pore which enables granzymes to enter the cell. In the cytosol, granzymes, which belong to the group of serine proteases, activate the pro-caspase-3 and -7, initiating apoptosis of the target cell [16]. The described perforin/granzyme pathway is also involved in the ADCC process [17].

In addition to perforin and granzymes, cytotoxic granules of human, but not rodent NK cells contain the antimicrobial peptide granzysin [18]. Granzysin can selectively destroy cholesterol-poor microbial membranes, leading to programmed cell death of microbes, called microptosis [19]. In 2016, Dotiwala and colleagues showed that using this process, granzymes can be delivered to different protozoan parasites, including *T. cruzi*, without the contribution of Perforin. Following this, the parasites are killed caspase-independently through the production of reactive oxygen species. With the additional involvement of perforin, intracellular parasites can also be killed. Perforin allows granzysin and granzymes to enter the infected cell, whereupon these mediators attack the parasites in the cytosol [20].

The other pathway of NK cell-mediated cytotoxicity is accomplished through the binding of apoptosis-mediating death receptors on target cells by respective ligands expressed by NK cells. Death receptor ligands such as Fas ligand (FasL) and tumor necrosis factor-related apoptosis-inducing ligand (TRAIL) are members of the tumor necrosis factor (TNF) family. The interaction triggers the recruitment of various intracellular adaptor molecules in the target cell, resulting in the formation of the death inducing-signaling complex (DISC). Subsequently, the complex activates the pro-caspases 8 and 10, initiating the caspase cascade and finally resulting in the apoptosis of the target cell [21], [22].

Besides the cytotoxic effector functions, appropriately stimulated NK cells secrete different chemokines, like the monocyte chemoattractant protein-1 (MCP-1), that facilitate the recruitment of further immune cells to the site of inflammation [23]. Moreover, NK cells secrete proinflammatory cytokines such as TNF- α and Interferon (IFN)- γ as well as

immunosuppressive cytokines like Interleukin (IL)-10 [12], [23]. IFN- γ participates in a variety of different processes. For instance, it mediates macrophage activation and an increased antigen presentation by MHC-I and -II molecules [24]. Additionally, NK cell secretion of TNF- α and IFN- γ is functionally associated with their cytolytic activity. The cytokines mediate the upregulation of intercellular adhesion molecule 1 (ICAM-1) on the target cell surface, which facilitates the conjugate formation with NK cells [25].

1.1.3 Regulation of NK cell activity

NK cell activity is regulated by a dynamic equilibrium of signals from inhibitory and activating receptors. The respective signal strength is dependent on the composition and expression intensity of NK cell receptors and ligands on target cells as well as cytokines in the environment.

During steady state, somatic cells express classical and non-classical MHC-I molecules, which are bound by inhibitory NK cell receptors (figure 1.2A). The individual receptors are specified in detail in section 1.1.4. Despite the binding of a few activating receptors, inhibitory signaling predominates due to normal MHC-I expression, resulting in NK cell tolerance. MHC-I expression can be modulated or downregulated in cancerous or infected cells (figure 1.2B). Due to the lack of inhibitory signals, activating signals become predominant [26]. Consequently, target cells escape recognition by CD8⁺ T cells due to modulation or absence of MHC-I, but are recognized and lysed by NK cells. This mechanism was first described in 1990 as the “*missing self* hypothesis” [27] and is thus the longest-known mechanism of NK cell activation. On the other hand, stress mediated by tumor transformation or infection can induce the upregulation of stimulatory NK cell ligands, shifting the equilibrium towards the stimulatory side, resulting in NK cell activation (Figure 1.2C) [28]. Besides the contact-dependent mechanisms, NK cells can be stimulated indirectly by various cytokines, like different IFNs, IL-2, IL-12, IL-15, IL-18 and IL-21 (Figure 1.2D) [29].

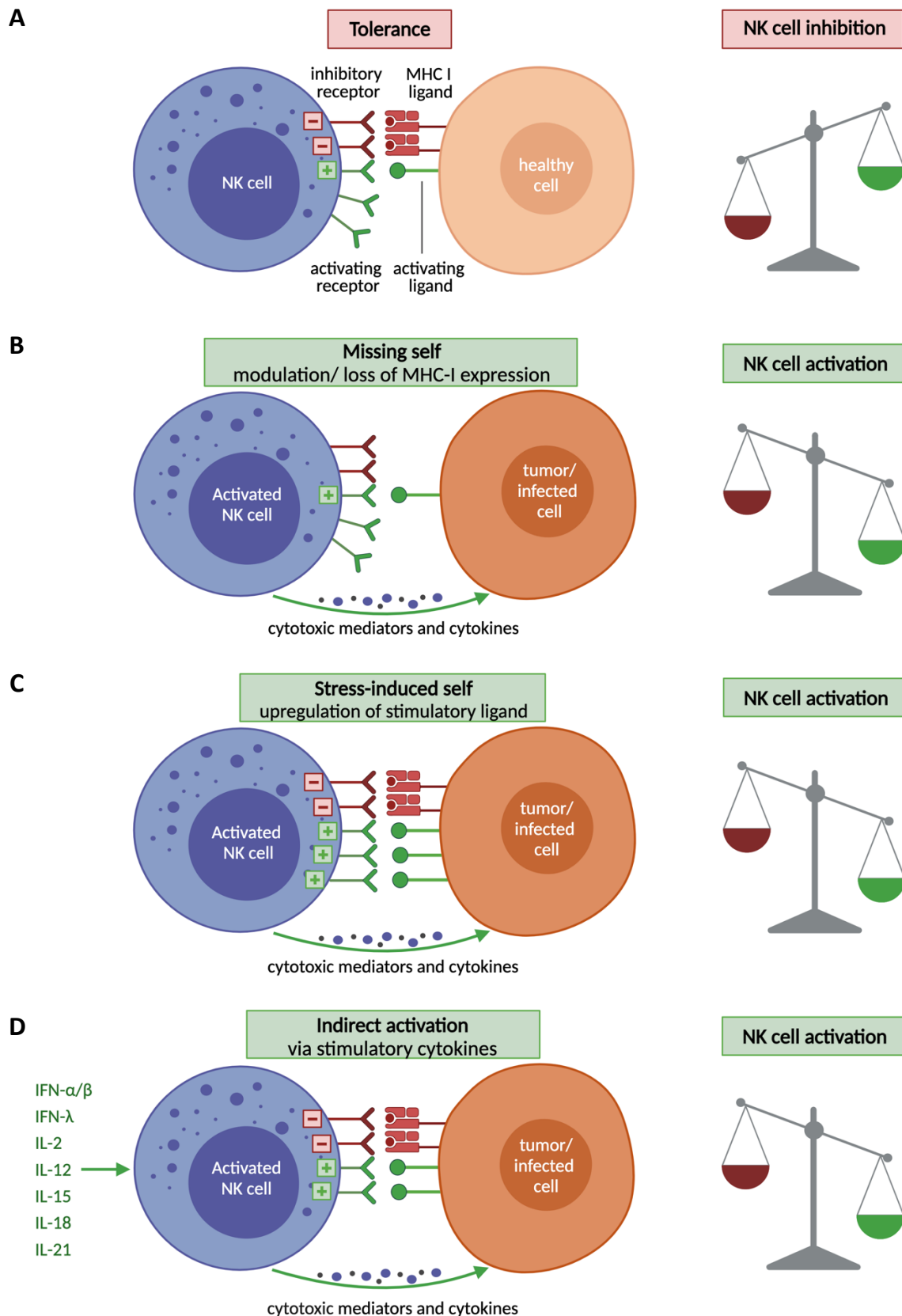


Figure 1.2: Recognition of tumorous or infected cells by NK cells. NK cell tolerance in steady state is mediated by a predominance of inhibitory signals due to normal MHC-I expression (A). NK cell activation can be mediated by modulation or loss of MHC-I expression according to the *missing self* hypothesis (B), by stress-induced upregulation of stimulatory ligands (C) and by stimulatory cytokines (D). Modified from Zwirner and Domaica, 2010 [29] and Vivier *et al.*, 2012 [30]. Created with Biorender.com.

1.1.4 NK cell receptors and their ligands

NK cells express a multitude of different receptors for cellular and pathogen-encoded ligands as well as cytokines and chemokines. In the following, the most important and, in the context of the present thesis, relevant receptors are described. Figure 1.3 shows the main human NK cell receptors and their respective interaction partners.

Inhibitory NK cell receptors transmit signals via cytoplasmic immunoreceptor tyrosine-based inhibitory motifs (ITIMs). After binding to the appropriate ligand, phosphatases are recruited to the ITIMs, which dephosphorylate downstream signaling molecules, leading to their inactivation and thus to inhibition of NK cell effector functions [31]. Most of the inhibitory NK cell receptors recognize classical or non-classical MHC-I molecules. In addition, similarly to T cells, NK cells express checkpoint receptors such as T cell immunoreceptor with immunoglobulin and ITIM domains (TIGIT) and B and T lymphocyte attenuator (BTLA), which can dampen NK cell effector function [9], [32], [33]. Ligands of inhibitory receptors can also often be recognized by activating receptors. Nevertheless, various studies have shown that in most cases inhibitory interactions exhibit a higher binding affinity compared to their activating counterpart [34]–[36]. If the ligand expression increases due to an infection or tumor transformation, the ligand can additionally form bonds to its activating receptor. Depending on the receptor expression level on the NK cell, this process results in inhibition or activation of NK cell effector functions [34].

Furthermore, NK cells express a variety of different activating receptors that can stimulate NK cells in synergy [31]. Most of the activating NK cell receptors mediate stimulatory signals via immunoreceptor tyrosine-based activation motifs (ITAMs), which are expressed by intracellularly associated adaptor molecules like the DNAX-activating protein 12 (DAP12). Moreover, some activating receptors use associated Fc ϵ R1 γ and CD3 ζ chains for transduction of activating signals. Binding of the appropriate ligand leads to recruitment and activation of tyrosine kinases, resulting in phosphorylation of downstream signaling molecules and subsequent NK cell stimulation [37]. Activating NK cell receptors mainly recognize cellular ligands, which are upregulated in response to stress due to infection or tumor transformation [38]. Besides that, natural cytotoxicity receptors (NCRs) can also directly detect pathogen-encoded ligands [39]. Furthermore, CD16 detects cells coated with pathogen- or tumor-specific immunoglobulin G (IgG), leading to ADCC [40].

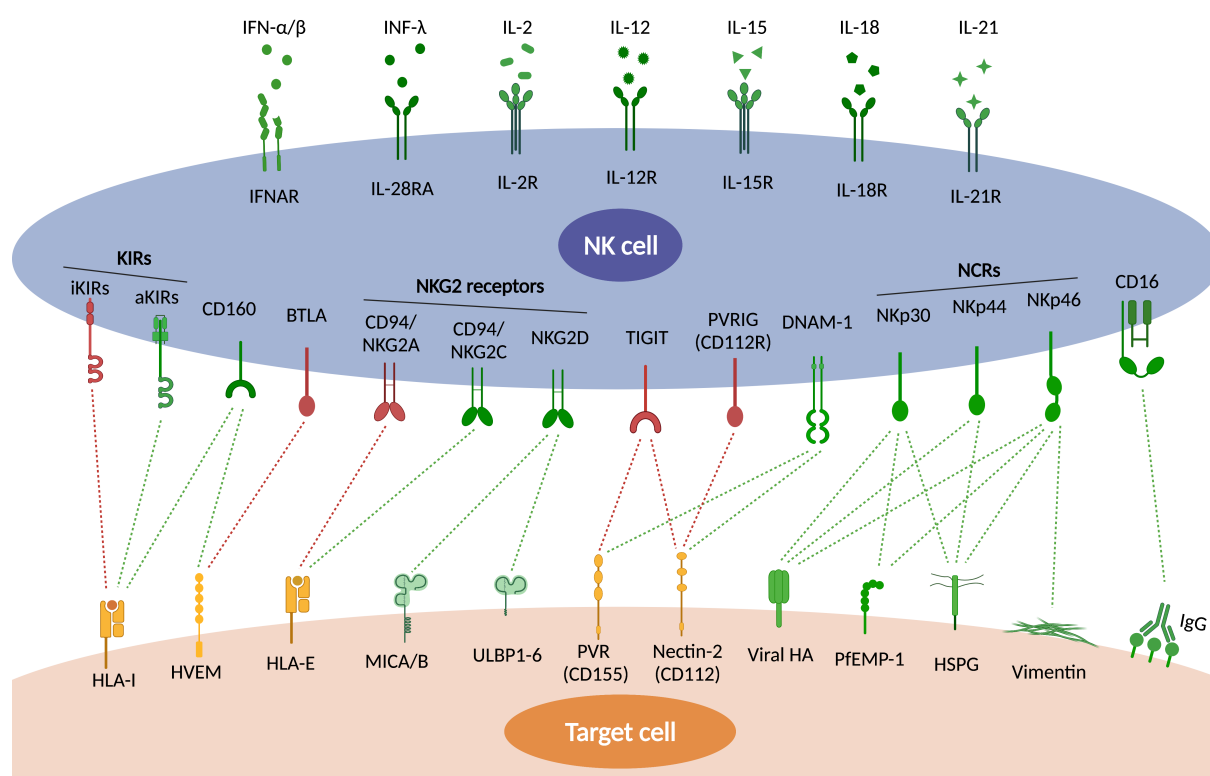


Figure 1.3: Selected human NK cell receptors, their ligands, and the effect of the interaction on the NK cell response. Inhibitory NK cell receptors and interactions are depicted in red, whereas activating NK cell receptors and interactions are shown in green. Ligands detected by inhibitory and activating receptors are shown in yellow, whereas ligands solely bound by activating receptors are depicted in green. Composed on basis of Le Bouteiller *et al.*, 2002 [41]; Bryceson *et al.*, 2006 [42]; Swann *et al.*, 2007 [43]; Ho *et al.*, 2008 [44]; Hecht *et al.*, 2009 [45]; Šedý *et al.*, 2013 [32]; Chan *et al.*, 2014 [46]; Romee *et al.*, 2014 [47]; Souza-Fonsera-Guimaraes *et al.*, 2015 [48]; Pazina *et al.*, 2017 [49]; Stein *et al.*, 2017 [50]; Gonzalez-Rodriguez *et al.*, 2019 [51] as well as Holder and Grant, 2020 [52]. Created with Biorender.com.

1.1.4.1 Killer cell immunoglobulin-like receptors and their MHC-I ligands

The KIR family comprises 15 functional genes encoding for activating and inhibitory members, as well as two pseudogenes. They are exclusively expressed in humans and higher primates [53]. As a functional equivalent, mice express the structurally different Ly49 receptors that evolved independently of KIRs [54], [55]. In addition to NK cells, various T cell subsets, such as effector/memory T cells, $\gamma\delta$ T cells and Natural Killer T cells (NKT cells), are described to express KIRs in humans [56], [57]. The KIR family is characterized by a massive variability, caused by extensive polymorphisms in addition to the described polygenicity, and is comparable to the variability of MHC molecules [58]. Regarding the composition of KIR genes, two different haplotype groups are described. Whereas group A haplotypes exclusively contain inhibitory KIR genes, apart from KIR2DS4, group B haplotypes are more variable and consist of more than one activating KIR gene [59]. Moreover, the frequency and expression

level of different encoded KIRs can differ between individuals due to copy number and allelic variations [60]. Furthermore, within an individual, not all encoded KIRs are expressed by every NK cell. Each individual NK cell clone stochastically expresses different combinations of the encoded KIRs [61].

The KIR nomenclature is based on the extra- and intracellular structure. Extracellularly, KIRs are composed of two (2D) or three (3D) immunoglobulin-like domains. The intracellular structure determines the function of the receptor. Inhibitory KIRs comprise a long (L) intracellular domain with ITIMs mediating inhibitory downstream signaling. In contrast, activating KIRs only feature a short (S) intracellular domain, that is linked to a DAP12 adaptor molecule containing ITAM sequences, which transmit stimulatory signals [53].

As shown in table 1.1, the different KIR molecules bind to different MHC-I ligands, which in humans are also known as human leukocyte antigen class I (HLA-I). In addition to NKG2A (section 1.1.4.2), inhibitory KIRs are responsible for maintenance of self-tolerance to healthy cells. As described in section 1.1.3, infection or malignant transformation can lead to modulation or downregulation of MHC-I expression. This absence of inhibitory signals renders the target cell vulnerable for NK cell-mediated killing [27].

Examples of inhibitory KIRs are KIR2DL1, KIR2DL2 and KIR2DL3, which bind to two different HLA-C allotypes. These allotypes are classified based on polymorphisms at the positions 77 and 80 of the HLA-I heavy chain. While KIR2DL1 binds HLA-C2, KIR2DL2 and KIR2DL3 preferentially bind HLA-C1 allotypes [62]. The KIR2DL1 – HLA-C2 interaction has been described to mediate stronger inhibitory signals compared to the KIR2DL2/L3 – HLA-C1 interaction [63]. In addition, activating KIRs have also been shown to recognize HLA-C molecules. Whereas KIR2DS1 binds to HLA-C2, KIR2DS2 recognizes HLA-C1 allotypes due to their extracellular structure, which is similar to that of their inhibitory counterparts. Nevertheless, activating KIRs have generally been shown to exhibit lower binding affinities and partially higher peptide selectivity compared to their opponents [64], [65]. Thus, the ligand and the receptor expression intensity as well as the presented peptides determine the engagement of the respective activating KIRs.

Table 1.1: KIRs, their identified ligands and the effect of the interaction on the NK cell response. Adapted from Nowak *et al.*, 2017 [62].

Receptor	Ligand	Function
KIR2DL1	HLA-C2 (C*02, C*04, C*05, C*06)	Inhibitory
KIR2DL2	HLA-C1 (C*01, C*03, C*07, C*08) Some HLA-C2 (C*0501, C*0202, C*0401) Some HLA-B (B*4601, B*7301)	Inhibitory
KIR2DL3	HLA-C1 (C*01, C*03, C*07, C*08) Some HLA-C2 (C*0501, C*0202) Some HLA-B (B*4601, B*7301)	Inhibitory
KIR2DL4	HLA-G	Inhibitory/activating
KIR2DL5A and KIR2DL5B	Unknown	Inhibitory
KIR2DS1	HLA-C2 (C*02, C*04, C*05, C*06)	Activating
KIR2DS2	HLA-A*1102 HLA-C1 (C*01, C*03, C*07, C*08)	Activating
KIR2DS3	Unknown	Activating
KIR2DS4	HLA-A*1102 Some HLA-C (C*0501, C*1601, C*0202)	Activating
KIR2DS5	Unknown	Activating
KIR3DL1	HLA-A expressing Bw4 epitope (A*23, A*24, A*32) HLA-B expressing Bw4 epitope (B*08, B*27, B*57, B*58)	Inhibitory
KIR3DL2	Some HLA-A (A*03, A*11) HLA-B27 HLA-F	Inhibitory
KIR3DL3	Unknown	Inhibitory
KIR3DS1	HLA-Bw4 epitope HLA-B*5701 HLA-F	Activating

1.1.4.2 Natural Killer Group 2 receptors and their cellular ligands

The Natural Killer Group 2 (NKG2) receptor family belongs to the C-type lectin-like receptors. They are selectively expressed by NK cells and CD8⁺ T cells. The family contains the inhibitory member NKG2A as well as the two activating members NKG2C and NKG2D [66].

NKG2A is associated with CD94 as a heterodimer and mediates inhibitory signaling via two integrated ITIM domains [67], [68]. In humans, NKG2A binds to the non-classical MHC-I molecule HLA-E (figure 1.3) that presents peptides derived from signal sequences of classical MHC-I molecules [69]. Thus, their presence on the cell surface additionally reflects the general MHC-I expression.

The activating NKG2C is also associated with CD94 as a heterodimer and transmits stimulatory signals through the intracellularly-associated adaptor molecule DAP12 and the comprised ITAM sequences [70]. NKG2C also binds HLA-E, but with lower affinity than the inhibitory NKG2A [35], [67], [71], [72]. In addition, NKG2C has been shown to specifically recognize viral peptides loaded on HLA-E molecules upon infection with human cytomegalovirus (HCMV).

This interaction is linked to the generation of memory-like/adaptive NK cells, which share properties with the adaptive immune system [73], [74].

In contrast to other family members, NKG2D is a homodimer. It is intracellularly associated to a DAP10 adaptor molecule, which transmits stimulatory signals using a tyrosine-x-x-methionine (YXXM) sequence [75]. NKG2D molecules recognize cellular ligands, which are upregulated in response to cell stress due to infection or malignant transformation [76]. In humans, these ligands are the MHC-I chain-related protein A/B (MICA/B) as well as the UL16 binding proteins 1-6 (ULBP1-6), as depicted in figure 1.3 [77], [78].

1.1.4.3 Natural cytotoxicity receptors and their cellular or pathogen-encoded ligands

Natural cytotoxicity receptors (NCRs) belong to the immunoglobulin superfamily and include the three transmembrane receptors NKp30, NKp44 and NKp46. NCRs mediate stimulatory signaling via the engagement of intracellularly-associated DAP12 adaptor molecules in the case of NKp44 or CD3 ζ , as well as Fc γ chains in the case of NKp30 and NKp46 [39]. Besides NK cells, also CD8⁺ T cells [79], [80], $\gamma\delta$ T cells [81]–[83] and some innate lymphoid cells (ILCs) [84], [85] have also been described to express NCRs. Different host as well as pathogen-encoded molecules have been shown to serve as NCR ligands, a selection of which is depicted in figure 1.3. In addition to surface expression, NCR ligands can be secreted, shedded or incorporated into the extracellular matrix [39].

NKp30 is constitutively expressed on mature resting and activated NK cells [86]. An example for a host-encoded ligand is heparan sulfate proteoglycan (HSPG), which is present on all cells but overexpressed on malignant transformed cells [45], [87]. Pathogen-encoded ligands for NKp30 are, for instance, viral hemagglutinin (HA) from poxviruses [88] and the *Plasmodium falciparum* erythrocyte membrane protein 1 (PfEMP1) [89].

NKp44 is expressed exclusively after cell activation [90]. Similar to NKp30, it has been shown to recognize HSPG as a cellular ligand [45] and viral HA from influenza as a pathogen-encoded ligand [44].

Like NKp30, NKp46 is constitutively expressed regardless of the activation status [91]. Besides HSPG, vimentin expressed on the surface of *Mycobacterium tuberculosis* infected monocytes has also been described to serve as a cellular ligand for NKp46 [45], [92]. Similar to NKp30, NKp46 recognizes viral HAs and PfEMP1 as pathogen-encoded ligands [88], [93].

1.1.4.4 CD160 and its ligand HVEM

CD160 engagement mediates bidirectional signaling depending on the expressing cell type and the context of engagement. It is expressed on NK cells, T cells, intraepithelial lymphocytes and endothelial cells [94]–[96]. Whereas CD160 has been shown to act as a co-inhibitory molecule for CD4⁺ T cells [97], its role for CD8⁺ T cells is controversial. Different studies revealed a co-stimulatory effect of CD160 on CD8⁺ T cells during human immunodeficiency virus (HIV) and *Listeria monocytogenes* infection [98], [99]. However, a study on experimental cerebral malaria instead suggested a co-inhibitory function for CD8⁺ T cells [100]. For NK cells, CD160 engagement has been shown to exclusively act in a stimulatory manner and induce cytotoxicity and cytokine production with a major focus on IFN- γ [41], [101]–[104].

CD160 is a member of the immunoglobulin superfamily and is mainly expressed in a Glycosylphosphatidyinositol (GPI)-anchored form, which can be secreted by activated NK cells [95], [105]. Furthermore, a transmembrane isoform was found solely on activated peripheral NK cells and NK cell lines [106]. In contrast to other activating receptors, CD160 is not associated to adaptor molecules that transmit stimulatory signals. The GPI-anchored form does not contain a transmembrane or intracellular domain, which means that it cannot transmit stimulatory signals itself. It is presumed that signal transduction is mediated through interaction with other receptors in lipid rafts such as the co-stimulatory receptor CD2 [107], [108].

As visualized in figure 1.3, CD160 interacts with MHC-I molecules [41], [101], [103] as well as the herpes virus entry mediator (HVEM) with higher affinity [32], [97]. In the context of human NK cells, the MHC-I molecule HLA-C was shown to stimulate NK cell activity via CD160 engagement [41], [103]. HVEM is primarily known to interact with CD160 on T cells mediating inhibitory and stimulating signaling [97], [100]. In 2013, Šedý and colleagues demonstrated its relevance for CD160-mediated NK cell activation in the context of HCMV infection [32]. Aside from CD160, the co-inhibitory molecule BTLA has also been described to interact with HVEM [109]. However, NK cell treatment with HVEM-Fc constructs resulted in increased NK cell activity, presumably due to higher frequency and expression intensity of CD160 compared to BTLA on NK cells [32], [110].

1.1.4.5 TIGIT, PVRIG and DNAM-1 and their ligand nectin-2

As depicted in figure 1.3, nectin-2 (CD112) has been shown to interact with the three receptors TIGIT, Poliovirus receptor related immunoglobulin domain containing (PVRIG; also known as CD112R) and DNAX accessory molecule 1 (DNAM-1) [111]–[113]. However, the receptors exhibit opposite effects on the expressing immune cells [50]. Whereas TIGIT and PVRIG act as co-inhibitory receptors, DNAM-1 has been shown to mediate stimulatory signals. Both co-inhibitory receptors are expressed on the surface of NK cells, T cells as well as NKT cells and mediate antagonistic signaling via ITIM sequences within their cytoplasmatic domains [36], [113]–[115]. DNAM-1 is described to be expressed on NK cells, T cells as well as monocytes, and mediates stimulatory signals via an immunoreceptor tyrosine tail (ITT)-like motif within its cytoplasmatic domain [116], [117]. The binding affinity of nectin-2 to the various receptors differs widely, with the highest affinity being demonstrated for PVRIG [50], [113].

Besides nectin-2, the Poliovirus receptor molecule (PVR) is shown to serve as another ligand for TIGIT and DNAM-1 with higher binding affinity to TIGIT [50].

1.1.4.6 Cytokine receptors

In addition to the direct cell-cell interaction at the immunological synapse, soluble factors such as cytokines can influence NK cell function. Furthermore, various cytokines are also crucial for NK cell development and differentiation [118]. NK cell effector functions of mature NK cells can mainly be modulated by IL-2, IL-12, IL-15, IL-18 as well as type I and type III IFNs as depicted in figure 2 and figure 3. These cytokines can act by themselves or in synergy with cellular ligands [43], [47], [48]. Based on their relevance for this thesis, the following section will focus on NK cell stimulation by type I and type III IFNs.

In the context of NK cells, IFN- α and IFN- β are the most important members of the type I IFN group. They have been described to influence the NK cell response against infections and tumorigenesis [43], [119]. During infection, type I IFNs can be secreted by a variety of different cell types, including dendritic cells (DCs), monocytes, endothelial cells and fibroblasts [120]. Their induction is mediated by the engagement of pattern recognition receptors (PRRs), for example by pathogen products [121]. The secreted type I IFNs are recognized by the receptor IFNAR, which is expressed on B cells, T cells, NK cells, neutrophils and monocytes [122]. The binding of a type I IFN molecule to one of the subunits, IFNAR1 or IFNAR2, leads to the

recruitment of the remaining subunit [123]. The receptor dimerization results in autophosphorylation of the Janus kinase (JAK), which is non-covalently associated to the cytoplasmic domain, inducing JAK/signal transducer and activator of transcription (STAT) signaling [124]. The signaling results in the transcription of IFN-stimulated genes (ISGs) that exhibit a broad range of functions [123], [125]. For instance, they execute direct antiviral functions, such as preventing virus entry into the host cell or inhibiting virus replication [126]. Furthermore, type I IFNs are described to increase the expression of MHC-I molecules [127] and enhance the production of other NK cell-stimulating cytokines like IL-15 [121]. In regard to their direct effect on NK cells, IFN- α and - β have been shown to enhance NK cell cytotoxicity [128], [129].

Type III IFNs consist of the four IFN- λ molecules IFN- λ 1 (IL-29), IFN- λ 2 (IL-28A), IFN- λ 3 (IL-28B) and IFN- λ 4. Similar to type I IFNs, they have been described to be secreted by different hematopoietic cells as well as endothelial cells in response to engagement of PRRs [130]. The corresponding receptor IL-28R is expressed by NK cells and DCs [48], [131]. The functional form of the receptor is a heterodimer consisting of the IL-28R alpha chain (IL-28R α), which is responsible for ligand recognition, and the IL-10 beta chain (IL-10R2), which mediates signal transduction [132], [133]. After binding of a type III IFN molecule to IL-28R α , IL-10R2 is recruited. The induced JAK/STAT signaling results in similar gene expression to type I IFN/IFNAR interaction [130]. With regard to NK cells, type III IFN recognition has been shown to stimulate the NK cell-mediated IFN- γ production [134].

1.2 *Trypanosoma cruzi* and Chagas disease

T. cruzi is the causative agent of Chagas disease, also known as American trypanosomiasis. This disease can cause severe symptoms, such as cardiomyopathy or damage to the nerves of the digestive tract, especially during the chronic phase.

The main transmission route of the protozoan parasite is vector-borne [135]. Therefore, the skin is the main site of entry, which makes it the focus of interest in this study.

1.2.1 Morphology and life cycle

T. cruzi is an obligate intracellular protozoan parasite of the genus *Kinetoplastida*. Its life cycle (figure 1.4) is characterized by a host shift between an arthropod vector and a vertebrate host. The parasite shows a very broad vertebrate host specificity, but is mainly found in mammals like humans, dogs, opossums and other rodents such as rats [136], [137]. Transmission to humans is mainly mediated by different species of triatomine bugs [136], [137]. The metacyclic trypomastigote form of the parasite is excreted through the bugs' feces or urine in parallel to the blood meal and enters the skin at the bite injury or the ocular or oral mucosa through unconscious scratching [138]. Trypomastigotes are the extracellular, infectious, non-replicating form of the parasite that is morphologically characterized by an elongated S-shape carrying a flagellum, enabling locomotion in the blood. In principal, trypomastigotes are able to infect all nucleated cells, but preferentially invade macrophages, fibroblasts, muscle cells, cells of the central nervous system and adipose tissue [139]. With regard to the initial infection via the skin, dermal fibroblasts and tissue-derived macrophages should be the primary infected cell types. Trypomastigotes are able to actively enter their host cells by binding host cell ligands such as lectins or sialic acids via specific receptors [140], [141]. Consequently, host cell lysosomes are recruited and fuse with the plasma membrane, resulting in the formation of a parasitophorous vacuole [142]. The subsequent fusion of this vacuole with a lysosome leads to acidification of the compartment. This acidification causes the secretion of pore-forming molecules by the trypomastigotes and their release to the cytoplasm [143]. Here, the parasites differentiate into their intracellular, replicating amastigote form. Amastigotes are morphologically characterized by their oval shape without an external flagellum. The parasites replicate through longitudinal division for 3 – 5 days until the host cell is entirely filled and differentiate back to their motile trypomastigote form [144],

[145]. Subsequently, trypomastigotes are released by mechanical cell rupture, which enables infection of adjacent cells, the spread to other tissues through the blood stream or an uptake by another arthropod vector during its blood meal [139]. After reaching the bug's midgut, the parasites invade epithelial cells and differentiate first to the amastigote and afterwards to the epimastigote form. Epimastigotes appear exclusively during the arthropod stage. They are able to replicate through longitudinal division, and the elongated form of the flagellum grants them additional mobility. Finally, the parasites differentiate into the infectious metacyclic trypomastigote form in the bug's rectum and can be excreted [146].

Besides the vector-borne transmission, *T. cruzi* can be transmitted orally through contaminated food, congenitally during pregnancy, through sexual contact or through organ transplantation and blood transfusion [135], [147].

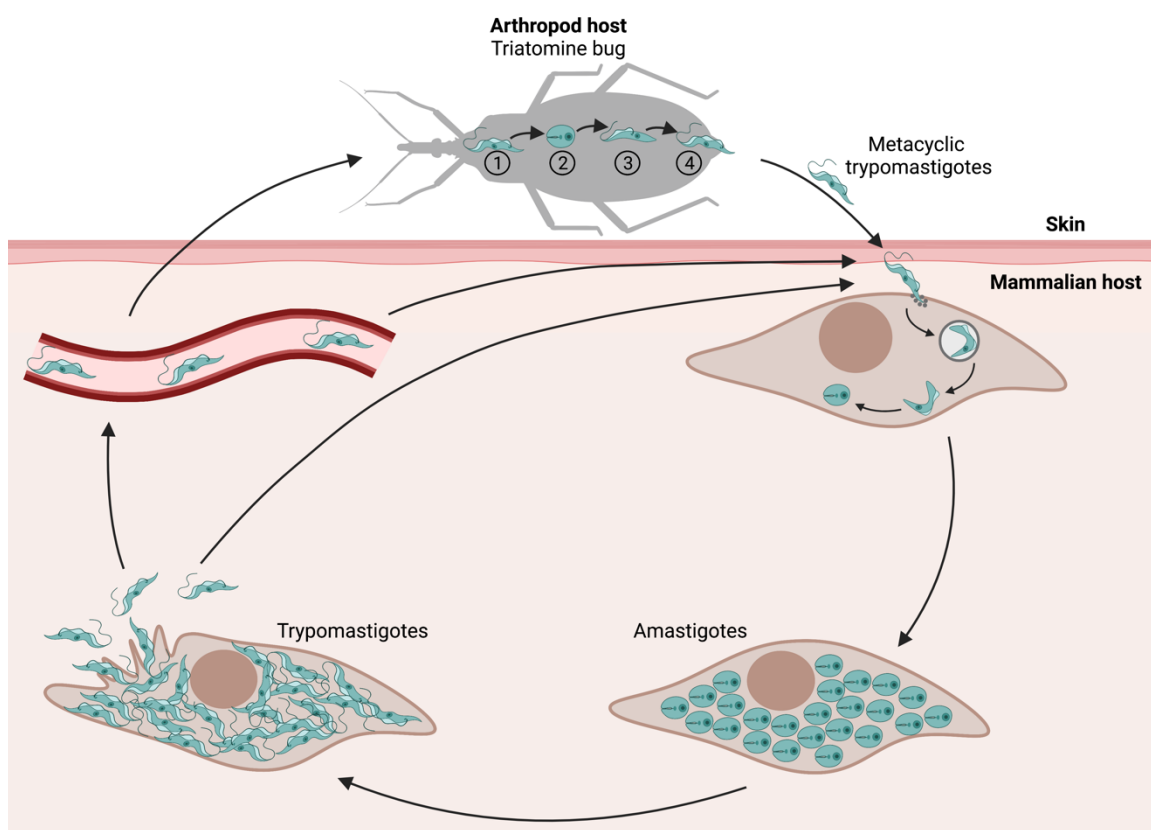


Figure 1.4: *T. cruzi* life cycle. Metacyclic trypomastigotes are excreted with feces or urine of an infected arthropod host in parallel to its blood meal. The parasites mainly enter the mammalian host skin at the bite injury, where they invade primary dermal fibroblasts and tissue-resident macrophages. After escaping from the parasitophorous vacuole into the cytosol, the trypomastigotes differentiate into the intracellular amastigote form and replicate through longitudinal division. Subsequently, the parasites differentiate back to the motile trypomastigote form and finally burst the host cell for further spreading or uptake by another arthropod vector. The trypomastigotes (1) invade epithelial cells in the bug's midgut and replicate after differentiation into amastigotes (2) and subsequently epimastigotes (3). Finally, the parasites differentiate to the infective metacyclic trypomastigotes (4) for further transmission. Image was created with BioRender.com.

1.2.2 Epidemiology

An infection with *T. cruzi* leads to the development of Chagas disease. The World Health Organization (WHO) placed Chagas disease on the list of the 20 neglected tropical diseases. It is estimated that about 6 – 7 million people are infected worldwide, with around 12,000 deaths per year [135], [148]. Initially, *T. cruzi* infections were restricted to rural regions in Latin America due to the distribution of the arthropod vector. The triatomine bugs stay there in cob walls and palm roofs of the human dwellings [149]. To this end, vector-borne transmission is strongly associated with poverty and rural housing [150]. Although Chagas disease is endemic in these regions, in recent decades it has been spread to non-endemic regions through urbanization and migration to other continents. Nowadays, a large number of countries, such as the USA, Canada, the Western Pacific and European countries are affected [135], [151], [152]. In Europe, the prevalence among Latin American immigrants is estimated at 4.2% [153]. In these non-endemic regions, transmission takes place via the described non-vector routes [154].

1.2.3 Pathogenesis

Chagas disease is divided into an acute and a chronic stage. The acute stage is driven by the intracellular proliferation process of the parasites and is characterized by high blood parasitemia and parasite burden in the tissue. Since most of the cases are asymptomatic or manifest mild and unspecific symptoms, the diagnosis is difficult [154]. Less than half of acutely infected individuals show dermatological manifestations such as inflammatory lesions at the inoculation site (Chagoma) or a purplish swelling of an eyelid (Romaña's sign) [138]. In rare cases, severe, life-threatening inflammations of the heart muscle and brain can occur [139]. The host immune response achieves a strong decrease of parasite number within 4 – 8 weeks, but fails to establish sterility [155].

If the patient is not treated during the acute stage, the chronic stage is entered after the parasite number is decreased. Here, parasites persist in the tissue, especially in muscle cells, the adipose tissue and the skin [156]–[158]. The chronic stage is initially asymptomatic and remains without symptoms in approximately 60 – 70% of cases. This asymptomatic, chronic stage is also referred to as the indeterminate stage. After 10 – 30 years, 30 – 40% of the infected individuals develop severe and partially life-threatening symptoms [159]. Whereas

about 30% of chronically infected individuals suffer from a cardiac manifestation, commonly called Chronic Chagas Cardiomyopathy, approximately 10% develop gastrointestinal symptoms such as megaesophagus or megacolon, or a mixed manifestation [135], [160], [161]. The reasons for the different progressions are not yet fully understood. However, it is assumed that different genetic factors of the host and parasite, host defense mechanisms, the infective load and the infection route contribute to the different manifestations [162]. Several studies indicate that molecular mimicry of the parasite triggers the onset of the symptoms. For instance, infection-induced autoantibodies cause a self-reactive immune response and consequently tissue damage [163], [164].

1.2.4 Treatment and prevention

Treatment of a *T. cruzi* infection is currently limited to the two drugs benznidazole and nifurtimox. Both have a direct toxic effect on the parasites, meaning that they are particularly effective in the acute phase, which is characterized by high parasitemia in the blood. Treatment efficiency decreases proportionally to the duration of infection [165]. Furthermore, both drugs show a high incidence of severe adverse events, partly due to the long treatment duration of at least two months [166].

Despite great efforts, no approved vaccination exists to combat Chagas disease [167]. The main focus of prophylaxis is on the destruction of the arthropod vector through the use of insecticides [168]. Although this has led to great progress in Latin America, there have been relapses in regions without sustained action [169], [170]. In addition, systemic blood screenings are carried out to prevent transmission through blood transfusions and transplants [135].

1.2.5 Immune response against *T. cruzi*

The immune response to *T. cruzi* infection is complex and involves both humoral and cellular mechanisms. The innate immune response, which is characterized by rapid reaction, is mainly driven by the complement system, phagocytic cell types, such as macrophages, DCs and neutrophils, as well as NK cells.

Phagocytes are rapidly activated via their PRRs after recognition of pathogen-associated molecular patterns (PAMPs). They detect *T. cruzi* parasites and their components primarily via

PRRs of the Toll-like receptor (TLR) group [171]. In particular, macrophages and DCs play an important role for antigen presentation and thus the initiation of the adaptive immune response [172]. Furthermore, they shape the immune response by secretion of various cytokines such as IL-12. This cytokine polarizes the immune response, for example via stimulation of IFN- γ production by NK cells [173], [174].

Since *T. cruzi* is an obligate intracellular parasite, NK cells are crucial for the rapid immune response against it. With increasing knowledge about their role during the infection, their relevance has become more evident. In an experimental mouse model as well as a study using human blood, it has been shown that NK cells are the main producers of IFN- γ during the initial phase of a *T. cruzi* infection [175], [176]. Several studies have demonstrated that IFN- γ is crucial for the parasite control [175], [177]. Among other things, this cytokine increases the macrophage effector activity [178], [179] and promotes the immunoglobulin switch to IgG subclasses, improving opsonization and complement activation [180]. Furthermore, IFN- γ promotes the production of reactive oxygen species in *T. cruzi*-infected fibroblast-like L929 cells [181]. Moreover, NK cells have been shown to directly kill extracellular trypomastigotes through a rapid formation of cell-cell contact and subsequent prevention of parasite motility and perforin-independent killing [182]. Besides their relevance during the acute stage, there is increasing evidence that NK cell function impacts the course of the chronic stage. Flow cytometry analyses revealed a higher amount of mature NK cells in the peripheral blood of asymptomatic compared to cardiac patients [183], [184]. In addition, microarray-based transcriptomic analyses showed an upregulation of NK cell cytotoxicity-related genes in the blood of asymptomatic patients and patients with mild cardiomyopathy and a downregulation of those genes in patients with severe cardiomyopathy [185]. Taken together, these data suggest that NK cell cytotoxicity plays an important role during the chronic stage of Chagas disease by promoting the maintenance of the asymptomatic status.

The adaptive immune response against *T. cruzi* is driven by B cells and T cells. Compared to the innate immune response, the onset of the adaptive immune response is delayed, but acts pathogen-specifically. This specificity is achieved by recombination of B cell and T cell receptors and subsequent clonal expansion [186].

The relevance of antibody-producing B cells was revealed in studies using B cell-deficient mice and rats, which were not able to control the *T. cruzi* infection [187], [188]. The produced parasite-specific antibodies facilitate the parasite phagocytosis by macrophages and neutrophils and are crucial for the activation of the complement system [188]–[190]. Additionally, activation of NK cells via ADCC seems to play a substantial role during initial killing of parasites. Adoptive transfer of serum, together with NK cells from mice, which were immunized with an attenuated *T. cruzi* strain, protected recipient mice from developing parasitemia after challenge [177].

Activation of CD4⁺ T cells, also known as T helper cells (T_h cells), requires the recognition of specific antigens presented on MHC-II molecules on the surface of professional antigen presenting cells such as macrophages or DCs. CD4⁺ T cells influence the immune response particularly through the secretion of cytokines [186]. In the context of a *T. cruzi* infection, protection is primarily mediated by the subgroup of T_h1 cells, especially through secretion of IFN- γ [191], [192].

Due to the obligatory intracellular life cycle of *T. cruzi*, CD8⁺ T cells, also known as cytotoxic T lymphocytes (CTLs), are the main drivers of the adaptive immune response. Their cytotoxic effector mechanisms are directed towards infected cells presenting specific antigens on MHC-I molecules. The strong impact of CD8⁺ T cells was demonstrated for the acute as well as the chronic stage of the infection. Whereas CD8⁺ T cell-deficient or depleted mice did not survive the acute stage [193], [194], CD8⁺ T cell depletion during the chronic stage caused an increased parasitic load in muscle and adipose tissue [195]. Besides their cytotoxic activity, CD8⁺ T cells secrete proinflammatory cytokines like TNF- α and IFN- γ [194]–[198].

Although the immune response is able to strongly reduce the parasite number during the acute stage, it fails to establish sterility, resulting in parasite persistence and advancement to the chronic stage [155]. The reason is thought to be a variety of immune evasion strategies of *T. cruzi* that have evolved through long coevolution. For instance, the parasites express surface proteins such as calreticulin, which impede the initial binding of the first components of the complement system and thus complement activation [199]. Moreover, they display a multitude of different antigens of highly polymorphic multigenic protein families such as trans-sialidases or mucins, which prohibit the activation of specific B cell clones [200]. In addition, the parasites secrete B cell mitogens which promote polyclonal B cell activation. As

a consequence, unspecific antibodies predominate over the specific ones, resulting in their reduced efficiency [201].

1.3 Aim of the study

During the natural, vector-borne transmission of *T. cruzi*, the skin is the primary site of infection. Accordingly, the early parasite defense in the skin has the potential to influence the further dissemination of the parasites to other tissues and organs. Since *T. cruzi* is an obligatory intracellular parasite, NK cells are presumed to be the main drivers of the innate immune response and to contain the parasite load until the onset of the adaptive immune response.

In this regard, the overall aim of this study was the characterization of the NK cell response against *T. cruzi*-infected dermal fibroblasts as well as its underlying mechanisms. In order to investigate this, the first question to be answered was whether *in vitro* *T. cruzi*-infected primary human dermal fibroblasts directly activate NK cells. A further aim of this study was to determine mechanisms which can promote or limit NK cell activation by *T. cruzi*-infected dermal fibroblasts. Due to the limited cell number of primary fibroblasts, the foreskin fibroblast cell line BJ was examined for its suitability for further analyses using comparative transcriptome analysis. Since it showed very similar changes in response to the infection, the cell line was used for mechanistic analyzes.

Different stimulatory and inhibitory interactions between NK cells and fibroblasts were investigated in three stages. First, the expression of NK cell receptor ligands on the fibroblast surface was determined. Second, the binding of the respective receptor was analyzed. Third, the impact of the respective receptor-ligand-interaction on NK cell effector function was investigated by blocking the respective receptor on the NK cell site or by knocking out the ligand at the target cell site.

In addition to contact-dependent interactions, the role of potential parasite- or fibroblast-derived soluble factors and their influence on the NK cell response was examined. After identifying potential factors, they were neutralized wherever possible to determine their impact on the NK cell response as described above.

2 Materials

2.1 Laboratory equipment

Table 2.1: Laboratory equipment

Name	Company
Agarose gel electrophoresis chamber	BioRAD, Munich, Germany
Analytical scales	Satorius AG, Göttingen, Germany
Autoclave 6464L	Schlumbohm Medizintechnik, Hamburg, Germany
Benchtop centrifuge 5810 R	Eppendorf, Hamburg, Germany
Bioanalyzer System Agilent 2100	Agilent technologies, Santa Clara, USA
Cell separator magnet EasySep™	Stemcell Technologies, Vancouver, Canada
Cell sorter FACSAria™III	Becton Dickinson, Heidelberg, Germany
Centrifuge Heraeus Megafuge X3R	Thermo Fisher Scientific, Walham, USA
ChemiDoc Touch Imaging System	BioRAD, Munich, Germany
CO ₂ incubator Hera Cell 150	Heraeus instruments, Hanau, Germany
Flow cytometer Accuri C6	Becton Dickinson, Heidelberg, Germany
Flow cytometer BD LSRFortessa™	Becton Dickinson, Heidelberg, Germany
Flow cytometer Cytex™ Aurora CS	Cytex Biosciences, Fremont, USA
Fluorescence microscope Axio Imager M.1	Carl Zeiss AG, Oberkochen, Germany
Freezer (-20°C/-70°C)	Liebherr, Biberach, Germany
Fridge (4°C)	Liebherr, Biberach, Germany
Laminar Flow FlowSafe B-(MaxPro) ³ -130	Berner, Elmshorn, Germany
Liquid nitrogen tank	Tec-Lab GmbH, Idstein, Germany
Microscope CKX41SF	Olympus, Hamburg, Germany
Microscope Wilovert	Helmut Hund, Wetzlar, Germany
Microwave	Panasonic, Wiesbaden, Germany
Milli-Q purification system	Merck Millipore, Burlington, USA
Mr. Frosty freezing device	Zefa Laborservice, Harthausen, Germany
Multichannel pipettes	Eppendorf, Hamburg, Germany
nanoACQUITY UPLC system	Waters Corporation, Milford, USA
NanoDrop 2000 microvolume spectrophotometer	Thermo Fisher Scientific, Walham, USA
NextSeq 550 system	Illumina, San Diego USA
Thermocycler (PeqSTAR 96X Universal Gradient)	Peqlab, Erlangen, Germany

pH meter	Hanna Instruments, Kehl am Rhein, Germany
Pipetboy accu-jet® pro	Brand, Wertheim, Germany
Pipettes (10 µl, 20 µl, 100 µl, 200 µl, 1000 µl)	Eppendorf, Hamburg, Germany; Gilson, Middleton, USA
Power supply	BioRAD, Munich, Germany
Q Exactive™ Quadrupole Orbitrap hybrid mass spectrometer	Thermo Fisher Scientific, Walham, USA
Thermomixer 5436	Eppendorf, Hamburg, Germany
Vortex V1 plus	Kisker Biotech GmbH & Co. KG i.G, Steinfurt, Germany
Vortex VF2	IKA-Werke GmbH & Co. KG, Staufen, Germany
Water bath	Lauda Dr. R. Wobser GmbH & Co. KG, Lauda-Königshofen, Germany

2.2 Glass and consumables

Table 2.2: Glass and consumables

Name	Company
Cell culture flasks (T25, T75, T175)	Sarstedt, Nümbrecht, Germany
Cell culture plates (6-well F-bottom, 12-well F-bottom, 24-well F-bottom, 48-well F-bottom, 96-well F-bottom, 96 well U-bottom)	Sarstedt, Nümbrecht, Germany
Cell scaper (16 cm)	Sarstedt, Nümbrecht, Germany
Cell strainer (70 µm, sterile)	Sysmex, Norderstedt, Germany
Chamber slides (16-well)	Nunc, Roskilde, Denmark
Cover slips	Paul Marienfeld GmbH & Co. KG, Lauda-Königshofen, Germany
CryoTube™ vials	Nunc, Roskilde, Denmark
Falcon tubes (15 ml, 50 ml)	Sarstedt, Nümbrecht, Germany
Filter tips (10 µl, 20 µl, 100 µl, 200 µl, 1000 µl)	Sarstedt, Nümbrecht, Germany
Glass bottles	Schott AG; Mainz, Germany
Microplate 96-well polypropylene V-bottom	Greiner Bio-One GmbH, Frickenhausen, Germany
Neubauer chambers (0.1 mm x 0.0025 mm ² , 0.02 mm x 0.0025 mm ²)	Paul Marienfeld GmbH & Co. KG, Lauda-Königshofen, Germany
Nunc™ Lab-Tek™ II Chamber slides (16-well)	Thermo Fisher Scientific, Waltham, USA
Pipette tips (10 µl, 200 µl, 1000 µl)	Sarstedt, Nümbrecht, Germany
Round-bottom flow cytometry tubes (5 ml)	Sarstedt, Nümbrecht, Germany
Round-bottom polystyrene tubes with caps (5 ml)	Stemcell, Vancouver, Canada
Safety-Multifly® needle	Sarstedt, Nümbrecht, Germany

SepMate™ PBMC isolation tubes (50 ml)	Stemcell, Vancouver, Canada
Serological pipettes (5 ml, 10 ml, 25 ml)	Sarstedt, Nümbrecht, Germany
S-Monovette 9 ml K3E EDTA blood collection tubes	Sarstedt, Nümbrecht, Germany
Stericup® quick release vacuum driven filtration system	Merck KGaA, Darmstadt, Germany
Sterile filters 0.2 µm	Sarstedt, Nümbrecht, Germany
Tubes (0.5 ml, 1.5 ml, 2 ml)	Eppendorf, Hamburg, Germany

2.3 Chemicals and reagents

Table 2.3: Chemicals and reagents

Name	Company
Agarose	Biomol, Hamburg, Germany
Ampuwa water	Fresenius, Graz, Austria
BSA (Bovine serum albumin)	SERVA GmbH & Co. KG, Heidelberg, Germany
Descosept	Dr. Schumacher, Malsfeld, Germany
Dulbecco's Modified Eagle's Medium (DMEM)	PAN-Biotech, Aidenbach, Germany
Dimethyl sulfoxide (DMSO)	Sigma-Aldrich, St. Luis, USA
DNA loading buffer (6 x)	Thermo Fisher Scientific, Waltham, USA
Deoxyribonucleic triphosphates (dNTPs)	Thermo Fisher Scientific, Waltham, USA
Dulbecco's Phosphate-Buffered Saline (DPBS)	PAN-Biotech, Aidenbach, Germany
Ethylenediaminetetraacetic acid (EDTA)	Merck Millipore, Burlington, USA
Ethanol	Merck KGaA, Darmstadt, Germany
Ethidium bromide	Sigma-Aldrich, St. Luis, USA
Fetal calf serum (FCS)	Capricorn Scientific GmbH, Ebsdorfergrund, Germany
Ficoll-Paque™ Plus	GE Healthcare, Little Chalfont, England
Foxp3/Transcription Factor Staining Buffer Set	Thermo Fisher Scientific, Waltham, USA
GeneRuler 1 kb DNA ladder	Thermo Fisher Scientific, Waltham, USA
GeneRuler 100 bp DNA ladder	Thermo Fisher Scientific, Waltham, USA
Gentamycin sulfate	Lonza, Basel, Switzerland
4-(2-hydroxyethyl)-1-piperazineethanesulfonic acid (HEPES)	Sigma-Aldrich, St. Luis, USA
Human recombinant IFN-γ (hrIFN-γ)	PeptoTech, Hamburg, Germany
Human recombinant IL-15 (hrIL-15)	PeptoTech, Hamburg, Germany
Human serum, Seraclot, Type AB	PAN-Biotech, Aidenbach, Germany

Incidin liquid	Ecolab, Düsseldorf, Germany
L-glutamine	PAA Laboratories GmbH, Cölbe, Germany
Medium 199	PAN-Biotech, Aidenbach, Germany
Penicillin/streptomycin solution	Capricorn Scientific GmbH, Ebsdorfergrund
Paraformaldehyd (PFA)	Merck KGaA, Darmstadt, Germany
Plasmid transfection medium	Santa Cruz Biotechnology, Dallas, USA
Puromycin	Capricorn Scientific GmbH, Ebsdorfergrund
Roti-Mount FluorCare 4',6-diamidino-2-phenylindole (DAPI) embedding medium	Carl Roth, Karlsruhe, Germany
RPMI-1640 (Roswell Park Memorial Institute Medium 1640)	PAN-Biotech, Aidenbach, Germany
UltraComp eBeads™	Thermo Fisher Scientific, Waltham, USA
Tris-HCl	Promega, Wisconsin, USA
Triton X-100	Sigma-Aldrich, St. Luis, USA
Trypan Blue	Sigma-Aldrich, St. Luis, USA
Trypsin-EDTA (0.05%)	PAA Laboratories GmbH, Cölbe, Germany
TrypsinLE™ Express	Thermo Fisher Scientific, Waltham, USA
UltraCruz® plasmid transfection reagent	Santa Cruz Biotechnology, Dallas, USA
X-VIVO 15™ Serum-free Hematopoietic Cell Medium	Lonza, Basel, Switzerland
Zombie NIR™ fixable viability dye	BioLegend, San Diego, USA

2.4 Buffers and solutions

Table 2.4: Buffers and solutions

Name	Content	Application
FACS buffer	DPBS 2% (v/v) FCS 2 mM EDTA	Flow cytometry
Fix/perm solution	1 part Fixation/Permeabilization concentrate (Foxp3/Transcription Factor Staining Set) 3 parts Fixation/Permeabilization diluent (Foxp3/Transcription Factor Staining Set)	Flow cytometry
Perm/wash buffer	1 part 10 x Permeabilization buffer (Foxp3/Transcription Factor Staining Set) 9 parts ddH ₂ O	Flow cytometry
Sorting buffer	5% (w/v) BSA in DPBS	Cell sorting

Binding assay buffer	5% (v/v) FCS 2 mM EDTA in DPBS	Receptor-Fc/ hrCD160 binding assay
FACS buffer	DPBS 2% (v/v) FCS 2 mM EDTA	Flow cytometry
Fixation solution	4% PFA in DPBS	Immunofluorescence microscopy
Permeabilization buffer	0.1% Triton X-100 in DPBS	Immunofluorescence microscopy
Antibody diluent	1% BSA 0.1% Tween 20 in DPBS	Immunofluorescence microscopy
MojoSort buffer	0.5% BSA 2 mM EDTA in DPBS	NK cell isolation
RLT cell lysis buffer	1% β -mercaptoethanol in RLT cell lysis buffer (RNeasy Mini Kit)	RNA isolation
Tris-HCl	10 mM Tris-HCl pH 8 in H ₂ O (Ampuwa water)	DNA isolation
TAE buffer	40 mM Tris base 45 mM acetic acid 0.5 mM EDTA pH 8 in H ₂ O	Gel electrophoresis
Ethidium bromide solution	10 mg/ml in H ₂ O	Gel electrophoresis

2.5 Cell culture media

Table 2.5: Cell culture media

Name	Application	Content
BJ medium	Cultivation of BJ cells	10% (v/v) FCS 10% Medium 199 2 mM L-glutamine 100 U/mL penicillin 100 U/mL streptomycin in RPMI-1640

HEK293 medium	Cultivation of HEK293 cells	10% (v/v) FCS 2 mM L-glutamine 100 U/mL penicillin 100 U/mL streptomycin 25 mM HEPES in DMEM
86-HG-39 medium	Cultivation of 86-HG-39 cells	10% (v/v) FCS 2 mM L-glutamine 50 µg/mL gentamycin sulfate in RPMI-1640
Jurkat cell medium	Cultivation of β_2m deficient Jurkat cells with and without transfected NKp46 ζ construct	20% (v/v) FCS 2 mM L-glutamine 100 U/mL penicillin 100 U/mL streptomycin in RPMI-1640
NK cell medium	Cultivation of human NK cells	10% human AB serum 2 mM L-glutamine 25 mM HEPES 50 µg/mL gentamycin sulfate in RPMI-1640
Vero81 medium	Cultivation of Vero81 cells	10% (v/v) FCS 2 mM L-glutamine 100 U/mL penicillin 100 U/mL streptomycin in DMEM
Cell freezing medium	Freezing of eukaryotic cells	10% DMSO in FCS
Parasite freezing medium	Freezing of <i>T. cruzi</i> trypomastigotes	25% DMSO 25% FCS in RPMI-1640

2.6 Oligonucleotide primers

All listed oligonucleotide primers were obtained from Eurofins Genomics Germany GmbH, Ebersberg, Germany.

Table 2.6: Oligonucleotide primers

HLA allotype	Direction	Sequence	Amplicon size
HLA-C1/-C2	Forward	5'- CGCCGCGAGTCCGAGAGG - 3'	
HLA-C1	Reverse	5'- GTTGTAGTAGCCGCGCAGG - 3'	139 bp
HLA-C2	Reverse	5'- GTTGTAGTAGCCGCGCAGT - 3'	139 bp

2.7 Plasmids

Table 2.7: Plasmids

Name	Amount per transfection	Company
HLA-C CRISPR/Cas9 KO Plasmid (h)	2 µg	Santa Cruz Biotechnology, Dallas, USA
HLA-C HDR Plasmid (h)	2 µg	Santa Cruz Biotechnology, Dallas, USA

2.8 Antibodies, immune sera and recombinant constructs

Table 2.8: Fluorochrome-labeled antibodies

Epitope	Species	Fluorophore	Clone	Dilution	Application	Company
CD3	Human	BV510	UCHT1	1:200	Flow cytometry	BioLegend, San Diego, USA
CD3	Human	APC/Cy7	HIT3a	1:400	Flow cytometry	BioLegend, San Diego, USA
CD8	Human	AF700	RPA-T8	1:400	Flow cytometry	BioLegend, San Diego, USA
CD16	Human	PE/Dazzle 594	3G8	1:100	Flow cytometry	BioLegend, San Diego, USA
CD56	Human	BUV395	NCAM16.2	1:100	Flow cytometry	BD Biosciences, New Jersey, USA
CD107a	Human	PE/Cy7	H4A3	1:100	Flow cytometry	BioLegend, San Diego, USA
Histidine (His)	-	PE	J095G46	1:50	Recombinant receptor binding assay	BioLegend, San Diego, USA
HLA-A,B,C	Human	Pacific Blue	W6/32	1:200	Flow cytometry	BioLegend, San Diego, USA
HLA-C	Human	APC	DT-9	1:20	Cell sorting	BD Biosciences, New Jersey, USA
HLA-C	Human	BUV395	DT-9	1:20	Flow cytometry	BD Biosciences, New Jersey, USA
HLA-C	Human	PE	DT-9	1:50	Flow cytometry	BD Biosciences, New Jersey, USA
HLA-E	Human	BV421	3D12	1:100	Flow cytometry	BioLegend, San Diego, USA
IgG Fc	Human	PE	-	1:50	Receptor-Fc binding assay	Thermo Fisher Scientific, Waltham, USA
IgG (L+H)	Mouse	FITC	-	1:200	Immunofluorescence microscopy	Jackson Immuno Research, Cambridgeshire, UK
NKp46	Human	AF700	9E2	1:100	Flow cytometry	BioLegend, San Diego, USA

Table 2.9: Blocking/neutralizing antibodies and isotype controls

Epitope	Species	Clone	Final concentration	Company
CD160	Human	BY55	20 µg/ml	BioLegend, San Diego, USA
NKp46	Human	9E2	20 µg/ml	BioLegend, San Diego, USA
IFN-β	Human	IFNb/A1	30 µg/ml	BioLegend, San Diego, USA
IgG1	Mouse	MG1-46	30 µg/ml	BioLegend, San Diego, USA

Table 2.10: Immune sera

Serum	Dilution	Origin
Murine anti- <i>T. cruzi</i> Brazil serum	1:200	Bernhard Nocht Institute for Tropical Medicine (BNITM), Hamburg, Germany

Table 2.11: Recombinant constructs

Construct	Final concentration	Company
Human recombinant NKp46-Fc chimera protein	10 µg/ml	R & D Systems, Minneapolis, USA
Human recombinant KIR2DL1-Fc chimera protein	1.5 µg/ml	R & D Systems, Minneapolis, USA
Human recombinant KIR2DL2-Fc chimera protein	10 µg/ml	R & D Systems, Minneapolis, USA
Human recombinant CD160 (hrCD160) protein with C-terminal 6-His tag	25 µg/ml	R & D Systems, Minneapolis, USA

2.9 Primary cells

Table 2.12: Primary cells

Name	Feature	Description
Peripheral blood mononuclear cells (PBMCs)/NK cells	Suspension cells	Isolated from peripheral whole blood from healthy donors at the BNITM, Hamburg, Germany. <i>Species: Homo sapiens</i> <i>Age at sampling:</i> Adult (24 – 39 years; median: 27 years) <i>Sex:</i> 10 x female; 4 x male
Dermal fibroblasts	Adherent cells	Isolated from skin biopsies from healthy donors at the Elbe Klinikum Buxtehude, Germany. <i>Species: Homo sapiens</i> <i>Age at sampling:</i> Adult (52 – 61 years; median: 55 years) <i>Sex:</i> 3 x female; 3 x male

2.10 Eukaryotic cell lines

Table 2.13: Eukaryotic cell lines

Name	Feature	Description
BJ fibroblasts	Adherent cells	Foreskin fibroblast cell line <u>Species</u> : <i>Homo sapiens</i> <u>Age at sampling</u> : Newborn (<1 year) <u>Sex</u> : Male
HEK293	Adherent cells	Embryonal kidney cell line <u>Species</u> : <i>Homo sapiens</i> <u>Age at sampling</u> : Fetus <u>Sex</u> : Female
86-HG-39	Adherent cells	Glioblastoma cell line <u>Species</u> : <i>Homo sapiens</i> <u>Age at sampling</u> : Adult <u>Sex</u> : Male
Vero 81	Adherent cells	Kidney cell line <u>Species</u> : <i>Cercopithecus aethiops</i> (African green monkey) <u>Age at sampling</u> : Adult <u>Sex</u> : Female
β_2m deficient Jurkat cells	Suspension cells	T lymphocyte cell line – modified for β_2m deficiency via Cas9-mediated deletion [202] <u>Species</u> : <i>Homo sapiens</i> <u>Age at sampling of original cells</u> : Child (14 years) <u>Sex</u> : Male Provided by Prof. Dr. Marcus Altfeld and Dr. Christian Körner, Heinrich Pette Institute, Leibniz Institute for Experimental Virology, Hamburg, Germany.

NKp46ζ Jurkat reporter cells	Suspension cells	<p>T lymphocyte cell line – modified for β_2m deficiency via Cas9-mediated deletion [202] and subsequent lentiviral transfection of a NKp46ζ construct. The NKp46ζ construct consists of the extracellular NKp46 domain, the transmembrane domain of KIR3DL1 and the cytoplasmic domain of the CD3ζ chain [203].</p> <p><u>Species:</u> <i>Homo sapiens</i></p> <p><u>Age at sampling of original cells:</u> Child (14 years)</p> <p><u>Sex:</u> Male</p> <p>Provided by Prof. Dr. Marcus Altfeld and Dr. Christian Körner, Heinrich Pette Institute, Leibniz Institute for Experimental Virology, Hamburg, Germany.</p>
------------------------------	------------------	---

2.11 Parasites

Table 2.14: Parasites

Name	Origin
<i>T. cruzi</i> Brazil strain	Dr. Maria Fatala Chaben, Instituto Nacional de Parasitologia, Buenos Aires, Argentina

2.12 Kits

Table 2.15: Kits

Name	Company
Agilent RNA 6000 Pico Kit	Agilent technologies, Santa Clara, USA
DreamTaq™ Hot Start DNA Polymerase Kit	Thermo Fisher Scientific, Waltham, USA
KIR Typing Kit	Miltenyi Biotec, Bergisch Gladbach, Germany
LEGENDplex™ Human CD8/NK Panel with V-bottom plate (13-plex: IL-2, IL-4, IL-10, IL-6, IL-17A, TNF-α, sFas, sFasL, IFN-γ, granzyme A, granzyme B, perforin, granulysin)	BioLegend, San Diego, USA
LEGENDplex™ Human Type I/II/III Interferon Panel with V-bottom plate (5-plex: IFN-α2, IFN-β, IFN-λ1, IFN-λ2/3, IFN-γ)	BioLegend, San Diego, USA
MojoSort™ Human NK Cell Isolation Kit	BioLegend, San Diego, USA
QIAamp DNA Mini Kit	Qiagen, Hilden, Germany
QIAseq Stranded mRNA Select Kit	Qiagen, Hilden, Germany
RNeasy Mini Kit	Qiagen, Hilden, Germany
Human Vimentin ELISA Kit (Colorimetric)	Abnova, Taipei, Taiwan

2.13 Software and web-based tools

Table 2.16: Software and web-based tools

Name	Purpose	Company/Developers
Agilent 2100 Expert Software	Determination of RNA Integrity Number (RIN)	Agilent technologies, Santa Clara, USA
AxioVision 4.7	Acquisition of fluorescence microscopic images	Carl Zeiss, Oberkochen, Germany
BD FACSDiva™ Software	Acquisition of flow cytometric data at the LSRFortessa™ flow cytometer	BD Biosciences, New Jersey, USA
BD Accuri™ C6 Software	Acquisition of flow cytometric data for LEGENDplex™ analysis at the Accuri C6 flow cytometer	BD Biosciences, New Jersey, USA
BioLegend LEGENplex Software (https://legendplex.qognit.com)	Analysis of LEGENDplex™ data	BioLegend, San Diego, USA
Biorender (https://biorender.com)	Preparation of illustrations	©bioRender, Toronto, Canada
FlowJo 10	Analysis of flow cytometry data	Tree Star, Inc., Ashland, USA
Graphpad Prism 9	Statistical analysis and creation of graphs	GraphPad Software, Inc., La Jolla, USA
ImageJ with Fiji plugin	Composition of fluorescence microscopic images	Wayne Rasband, National Institutes of Health (NIH), Bethesda, USA
Image Lab 5	Analysis of digital image data from electrophoresis gels	Bio-Rad Laboratories, Hercules, USA
Mendeley	Citation of references	Mendeley Ltd., London, UK
Microsoft Office	Preparation of written documents and illustrations	Microsoft Corporation, Washington, USA
Nanodrop 2000 Software	Determination of nucleic acid concentrations and purity	Thermo Fisher Scientific, Waltham, USA
SpectralFlo® Software	Acquisition of flow cytometric data at the Cytex™ Aurora CS spectral flow cytometer	Cytex Biosciences, Fremont, USA
Webgestalt (http://www.webgestalt.org)	WEB -based GENe SeT AnaLysis Toolkit used for pathway analysis of transcriptome and proteome data	Yuxing Liao, Zhiao Shi and Bing Zhang at the Zhang Lab, Oak Ridge, USA

3 Methods

3.1 Cell culture

All cell culture work was performed under sterile conditions using class II laminar airflow cabinets. Cells were cultivated using the medium specified in table 2.5 at 37°C and 5% CO₂ in a Hera Cell 150 incubator.

Suspension cells were directly harvested in Falcon tubes, washed by centrifugation (500 rcf, 5 min, room temperature (RT)) and, after discarding the supernatant, resuspended in fresh culture medium and seeded in a 1:10 – 1:20 dilution.

Adherent cells were harvested by trypsinization. To this end, the culture medium was removed, cells were washed with DPBS and 20 µl Trypsin/EDTA was added per cm². After incubation for 5 min at 37°C, the reaction was stopped with the 10fold volume of the respective culture medium. Cells were harvested, centrifuged as described above, resuspended in culture medium and seeded in a 1:5 – 1:10 dilution.

For long-term storage, cells were harvested, washed and resuspended in ice-cold cell freezing medium at a concentration of 1 – 5 × 10⁶ cells/ml. Then, 1 ml of the obtained cell suspension was transferred into a pre-cooled cryo tube and slowly chilled at -80°C for 24 h using a Mr. Frosty™ freezing container. Finally, the tubes were transferred to liquid nitrogen. To resume the culture, the frozen cell suspension was thawed in a water bath at 37°C, immediately transferred to 10 ml prewarmed medium and mixed gently by inverting. The cells were washed twice (500 rcf, 5 min, RT) and finally seeded in the respective medium.

3.2 Cultivation of *T. cruzi* parasites *in vitro*

Since *T. cruzi* is an obligatory intracellular parasite, host cells are indispensable for the *in vitro* culture. Here, the human glioblastoma cell line 86-HG-39 was chosen, which enables an efficient and secular infection. The 86-HG-39 cells were cultured in T175 flasks until a confluency of 60 – 80% was reached and infected with 5 – 10% of the culture supernatant from the previously *T. cruzi*-infected cell culture flask. The first parasites were released 3 – 4 days post infection and could be used for *in vitro* experiments.

To this end, the supernatant of 1 – 4 T175 flasks was harvested into 50 ml Falcon tubes and centrifuged at 300 rcf for 5 min at RT to remove detached 86-HG-39 host cells. After that, the supernatant was transferred to fresh tubes and centrifuged at 2670 rcf for 15 min at RT to pellet the parasites. After the supernatant was carefully removed by pipetting, the pellet was resuspended in 1 – 10 ml of the respective required culture medium, depending on the cellularity. Parasites were counted as described in section 3.3.

3.3 Cell counting

To assess the number of eukaryotic cells, an aliquot of appropriately diluted cell suspension was mixed 1:2 with Trypan Blue solution. Then, 10 μ l of the suspension were loaded on a Neubauer chamber with a height of 0.1 mm. Unstained, viable cells were counted in 4 big squares and the cell concentration was calculated using the following formula:

$$\text{Cells/ml} = \frac{\text{counted cells}}{4 \text{ big squares}} \times \text{dilution factor} \times 10^4$$

For the determination of the parasite count, 5 μ l of parasite suspension were loaded on a Neubauer chamber with a height of 0.02 mm. Motile trypomastigotes were counted in 4 big squares, whereupon the parasite concentration was calculated via the stated below formula. Due to the reduced chamber height, a chamber factor of 5 had to be considered.

$$\text{Parasites/ml} = \frac{\text{counted cells}}{4 \text{ big squares}} \times \text{dilution factor} \times \text{chamber factor} \times 10^4$$

3.4 *T. cruzi* in vitro infection

Unless otherwise stated, fibroblasts or Vero81 cells were seeded at 4×10^4 cells/cm² in flat-bottom (F-bottom) cell culture plates and cultured for 24 h at 37°C and 5% CO₂. A dedicated well was harvested by trypsinization and cells were counted (section 3.3) to determine the final required *T. cruzi* trypomastigote number per well. Before infection, culture medium was exchanged. After that, *T. cruzi* trypomastigotes were harvested, resuspended in respective culture medium and counted. The required volume of parasite suspension for a multiplicity of infection (MOI) of 3 was added to designated wells. For mock controls, the equivalent volume

of culture medium was added to the dedicated wells. The cells were cultured for 24 h at 37°C and 5% CO₂, before culture medium was exchanged to remove not-infiltrated parasites.

3.5 Immunofluorescence microscopy

Immunofluorescence staining was performed to visualize the intracellular proliferation process of *T. cruzi* in fibroblasts.

Initially, fibroblasts were seeded into a 16-well chamber slide with a density of 1×10^4 cells/well and infected 24 h later with an MOI of 3, as described previously. All the following steps were performed at RT unless otherwise stated. At indicated time points, fibroblasts were washed twice with DPBS, fixed with 4% PFA solution for 15 min and washed twice with DPBS again. Afterwards, fibroblasts were permeabilized with 0.1% Triton X-100 solution for 5 min. For the pathogen detection, fibroblasts were incubated with murine *T. cruzi* Brazil immune serum diluted in antibody diluent for 1.5 h at 37°C and washed three times with DPBS. Subsequently, a FITC-conjugated goat anti-mouse IgG secondary antibody diluted in antibody diluent was added for 45 min. After double washing, the chambers were removed from the microscope slide, which was afterwards coated with Roti®-Mount FluorCare DAPI embedding medium and covered with a cover slip. The embedding medium dried overnight in the dark. Finally, the microscope slides were stored at -4°C for the microscopic analysis via the Axio Imager M.1 fluorescence microscope.

3.6 Flow cytometry

Flow cytometric analysis allows the characterization of single cells based on size (forward scatter, FSC), granularity (sideward scatter, SSC) and fluorescence-labeled cellular structures. Cells of interest were stained in 96-well U-bottom plates. To exclude dead cells, samples were washed with DPBS (500 rcf, 5 min, 4°C), then incubated, if indicated, with Zombie NIR™ fixable viability dye diluted 1:1000 in DPBS for 15 min at 4°C and washed again with DPBS. Afterthat, antibodies against surface molecules diluted in FACS buffer (table 2.8) were added for 30 min at 4°C and removed by washing twice with FACS buffer. The samples were fixed and permeabilized using 150 µl fix/perm solution per well for 45 min in the dark at RT and washed twice with perm/wash buffer. The samples were resuspended in 120 µl perm/wash buffer, respectively.

Apart from HLA-C knockout (KO) fibroblasts (section 3.14.2), all cells were measured at the LSRFortessa™ flow cytometer using the FACSDiva software. Due to the expression of red fluorescent protein (RFP) in HLA-C KO fibroblasts, these cells were measured using the Cytek™ Aurora CS spectral flow cytometer. On account using the full spectrum instead of particular wavelengths, this flow cytometer allows more precise discrimination between the expressed RFP and the fluorochrome PE used for binding assays (section 3.10).

3.7 Flow cytometric bead-based immunoassay - LEGENDplex™

BioLegend's LEGENDplex™ bead-based immunoassays were used to analyze soluble factors released by fibroblasts in reaction to infection (Human Type I/II/III Interferon Panel, 5-plex) and NK cells in response to infected fibroblasts (Human CD8/NK Panel, 13-plex).

Respectively indicated culture supernatants were processed according to the manufacturer's instructions without prior pre-dilution. This method uses the same principle as a sandwich immunoassay. They contain beads, which can be distinguished by size and internal fluorescence intensity in the APC channel, resulting in a distinct bead population for each analyte. The different bead populations are coupled to analyte-specific antibodies, which bind the analytes in the investigated culture supernatant. In the next step, the analytes are bound by biotinylated secondary antibodies, which are finally detected by Streptavidin PE. The fluorescence intensity in the PE channel provides information on the amount of the considered analyte. All samples were measured using the Accuri C6 flow cytometer. Finally, the concentration of the respective analytes was calculated on the basis of a standard series using the web-based LEGENDplex software.

3.8 ELISA (enzyme-linked immuno-sorbent assay)

Abnova's Human Vimentin ELISA Kit is based on the principle of a sandwich ELISA and was used to determine the concentration of soluble vimentin released by mock and *T. cruzi*-infected fibroblasts. Culture supernatants were analyzed without prior pre-dilution according to manufacturer's instructions (version 24). Briefly, test samples and serially diluted standard solution were added to a provided 96-well plate that had been pre-coated with a purified anti-vimentin antibody. Then, a horse radish peroxidase (HRP)-conjugated anti-vimentin antibody was used for detection. After removing unbound conjugates,

3,3',5,5'-Tetramethylbenzidine (TMB) substrate was added to enable the enzymatic reaction catalyzed by HRP, resulting in a blue color product that turns yellow after addition of acidic stop solution. The color intensity is proportional to the amount of vimentin and was measured via the optical density (OD) absorbance at 450 nm in a microplate reader. The vimentin concentrations in the tested samples were calculated based on the standard series.

3.9 Expression analysis of NK cell receptor ligands on fibroblasts

In order to analyze the expression of NK cell receptor ligands on *T. cruzi*-infected fibroblasts, the cells were seeded in 12-well F-bottom cell culture plates and infected with *T. cruzi* trypomastigotes with an MOI of 3, as described in section 3.4. At the indicated time points, the fibroblasts were washed with DPBS and harvested treating the cells with 200 μ l TrypsinLE™ solution per well at 37°C and 5% CO₂ for 3 min. Subsequently, the digestion was stopped by adding 800 μ l complete medium per well. After cell counting (section 3.3), 1.5×10^5 fibroblasts per condition were transferred to a 96-well U-bottom plate, centrifuged at 500 rcf for 5 min at 4°C and used for flow cytometric staining (section 3.6) of HLA-A,B,C as well as HLA-C, HLA-E, HVEM, nectin-2 and vimentin. In the case of vimentin expression analysis, permeabilized cells were also stained using the Zombie NIR™ viability dye beforehand to avoid false positive signals from intracellularly stained vimentin.

In addition, whether altered ligand expression was due to direct *T. cruzi* infection or to soluble factors released by infected fibroblasts was investigated. To this end, pre-seeded fibroblasts were treated for 24 h with sterile-filtered supernatants of mock and *T. cruzi*-infected fibroblasts from the indicated time points. Afterwards, supernatant-treated fibroblasts were harvested and stained as described above.

3.9.1 Neutralization of IFN- β in fibroblasts supernatants

IFN- β neutralization of supernatants from mock and *T. cruzi*-infected fibroblasts was performed to determine the influence of fibroblast-derived IFN- β on the expression of MHC-I ligands on the fibroblast surface.

To this end, fibroblasts were seeded and infected with *T. cruzi* as previously described (section 3.4). After 24 h, medium was exchanged and fibroblasts were cultured until 48 hpi,

whereupon supernatants from infected fibroblasts and mock controls were harvested and sterile filtered. In order to neutralize secreted IFN- β , the supernatants were pre-treated with 30 $\mu\text{g}/\text{ml}$ of the anti-IFN- β antibody clone IFNb/A1 or an IgG1 isotype control for 1 h at 4°C. Afterwards, pre-seeded fibroblasts were treated with the described supernatants for 24 h. Finally, the cells were harvested and stained for flow cytometric analysis (section 3.6) of HLA-A,B,C and HLA-C expression.

3.10 Receptor-Fc/recombinant receptor binding assay

To investigate the binding of the NK cell receptors NKp46, KIR2DL1, KIR2DL2 and CD160, fibroblasts were seeded and infected with *T. cruzi* trypomastigotes with an MOI of 3 (section 3.4). Fibroblasts were harvested 48 hpi by TrypsinLE™ treatment as described in section 3.9. 1.5×10^5 fibroblasts per condition were transferred to a 96-well U-bottom plate and incubated with NKp46-Fc, KIR2DL1-Fc or KIR2DL2-Fc chimera constructs for 1 h on ice or with recombinant CD160 protein diluted in binding assay buffer for 1 h at 37°C. The concentrations used are listed in table 2.11. Afterwards, the cells were washed three times with binding assay buffer and treated with the respective secondary antibody diluted in binding assay buffer (table 2.8) for 20 min at 4°C in the dark. Fc-chimera molecule-treated fibroblasts were incubated with a PE-conjugated goat anti-human IgG secondary antibody, whereas recombinant CD160 protein-bound fibroblasts were detected using a PE-conjugated anti-His secondary antibody, targeting the His-tag of the recombinant CD160 protein. After two washing steps with DPBS, fibroblasts were fixed with 150 μl fix/perm solution per well for 45 min at RT in the dark, washed twice with perm/wash buffer and finally resuspended in 120 μl perm/wash buffer for flow cytometric analysis.

3.11 Reporter cell assay

A reporter cell assay was applied to prove the functional binding of NKp46 to fibroblasts. Jurkat cells modified for β_2 -microglobulin ($\beta_2\text{m}$) deficiency via Cas9-mediated deletion [202] and subsequent lentiviral transfection of an NKp46 ζ construct were used. The NKp46 ζ construct consists of the extracellular NKp46 domain, the transmembrane domain of KIR3DL1 and the cytoplasmatic domain of the CD3 ζ chain [203]. The CD3 ζ chain mediates the signal transduction after ligand binding and thus the subsequent expression of the activation marker

CD69 on the Jurkat cell surface. β_2m -deficient Jurkat cells without transfected NKp46 ζ construct were used as a background control. To avoid background signals due to nutrient deficiency, Jurkat cells were seeded 24 h before stimulation with a density of 2.5×10^5 cells/ml.

3.11.1 Stimulation by coculture with fibroblasts

Fibroblasts were seeded in 48-well F-bottom cell culture plates and infected with *T. cruzi* trypomastigotes with an MOI of 3 as previously described (section 3.4). To determine the required number of Jurkat cells for subsequent coculture with an effector to target (E:T) ratio of 10:1, a dedicated well was trypsinized 30 hpi and fibroblasts were counted (section 3.3). Jurkat cells were harvested, counted, spun down (500 rcf, 5 min, RT) and resuspended in the appropriate volume of Jurkat cell medium. After removing medium from fibroblasts and washing the wells with Jurkat cell medium, 200 μ l/well Jurkat suspension was added. To ensure optimal cell-cell contact, plates were centrifuged at 100 rcf for 30 sec at RT. Afterwards, the cells were cocultured for 18 h at 37°C with 5% CO₂. Jurkat cells were harvested by pipetting up and down and transferred to a 96-well U-bottom plate for subsequent flow cytometric staining (section 3.6) of CD3, NKp46 and CD69 following a live/dead staining using the Zombie NIR™ viability dye.

3.11.2 Stimulation by supernatant from fibroblasts

In order to stimulate NKp46 ζ reporter Jurkat cells and β_2m -deficient controls with supernatant from mock or *T. cruzi*-infected fibroblasts, fibroblasts were infected as previously described (section 3.4). Supernatants were harvested 48 hpi and sterile filtered. Jurkat cells were harvested, counted (section 3.3), spun down (500 rcf, 5 min, RT) and resuspended in Jurkat cell medium at a concentration of 1.25×10^6 cells/ml. 20 μ l (2.5×10^4 cells) of the respective Jurkat cell suspension were mixed with 180 μ l fibroblast supernatant in a 48-well F-bottom cell culture plate and cultured for 18 h at 37°C with 5% CO₂. Afterwards, the cells were transferred to a 96-well U-bottom plate and stained for flow cytometric analysis as described in section 3.11.1.

3.12 Isolation of NK cells from whole blood

In the first step, PBMCs were isolated from fresh human blood drawn in EDTA collection tubes. The blood was transferred to 50 ml Falcon tubes and diluted 1:1 with DPBS. SepMate™ tubes were prepared by pipetting 15 ml Ficoll-Paque™ Plus through the intended hole. Subsequently, the diluted blood was carefully layered on top, followed by centrifugation at 1200 rcf for 15 min at RT to separate erythrocytes and granulocytes below the membrane and PBMCs and plasma above. The PBMC/plasma mixture was transferred to a 50 ml Falcon tube each and filled up to 50 ml with X-VIVO 15™ medium. The Falcon tubes were centrifuged at 550 rcf for 15 min at RT to pellet the PBMCs. The cells were washed a second time with X-VIVO 15™ medium, resuspended in 10 – 40 ml, depending on the cellularity, and counted (section 3.3).

Afterwards, NK cells were isolated from purified PBMCs using BioLegend's MojoSort™ Human NK Cell Isolation Kit according to the suppliers' protocol. The method is based on negative selection of NK cells using a biotin antibody cocktail against surface antigens expressed on other immune cells and erythrocytes. The following treatment with magnetic streptavidin nanobeads and a magnetic separator allows the retainment of the labeled fraction and the collection of untouched NK cells in the decanted liquid. The purity of the obtained NK cells was determined by flow cytometric analysis (section 3.6) of CD3, CD14, CD19 and CD56. NK cells were rested overnight in NK cell medium with 5 ng/ml hrIL-15 for regeneration after the isolation process.

3.13 NK cell stimulation by *T. cruzi*-infected fibroblasts

Different approaches were used to investigate the effect of *T. cruzi*-infected fibroblasts and their secreted soluble factors on the activity of NK cells.

3.13.1 Degranulation assay after coculture

The activation status of NK cells can be measured by their release of cytotoxic granules. The granule lipid bilayer contains lysosomal-associated membrane glycoproteins (LAMPs), including CD107a (LAMP-1), which can be detected on the NK cell surface after degranulation [204].

To analyze NK cell degranulation in response to mock and *T. cruzi*-infected fibroblasts, fibroblasts were seeded in fibroblast medium in a 24-well F-bottom cell culture plate and infected 24 h later with an MOI of 3 (section 3.4). In parallel, human NK cells were isolated from purified PBMCs from fresh blood of healthy donors and rested overnight (section 3.12). Not-infiltrated trypomastigotes were removed from fibroblasts 24 hpi by washing three times with DPBS. A dedicated well was trypsinized and the fibroblast number/well was determined by counting (section 3.3). NK cells were harvested, washed (500 rcf, 5 min, RT), counted and adjusted to the required cell concentration. Coculture with mock and *T. cruzi*-infected fibroblasts was prepared with an E:T ratio of 1:10 in a total volume of 200 µl NK cell medium per well. To ensure direct cell-cell contact, plates were centrifuged at 100 rcf for 30 sec at RT. After that, fibroblasts and NK cells were cocultured for 24 h at 37°C and 5% CO₂.

To prove the general responsiveness of used NK cells, an additional coculture with HEK293 cells, which are described to highly express ligands for the NK cell-activating receptor NKG2D [205], was performed as positive control. Here, coculture was performed for 5 h instead of 24 h to prevent NK cell overactivation and cell death.

To optimally display NK cell degranulation, the internalization of CD107a was impeded by adding 1.5 µl PE/Cy7-labelled anti-CD107a antibody per well for the last 5 h of coculture. Finally, NK cells were harvested and transferred to a 96-well U-bottom plate for flow cytometry staining (section 3.6) of CD3, CD14, CD19 and CD56.

3.13.2 Degranulation assay after stimulation by supernatants

NK cells were stimulated with supernatants from mock and *T. cruzi*-infected human fibroblasts and Vero81 cells from the African green monkey to evaluate whether cellular or parasitic soluble factors induce NK cell activation.

Fibroblasts and Vero81 cells were seeded in the respective culture medium in 24-well F-bottom cell culture plates and infected 24 h later with an MOI of 3 (section 3.4). After 24 h, the medium was exchanged to 200 µl/well NK cell medium after one washing step. Fibroblasts and Vero81 cells were incubated for a further 24 h at 37°C with 5% CO₂. In parallel, NK cells were purified and rested overnight as described previously (section 3.12). BJ fibroblast and Vero81 culture supernatants were harvested 48 hpi and centrifuged at 500 rcf for 5 min at 4°C to remove cell debris. This was followed by two centrifugation steps with 2670 rcf for 15 min at 4°C to remove remaining parasites. NK cells were harvested, washed and adjusted to

2.25×10^6 cells/ml in NK cell medium. Afterwards, 20 μ l NK cell suspension (4.5×10^5 cells) were mixed with 180 μ l BJ fibroblast or Vero81 culture supernatant in a 24-well F-bottom cell culture plate and incubated for 24 h at 37°C with 5% CO₂. As described above, PE/Cy7-labelled anti-CD107a antibody was added for the last 5 h of stimulation before further flow cytometric staining (section 3.6) of CD3, CD14, CD19 and CD56 was performed in a 96-well U-bottom plate.

3.13.3 Analysis of secreted NK cell effector molecules during coculture

Besides illustrating the release of cytotoxic granules via flow cytometric analysis of CD107a, different secreted NK cell effector molecules were also analyzed in the coculture supernatants.

Fibroblasts were seeded in a 48-well F-bottom cell culture plate and infected 24 h later with *T. cruzi* trypomastigotes an MOI of 3 (section 3.4). As described in section 3.12, NK cells were isolated and rested overnight. 24 hpi, fibroblasts were washed three times with DPBS to remove not-infiltrated trypomastigotes. A dedicated well was utilized to determine fibroblast number per well (section 3.3). NK cells were harvested, washed (500 rcf, 5 min, RT), counted and adjusted to the required cell concentration. The coculture with mock and *T. cruzi*-infected fibroblasts was prepared with an E:T ratio of 1:2.5 in a total volume of 100 μ l NK cell medium per well. The higher E:T ratio compared to the degranulation assay enabled higher concentrations of the subsequently analyzed effector molecules. After centrifugation at 100 rcf for 30 at RT, fibroblasts and NK cells were cocultured for 24 h at 37°C and 5% CO₂. Then, supernatants were harvested in a 96-well U-bottom plate and centrifuged at 500 rcf for 5 min at 4°C to remove cell debris. Subsequently, supernatants were transferred to a new plate and centrifuged at 2670 rcf for 15 min at 4°C to eliminate remaining *T. cruzi* parasites. The process was repeated once. After transfer to a fresh 96-well U-bottom plate, supernatants were stored at -20°C until LEGENDplex™ analysis using the Human CD8/NK Panel (section 3.7).

3.14 Interruption of regulatory interactions

Different interactions between NK cells and *T. cruzi*-infected fibroblasts were examined for their physiological impact on the NK cell response. Accordingly, different approaches were used depending on the interaction to be analyzed.

3.14.1 Blockade of NKp46 and CD160 on NK cells

To investigate the impact of the engagement of the NK cell receptors NKp46 and CD160 on the NK cell activation by *T. cruzi*-infected fibroblasts, the receptors were blocked before NK cell fibroblast coculture was started.

Specifically, PBMCs and NK cells were isolated as described in section 3.12. During the overnight resting step, NK cells were treated with 20 µg/ml anti-NKp46 antibody (clone 9E2) or anti-CD160 antibody (clone BY55), respectively. Afterwards, an aliquot of 5×10^4 NK cells was used to verify the success of the blockade by flow cytometric staining (section 3.6) of the respective receptor. Blocking antibodies were removed by washing NK cells with NK cell medium and coculture with mock and *T. cruzi*-infected fibroblasts was prepared as described above, either for analysis of degranulation (section 3.13.1) or of secreted NK cell effector molecules (section 3.13.3).

3.14.2 HLA-C KO in fibroblasts

To investigate the impact of altered fibroblast HLA-C expression on the NK cell response, HLA-C KO of BJ fibroblasts was performed using clustered regulatory interspaced short palindromic repeats (CRISPR)/Cas9 technology.

3.14.2.1 Generation of HLA-C KO fibroblasts via CRISPR/Cas9 technology

Pre-designed KO and homology directed repair (HDR) plasmids, transfection reagent and transfection medium from Santa Cruz Biotechnology were used. Initially, fibroblasts were seeded in 6-well cell culture plates in antibiotic-free fibroblast culture medium and cultivated until a confluency of 70 – 80% was reached. Before transfection, medium was exchanged for 3 ml of fresh antibiotic-free fibroblast culture medium. Subsequently, a cotransfection of pre-designed HLA-C KO and HDR plasmids was performed according to the manufacturer's

instructions. Briefly, 10 μ l of UltraCruz[®] transfection reagent, 2 μ g of HLA-C KO and HDR plasmids each were prepared per well in transfection medium in a complete volume of 300 μ l. The mixture was added to the fibroblasts dropwise and distributed by gently swirling the culture plate.

The plasmids transfected in this way should subsequently mediate the HLA-C KO using CRISPR/Cas9 technology with subsequent HDR. To be precise, the provided HLA-C KO plasmids encode the two major components of the CRISPR/Cas9 system: the unspecific endonuclease Cas9 and one each of three different pre-designed single guide RNAs (sgRNAs) that contain a target-specific sequence. Usage of multiple sgRNAs is necessary to increase efficiency, since their specificity and activity can vary. Together, the endonuclease Cas9 and one sgRNA form a ribonucleoprotein (RNP) complex. The target-specific sequence of the sgRNA binds to the complementary sequence of the gene of interest, which is immediately upstream of a protospacer adherent motif (PAM), thus directing Cas9 to the target DNA. Cas9 binds to the target DNA at the PAM and mediates a double-strand break 3 – 4 nucleotides upstream of the motif [206]. In the absence of template DNA, repair proceeds via non-homologous end joining (NHEJ). This is often accompanied by insertions or deletions, resulting in a frameshift mutation of the target gene. However, higher efficiency can be achieved by HDR using a template sequence [207], as performed in this study. The HDR plasmid contains homologous regions to the cleavage site, which allows the incorporation of the HDR plasmid-encoded puromycin resistance gene and RFP gene by homologous recombination. Thus, the HLA-C gene should be replaced by the named genes, which facilitate the subsequent selection of successful HLA-C KO clones.

3.14.2.2 Selection of an HLA-C KO single-cell clone

After incubation for 48 h, the medium was exchanged for antibiotic-free culture medium. The fibroblasts were grown to a confluence of 70 – 80% before the selection of HLA-C KO single-cell clones was started. The selection was done in three main steps with increasing specificity.

First, cells that do not express the puromycin resistance gene, meaning that no homologous recombination has occurred, were mortified by treatment with 2.5 μ g/ml puromycin for 96 h. The remaining fibroblasts were cultured in antibiotic-free culture medium until a confluency of 70 – 80% was reached.

In the second step, the fibroblasts were sorted for the presence of RFP expression, the gene for which was also inserted by homologous recombination, and the absence of HLA-C expression. Since HLA-C expression of BJ fibroblasts was observed to be weak in steady state, it was enhanced by treatment with 1000 U/mL of human recombinant IFN- γ (hrIFN- γ) for 24 h before sorting. IFN- γ has been shown to upregulate antigen presentation by MHC-I molecules and thus the presence of MHC-I molecules on the cell surface [208]–[210]. Following IFN- γ stimulation, fibroblasts were harvested using TrypsinLE™, as described in section 3.9, washed with sorting buffer and stained with an APC-labeled anti-HLA-C antibody diluted 1:20 in a total volume of 300 μ l sorting buffer for 30 min at RT. After washing twice, the fibroblasts were resuspended in 500 μ l sorting buffer and sorted into antibiotic-free culture medium with 20% FCS at RT using a 70 mm nozzle. After collecting approximately 6×10^3 RFP⁺ HLA-C⁻ fibroblasts, the cells were pelleted at 300 rcf for 5 min at RT, resuspended in 500 μ l antibiotic-free culture medium with 20% FCS and seeded in one well of a 48-well F-bottom cell culture plate. The sorted fibroblasts were cultured until a confluency of 70 – 80% was reached, enabling the fibroblasts to recover from the sorting procedure.

Finally, single-cell clones were selected based on HLA-C expression in response to *T. cruzi* infection. For this purpose, the serial dilution method was applied. The sorted fibroblasts were seeded in 96-well F-bottom cell culture plates at a theoretical density of 0.3 cells/well, 1 cell/well, or 3 cells/well. The cells were seeded in 5 plates per condition to obtain a sufficient number of single-cell clones. Feeder cells were not required here. The fibroblasts were cultured until the first 24 wells showed a confluent cell layer. These 24 clones were subsequently divided into 2 wells each in 24-well F-bottom cell culture plates. While the first plate was used for expansion, the second plate was utilized for stimulation by *T. cruzi* infection for further screening. Wildtype (WT) BJ fibroblasts were used as a control. Single-cell HLA-C KO and WT fibroblasts were infected with an MOI of 3 (section 3.4) and analyzed 48 hpi for their HLA-A,B,C and HLA-C expression by flow cytometric analysis (section 3.6). Analysis of general expression of MHC-I molecules, including HLA-A, -B and -C, was performed to identify possible off-target effects during the CRISPR/Cas9-mediated KO, resulting in the impairment of MHC-I molecules apart from HLA-C. A single-cell clone was selected that lacked HLA-C expression while having the least impaired HLA-A,B,C expression. To verify, that the HLA-C KO of the selected clone was functional, the binding of corresponding KIRs KIR2DL2 and KIR2DL1 to HLA-C1 and HLA-C2 was investigated using receptor-Fc binding assays (section 3.10).

3.14.2.3 Use in coculture experiments

Following the expansion of this HLA-C KO fibroblast single-cell clone, the cells were used for coculture experiments with NK cells. These were performed as previously described in sections 3.12.1 and 3.12.3, comparing NK cell degranulation and secretion of effector molecules in response to mock and *T. cruzi*-infected WT and HLA-C KO BJ fibroblasts.

3.14.3 Neutralization of IFN- β in the supernatant

Furthermore, the impact of IFN- β secreted by *T. cruzi*-infected fibroblasts on NK cell activity was investigated. To this end, two possible modes of action were analyzed. Firstly, the direct effect of IFN- β on NK cells and secondly, the indirect effect on NK cell activation via the modulation of ligand expression on fibroblasts.

The direct effect of IFN- β secreted by *T. cruzi*-infected fibroblasts on NK cell activity was determined by neutralization of IFN- β in fibroblast supernatant that was later used for NK cell stimulation. Specifically, supernatants from mock and *T. cruzi*-infected fibroblasts were generated as described in section 3.13.2. Harvested supernatants were pre-treated with 30 $\mu\text{g}/\text{ml}$ of the anti-IFN- β antibody clone IFNb/A1 or an IgG1 isotype control for 1 h at 4°C. Isolated and rested NK cells (section 3.12) were harvested, washed and adjusted to a concentration of 2.25×10^6 cells/ml in NK cell medium. Subsequently, 20 μl NK cell suspension (4.5×10^5 cells) were mixed in a 24-well F-bottom plate with 180 μl of one of the pre-treated fibroblast supernatants and incubated for 24 h at 37°C with 5% CO₂. The NK cell response was measured by their degranulating activity. To this end, PE/Cy7-labelled anti-CD107a antibody was added for the last 5 h of stimulation, before further flow cytometric staining (section 3.6) of CD3, CD14, CD19 and CD56 was performed in a 96-well U-bottom plate.

The indirect effect of IFN- β on NK cell activity by modulating the ligand expression on fibroblasts was determined by IFN- β neutralization during NK cell coculture with mock and *T. cruzi*-infected fibroblasts. First, cocultures were prepared for analysis of NK cell degranulation and secretion of effector molecules as described in section 3.13.1 and section 3.13.3. Before starting the 24 h incubation at 37°C and 5% CO₂, 30 $\mu\text{g}/\text{ml}$ of the anti-IFN- β antibody clone IFNb/A1 or an IgG1 isotype control were added to the coculture medium. This

approach was intended to directly neutralize newly secreted IFN- β during coculture. NK cell degranulation and secretion of effector molecules was determined as indicated in section 3.13.1 and section 3.13.3.

3.15 HLA-C and KIR genotyping

Since different inhibitory and activating KIRs have been shown to interact with distinct HLA-C allotypes [62], BJ fibroblasts were genotyped for allotypes of the HLA-C1 and C2 group to examine whether all interactions of interest can be investigated properly using the BJ fibroblast model.

Moreover, the composition of KIR genes of all NK cell donors was determined to analyze the impact of individual HLA-C corresponding KIRs on NK cell activation by *T. cruzi*-infected BJ fibroblasts.

3.15.1 DNA Isolation

DNA was isolated from 2×10^6 BJ fibroblasts or 5×10^6 PBMCs via Qiagen's QIAamp DNA Mini Kit using silica membrane spin columns according to the manufacturer's instructions. The fibroblast DNA for HLA-C genotyping was eluted in 200 μ l supplied buffer AE. PBMC DNA was eluted in 100 μ l Tris-HCl solution as indicated in the manufacturer's instructions for the following KIR genotyping (section 3.15.3). Subsequently, the DNA concentration was determined using a NanoDrop 2000 microvolume spectrophotometer and the NanoDrop 2000 Software.

3.15.2 HLA-C typing by polymerase chain reaction (PCR)

The PCR method is utilized to amplify a defined nucleic acid sequence *in vitro*. In this case, PCR was performed using primer sequences and a PCR program published by Gamliel *et al.*, 2016 [211] to determine whether BJ fibroblasts are homozygous for HLA-C1, homozygous for HLA-C2 or heterozygous. While the forward primer binds the same sequence for both HLA-C1 and -C2 within the HLA-C gene, the different reverse primers distinguish encoded asparagine (HLA-C1) or lysine (HLA-C2) at position 80 of the encoded protein.

Reaction mixtures were prepared from 2 ng template DNA, 0.2 mM dNTPs, 0.5 μ M forward and reverse primer, 2 μ l 10 x DreamTaq buffer, and 1 U DreamTaq polymerases. A total volume of 20 μ l was reached by adding Ampuwa water. Additionally, a negative control without template DNA was prepared to exclude false positive signals through DNA contamination.

The following PCR program was performed using the thermocycler PeqSTAR 96X:

Initial melting	95°C	180 sec	
Denaturation	95°C	10 sec	} 10 x
Primer annealing	65°C	30 sec	
Elongation	72°C	45 sec	
Denaturation	95°C	10 sec	} 22 x
Primer annealing	58°C	30 sec	
Elongation	72°C	45 sec	
Final elongation	72°C	600 sec	
Storage	4°C	∞	

The amplification success of the respective sequences was verified by agarose gel electrophoresis (section 3.15.4).

3.15.3 KIR genotyping PCR

Since not all of the 15 KIR genes are present in every individual, the KIR genotype of every NK cell donor was determined by PCR using the KIR Typing Kit from Miltenyi Biotec according to the manufacturer's instructions. The kit contains PCR plates with lyophilized enzyme mixes and KIR-specific primers, enabling the detection of all known human KIR genes and two pseudogenes. In addition, a second primer pair detecting β -actin was added to each PCR reaction. This served as an internal control to verify the success of the amplification. Besides the KIR typing PCR mixes, the kit contains a positive control for the PCR reaction with only β -actin-specific primers and a negative control, to which no template DNA is added.

After the addition of purified template DNA diluted in the provided resuspension buffer to the lyophilized mixes, the following PCR program was performed utilizing the thermocycler PeqSTAR 96X:

Initial melting	95°C	60 sec	
Denaturation	94°C	20 sec	} 28 x
Primer annealing	63°C	20 sec	
Elongation	72°C	90 sec	
Storage	4°C	∞	

Agarose gel electrophoresis was used to monitor the presence of amplicons for the respective KIR genes and controls (section 3.15.4).

3.15.4 Agarose gel electrophoresis

Agarose gel electrophoresis was used to evaluate HLA-C and KIR genotyping. In this process, PCR products, in this case, are separated according to their size by an electric field, which allows the identification of the different amplicons.

Agarose gels for the evaluation of the HLA-C genotype were prepared with 1.5% (w/v) agarose in TAE buffer, or with 2% (w/v) agarose for the evaluation of the KIR genotype. After boiling the agarose/TAE buffer mixture to melt the agarose, the DNA-intercalating dye ethidium bromide was added. It allows the detection of DNA bands under UV light following electrophoresis. The gel was poured into a gel chamber to cool down, allowing the polymerization of the agarose. In the case of HLA-C genotyping, 10 µl PCR product were mixed with 2 µl 6 x loading buffer. This step was not necessary for PCR products for KIR genotyping, since the provided enzyme mixes already contained the buffer. The glycerol contained in the loading buffer ensures that the DNA in the sample forms a layer on the bottom of the well. Furthermore, two included dyes allow the visualization of the DNA during electrophoresis. The fragment sizes were determined by the GeneRuler 100 bp DNA ladder in the case of HLA-C typing and a combination of the GeneRuler 100 bp and 1 kb DNA ladder in the case of KIR genotyping. The electrophoresis was carried out at 80 V for 1 h. Subsequently, the gels were

exposed to UV light in the ChemiDoc Touch Imaging System and images were captured using the associated software.

3.16 Transcriptomic analysis

Transcriptome analysis, also referred as RNA sequencing, of mock and *T. cruzi*-infected primary dermal fibroblasts and the fibroblast cell line BJ was performed to evaluate the suitability of BJ fibroblasts for an *in vitro* model of a dermal *T. cruzi* infection. In addition, the induced gene signatures after *T. cruzi* infection should provide information on possible mechanisms for the modulation of NK cell activity.

The required RNA samples were prepared as follows. Depending on the available number of cells, 2 – 3 x 10⁵ fibroblasts per condition were seeded in 6-well F-bottom cell culture plates and infected with *T. cruzi* trypomastigotes with an MOI of 3 (section 3.4). Due to the limited cell number of primary fibroblasts, replicates could not be generated here. In the case of BJ fibroblasts, biological replicates were generated though two independent infections. 48 hpi, the medium was removed, fibroblasts were washed once with DPBS and harvested by scraping in DPBS. After transfer into a 1.5 ml tube, the fibroblasts were pelleted at 500 rcf for 5 min at 4°C and resuspended in 350 µl RLT cell lysis buffer provided in Qiagen's RNeasy Mini Kit with 1% β-mercaptoethanol.

3.16.1 Total RNA isolation

Total RNA was isolated using Qiagen's RNeasy Mini Kit according to the manufacturer's instructions using silica membrane spin columns. In the final step, RNA was eluted with 30 µl of RNase-free water provided in the kit. The procedure was repeated once with the first eluate to obtain a higher yield. Subsequently, the RNA concentration was determined using the NanoDrop 2000 microvolume spectrophotometer and the associated. The RNA was aliquoted and stored at -80°C until further procedure.

3.16.2 Determination of RNA Integrity Number (RIN)

To exclude a possible degradation of the isolated RNA, for example due to unavoidable freezing and thawing, the RIN was determined using the Bioanalyzer System Agilent 2100. To

this end, RNA samples were prepared using the Agilent RNA 6000 Pico Kit according to the manufacturer's instructions. Here, the RNA was treated with an interacting fluorescent dye, loaded onto the provided RNA Pico Chip and separated by fragment size using electrophoresis. The Agilent 2100 Expert Software evaluates the data and calculates the RIN with values between 1 and 10 using a specially developed algorithm. The level of the value correlates with the integrity of the RNA, with a RIN > 8 needed to ensure sufficient RNA quality for subsequent sequencing.

3.16.3 RNA sequencing library preparation and next-generation sequencing (NGS)

The following steps were performed by the NGS core facility of the BNITM by Dr. Dániel Cadar and Heike Baum. In brief, using Qiagen's QIAseq Stranded mRNA Select Kit, mRNA was enriched from the previously purified RNA based on its polyadenylation. Moreover, the kit was used to prepare the RNAseq library for NGS. Subsequently, the sequencing was performed using Illumina's NextSeq 500/550 Mid Output Kit and Illumina's NextSeq 550 system. The first bioinformatic evaluation was performed by Dr. Dániel Cadar, providing the Reads per kilobase of transcript per Million mapped reads (RPKM) values that were used for further analysis.

3.16.4 Transcriptome data analysis

RPKM values of biological replicates were used as mean values for further analysis. The fold change was calculated by the ratio of RPKM values of *T. cruzi*-infected fibroblasts and the corresponding mock controls. Subsequently, the values were \log_2 -transformed to model proportional changes. Statistical significance was evaluated using the GraphPad Prism 9 software using multiple paired t-tests. Changes with a p-value ≤ 0.05 were considered statistically significant.

Unless otherwise stated, the following analyses were performed using the GraphPad Prism 9 software to compare changes in gene expression after *T. cruzi* infection of primary fibroblasts and the fibroblast cell line BJ. To this end, \log_2 -transformed RPKM values of significantly differentially expressed genes (DEGs) were used to perform principal component analysis. Here, all variables were combined into two principal components, enabling the depiction of

the degree of similarity between individual samples. For further visualization, a heat map was created to show the relative expression of significant DEGs using \log_2 -transformed RPKM values in relation to the mean RPKM value of all genes considered.

For a more detailed evaluation of potentially biologically relevant genes, a volcano plot was created. This representation of the RNA sequencing data enables the identification of individual genes with a high fold change and statistical significance.

In addition, pathway analysis of significantly upregulated genes was conducted. To this end, an over-representation analysis was performed using the web-based tool webgestalt.org on the basis of the reactome pathway database. The top 5 significant pathways were calculated.

3.17 Proteomic analysis

Proteomic analysis of *T. cruzi*-infected BJ fibroblasts and mock controls was performed to validate induced genes and signalling pathways which were identified in the previous transcriptome analysis.

Here, BJ fibroblasts were seeded in 6-well F-bottom cell culture plates for each condition and infected with *T. cruzi* trypomastigotes with an MOI of 3 (section 3.4). The fibroblasts were harvested 48 hpi by removing the medium, washing with DPBS 3 times and scraping the cells in ice cold DPBS. After transfer into a 1.5 ml tube, the fibroblasts were pelleted at 500 rcf for 5 min at 4°C. Supernatants were removed as completely as possible by pipetting. The samples were snap frozen in liquid nitrogen and stored at -20°C until further processing.

3.17.1 Sample processing and liquid chromatography tandem mass spectrometry (LC-MS/MS)

The following steps were performed by the core facility for mass spectrometry proteomics of the University Medical Center Hamburg-Eppendorf by Dr. Christoph Krisp and Bente Siebels. In brief, proteins were extracted by sonification, disulfide bounds were reduced with dithiothreitol (DTT) and cysteine residues were alkylated with iodoacetamide (IAA). Subsequently, tryptic digestion was performed to fragment the proteins into peptides. The generated peptides were separated by ultra performance liquid chromatography (UPLC) using the nanoACQUITY UPLC System from Waters Corporation. The following tandem mass

spectrometry was performed using Thermo Fisher Scientific's Q Exactive™ Quadrupole Orbitrap hybrid mass spectrometer. The relative abundances determined in this process were used for subsequent analyses.

3.17.2 Proteome data evaluation

The fold change was calculated by the ratio of relative abundances of peptides from *T. cruzi*-infected fibroblasts and the corresponding mock controls. Statistical significances were evaluated using multiple t-tests. Changes with a p-value ≤ 0.05 were considered statistically significant.

Analogously to the transcriptome analysis, a volcano plot was generated, enabling the identification of individual proteins with a high fold change and statistical significance. Analysis of upregulated signaling pathways was also performed here using the web-based tool webgestalt.org. Analogous to section 3.16.4, an over-representation analysis was conducted on the basis of the reactome database and the top 5 significant pathways were calculated.

3.18 Statistical analysis

The GraphPad Prism 9 software was used to perform all statistical analyses. If indicated, outliers were identified using the ROUT method. Gaussian distribution was tested using a Shapiro-Wilk test. If all groups to be compared were normally distributed, statistical significance was tested for unpaired values using unpaired t-tests and for paired values using paired t-tests. If at least one of the groups being compared was not normally distributed, statistical significance was determined for unpaired values by Mann-Whitney test and for paired values by Wilcoxon test. P-values were indicated as * $p \leq 0.05$; ** $p \leq 0.01$; *** $p \leq 0.001$; **** $p \leq 0.0001$. For clarity, only differences tested as significant are labeled. As an exception, p-values < 0.1 were stated to indicate a strong tendency.

4 Results

The skin is the initial site of infection during the vector-borne transmission of the protozoan parasite *T. cruzi*, the causative agent of Chagas disease. In this study, *in vitro* infections of dermal fibroblasts with the *T. cruzi* strain Brazil were utilized to mimic this incipient phase. The early immune response against infected dermal fibroblasts is thought to influence further distribution of parasites to other tissues and organs. Since *T. cruzi* is an obligate intracellular parasite, it can be assumed that NK cells are the main drivers of the innate immune response and contain the parasite load until the onset of the adaptive immune response. Accordingly, the NK cell response and underlying stimulatory and inhibitory mechanisms were characterized in the context of this study.

4.1 Activation of human NK cells by *T. cruzi*-infected dermal fibroblasts

First, it was investigated whether *T. cruzi*-infected primary human dermal fibroblasts (HDF) were able to directly activate NK cells. For this purpose and for further experiments, a protocol was established for a heterologous coculture of isolated NK cells from healthy donors and *in vitro* *T. cruzi*-infected fibroblasts (figure 4.1 A).

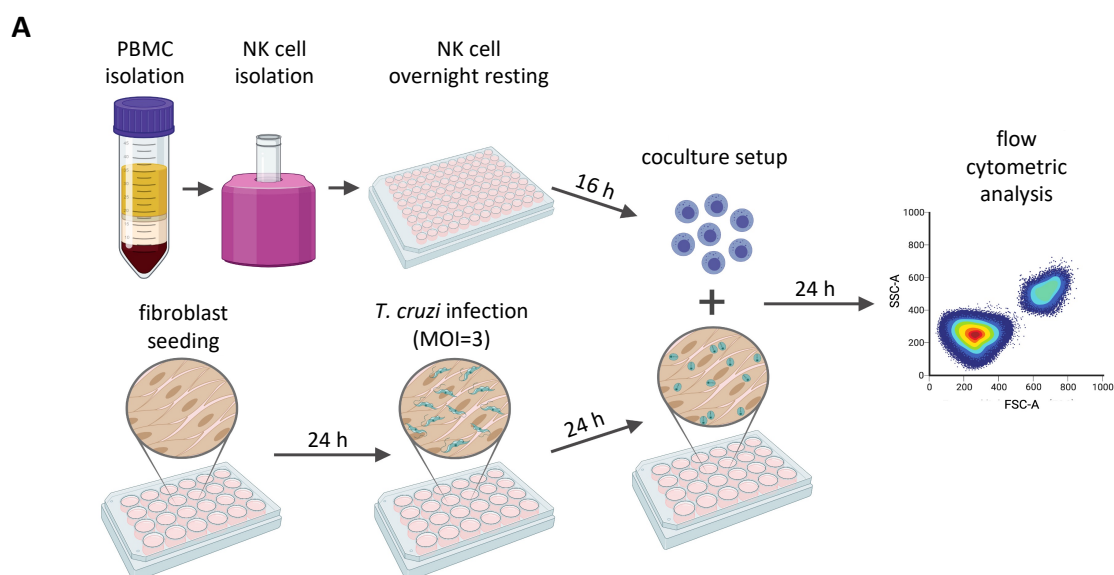
Peripheral blood mononuclear cells (PBMCs) isolated from whole blood of healthy donors were processed for NK cell isolation. The NK cell purification success was verified by flow cytometric staining. A representative plot is depicted in figure 4.1 B. While NK cells accounted for approximately 5 – 15% of PBMCs before purification, the percentage increased to approximately 85 – 95% after purification. Before starting the coculture the following day, the purified NK cells were rested overnight to allow them to recover from the isolation procedure. In parallel, the fibroblasts were seeded and infected *in vitro* with *T. cruzi* trypomastigotes with an MOI of 3. Using this MOI, constant infection rates of 50 – 70% were reached as observed by light microscopy (data not shown).

Cocultures with rested NK cells and mock or *T. cruzi*-infected fibroblasts were set up 24 hpi using an effector to target (E:T) ratio of 1:10 to ensure optimal NK cell stimulation for the following analysis. The cells were cocultured for 24 h and NK cell degranulation was evaluated via flow cytometric analysis of CD107a on the NK cell surface.

Before evaluating the NK cell response to *T. cruzi*-infected fibroblasts, the general responsiveness of NK cells to adherent cells was tested. For this positive control, the purified

and rested NK cells were cocultured with HEK293 cells for 5 h. This cell line has been shown to highly express ligands for the activating NK cell receptor NKG2D [205]. The short duration of coculture was chosen due to the high NK cell stimulating capacity of HEK293 cells, which led to NK cell exhaustion and cell death in response to longer stimulations (data not shown). As displayed in a representative histogram in figure 4.1 C, all tested NK cells exhibited strong degranulation in response to coculture with HEK293 cells.

After general NK cell responsiveness against adherent cells was confirmed, the NK cell response against *T. cruzi*-infected HDF and respective mock controls was evaluated. Figure 4.1 D depicts the NK cell degranulation displayed by the frequency of CD107a⁺ NK cells in response to the respective cocultures. As illustrated in the representative histogram, CD107a gating was performed based on CD107a expression on NK cells cultured without target cells. Based on this, about 18% of NK cells cocultured with mock-infected HDF displayed CD107a on their cell surface. In contrast, coculture with *T. cruzi*-infected HDF resulted in significantly higher NK cell degranulation ($p \leq 0.0001$) with around 66% CD107a⁺ NK cells. These results indicate that *T. cruzi*-infected human dermal fibroblasts directly activate NK cells.



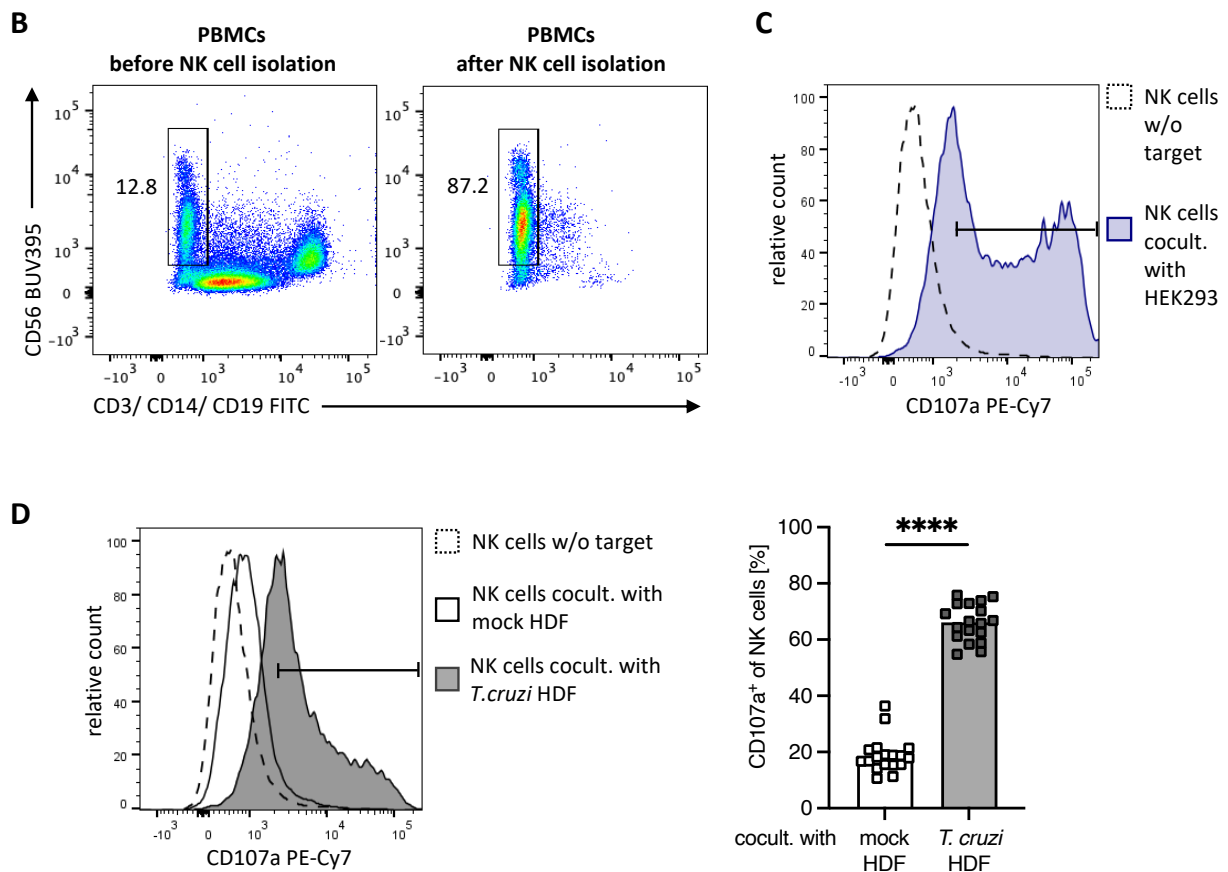


Figure 4.1: Coculture of human NK cells and *T. cruzi*-infected primary human dermal fibroblasts (HDF) results in NK cell degranulation. (A) Experimental layout of heterologous coculture of isolated NK cells from healthy donors and mock or *T. cruzi*-infected HDF (MOI=3). Coculture was started 24 hpi with an E:T ratio of 1:10. Cells were cocultured for 24 h, after which flow cytometric analysis of NK cells was performed. (B) Representative plots of PBMCs before and after NK cell isolation to verify purification success. (C) Representative histogram to verify general responsiveness of used NK cells to adherent cells using coculture with the cell line HEK293, which is described to highly express ligands for the NK cell-activating receptor NKG2D. This coculture was performed for 5 h instead of 24 h to prevent NK cell overactivation and cell death. NK cell degranulation was visualized by the presence of CD107a on the NK cell surface. The gating was performed on the basis of NK cells cultured without target cells. (D) NK cell degranulation after heterologous coculture with mock and *T. cruzi*-infected HDF. Left: representative histogram. Right: diagram illustrating 18 coculture combinations of NK cells isolated from 3 donors with HDF originating from 6 donors. Respective medians for each group are depicted by bars. After positive test for normal distribution, statistical significance was analyzed by paired t-test: **** $p \leq 0.0001$.

4.2 Implementation of BJ fibroblasts as a model for dermal *T. cruzi* infection and related NK cell activation

Due to the limited cell number of primary fibroblasts due to finite expansion, it was not feasible to use these for subsequent analyses. Therefore, a fibroblast cell line was used to mimic the acute, dermal *T. cruzi* infection and decipher the mechanisms of NK cell modulation by infected fibroblasts. To this end, the foreskin fibroblast cell line BJ was first examined for similarity of response to *T. cruzi* infection. Both HDF and BJ fibroblasts exhibited comparable infection rates of approximately 50 – 70% using an MOI of 3, as observed by light microscopy (data not shown). Afterwards, RNA sequencing of mock and *T. cruzi*-infected HDF from 5 donors and BJ fibroblasts was conducted 48 hpi to perform a comparative transcriptome analysis. Out of all 67×10^3 identified genes, 581 genes were found to be significantly ($p \leq 0.05$) differentially expressed with a \log_2 fold change of ≥ 1 or ≤ -1 . This reflects a doubling or halving of the expression. These significantly differentially expressed genes (DEGs) were used for principal component analysis. Here, all variables, thus the expression intensities of all analyzed genes, were combined into two principal components (PC1 and PC2). Using this approach, the degree of similarity between all individual samples could be illustrated. The greater the distance between samples, the more they differ from each other. The results are depicted in figure 4.2 A. Two clusters were found, one formed from all infected fibroblasts and the other from mock controls. Although mock and *T. cruzi*-infected BJ fibroblasts were located higher in PC2 than their respective HDFs, the shift in PC1 correlated to the infection was very similar for HDF and BJ fibroblasts.

The comparable reaction of HDF and BJ fibroblasts to *T. cruzi* infection was further visualized by a heatmap displaying the relative expression of significantly ($p \leq 0.05$) DEGs. For optimal clarity, the cutoff for the \log_2 fold change was set to ≥ 2 or ≤ -2 , corresponding to a quadrupling and reduction to a quarter of the expression. This cutoff resulted in 99 genes being displayed (figure 4.2 B). The generated heatmap shows comparable expression patterns of *T. cruzi*-infected HDF and BJ fibroblasts and the respective mock controls, respectively.

Thus, a similar response of HDF and BJ fibroblasts to *T. cruzi* infection was confirmed.

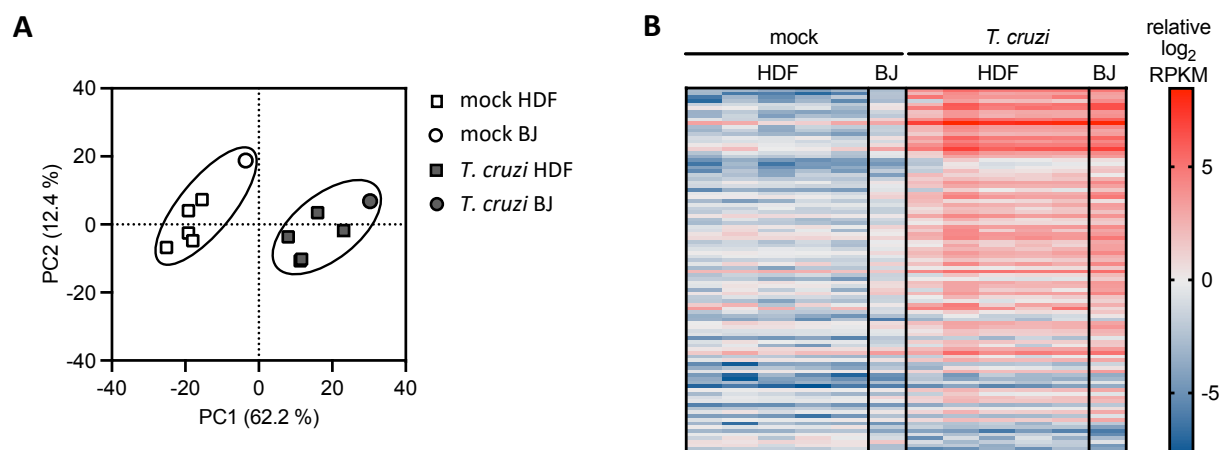


Figure 4.2: Transcriptome analysis reveals comparable transcriptional changes of HDFs and BJ fibroblasts in response to *T. cruzi* infection. RNA sequencing was performed using mock and *T. cruzi*-infected HDFs and BJ fibroblasts 48 hpi (MOI=3). HDFs from 5 healthy donors were compared with BJ fibroblasts. In the case of BJ fibroblasts, the mean from 2 independent infections was used. **(A)** Principal component analysis of significantly ($p \leq 0.05$) differentially expressed genes (DEGs) with a \log_2 fold change of ≥ 1 or ≤ -1 . **(B)** Heatmap displaying the relative expression of significantly ($p \leq 0.05$) DEGs with a \log_2 fold change of ≥ 2 or ≤ -2 using \log_2 -transformed Reads per kilobase of transcript per Million mapped reads (RPKM) values in relation to the mean RPKM value of all considered genes.

In the next step it was investigated, whether a *T. cruzi* infection in BJ fibroblasts results in enhanced NK cell degranulation, as observed for infected HDFs. To this end, coculture experiments were performed analogous to section 4.1. Here, a significant increase ($p \leq 0.001$) in the frequency of CD107a⁺ NK cells after coculture with *T. cruzi*-infected BJ fibroblasts was observed compared to the coculture with mock controls (figure 4.3). Whereas around 15% of NK cells cocultured with mock controls exhibited CD107a on their surface, approximately 75% of NK cells cocultured with infected BJ fibroblasts were CD107a⁺. The effect was comparable to the increased NK cell degranulation after coculture with mock or *T. cruzi*-infected HDFs, respectively.

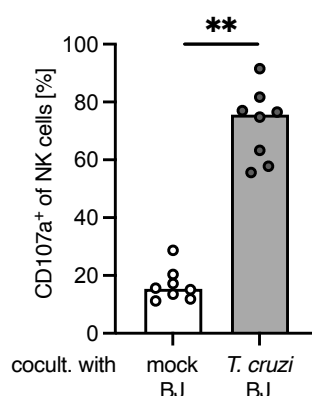


Figure 4.3: Coculture of human NK cells and *T. cruzi*-infected BJ fibroblasts induces NK cell degranulation. Coculture was started 24 hpi (MOI=3) with an E:T ratio of 1:10 using NK cells derived from 8 healthy donors. Cells were cocultured for 24 h and NK cell degranulation was visualized by flow cytometric analysis of the presence of CD107a on NK cell surfaces. Bars display respective medians. After negative test for normal distribution, statistical significance was analyzed by paired Wilcoxon test: ** $p \leq 0.01$.

Based on comparable transcriptional changes of HDFs and BJ fibroblasts after *T. cruzi* infection and the comparable induction of NK cell degranulation after coculture, BJ fibroblasts were used for subsequent mechanistic analyses.

4.3 *T. cruzi*-infected fibroblasts exhibit no reduction of MHC-I expression

The oldest-known mechanism of NK cell activation is the reduction of inhibitory signals by MHC-I-recognizing receptors [27]. Therefore, the MHC-I expression of BJ fibroblasts was investigated during *T. cruzi* infection between 24 and 72 hpi. As shown by fluorescence microscopy in figure 4.4 A, the intracellular multiplication process of the parasites in the amastigote stage takes place during this time. Whereas the first replications of *T. cruzi* amastigotes started 24 hpi and 2 – 4 parasites were usually present per fibroblast, at 72 hpi the first fibroblasts were already filled by the parasites.

The MHC-I expression on BJ fibroblasts in the course of a *T. cruzi* infection was evaluated by flow cytometry using an antibody clone detecting all classical human MHC-I molecules, HLA-A, -B and -C (figure 4.4 B). Since nearly all fibroblasts were positive for HLA-A,B,C as displayed in the representative histogram, the mean fluorescence intensity (MFI), displaying the density of the expressed HLA-A,B,C molecules, was evaluated. All MFI values were normalized to the average MFI of all respective mock controls. A slight increase in HLA-A,B,C expression was observed in the course of infection. Whereas a trend was apparent at 24 hpi, normalized

HLA-A,B,C MFIs were significantly ($p < 0.05$) increased by approximately 12% compared to controls at 48 and 72 hpi.

Since no reduction of HLA-A,B,C expression was observed in response to the infection, other potential mechanisms of NK cell activation were investigated.

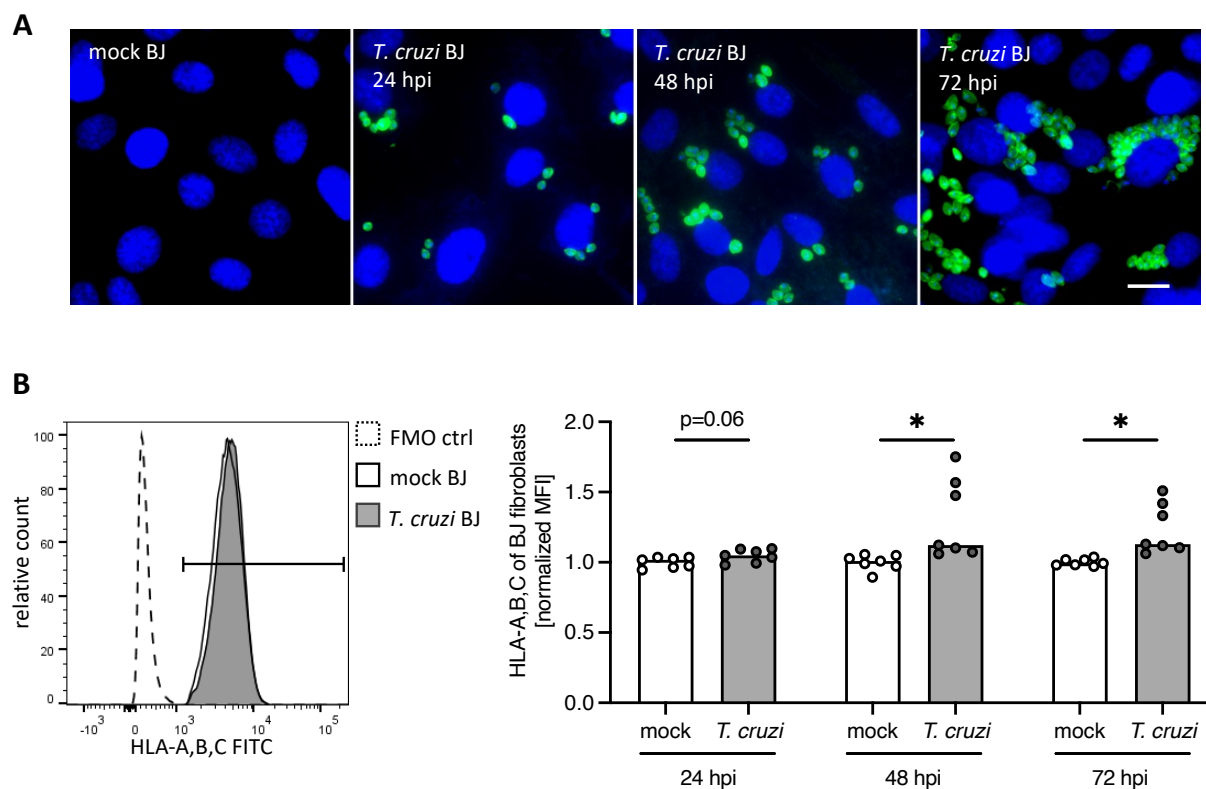


Figure 4.4: Expression of the classical MHC-I molecules HLA-A,B,C is slightly increased on the BJ fibroblast surface in the course of *T. cruzi* infection. (A) Representative immunofluorescence microscopy of *T. cruzi*-infected BJ fibroblasts 24, 48 and 72 hpi (MOI=3). Fibroblast nuclei were visualized via DAPI (blue); intracellular *T. cruzi* parasites were stained with murine anti-*T. cruzi* Brazil immune serum and a FITC-labeled anti-mouse IgG secondary antibody (green). Scale: 10 μ m. (B) Flow cytometric analysis of HLA-A,B,C expression on the BJ fibroblast surface. Left: representative histogram, 48 hpi; right: normalized HLA-A,B,C MFI in the course of infection (24, 48, 72 hpi; MOI=3). MFI values were normalized to the average MFI of all mock controls. Bars display respective medians (n=9). After positive test for normal distribution, statistical differences were calculated by unpaired t-test with Welch's correction: * $p < 0.05$.

4.4 NK cell response to *T. cruzi*-infected fibroblasts is facilitated by the engagement of NKp46

Another way to induce NK cell activation is the enhancement of stimulatory interactions. One activating NK cell receptor is the natural cytotoxicity receptor NKp46, which has been shown to interact with cell surface vimentin (csVimentin) as a cellular ligand promoting NK cell activation [92].

4.4.1 Increased presence of csVimentin on fibroblasts in response to *T. cruzi* infection

Since vimentin is expressed intracellularly by fibroblasts as an intermediate filament, the possibility of it being present on the fibroblast surface in response to *T. cruzi* infection was examined. In this context, flow cytometric analysis of csVimentin was performed during infection between 24 and 72 hpi (figure 4.5). The gating was set based on fluorescence minus one (FMO) controls as depicted in the representative histogram. The FMO controls were prepared by staining a mixture of mock and *T. cruzi*-infected BJ fibroblasts with all fluorochrome-labeled antibodies used in the experiment except the FITC-labeled anti-vimentin antibody. Although a small fraction of approximately 10% of the mock controls displayed csVimentin, there was a significant increase in csVimentin in the course of the infection. Whereas 24 hpi the frequency of csVimentin⁺ BJ fibroblasts was around 20% ($p \leq 0.0001$), the fraction increased to 42% ($p \leq 0.0001$) 48 hpi and to 48% ($p \leq 0.001$) 72 hpi.

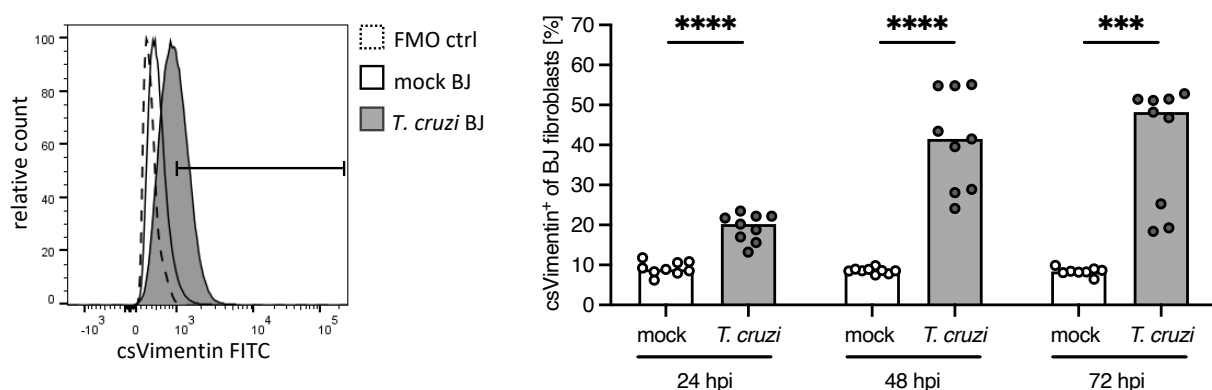


Figure 4.5: BJ fibroblasts show increased presence of vimentin on their cell surface in the course of *T. cruzi* infection. Flow cytometric analysis of csVimentin on mock and *T. cruzi*-infected BJ fibroblasts (MOI=3). Left: representative histogram, 48 hpi. Right: frequency of csVimentin⁺ BJ fibroblasts in the course of infection (24, 48 and 72 hpi). Bars display respective medians (n=9). After negative test for normal distribution, statistical differences were calculated by Mann-Whitney test: *** $p \leq 0.001$, **** $p \leq 0.0001$.

4.4.2 Increased binding of NKp46 to *T. cruzi*-infected fibroblasts

The binding of the NK cell receptor corresponding to csVimentin, NKp46, was investigated. Here, like for later analyses, fibroblasts were examined 48 hpi. This time point was chosen since the presence of the ligand was already strongly increased (figure 4.5), but intracellular parasites had not yet completely filled their host cells, thereby destabilizing them (figure 4.4 A).

Two different approaches were utilized to study the NKp46 binding to mock and *T. cruzi*-infected fibroblasts. First, a binding assay using NKp46-Fc chimera molecules, which were detected by a fluorochrome-labeled secondary anti-human IgG Fc antibody, was performed (figure 4.6 A). As shown in the representative histogram on the left, gating was performed based on BJ fibroblasts stained only with the fluorochrome-labeled secondary anti-human IgG-Fc antibody without prior treatment with NKp46-Fc chimera molecules. The results showed a significantly ($p \leq 0.0001$) higher frequency of NKp46-Fc bound *T. cruzi*-infected BJ fibroblasts (median $\sim 10\%$) compared to the mock controls (median $\sim 1.6\%$). Furthermore, the functionality of the NKp46 binding to BJ fibroblasts was verified by a reporter cell assay (figure 4.6 B). Here, β_2m -deficient Jurkat cells transfected with an NKp46 ζ construct were cocultured with mock or *T. cruzi*-infected BJ fibroblasts for 18 h (figure 4.6 B above). Subsequently, the reporter cells were assessed for their activation status by flow cytometric analysis of cell surface expression of the activation marker CD69, which is expressed after functional ligand binding to the NKp46 ζ construct in response to signaling transduction induced by the intracellular ζ -chain [203]. To exclude unspecific responses, β_2m -deficient Jurkat cells without an NKp46 ζ construct were used as background controls (figure 4.6 B below). As depicted in the representative histograms on the left, gating was performed on the basis of FMO controls. Only NKp46 ζ^+ Jurkat reporter cells showed a clear and differentiated activation after coculture with BJ fibroblasts. The frequency of CD69 $^+$ out of NKp46 ζ^+ Jurkat reporters was significantly ($p \leq 0.0001$) higher after coculture with *T. cruzi*-infected BJ fibroblasts (median $\sim 20\%$) compared to mock controls (median $\sim 13\%$). These results confirm an increased interaction of NKp46 with fibroblasts after *T. cruzi* infection.

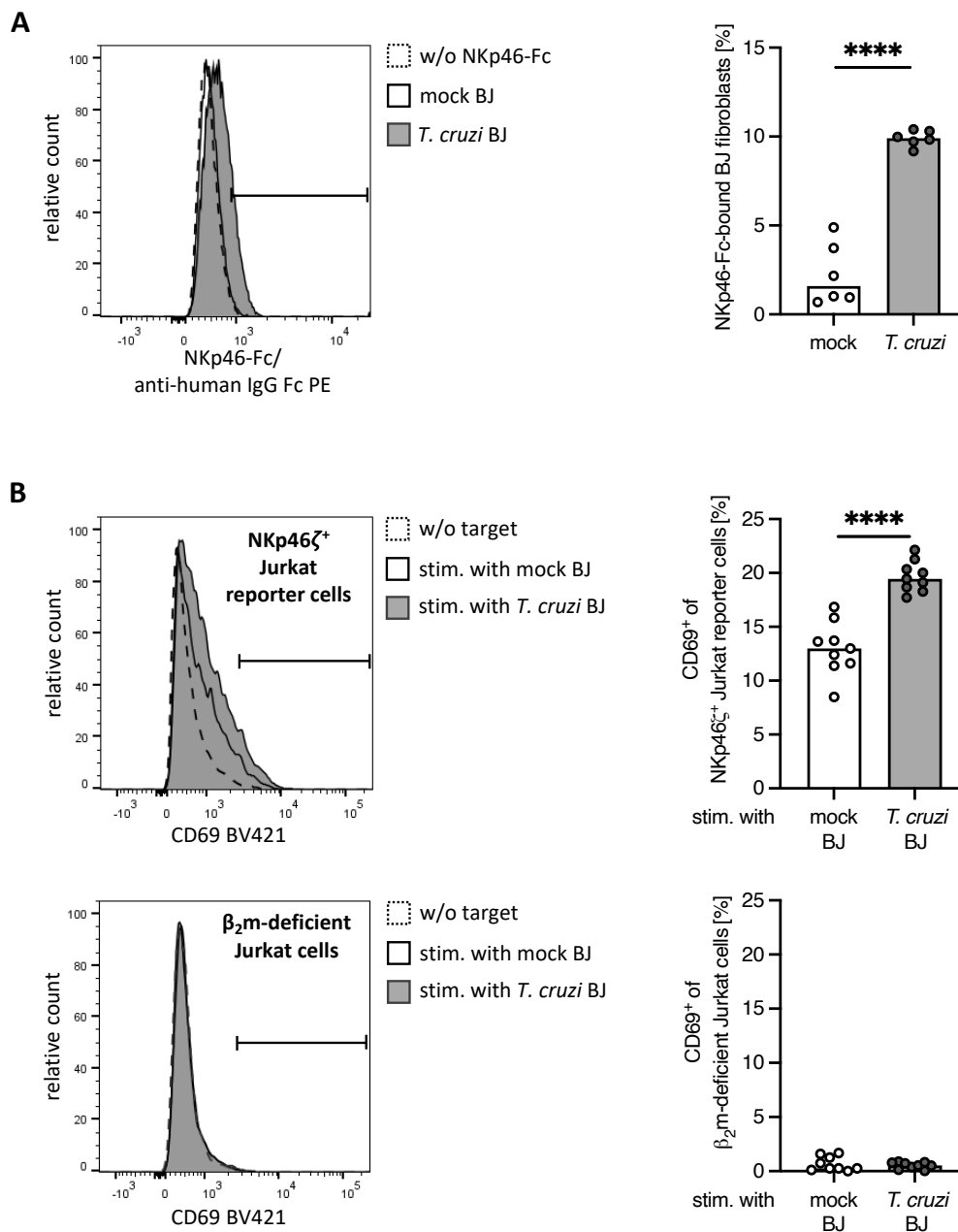


Figure 4.6: Binding of NKp46 to fibroblasts is increased after *T. cruzi* infection. (A) Receptor-Fc binding assay was conducted with mock or *T. cruzi*-infected BJ fibroblasts 48 hpi (MOI=3) using NKp46-Fc chimera molecules and anti-human IgG Fc secondary antibody with subsequent flow cytometric analysis. Left: representative histogram, 48 hpi. Right: frequency of NKp46-Fc bound BJ fibroblasts. Bars display respective medians (n=6). After positive test for normal distribution, statistical differences were calculated by unpaired t-test with Welch's correction: **** p<0.0001. (B) Reporter cell assay was performed using β_2m -deficient Jurkat cells with (above) or without (below) the transfected NKp46 ζ construct. They were cocultured with mock or *T. cruzi*-infected BJ fibroblasts (MOI=3) for 18 h between 30 and 48 hpi. The Jurkat cell activation status was monitored via the activation marker CD69 on the cell surface. Left: representative histogram, 48 hpi. Right: frequency of CD69 $^+$ Jurkat cells. Bars display respective medians (n=9). After positive test for normal distribution, statistical differences were calculated by unpaired t-test with Welch's correction: **** p<0.0001.

Subsequently, it was investigated whether the engagement of NKp46 is solely dependent on cell-cell contact or whether soluble factors in the fibroblast culture supernatants, such as soluble vimentin, also interact with this activating NK cell receptor. To this end, NKp46 ζ^+ Jurkat reporter cells were stimulated by coculture with mock or *T. cruzi*-infected BJ fibroblasts or solely with the culture supernatants of the respective cells (figure 4.7 A). As previously observed, the reporter cells showed a significantly ($p \leq 0.0001$) higher frequency of CD69 $^+$ cells after coculture with *T. cruzi*-infected BJ fibroblasts (median $\sim 13\%$) compared to mock controls (median $\sim 19.5\%$). In contrast, stimulation of NKp46 ζ^+ Jurkat reporter cells solely with the culture supernatant of *T. cruzi*-infected BJ fibroblasts resulted in significantly ($p \leq 0.0001$) lower activation compared to the mock controls. Whereas around 9% CD69 $^+$ reporter cells were detected after stimulation with supernatant from infected BJ fibroblasts, only about 1.5% CD69 $^+$ reporter cells were found in response to stimulation with the mock control supernatants.

These results were supported by the measurement of soluble vimentin in the culture supernatants of mock and *T. cruzi*-infected BJ fibroblasts via ELISA (figure 4.7 B). Although not significant, a trend toward lower levels of soluble vimentin was measured in the supernatants of infected BJ fibroblasts compared to mock controls.

Taken together, these results indicate a cell-cell contact-dependent engagement of NKp46 in the context of *T. cruzi*-infected BJ fibroblasts.

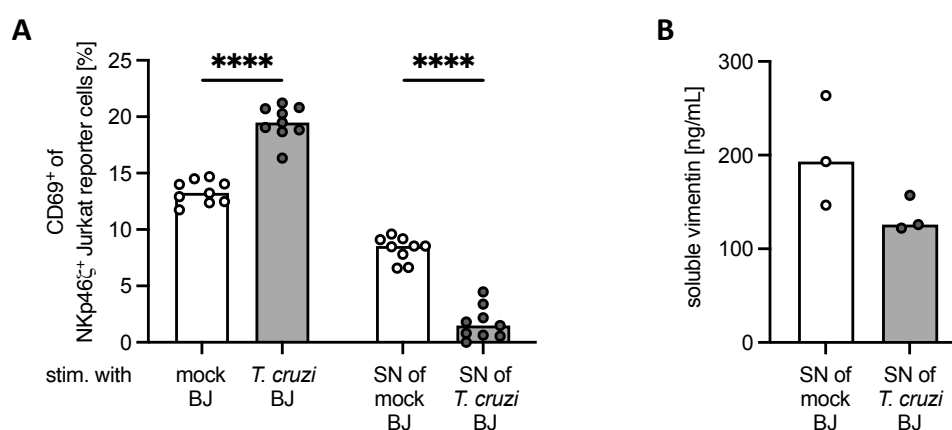


Figure 4.7: Engagement of NKp46 in the context of *T. cruzi*-infected BJ fibroblasts is dependent on cell-cell contact. (A) Reporter cell assay using NKp46 ζ^+ Jurkat reporter cells stimulated with mock or *T. cruzi*-infected BJ fibroblasts 48 hpi (MOI=3) or solely with culture supernatant (SN) of the named fibroblasts. Bars display respective medians (n=9). After positive test for normal distribution, statistical differences were calculated by unpaired t-test with Welch's s correction: **** $p \leq 0.0001$. (B) Concentration of soluble vimentin in the culture supernatant of mock and *T. cruzi*-infected fibroblasts 48 hpi (MOI=3) was measured via ELISA. Bars display respective medians (n=3). After negative test for normal distribution, statistical differences were analyzed using Mann-Whitney test. No statistical differences were found.

4.4.3 NKp46 blockade reduces NK cell response to fibroblasts

Finally, the impact of NKp46 engagement on NK cell effector functions by *T. cruzi*-infected BJ fibroblasts in particular was investigated. In order to this, NKp46 was blocked on NK cells using the monoclonal antibody clone 9E2 before cocultures with mock and *T. cruzi*-infected BJ fibroblasts were started. The antibody clone was chosen for its proven blocking effect on NKp46 [213]. The efficiency of the blockade was validated by flow cytometric staining of the receptor (figure 4.8 A). While NKp46 could be found on a majority of the untreated NK cells, only a weak NKp46 staining was detectable on the NKp46 blocking antibody-treated NK cells. Based on these results, NKp46 blockade was assessed to be sufficiently efficient for subsequent coculture experiments. Here, the effect of NKp46 blockade on different NK cell effector functions was investigated.

First, NK cell degranulation was examined after coculture with an E:T ratio of 1:10 by flow cytometric analysis of CD107a (figure 4.8 B). NKp46 blockade resulted in significantly reduced frequencies of CD107a⁺ NK cells by approximately 75 – 80% following cocultures with mock ($p \leq 0.05$) as well as with *T. cruzi*-infected BJ fibroblasts ($p \leq 0.001$). However, since a higher frequency of NK cells generally degranulated in response to fibroblasts infected with *T. cruzi* compared with mock controls, degranulation was impeded in a higher amount of NK cells by blocking NKp46.

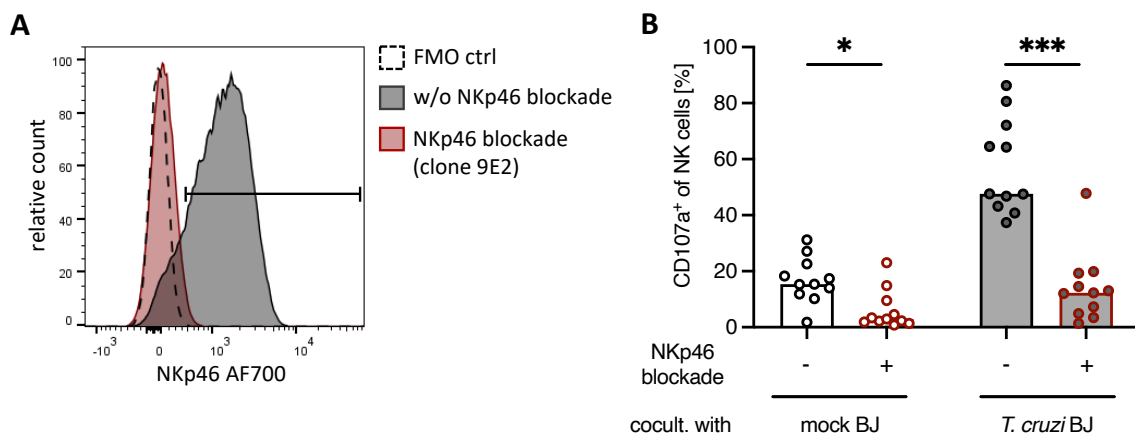
Second, coculture experiments were performed for the following analysis of the supernatants for different secreted effector molecules using the LEGENDplex™ Human CD8/NK Panel (figure 4.8 C). To ensure optimal amounts of secreted effector molecules, the E:T ratio was increased to 1:2.5. Only the mediators that were increased after coculture with *T. cruzi*-infected BJ fibroblasts compared to mock controls are displayed.

The cytotoxic NK cell effector function was assessed by measuring the amounts of granzyme A, granzyme B, perforin, and granulysin in addition to NK cell degranulation, as displayed previously by flow cytometric analysis of CD107a. Granzyme A, granzyme B and granulysin were secreted at significantly ($p \leq 0.01$, $p \leq 0.05$ and $p \leq 0.01$) lower levels in response to *T. cruzi*-infected BJ fibroblasts when NKp46 signaling was blocked. There was also a tendency for less perforin to be released after NKp46 blockade ($p = 0.08$). Regarding the coculture with mock controls, there was a significant ($p \leq 0.01$ and $p \leq 0.05$) effect of NKp46 blockade on the secretion of granzyme A and granzyme B, but not on the secretion of perforin and granulysin.

Moreover, NK cell-mediated cytotoxicity through the engagement of apoptosis-inducing death receptors was investigated by determining the levels of soluble Fas ligand (sFasL) in the coculture supernatant. NKp46 blockade resulted in a significantly ($p \leq 0.01$) lower concentration of sFasL after coculture with *T. cruzi*-infected fibroblasts, but not after coculture with mock controls.

Apart from cytotoxic NK cell effector functions, the secretion of the cytokine IFN- γ was quantified. IFN- γ is a potent modulator of the immune response and has been shown to be crucial for control of the *T. cruzi* parasite [175], [177]. When NKp46 was blocked, significantly ($p \leq 0.05$) lower secretion of IFN- γ was observed after both coculture with *T. cruzi*-infected BJ fibroblasts as well as with mock controls.

Taken together, the results demonstrate a reduced NK cell response to mock as well as to *T. cruzi*-infected BJ fibroblasts when NKp46 is blocked. Nevertheless, the effect seems more pronounced in coculture with infected fibroblasts compared to mock controls.



To be continued on the next page.

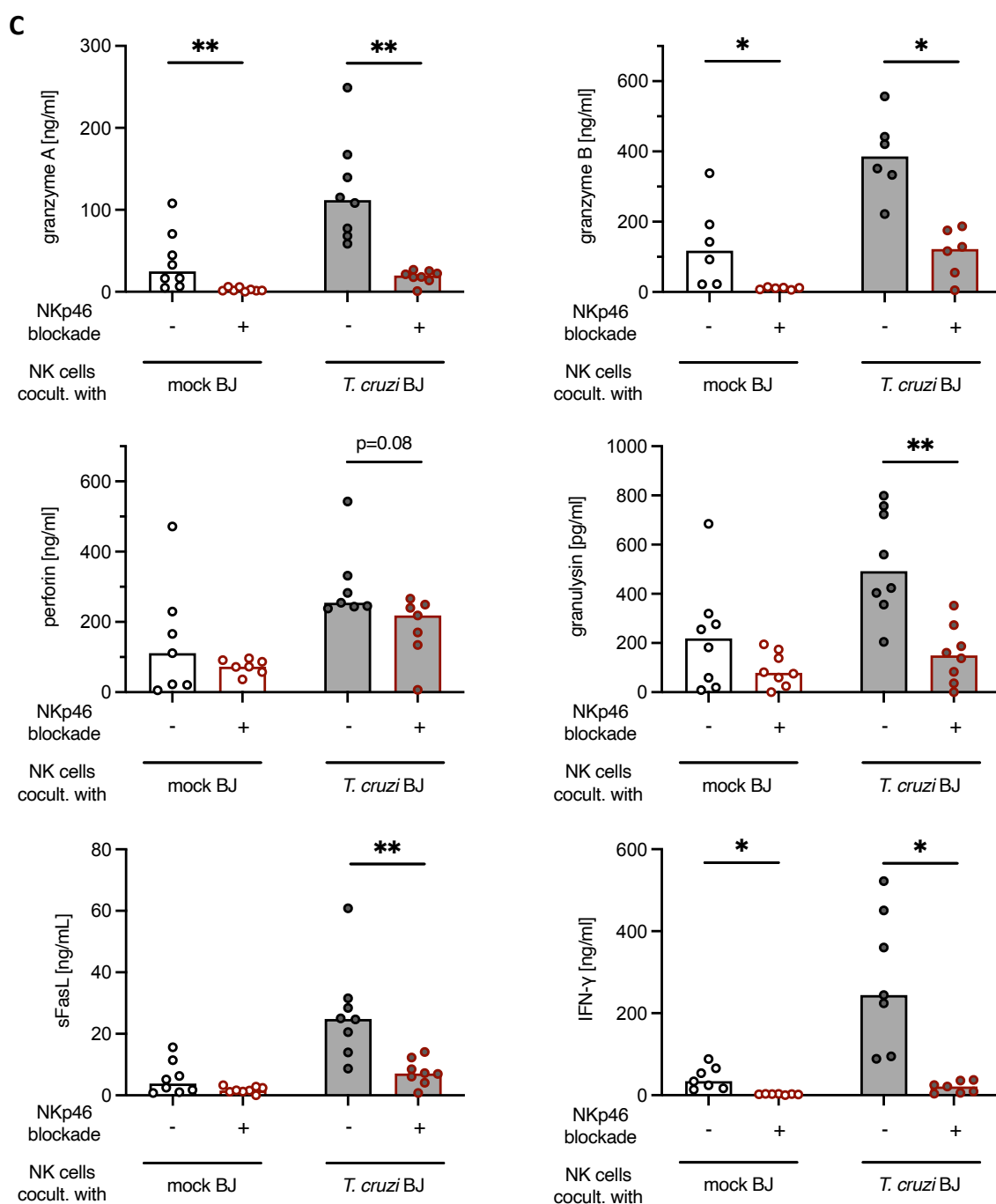


Figure 4.8: NKp46 blockade reduces NK cell response to fibroblasts. (A) Blockade of NKp46 on the NK cell surface by antibody clone 9E2 was validated before coculture setup by flow cytometric analysis. A representative histogram is depicted. (B) Flow cytometric analysis of CD107a on the NK cell (CD3⁺CD56⁺) surface after coculture with mock and *T. cruzi*-infected BJ fibroblasts without and with prior NKp46 blockade. Cocultures were started 24 hpi (MOI=3) with an E:T ratio of 1:10 using NK cells derived from 11 healthy donors. Cells were cocultured for 24 h before flow cytometric analysis was performed. Respective medians are depicted by bars. After negative test for normal distribution, statistical significances were calculated by paired Wilcoxon test: * p<0.05; *** p<0.001. (C) Analysis of supernatants after NK cell coculture with mock and *T. cruzi*-infected BJ fibroblasts without and with prior NKp46 blockade. Cocultures were started 24 hpi (MOI=3) with an E:T ratio of 1:2.5 using NK cells derived from 8 healthy donors. Cells were cocultured for 24 h before concentrations of granzyme A, granzyme B, perforin, granulysin, sFasL, and IFN- γ were determined using the Human CD8/NK Panel of the LEGENDplex™ kit. Outliers were identified by ROUT method and excluded. Respective medians are depicted by bars. After negative test for normal distribution, statistical significances were calculated by paired Wilcoxon test: * p<0.05; ** p<0.01.

4.5 NK cell response to *T. cruzi*-infected fibroblasts is promoted by the engagement of CD160

Since the activation of NK cells requires an interplay of several factors, the engagement of another stimulatory receptor was investigated in the context of NK cell activation by *T. cruzi*-infected fibroblasts. Here, the receptor CD160, which acts upon NK cells in a stimulatory manner, was chosen. Both HLA-C and HVEM have been described as ligands for CD160, with HVEM having a higher affinity [32], [97].

4.5.1 Increased expression of the CD160 ligand HVEM on fibroblasts in response to *T. cruzi* infection

Transcriptome analysis revealed a significantly ($p \leq 0.01$) increased expression rate of the HVEM-encoding gene *TNFRSF14* after *T. cruzi* infection of HDF as well as BJ fibroblasts 48 hpi (figure 4.9). In the case of BJ fibroblasts, *TNFRSF14* gene expression increased by nearly 40% in response to the infection. Although all HDF donors exhibited lower *TNFRSF14* gene expression overall, the increase in response to the infection was comparable. Based on these results, further analyses were performed using BJ fibroblasts.

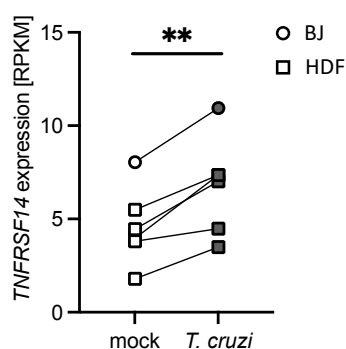


Figure 4.9: Transcriptome analysis reveals increased HVEM expression in BJ fibroblasts and HDF in response to *T. cruzi* infection. RNA sequencing was performed using mock and *T. cruzi*-infected HDFs and BJ fibroblasts 48 hpi (MOI=3). RPKM values display *TNFRSF14* (HVEM encoding) gene expression of BJ fibroblasts and 5 HDF donors. After positive test for normal distribution, statistical significance was analyzed by paired t-test: ** $p \leq 0.01$.

The HVEM protein expression on BJ fibroblasts was investigated during *T. cruzi* infection between 24 and 72 hpi by flow cytometric analysis (figure 4.10). The gating was performed based on FMO controls. While HVEM could be stained on about 3% of the mock controls, the frequency of HVEM⁺ BJ fibroblasts increased significantly and steadily over the course of the *T. cruzi* infection. The proportion of HVEM⁺ BJ fibroblasts increased at the to a median of around 5% 24 hpi ($p \leq 0.0001$), to around 9% 48 hpi ($p \leq 0.001$) and to approximately 14% 72 hpi ($p \leq 0.001$).

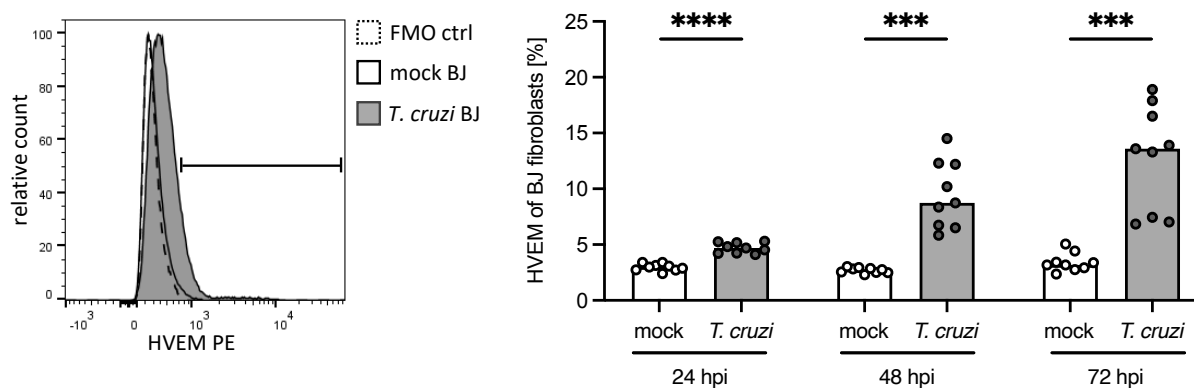


Figure 4.10: Expression of HVEM is increased on the BJ fibroblast surface in the course of *T. cruzi* infection. Flow cytometric analysis of HVEM on mock and *T. cruzi*-infected BJ fibroblasts (MOI=3). Left: representative histogram at 48 hpi. Right: frequency of HVEM⁺ BJ fibroblasts in the course of infection (24, 48 and 72 hpi). Bars display respective medians (n=9). After positive test for normal distribution, statistical differences were calculated by unpaired t-test with Welch's correction: *** $p \leq 0.001$; **** $p \leq 0.0001$.

4.5.2 Increased binding of CD160 to *T. cruzi*-infected fibroblasts

In the next step, the binding of the corresponding stimulatory NK cell receptor CD160 to HVEM was examined 48 hpi (figure 4.11). Since no receptor-Fc chimera molecules were available for human CD160, the receptor binding assay was modified. To this end, mock and *T. cruzi*-infected BJ fibroblasts were treated with human recombinant CD160 (hrCD160) proteins containing a His-tag. Subsequently, the recombinant proteins bound to the fibroblasts were detected by a fluorochrome-labeled anti-His secondary antibody. As depicted in the representative histogram on the left, gating was performed based on BJ fibroblasts stained only with the fluorochrome-labeled anti-His secondary antibody without prior treatment with hrCD160 molecules. Using this approach, significantly ($p \leq 0.001$) increased binding of CD160 to *T. cruzi*-infected BJ fibroblasts was observed compared to mock controls. The percentage of hrCD160-bound fibroblasts doubled from about 20% to approximately 40%.

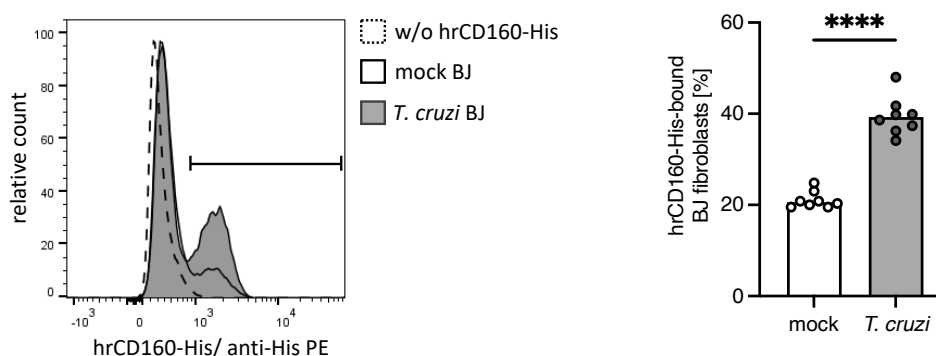


Figure 4.11: Binding of CD160 is increased after *T. cruzi* infection. A receptor binding assay was conducted with mock or *T. cruzi*-infected BJ fibroblasts 48 hpi (MOI=3) using human recombinant CD160 (hrCD160) molecules containing a C-terminal 6-His tag and anti-His secondary antibody with subsequent flow cytometric analysis. Left: representative histogram at 48 hpi. Right: frequency of hrCD160-His bound BJ fibroblasts. Bars display respective medians (n=8). After positive test for normal distribution, statistical differences were calculated by unpaired t-test with Welch's correction: *** p<0.001.

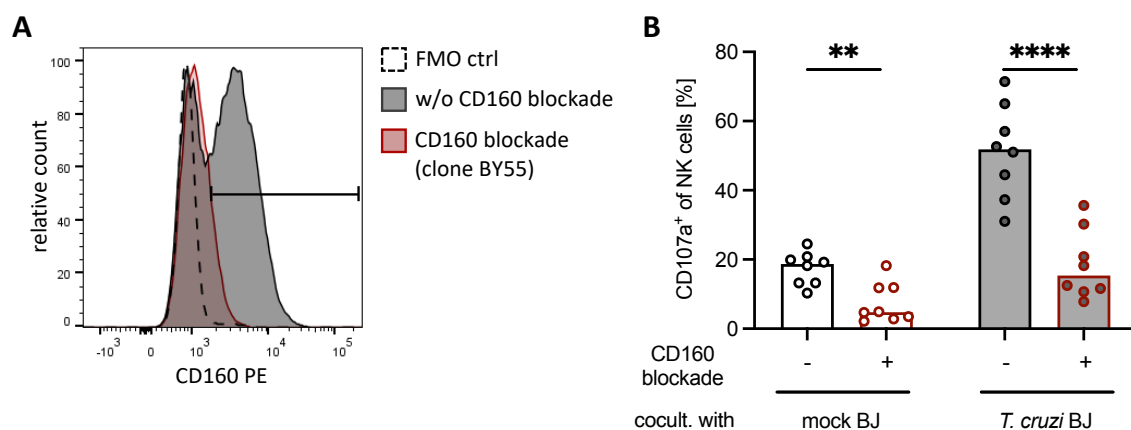
4.5.3 CD160 blockade reduces NK cell response to fibroblasts

Subsequently, the role of CD160 engagement in NK cell activation by mock and *T. cruzi*-infected BJ fibroblasts was studied. To this end, CD160 was blocked on NK cells using the antibody clone BY55 before cocultures with mock and *T. cruzi*-infected BJ fibroblasts were started. Prior to coculture, blocking efficiency was examined by flow cytometric staining of CD160 as depicted by the representative histogram in figure 4.12 A. Gating was performed based on FMO controls. Although a small proportion of NK cells were still stained with the fluorochrome-labeled anti-CD160 antibody after blockade, over 90% of CD160 molecules were covered after blockade compared to untreated NK cells. Therefore, the blockade was considered to be sufficiently efficient for subsequent coculture experiments to analyze different NK cell effector functions.

First, NK cell degranulation was examined by flow cytometric analysis of CD107a expression on the NK cell surface (figure 4.12 B) as previously described. The blockade of CD160 caused a reduced frequency of CD107a⁺ NK cells by around 70 – 75% following cocultures with *T. cruzi*-infected BJ fibroblasts (p<0.0001) as well as with mock controls (p<0.01). Since *T. cruzi*-infected fibroblasts induced degranulation in a higher fraction of NK cells than mock-treated fibroblasts, a higher number of NK cells was inhibited by the CD160 blockade. Further coculture experiments were performed to analyze the culture supernatants for secreted NK cell effector molecules (figure 4.12 C). As previously described in section 4.4.3, mediators that were increased in response to *T. cruzi*-infected BJ fibroblasts compared with

mock controls are depicted. When CD160 was blocked, the secretion of the cytotoxicity mediators granzyme A, granzyme B, perforin, granulysin and sFasL as well as the cytokine IFN- γ was significantly reduced after coculture with *T. cruzi*-infected BJ fibroblasts as well as with mock controls. *T. cruzi* infection did not affect the CD160 blockade effect, whereas, due to higher NK cell activity overall, the magnitude of reduction in secretion was higher for NK cells cocultured with infected fibroblasts.

In total, the results showed a reduced NK cell response to mock as well as to *T. cruzi*-infected BJ fibroblasts when CD160 was blocked. Although the effect was not specific for *T. cruzi*-infected fibroblasts, the activity of a higher number of NK cells appeared to be impacted by the blockade when NK cells were cocultured with infected fibroblasts compared to mock controls.



To be continued on the next page.

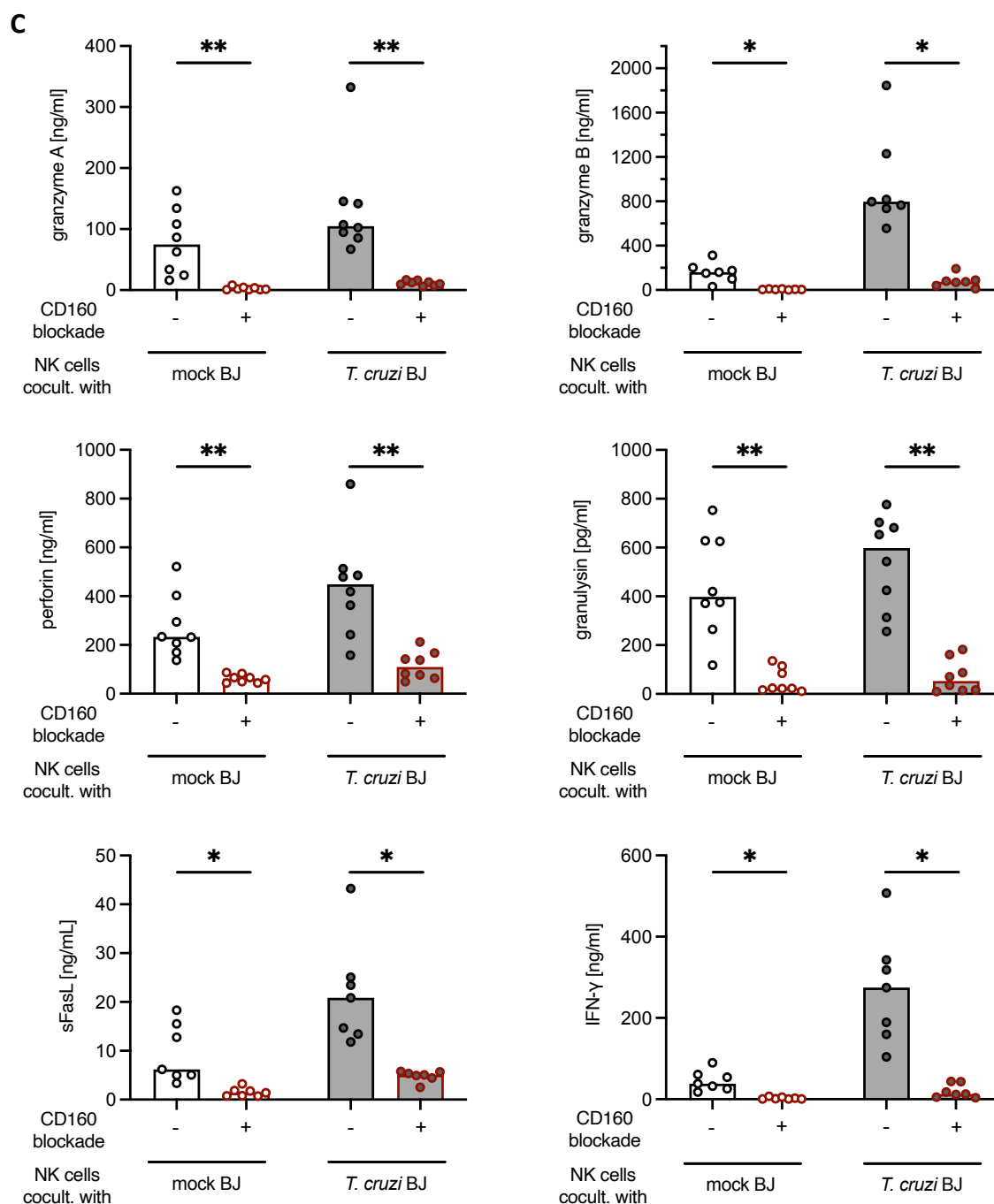


Figure 4.12: CD160 blockade reduces NK cell response to fibroblasts. (A) Blockade of CD160 on the NK cell surface by antibody clone BY55 was validated before coculture setup via flow cytometric analysis. Representative histogram is depicted. (B) Flow cytometric analysis of CD107a on the NK cell (CD3⁺CD56⁺) surface after coculture with mock and *T. cruzi*-infected BJ fibroblasts without and with prior CD160 blockade. Cocultures were started 24 hpi (MOI=3) with an E:T ratio of 1:10 using NK cells derived from 8 healthy donors. Cells were cocultured for 24 h before flow cytometric analysis was performed. Respective medians are depicted by bars. After positive test for normal distribution, statistical significances were calculated by paired t-test: ** $p \leq 0.01$; **** $p \leq 0.0001$. (C) Analysis of supernatants after NK cell coculture with mock and *T. cruzi*-infected BJ fibroblasts without and with prior CD160 blockade. Cocultures were started 24 hpi (MOI=3) with an E:T ratio of 1:2.5 using NK cells derived from 8 healthy donors. Cells were cocultured for 24 h before concentrations of granzyme A, granzyme B, perforin, granulysin, sFasL, and IFN- γ were determined using the Human CD8/NK Panel of the LEGENDplex™ kit. Outliers were identified by ROUT method and excluded. Respective medians are depicted by bars. After negative test for normal distribution, statistical significances were calculated by paired Wilcoxon test: * $p \leq 0.05$; ** $p \leq 0.01$.

4.6 Interferons secreted by *T. cruzi*-infected fibroblasts support NK cell effector function

Next, whether soluble factors also play a role in NK cell activation by *T. cruzi*-infected fibroblasts in addition to direct cell-cell interactions between NK and target cells was investigated.

4.6.1 NK cell degranulation is promoted by soluble cellular factors released by *T. cruzi*-infected fibroblasts

First, it was studied whether soluble cellular or parasitic factors released by *T. cruzi*-infected cells contribute to NK cell activation. To this end, NK cells were stimulated for 24 h with culture supernatants of mock and *T. cruzi*-infected human BJ fibroblasts or Vero81 cells, which are derived from African green monkey kidney cells (figure 4.13). Both cell types showed comparable infection kinetics and infection rates between 50% and 70% with an MOI of 3 when assessed by light microscopy (data not shown).

Figure 4.13 A shows a graphical modeling of the principle of the experiment, which should allow differentiation of the NK cell response against soluble cellular and parasitic factors. Activation of human NK cells with supernatants of infected BJ fibroblasts could theoretically be caused by both cellular and parasitic factors. Since Vero81 cells are not derived from humans, but from the African green monkey, it is assumed that human NK cell receptors cannot recognize cellular mediators secreted by Vero81. Therefore, it is likely, that activation of human NK cells by supernatants of infected Vero81 cells is induced solely by parasitic factors.

Following NK cell stimulation with the indicated culture supernatants, NK cell degranulation was examined by flow cytometric analysis of CD107a on the NK cell surface (figure 4.13 B). NK cell stimulation with supernatants from *T. cruzi*-infected BJ fibroblasts resulted in a significantly ($p \leq 0.05$) increased frequency of CD107a⁺ NK cells (median ~40%) compared to stimulation with supernatants from mock controls (median ~10%). However, the frequency of CD107a⁺ NK cells was 10 – 20% lower compared to NK cells directly cocultured with *T. cruzi*-infected BJ fibroblasts as observed in previous experiments (figure 4.3, 4.8 B and 4.12 B). In contrast to NK cell stimulation with BJ fibroblast supernatants, there were no differences in the frequency of CD107a⁺ NK cells after stimulation with supernatants from mock and *T. cruzi*-infected Vero81 cells.

Based on these results, it was concluded that soluble cellular factors secreted by *T. cruzi*-infected fibroblasts contribute to NK cell activation.

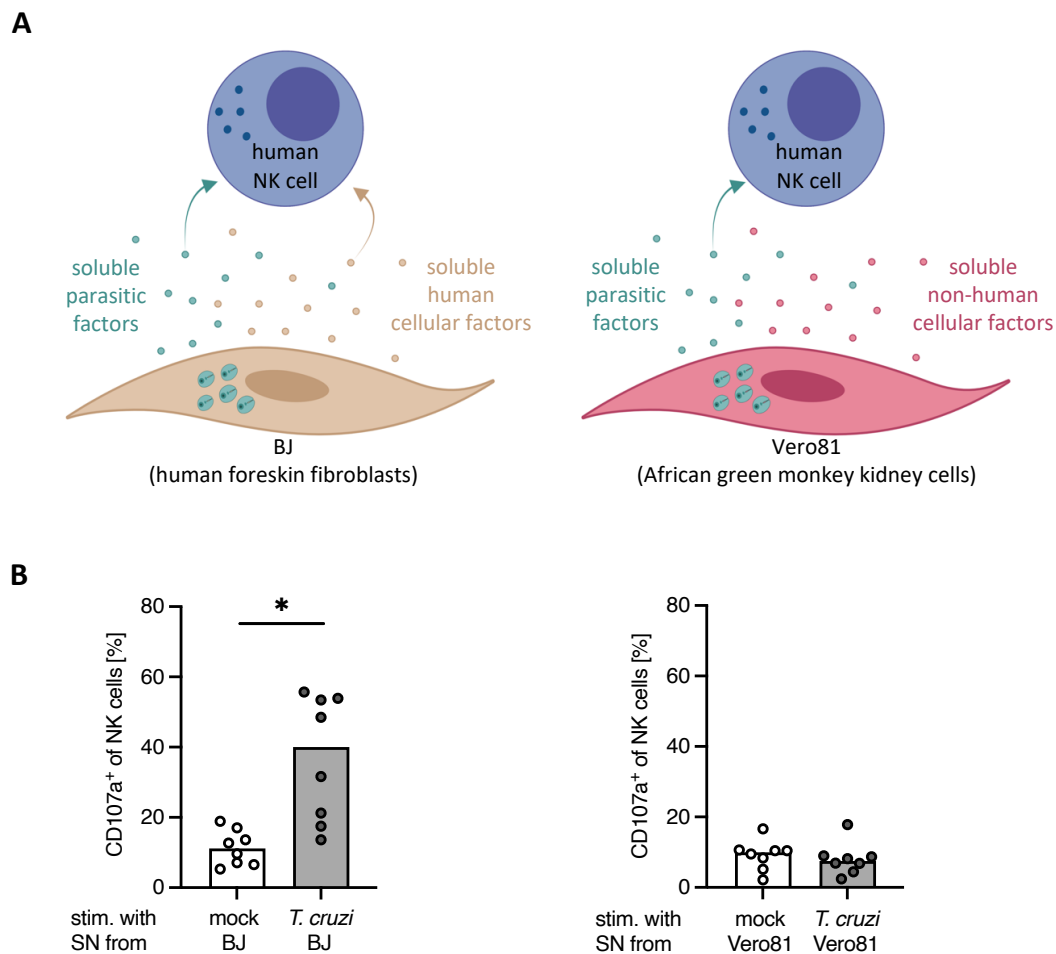


Figure 4.13: NK cells are stimulated by soluble cellular factors released by *T. cruzi*-infected fibroblasts. (A) Principle of the experiment to decipher whether NK cells are stimulated by soluble cellular or parasitic factors. Due to the human origin of BJ fibroblasts, activation of human NK cells with supernatants of infected BJ fibroblasts could potentially be induced by soluble parasitic and cellular factors. In contrast, Vero81 cells are not derived from humans, but from the African green monkey. Therefore, it is likely that human NK cell receptors cannot recognize cellular mediators secreted by Vero81, meaning that activation of human NK cells by supernatants of infected Vero81 cells can only be caused by parasitic factors. Created with Biorender.com. (B) Flow cytometric analysis of CD107a on the NK cell surface after 24 h stimulation with supernatants from mock and *T. cruzi*-infected BJ fibroblasts (left) and Vero81 cells (right). Supernatants were previously obtained from indicated cells cultured for 24 h in fresh culture medium between 24 and 48 hpi. NK cells from 8 healthy donors were stimulated. Respective medians are depicted by bars. After positive test for normal distribution, statistical significance was analyzed by paired t-test: * $p < 0.05$.

4.6.2 Fibroblasts secrete interferons in response to *T. cruzi* infection

The next step was to identify cellular factors secreted by fibroblasts infected with *T. cruzi* that may trigger NK cell activation. In order to do this, RNA sequencing data from mock and *T. cruzi*-infected HDF and BJ fibroblasts, already utilized in section 4.2, were analyzed in more detail.

Here, a volcano plot with all 67×10^3 determined human genes was created. This enabled the identification of individual genes with statistically significant ($p \leq 0.05$) differential expression and a high fold change in response to *T. cruzi* infections (figure 4.14 A). Significantly downregulated genes with a \log_2 fold change ≤ -1 were marked red, whereas significantly upregulated genes with a \log_2 fold change ≥ 1 were marked green. Out of these, immunologically relevant genes were named in the plot. They were found exclusively within the significantly upregulated genes. This approach revealed the induction of a variety of IFN-related genes, such as the IFN-induced GTP-binding protein 1 (MX1) and 2 (MX2), the IFN-stimulated gene 15 (ISG15), the IFN-induced protein with tetratricopeptide repeats 2 (IFIT2), 3 (IFIT3) and 5 (IFIT5) as well as the IFN-induced transmembrane protein 1 (IFITM1), 2 (IFITM2) and 3 (IFITM3).

To gain detailed insights into the pathways induced by *T. cruzi* infection, an over-representation analysis of all significantly ($p \leq 0.05$) upregulated genes with a \log_2 fold change ≥ 1 was conducted using the web-based tool webgestalt.org [214]. The top 5 significantly (false discovery rate (FDR) ≤ 0.05) induced pathways are shown in figure 4.14 B. The pathways "IFN- α / β signaling" and "IFN signaling" showed the highest enrichment ratios, meaning the highest ratio between the number of observed genes and the expected number of genes within the indicated pathway. Besides that, analyzed genes were significantly enriched in the pathways "cell cycle", "cell cycle, mitotic" and "cytokine signaling in immune system" in response to *T. cruzi* infection.

Overall, transcriptome data showed induction of IFN signaling in response to *T. cruzi* infection in BJ fibroblasts as well as in HDF, indicating enhanced expression of IFNs by infected fibroblasts.

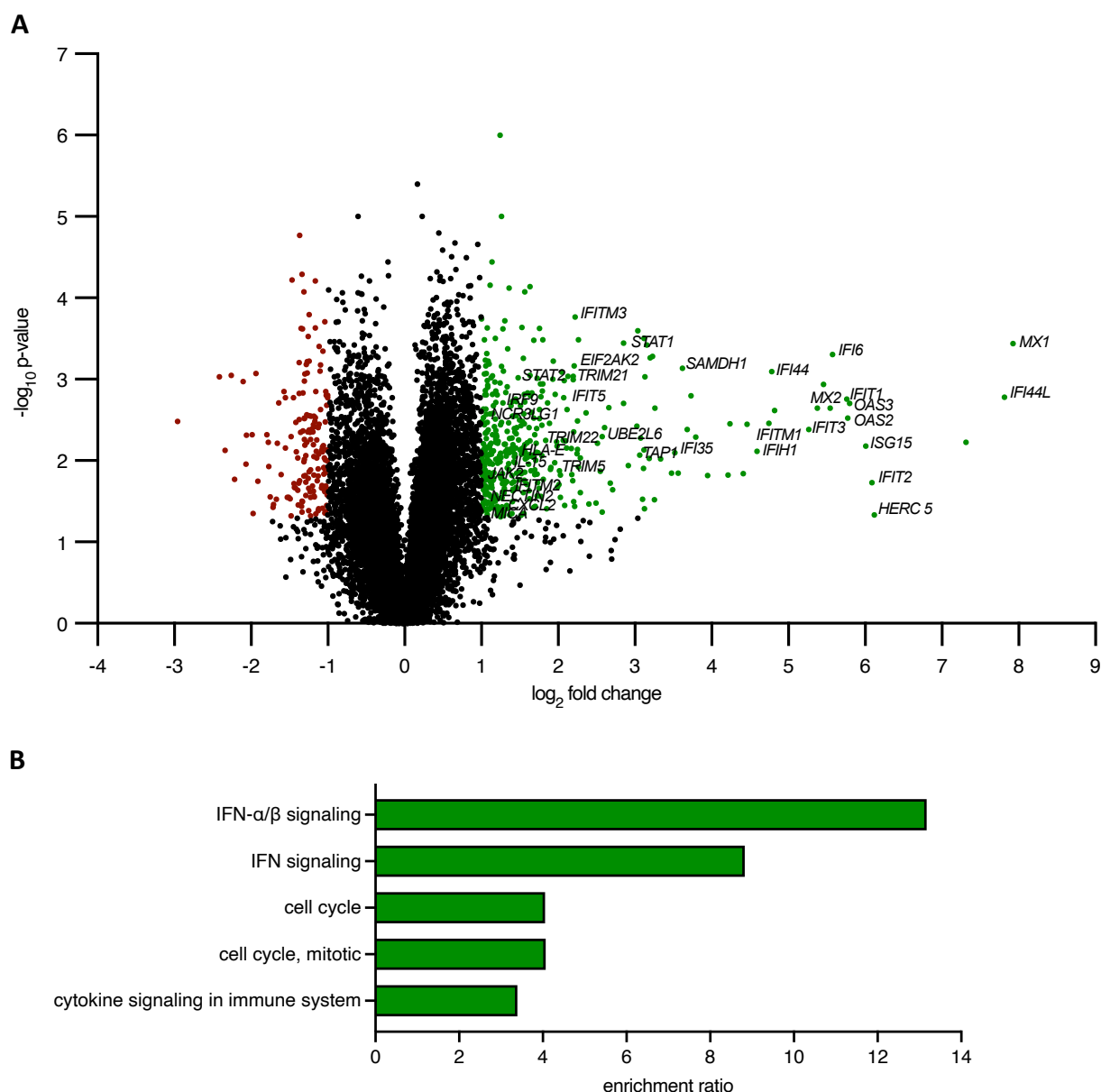


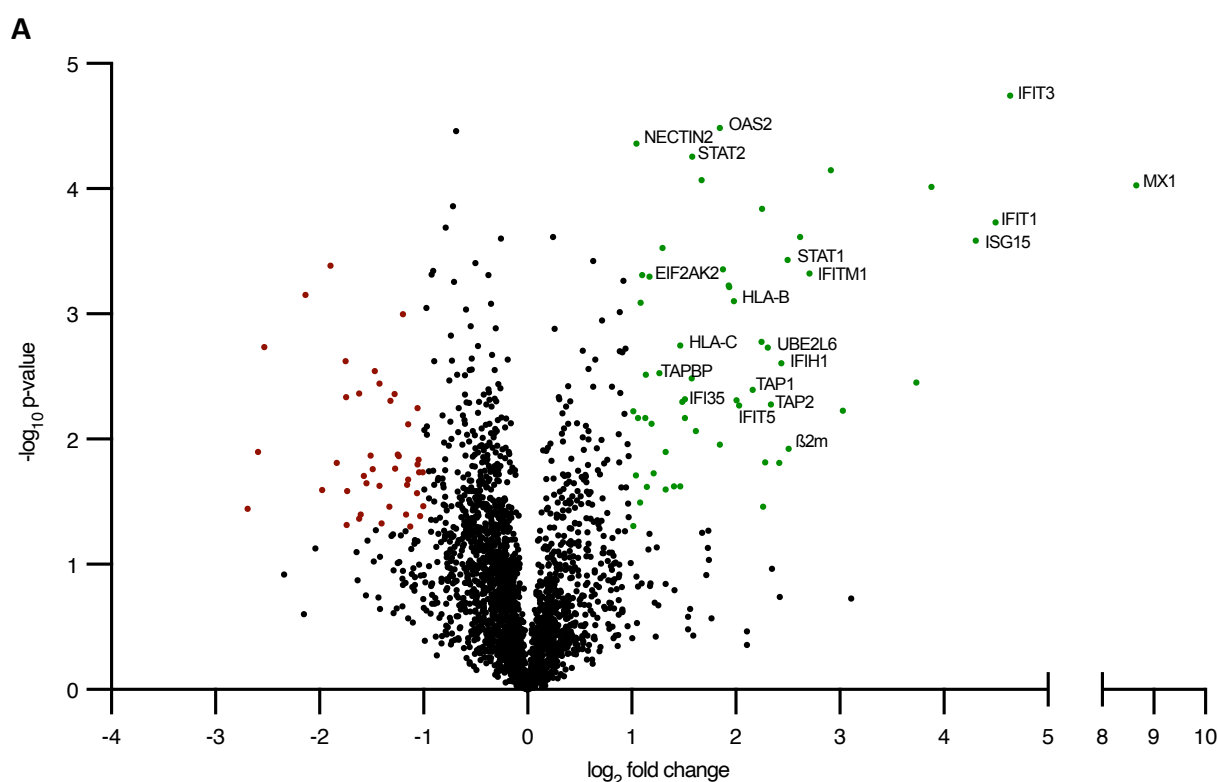
Figure 4.14: Transcriptome analysis of BJ fibroblasts and HDF reveals induction of IFN signaling in response to *T. cruzi* infection. RNA sequencing was performed using mock and *T. cruzi*-infected HDFs from 5 donors and BJ fibroblasts 48 hpi (MOI=3). **(A)** Volcano plot displaying the \log_2 fold change (x-axis) against the respective $-\log_{10}$ p-value calculated by paired t-test (y-axis) of all detected genes. Each gene is represented by a dot. Significantly ($p \leq 0.05$) downregulated genes with a \log_2 fold change of ≤ -1 are marked red. Significantly ($p \leq 0.05$) upregulated genes with a \log_2 fold change of ≥ 1 are marked green. Immunologically relevant genes are named. **(B)** Over-representation analysis of significantly upregulated genes ($p \leq 0.05$; \log_2 fold change of ≥ 1) was performed using the web-based tool webgestalt.org [214]. The top 5 pathways with $FDR \leq 0.05$ are depicted.

To corroborate transcriptional analysis results of HDF and BJ fibroblasts at protein level, mass spectrometric analysis was conducted. Due to the limited number of HDF, this analysis could only be performed with mock and *T. cruzi*-infected BJ fibroblasts. The resulting proteome data were evaluated analogously to the analysis of the transcriptome as described above.

Figure 4.15 A shows the generated volcano plot displaying all identified human 2.7×10^3 proteins, with red-marked significantly ($p \leq 0.05$) downregulated (\log_2 fold change ≤ -1) and green-marked significantly ($p \leq 0.05$) up-regulated proteins (\log_2 fold change ≥ 1). Of these, immunologically relevant differentially expressed proteins were designated. They were found solely within the group of significantly upregulated proteins. This illustration shows the clear induction of IFN-related proteins such as MX1, ISG15, IFIT1, IFIT3, IFIT5 as well as IFITM1.

Analogous to the transcriptome, an over-representation analysis was performed with all significantly ($p \leq 0.05$) up-regulated proteins with a \log_2 fold change of ≥ 1 to investigate signaling pathways induced at protein level. The top 5 significantly ($FDR \leq 0.05$) induced pathways are depicted in figure 4.15 B. The pathways "IFN- α - β signaling", "IFN- γ signaling" and "IFN signaling" showed the highest enrichment ratios indicating the induction of IFN-mediated processes at protein level. In addition, the pathways "cytokine signaling in immune system" and "immune system" were also induced in BJ fibroblasts in response to *T. cruzi* infection, but with lower enrichment ratios.

Thus, mass spectrometric analysis confirmed the induction of IFN signaling in fibroblasts in response to *T. cruzi* infection at protein level.



B

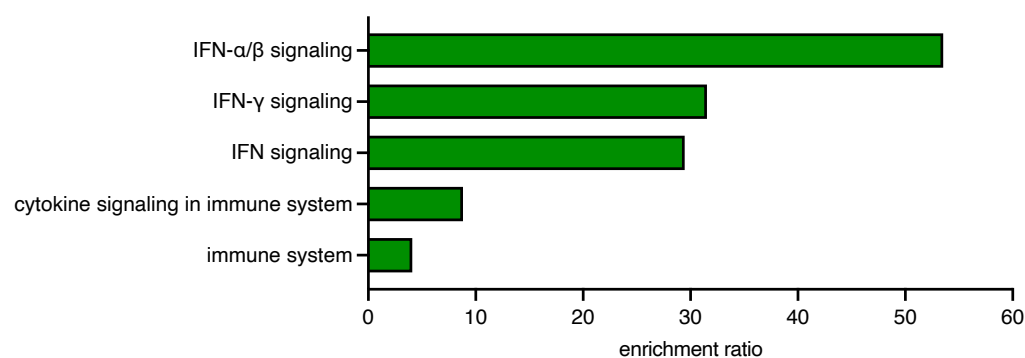


Figure 4.15: Proteome analysis of BJ fibroblasts confirms the induction of IFN signaling in response to *T. cruzi* infection. Mass spectrometric analysis of the proteome was performed using mock and *T. cruzi*-infected BJ fibroblasts 48 hpi (MOI=3). Samples were collected from 3 independent infections. (A) Volcano plot displaying the \log_2 fold change (x-axis) against the respective $-\log_{10}$ p-value calculated by unpaired t-test (y-axis) of all detected proteins. Each protein is represented by a dot. Significantly ($p \leq 0.05$) downregulated proteins with a \log_2 fold change of ≤ -1 are marked red. Significantly ($p \leq 0.05$) upregulated proteins with a \log_2 fold change of ≥ 1 are marked green. Immunologically relevant genes are named. (B) Over-representation analysis of significantly upregulated proteins ($p \leq 0.05$; \log_2 fold change of ≥ 1) was performed using the web-based tool webgestalt.org [214]. The top 5 pathways with $FDR \leq 0.05$ are depicted.

The increased IFN signaling in fibroblasts in response to *T. cruzi* infection revealed by transcriptome and proteomic analysis was indicative of increased IFN production.

Therefore, the secretion of IFN- α , - β , - γ as well as IFN- $\lambda 1$ and IFN- $\lambda 2/3$ by mock and *T. cruzi*-infected BJ fibroblasts during an infection kinetic between 24 and 72 hpi was studied using the LEGENDplex™ Human Interferon Panel (figure 4.16). IFN- α and IFN- γ were not detectable in any of the samples (data not shown). IFN- β as well as IFN- $\lambda 1$ and IFN- $\lambda 2/3$ were not detectable in the supernatants of mock controls, but were secreted by *T. cruzi*-infected fibroblasts with increasing intensity as the infection progressed.

Concentrations of the type I IFN IFN- β were significantly increased in the supernatant of infected BJ fibroblasts 48 hpi ($p \leq 0.05$) and 72 hpi ($p \leq 0.01$) compared to the respective mock controls. Whereas 48 hpi around 70 pg/ml IFN- β were found in the supernatant, the concentration increased to approximately 550 pg/ml at 72 hpi.

Of the type III IFNs, IFN- $\lambda 1$ was most strongly induced by *T. cruzi* infection. Its concentration was significantly ($p \leq 0.01$) increased in the supernatants of infected BJ fibroblasts 48 and 72 hpi. Approximately 140 pg/ml IFN- $\lambda 1$ were detected in the supernatant from BJ fibroblasts 48 hpi, whereas around 350 pg/ml were measured 72 hpi. Moreover, at 72 hpi, significantly ($p \leq 0.01$) increased IFN- $\lambda 2/3$ concentrations were measured in the supernatants of infected BJ fibroblasts, at about 110 pg/ml.

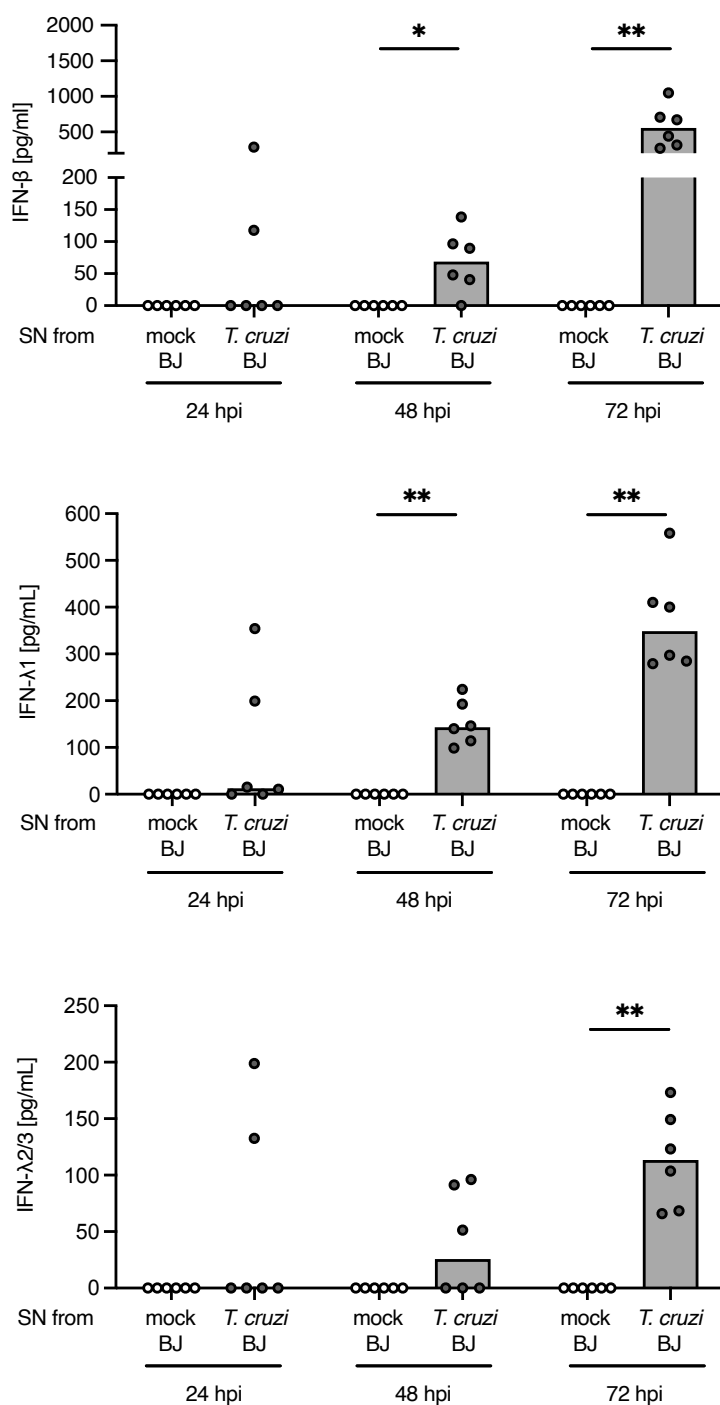


Figure 4.16: Type I IFN IFN-β and type III IFN IFN-λ1 and IFN-λ2/3 are secreted by BJ fibroblasts after *T. cruzi* infection. Concentration of type I, II and III IFNs in the culture supernatant of mock and *T. cruzi*-infected fibroblasts 48 hpi (MOI=3) were determined via LEGENDplex™ Human Interferon Panel. Measured concentrations of IFN-β, IFN-λ1 and IFN-λ2/3 are shown. Not detectable values were set as 0. Bars display respective medians (n=6). After negative test for normal distribution, statistical significances were calculated by Mann-Whitney test: * p<0.05; ** p<0.01.

4.6.3 IFN- β secreted by *T. cruzi*-infected fibroblasts contributes to increased NK cell activation

Previous results showed, first, that soluble cellular factors secreted by *T. cruzi*-infected BJ fibroblasts promote NK cell cytotoxicity, and second, that *T. cruzi*-infected BJ fibroblasts secrete IFNs such as IFN- β . Since the type I IFNs IFN- α and IFN- β have been shown to enhance NK cell cytotoxicity [128], [129], the effect of IFN- β secreted by infected BJ fibroblasts on NK cell degranulation was investigated below.

To this end, culture supernatants from mock and *T. cruzi*-infected BJ fibroblasts were harvested 48 hpi and treated with the IFN- β neutralizing antibody clone IFNb/A1 [215] or an IgG1 isotype control. Afterwards, the respective supernatants were used for a 24 h NK cell stimulation. The subsequent flow cytometric analysis of the NK cell degranulation via the presence of CD107a on the NK cell surface (figure 4.17) showed no impact of IFN- β neutralization on the NK cell response against the mock-treated BJ fibroblasts.

In contrast, a significantly ($p \leq 0.001$) lower frequency of CD107a⁺ NK cells was observed after stimulation with supernatants from *T. cruzi*-infected BJ fibroblasts when IFN- β was neutralized. The median frequency decreased from approximately 37% to around 26%. However, frequency of CD107a⁺ NK cells was not reduced to the level of mock controls, which was about 8%.

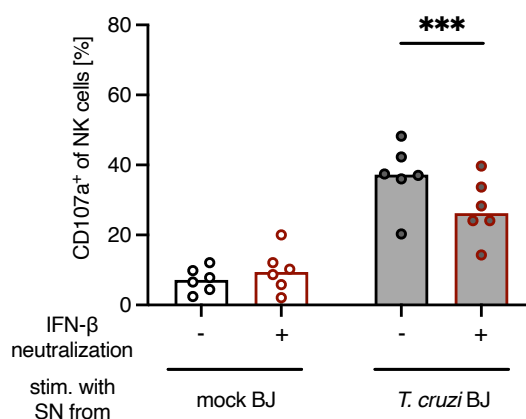


Figure 4.17: IFN- β secreted by *T. cruzi*-infected BJ fibroblasts contributes to increased NK cell activation. Flow cytometric analysis of CD107a on the NK cell surface after 24 h stimulation with supernatants from mock and *T. cruzi*-infected BJ fibroblasts (MOI=3) without and with IFN- β neutralization by antibody clone IFNb/A1. Supernatants were previously obtained from indicated BJ fibroblasts cultured for 24 h in fresh culture medium between 24 and 48 hpi. NK cells from 6 healthy donors were stimulated. Respective medians are depicted by bars. After positive test for normal distribution, statistical significances were calculated by paired t-test: *** $p \leq 0.001$.

4.7 NK cell response against *T. cruzi*-infected fibroblasts is inhibited by the engagement of KIR2DL molecules

In addition to mechanisms of NK cell stimulation, it was investigated whether *T. cruzi*-infected fibroblasts inhibit NK cell activity through the engagement of inhibitory NK cell receptors. In a previous part of the present study, increased expression of MHC-I was found after *T. cruzi* infection (figure 4.4 B). These data were confirmed by transcriptome and proteome analysis. Here, an upregulated expression of β_2m , Transporter associated with antigen processing 1 (TAP1) and 2 (TAP2) as well as TAP binding protein (TAPBP) was revealed (figure 4.14 A and 4.15 A). Whereas β_2m is a component of MHC-I molecules, TAP1, TAP2 and TAPBP are involved in the peptide loading process of MHC-I molecules, which is essential for their transport to the cell surface [216]. Therefore, increased expression of these molecules also suggests an increased presence of MHC-I molecules on the cell surface.

Based on these previous results, the interaction of mock and *T. cruzi*-infected BJ fibroblasts with their primary corresponding NK cell receptors, the inhibitory KIRs, was investigated. Here, the focus was set on the MHC-I molecule HLA-C, since a previous publication has already determined a relation between the composition of different HLA-C corresponding KIRs and the progression of Chagas disease [217].

4.7.1 Increased expression of the KIR ligand HLA-C on fibroblasts in response to *T. cruzi* infection

RNA sequencing data from mock and *T. cruzi*-infected HDF and BJ fibroblasts showed a tendency ($p=0.06$) towards increased expression of the *HLA-C* gene, which encodes for the HLA-C α -chain, in response to the infection at 48 hpi (figure 4.18). Although 3 out of 5 studied donors clearly exhibited a lower basal *HLA-C* gene expression than BJ fibroblasts, the infection-related increase in expression was comparable. Whereas the different HDF donors showed an increase of 225 – 500%, BJ fibroblasts exhibited an increase of 315%, reaching an *HLA-C* gene expression of around 500 RPKM. Based on these results, further analyses were performed using BJ fibroblasts.

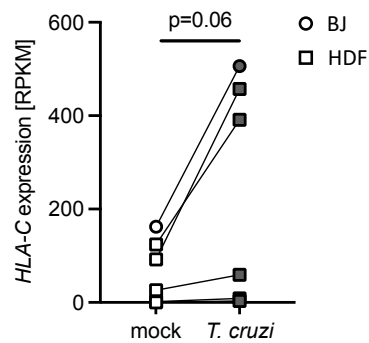


Figure 4.18: Transcriptome analysis confirms increased HLA-C expression in BJ fibroblasts and HDF in response to *T. cruzi* infection. RNA sequencing was performed using mock and *T. cruzi*-infected HDFs and BJ fibroblasts 48 hpi (MOI=3). RPKM values display *HLA-C* gene expression of BJ fibroblasts and 5 HDF donors. After positive test for normal distribution, statistical significance was analyzed by paired t-test.

The HLA-C protein expression was examined in the course of a *T. cruzi* infection between 24 and 72 hpi using flow cytometric analysis (figure 4.19). Gating was performed based on FMO controls, as depicted in the representative histogram on the left. In the mock controls, HLA-C could be detected in approximately 20% of BJ fibroblasts. While no infection-mediated effect was visible at 24 hpi, an increase in the frequency of HLA-C⁺ BJ fibroblasts to about 60% was detectable at 48 hpi. This frequency increased further to around 72% at 72 hpi. The infection-induced increase in HLA-C expression was highly significant ($p \leq 0.0001$) at both time points.

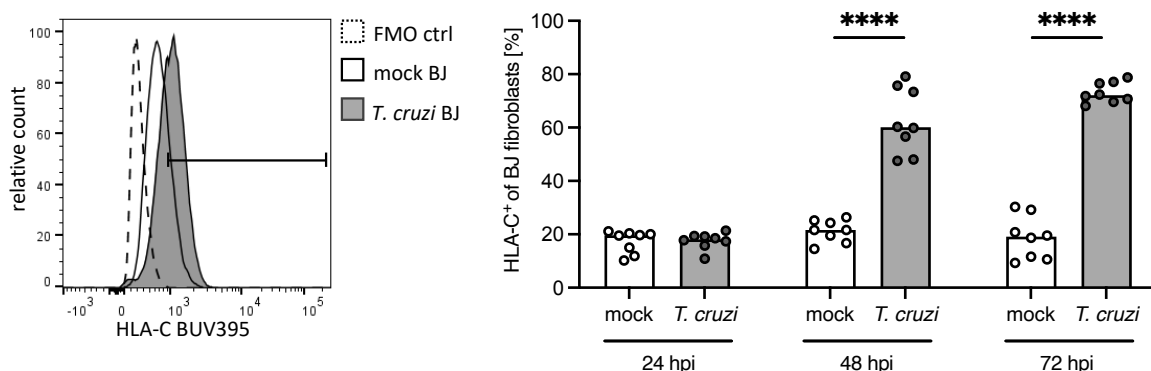


Figure 4.19: Expression of HLA-C is increased on the surface of BJ fibroblasts during the course of *T. cruzi* infection. Flow cytometric analysis of HVEM on mock and *T. cruzi*-infected BJ fibroblasts (MOI=3). Left: representative histogram at 48 hpi. Right: frequency of HLA-C⁺ BJ fibroblasts over the course of infection (24, 48 and 72 hpi). Bars display respective medians (n=8). After positive test for normal distribution, statistical differences were calculated by unpaired t-test with Welch's correction: **** $p \leq 0.0001$.

4.7.2 Increased HLA-C expression is mediated by soluble factors like IFN- β released by *T. cruzi*-infected fibroblasts

In addition, it was investigated whether an increase in HLA-C expression is induced by cell intrinsic processes of infected fibroblasts or whether soluble factors secreted by infected fibroblasts influence the HLA-C expression.

To this end, BJ fibroblasts were treated with culture supernatants from mock and *T. cruzi*-infected BJ fibroblasts from the indicated time points for 24 h (figure 4.20). Treatment with supernatants from infected BJ fibroblasts from all time points resulted in significantly increased HLA-C expression. The treatment with supernatant from infected fibroblasts from 24 hpi induced a mild increase in the frequency of HLA-C⁺ fibroblasts from around 18% in the mock controls to approximately 25% ($p \leq 0.001$). In contrast, treatment with supernatants of infected fibroblasts from 48 and 72 hpi caused a greater increase in HLA-C expression to around 52 and 56%, respectively ($p \leq 0.001$). This increased HLA-C expression after treatment with supernatants from infected fibroblasts was comparable to the increased HLA-C expression after direct infection, indicating an induction of HLA-C by soluble factors released by infected fibroblasts.

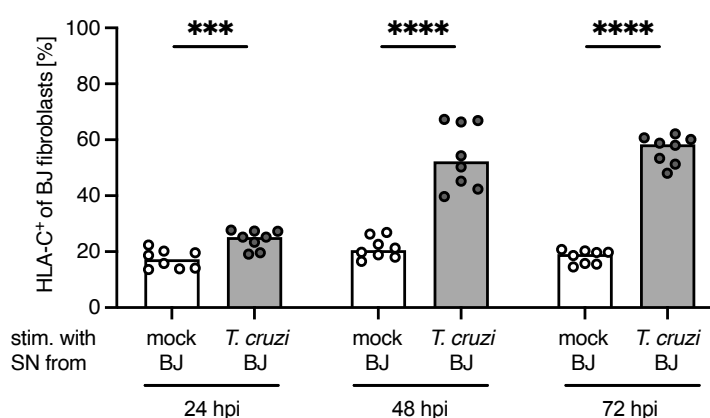


Figure 4.20: Increased HLA-C expression is mediated by soluble factors released by *T. cruzi*-infected BJ fibroblasts. Pre-seeded BJ fibroblasts were treated with parasite-free supernatants from mock and *T. cruzi*-infected BJ fibroblasts from indicated time points (24, 48 or 72 hpi; MOI=3) for 24 h and analyzed for HLA-C expression by flow cytometry. Bars display respective medians (n=8). After positive test for normal distribution, statistical differences were calculated by unpaired t-test with Welch's correction: *** $p \leq 0.001$; **** $p \leq 0.0001$.

IFN- β has been shown to increase MHC-I expression in synovial fibroblasts [127]. Since previous results of the present study revealed IFN- β secretion by *T. cruzi*-infected BJ fibroblasts, the effect of secreted IFN- β on HLA-C and overall MHC-I (HLA-A,B,C) expression

on BJ fibroblasts was examined (figure 4.21). To this end, culture supernatants from mock and *T. cruzi*-infected BJ fibroblasts were harvested 48 hpi and treated with the IFN- β neutralizing antibody clone IFNb/A1 or the respective IgG1 isotype control. Subsequently, the supernatants were used for a 24 h stimulation of pre-seeded BJ fibroblasts. The following flow cytometric analysis showed no impact of IFN- β neutralization on the HLA-C expression of fibroblasts treated with supernatants from mock controls (figure 4.21 left). In contrast, it revealed significantly ($p \leq 0.0001$) lower frequencies of HLA-C⁺ BJ fibroblasts after stimulation with supernatant from *T. cruzi*-infected fibroblasts treated with IFN- β -neutralizing antibody (median ~45%) compared to the isotype control (median ~55%). Accordingly, the infection-related increase in HLA-C expression was reduced by about 30%.

Regarding the general MHC-I expression (figure 4.21 right), IFN- β neutralization resulted in significantly reduced normalized MFIs of HLA-A,B,C on fibroblasts treated with supernatants from *T. cruzi*-infected BJ fibroblasts as well as the mock controls. When fibroblasts were stimulated with supernatants from mock-treated fibroblasts, the IFN- β neutralization caused a significant ($p \leq 0.05$) reduction of approximately 5%. In contrast, when fibroblasts were stimulated with supernatants from *T. cruzi*-infected fibroblasts, HLA-A,B,C expression was significantly ($p \leq 0.0001$) reduced by around 35% when IFN- β was neutralized.

These results suggest a contribution of IFN- β to the *T. cruzi* infection-mediated increase of MHC-I molecules such as HLA-C.

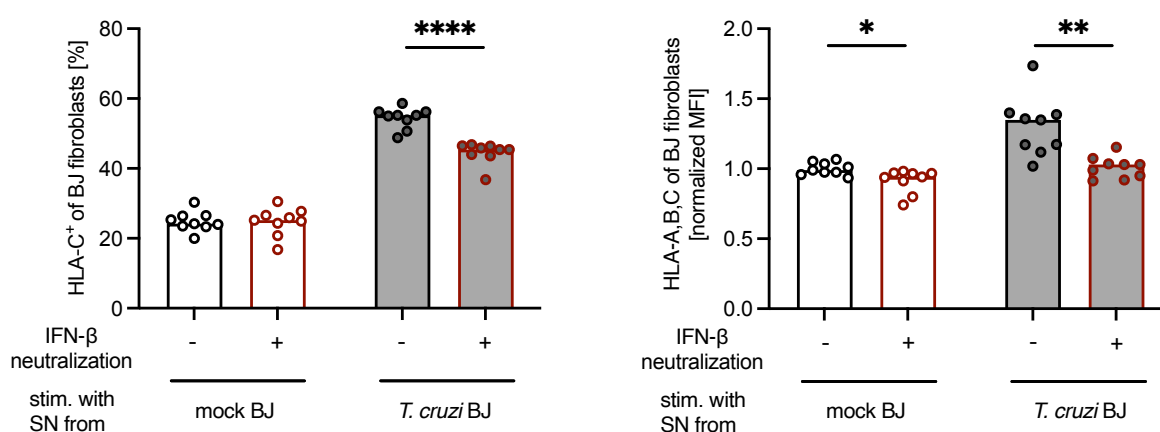


Figure 4.21: IFN- β secreted by *T. cruzi*-infected BJ fibroblasts contributes to increase of MHC-I molecules such as HLA-C. Pre-seeded BJ fibroblasts were treated with parasite-free supernatants from mock and *T. cruzi*-infected BJ fibroblasts (48 hpi; MOI=3) without and with IFN- β neutralization by antibody clone IFNb/A1. Supernatants were previously obtained from indicated BJ fibroblasts cultured for 24 h in fresh culture medium between 24 and 48 hpi. Left: frequency of HLA-C⁺ BJ fibroblasts. Right: normalized MFI of HLA-A,B,C. MFI values were normalized to the average MFI of all mock controls. Bars display respective medians (n=9). After negative test for normal distribution, statistical differences were calculated by Mann-Whitney test: * $p \leq 0.05$; ** $p \leq 0.01$; **** $p \leq 0.0001$.

4.7.3 Increased binding of KIR2DL1 and KIR2DL2 to *T. cruzi*-infected fibroblasts

Following the determination of HLA-C expression in response to *T. cruzi* infection, the binding of the corresponding inhibitory KIRs to infected BJ fibroblasts and mock controls was investigated. To this end, Fc receptor binding assays were performed 48 hpi. HLA-C genotyping of BJ fibroblasts showed heterozygosity for HLA-C1 and HLA-C2 (data not shown). Therefore, the binding of KIR2DL1, which primarily interacts with HLA-C2 allotypes, and KIR2DL2, which primarily binds to HLA-C1 allotypes [62], were examined (figure 4.22). As depicted in the representative histograms on the left side, gates were set using controls stained with secondary antibodies, without prior treatment with the respective receptor-Fc molecule. KIR2DL1-Fc molecules were bound by about 20% of the mock infected BJ fibroblasts. The frequency was significantly ($p \leq 0.0001$) increased in response to *T. cruzi* infection to approximately 72%. KIR2DL2-Fc molecules were bound by about 9% of mock controls, whereas the percentage increased significantly ($p \leq 0.0001$) to 63% in response to *T. cruzi* infection.

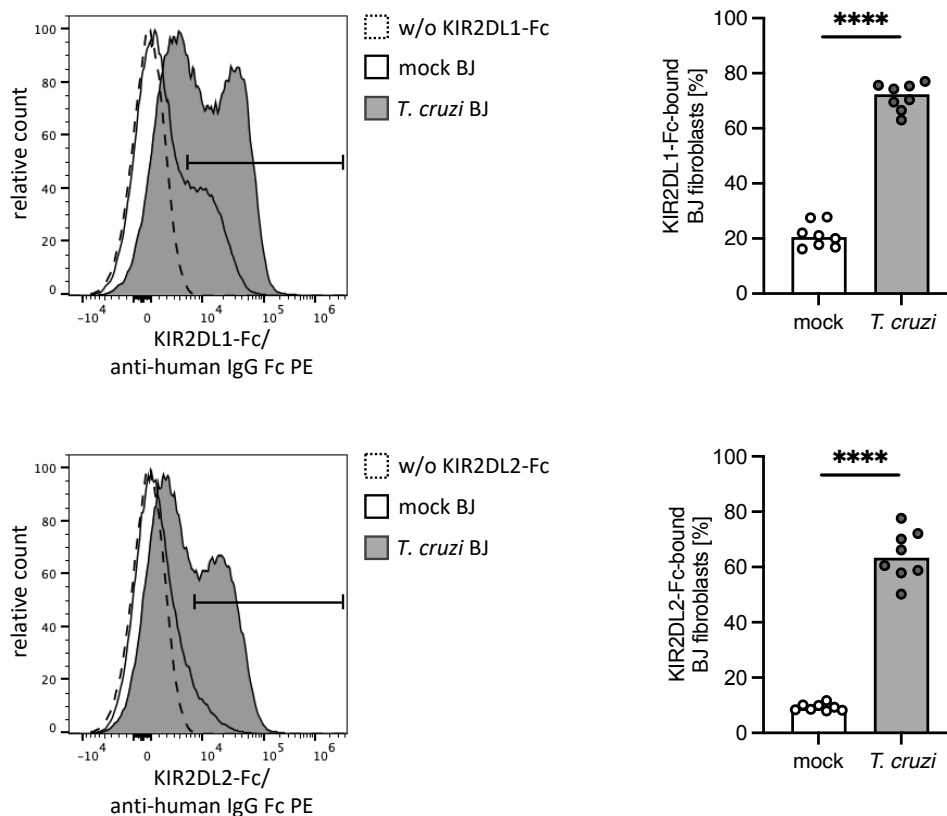


Figure 4.22: Binding of KIR2DL1 and KIR2DL2 to BJ fibroblasts is increased after *T. cruzi* infection. Receptor binding assay was conducted with mock or *T. cruzi*-infected BJ fibroblasts 48 hpi (MOI=3) using KIR2DL1-Fc (above) and KIR2DL2-Fc (below) chimera molecules and anti-human IgG Fc secondary antibody with subsequent flow cytometric analysis. Left: representative histograms at 48 hpi. Right: frequencies of KIR2DL1-Fc or KIR2DL2-Fc-bound BJ fibroblasts, respectively. Bars display respective medians (n=8). After positive test for normal distribution, statistical differences were calculated by unpaired t-test with Welch's correction: **** p<0.0001.

4.7.4 Generation of HLA-C KO BJ fibroblasts

Next, the impact of the *T. cruzi* infection-induced increased fibroblast HLA-C expression on NK cell activation was investigated. To this end, an HLA-C KO was generated in BJ fibroblasts using CRISPR/Cas9 technology (figure 4.23 A). To this end, predesigned HLA-C KO and HDR plasmids were cotransfected, resulting in a Cas9-induced double-strand break and HLA-C target gene replacement against an RFP and a puromycin resistance gene by homologous recombination.

After selection of puromycin-resistant RFP⁺ fibroblasts that showed no HLA-C expression after IFN- γ stimulation, single-cell clones were generated and tested for their HLA-C and overall MHC-I (HLA-A,B,C) expression in response to *T. cruzi* infection. This, on the one hand, was to confirm the successful HLA-C KO in the context of *T. cruzi* infection, and on the other hand, exclude the impairment of MHC-I, as well as HLA-C, through possible off-target effects during the CRISPR/Cas9-mediated KO. Figure 4.23 B depicts the results of flow cytometric analysis of wildtype (WT) BJ fibroblasts and HLA-C KO single-cell clone #8, which was selected for further analyses. Compared to WT controls, the selected HLA-C KO fibroblasts exhibited only mild background HLA-C staining, with no difference between *T. cruzi*-infected HLA-C KO fibroblasts and the corresponding mock controls. Additionally, the selected HLA-C KO fibroblasts showed no impairment of the total MHC-I expression.

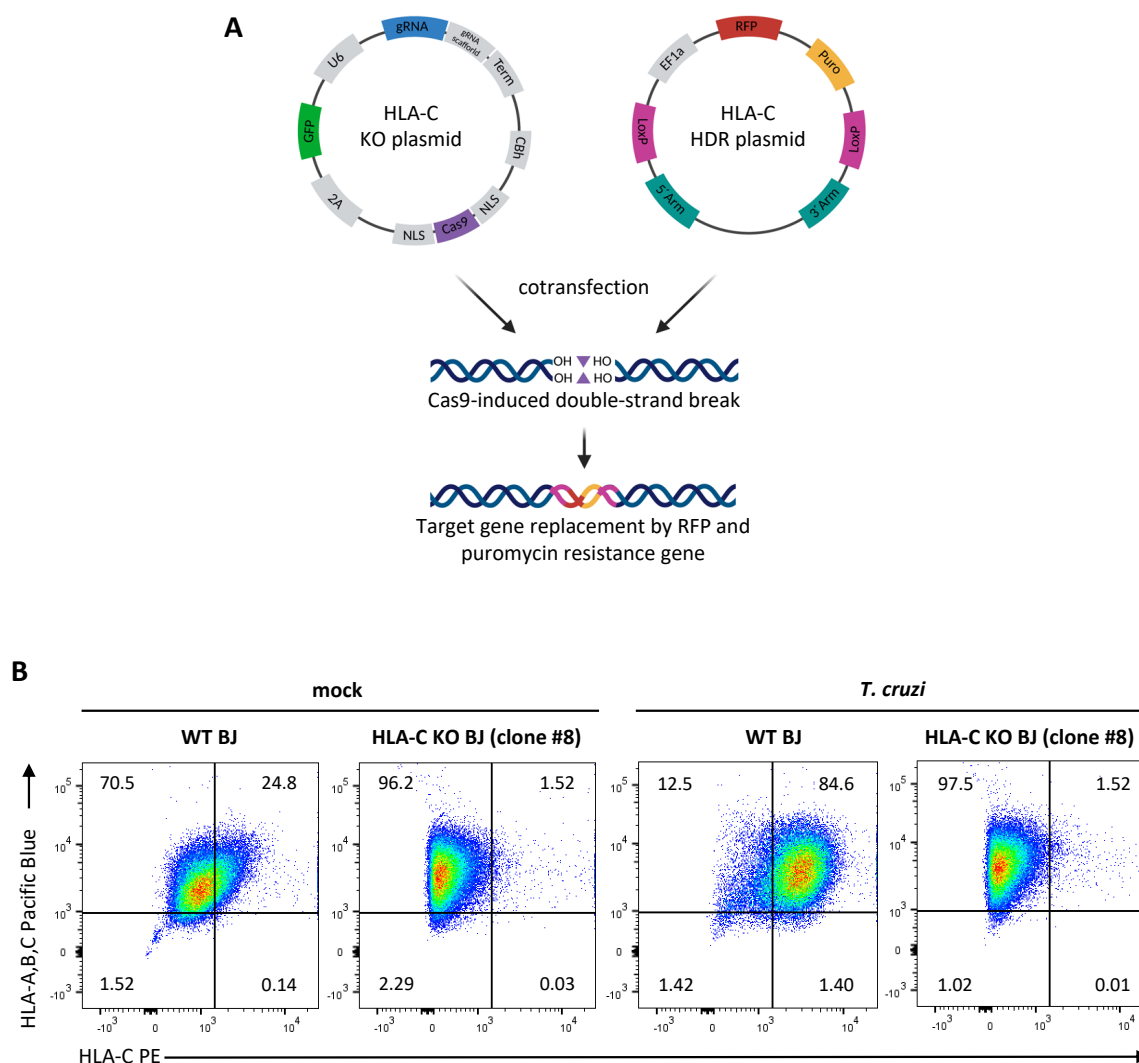


Figure 4.23: Generation of HLA-C KO BJ fibroblasts using CRISPR/Cas9 technology. (A) Scheme illustrating the cotransfection of HLA-C KO and HDR plasmids for the generation of a Cas9-induced double-strand break and HLA-C target gene replacement against an RFP and a puromycin resistance gene by homologous recombination. Created with biorender.com based on manufacturer's information. (B) Flow cytometric analysis of mock and *T. cruzi*-infected WT BJ fibroblasts and the selected HLA-C KO single-cell clone that was used for following experiments. The expression of HLA-C and of all classical MHC-I molecules (HLA-A,B,C) is depicted in representative plots.

In order to verify that the HLA-C KO of the selected clone was functional, the binding of the KIRs corresponding to HLA-C2 and HLA-C1, KIR2DL1 and KIR2DL2, respectively, was investigated using receptor-Fc binding assays (figure 4.24). The binding of KIR2DL1-/KIR2DL2-Fc molecules was compared for mock and *T. cruzi*-infected WT and HLA-C KO fibroblasts.

Under all tested conditions, KIR2DL1 and KIR2DL2-Fc binding to HLA-C KO fibroblasts was significantly ($p \leq 0.0001$) reduced compared to WT control. In contrast to WT BJ fibroblasts, no binding of KIR2DL1-Fc molecules by HLA-C KO fibroblasts was detectable. Furthermore, the

selected HLA-C KO fibroblasts exhibited a significantly reduced binding of KIR2DL2-Fc molecules compared to the WT controls. Whereas no binding of KIR2DL2-Fc molecules was detected for mock-infected HLA-C KO fibroblasts, approximately 2% of *T. cruzi*-infected HLA-C KO fibroblasts were bound by KIR2DL2-Fc molecules. However, KIR2DL2-Fc binding was reduced by more than 20-fold compared to the infected WT fibroblasts.

The HLA-C KO was thus considered as functional and the cells were used for subsequent analyses.

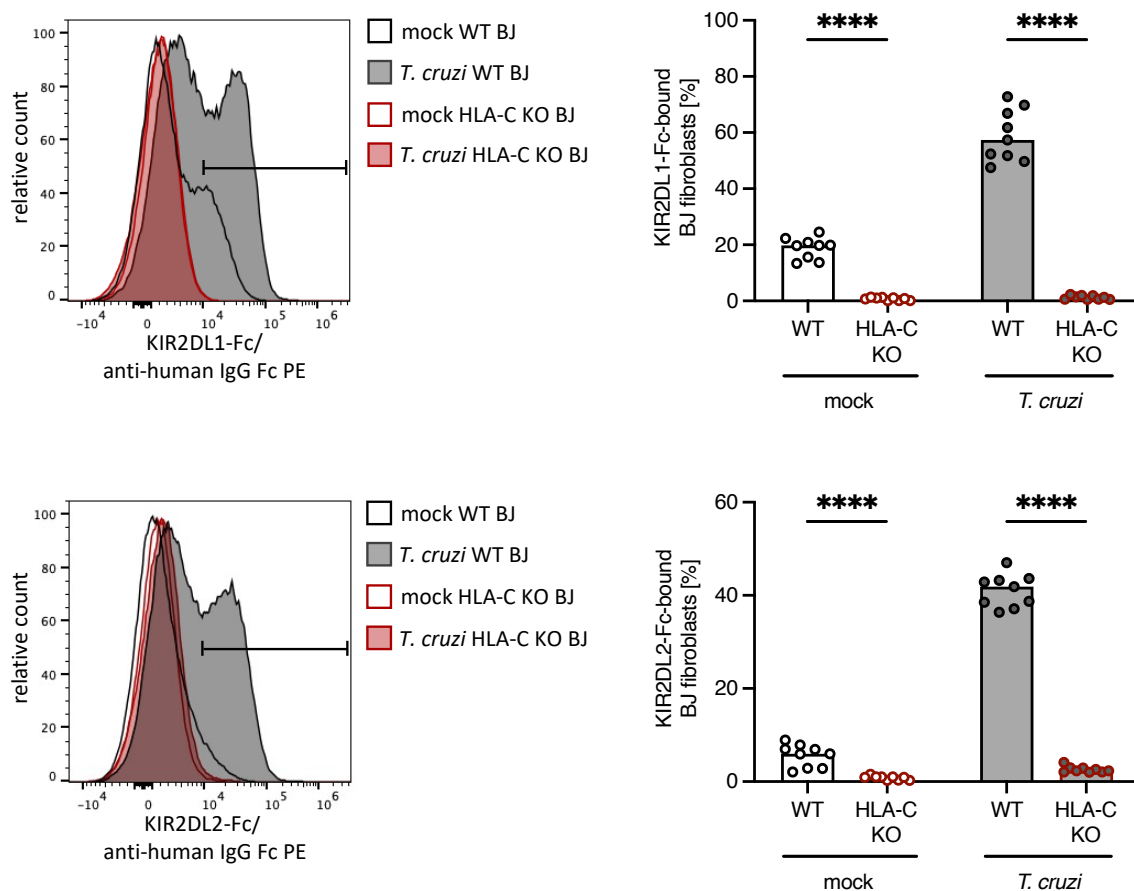


Figure 4.24: Successful HLA-C KO was confirmed by missing or strongly reduced binding of KIR2DL1 and KIR2DL2 to the selected HLA-C KO BJ fibroblast clone. Receptor binding assay was conducted with mock or *T. cruzi*-infected WT and HLA-C KO BJ fibroblasts 48 hpi (MOI=3) using KIR2DL1-Fc (above) and KIR2DL2-Fc (below) chimera molecules and anti-human IgG Fc secondary antibody. Left: representative histograms at 48 hpi. Right: frequencies of KIR2DL1-Fc or KIR2DL2-Fc-bound BJ fibroblasts, respectively. Bars display respective medians (n=8). After positive test for normal distribution, statistical differences were calculated by unpaired t-test with Welch's correction: **** $p < 0.0001$.

4.7.5 HLA-C expressed on fibroblasts reduces the NK cell response during coculture

Using the generated HLA-C KO BJ fibroblasts, the impact of upregulated HLA-C expression in response to *T. cruzi* infection was examined in terms of its effect on NK cell activation (figure 4.20). In this context, the genotype of the corresponding KIRs of all studied donors was determined (figure 4.25 A). This should subsequently allow conclusions to be drawn about possible differential effects of HLA-C KOs on the response of NK cells from different donors.

Afterwards, coculture experiments of NK cells with mock or *T. cruzi*-infected WT or HLA-C KO fibroblasts were performed to determine NK cell degranulation by flow cytometric analysis of CD107a (figure 4.25 B). NK cells cocultured with mock-treated HLA-C fibroblasts displayed a high spread in the presence of CD107a on the cell surface. No significant effect of the HLA-C KO could be detected. Coculture with *T. cruzi*-infected HLA-C KO fibroblasts resulted in a slightly but significantly ($p \leq 0.05$) higher frequency of CD107a⁺ NK cells (median ~62%) compared to the coculture with infected WT fibroblasts (median ~54%).

Additional coculture experiments were performed to analyze the coculture supernatants and thus the effector molecules secreted by NK cells (figure 4.25 C), as previously described. Despite a high spread, a tendency towards increased release of all depicted analytes was detected after coculture with HLA-C KO fibroblasts compared to WT fibroblasts. This applied to both coculture with mock and *T. cruzi*-infected fibroblasts. The increased concentration of granzyme B and sFasL after coculture with mock-treated HLA-C KO fibroblasts was statistically significant, as was the increase of granzyme A, perforin, sFasL, and IFN- γ after coculture with *T. cruzi*-infected HLA-C KO fibroblasts compared to the respective WT controls ($p \leq 0.05$).

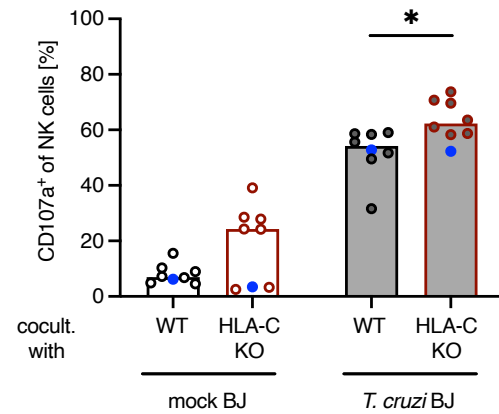
NK cells from donor A, highlighted in blue in figure 4.25, showed a different response to the HLA-C KO of fibroblasts compared to all other studied NK cell donors (figure 4.25 B and C). The response to mock-treated fibroblasts was rarely affected by the HLA-C KO. In contrast, donor A-derived NK cells responded to coculture with *T. cruzi*-infected fibroblasts when HLA-C was knocked out with lower secretion of granzyme B, granulysin and sFasL. Regarding the secretion of the other effector molecules and the frequency of CD107a⁺ NK cells, no change was observed through the KO of HLA-C on target cells. This NK cell donor uniquely exhibited the KIR genotype KIR2DL1⁺/2DL2⁻/2DL3⁺/2DS1⁺/2DS2⁻ (figure 4.25 A).

Collectively, these results suggest that upregulated HLA-C on fibroblasts in response to *T. cruzi* infection modulates the NK cell response depending on the KIR phenotype, leading to dampened NK cell activation in most cases.

A

NK cell donor	KIR 2DL1	KIR 2DL2	KIR 2DL3	KIR 2DS1	KIR 2DS2
A	+	-	+	+	-
B	+	-	+	-	-
C	+	-	+	-	-
D	+	+	+	+	+
E	+	+	+	-	+
F	+	+	+	+	+
G	+	-	+	-	-
H	+	-	+	-	-

B



To be continued on the next page.

4.7.6 Stimulatory effect of IFN- β on NK cell response tends to be predominant

Based on the previous results, IFN- β secreted by *T. cruzi*-infected BJ fibroblasts exhibits a bilateral effect on NK cell activity. On the one hand, secreted IFN- β directly promotes NK cell cytotoxicity (figure 4.17). On the other hand, it facilitates an increased HLA-C expression on BJ fibroblasts (figure 4.21). Coculture with WT and HLA-C KO BJ fibroblasts revealed a mainly inhibitory effect of HLA-C on the NK cell response (figure 4.25). Therefore, which of these two effects predominates was investigated here.

To this end, secreted IFN- β was neutralized by the antibody clone IFNb/A1 during coculture with mock and *T. cruzi*-infected BJ fibroblasts. All coculture experiments were performed using NK cells derived from donors with a KIR genotype that was associated with increased activation by HLA-C KO fibroblasts in comparison to WT controls (compare section 4.7.5). The determined genotypes for the corresponding KIRs are shown in figure 4.26 A. Coculture experiments without and with IFN- β neutralization were performed to determine NK cell degranulation by flow cytometric analysis of CD107a (figure 4.26 B). No significant differences in the frequency of degranulated NK cells were found as a result of IFN- β neutralization.

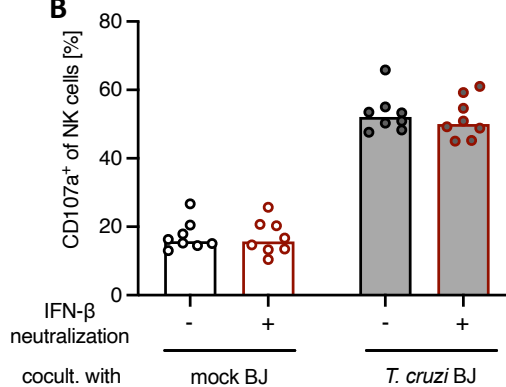
Subsequently, further coculture experiments were performed to analyze coculture supernatants for effector molecules secreted by NK cells (figure 4.26 C), as previously described. IFN- β neutralization resulted in a tendentially higher secretion of all studied analytes in response to coculture with mock-treated BJ fibroblasts. However, the spread was high and differences were not significant. In contrast, IFN- β neutralization led to lower concentrations of secreted NK cell effector molecules after coculture with *T. cruzi*-infected BJ fibroblasts. In the case of granzyme B, perforin, granulysin and sFasL, the effect was evident as a trend without statistical significance. The measured concentrations of granzyme A and IFN- γ were significantly lower ($p \leq 0.05$) when IFN- β was neutralized.

No differences in NK cell response were apparent with regard to the determined KIR genotype.

A

NK cell donor	KIR 2DL1	KIR 2DL2	KIR 2DL3	KIR 2DS1	KIR 2DS2
D	+	+	+	+	+
F	+	+	+	+	+
G	+	-	+	-	-
H	+	+	+	+	+
I	+	-	+	-	-
J	+	-	+	-	-
K	+	-	+	-	-
L	+	-	+	-	-

B



C

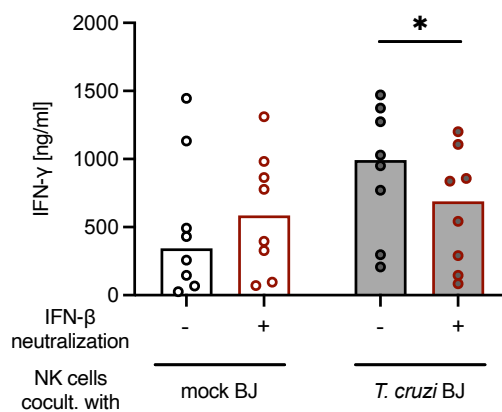
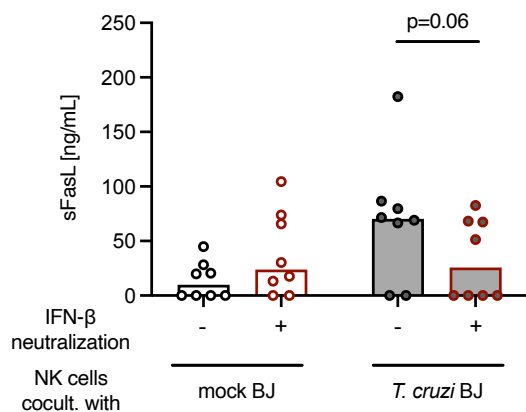
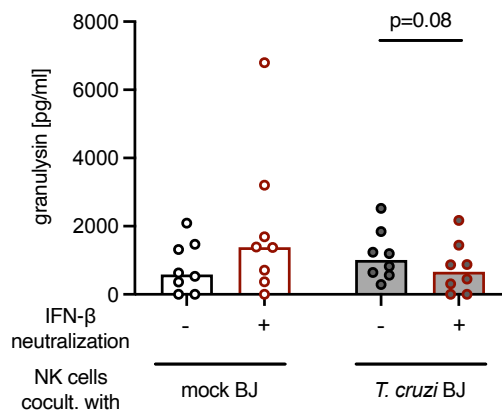
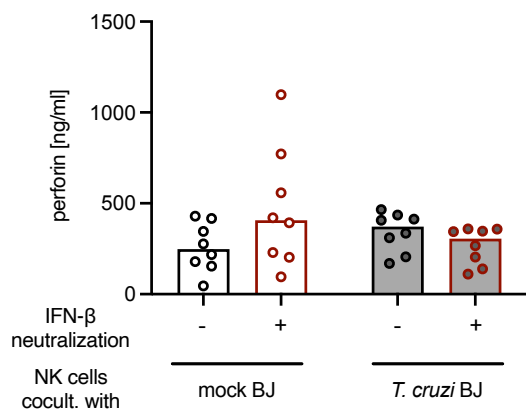
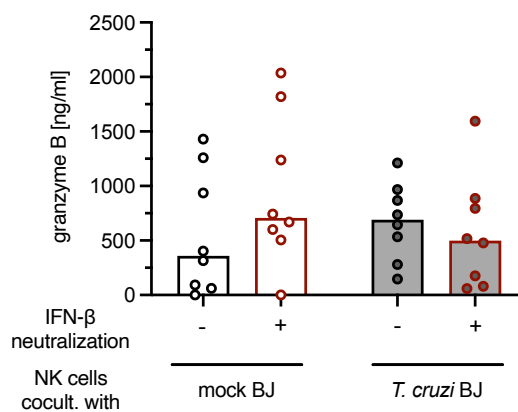
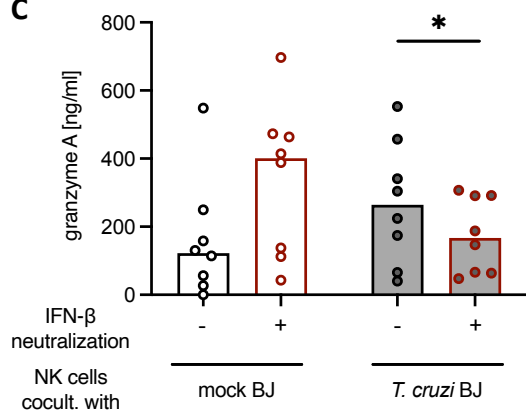


Figure 4.26: Despite the dual effect of IFN- β on the NK cell response to *T. cruzi*-infected BJ fibroblasts, the stimulatory effect tends to be predominant. (A) Genotype of KIRs of NK cell donors used for experiments. (B) Flow cytometric analysis of CD107a on the NK cell surface after coculture with mock and *T. cruzi*-infected BJ fibroblasts without and with IFN- β neutralization (antibody clone IFNb/A1). Cocultures were started 24 hpi (MOI=3) with an E:T ratio of 1:10 using NK cells derived from 8 healthy donors. Cells were cocultured for 24 h before flow cytometric analysis was performed. Respective medians are depicted by bars. After positive test for normal distribution, statistical significances were calculated by paired t-test: No statistically significant differences were found. (C) Analysis of supernatants after NK cell coculture with mock and *T. cruzi*-infected BJ fibroblasts without and with IFN- β neutralization. Cocultures were started 24 hpi (MOI=3) with an E:T ratio of 1:2.5 using NK cells derived from 8 healthy donors. Cells were cocultured for 24 h before concentrations of granzyme A, granzyme B, perforin, granulysin, sFasL and IFN- γ were determined using the Human CD8/NK Panel of the LEGENDplex™ kit. Outliers were identified by ROUT method and excluded. Respective medians are depicted by bars. After negative test for normal distribution, statistical significances were calculated by paired Wilcoxon test: * $p \leq 0.05$.

4.8 Nectin-2 and HLA-E are further potential modulators of the NK cell response against *T. cruzi*-infected fibroblasts

In addition to the mechanisms described above, two further potential modulators of the NK cell response against *T. cruzi*-infected fibroblasts were identified, both of which can interact with stimulatory as well as inhibitory NK cell receptors.

First, transcriptome analysis revealed a significantly ($p \leq 0.05$) increased expression of the *NECTIN2* gene in HDF and BJ fibroblasts in response to *T. cruzi* infection 48 hpi (figure 4.27 A). The gene expression increase ranged from approximately 60 to 270% in different HDF donors. In the case of BJ fibroblasts, *NECTIN2* gene expression was increased by around 140%.

Based on these results, nectin-2 protein expression was investigated by flow cytometric analyses of mock and *T. cruzi*-infected BJ fibroblasts 48 hpi (figure 4.27 B). Since almost all fibroblasts expressed nectin-2, as shown in the representative histogram on the left, the MFI, which indicates the expression intensity of nectin-2 molecules per cell, was evaluated. MFI values were normalized to the average MFI of all respective mock controls. The normalized nectin-2 MFI was significantly ($p \leq 0.0001$) increased by approximately 74% after *T. cruzi* infection compared to mock controls. Furthermore, it was investigated whether the increase in nectin-2 expression is induced by cell-intrinsic processes of infected fibroblasts or by soluble factors secreted by infected fibroblasts. To this end, pre-seeded BJ fibroblasts were treated with culture supernatants from mock or *T. cruzi*-infected BJ fibroblasts for 24 h (figure 4.27 C). This resulted in a significant ($p \leq 0.0001$) increase in normalized MFI after treatment with supernatants from infected BJ fibroblasts compared to mock controls. In this case, the normalized nectin-2 MFI was only increased by around 26%.

These data suggest an increased nectin-2 expression in dermal fibroblasts in response to *T. cruzi* infection that is at least partially mediated through soluble factors released by infected fibroblasts. The increased nectin-2 expression could potentially contribute to the modulation of the NK cell response by engaging the inhibitory receptors TIGIT and PVRIG or the activating receptor DNAM-1 on NK cells [50].

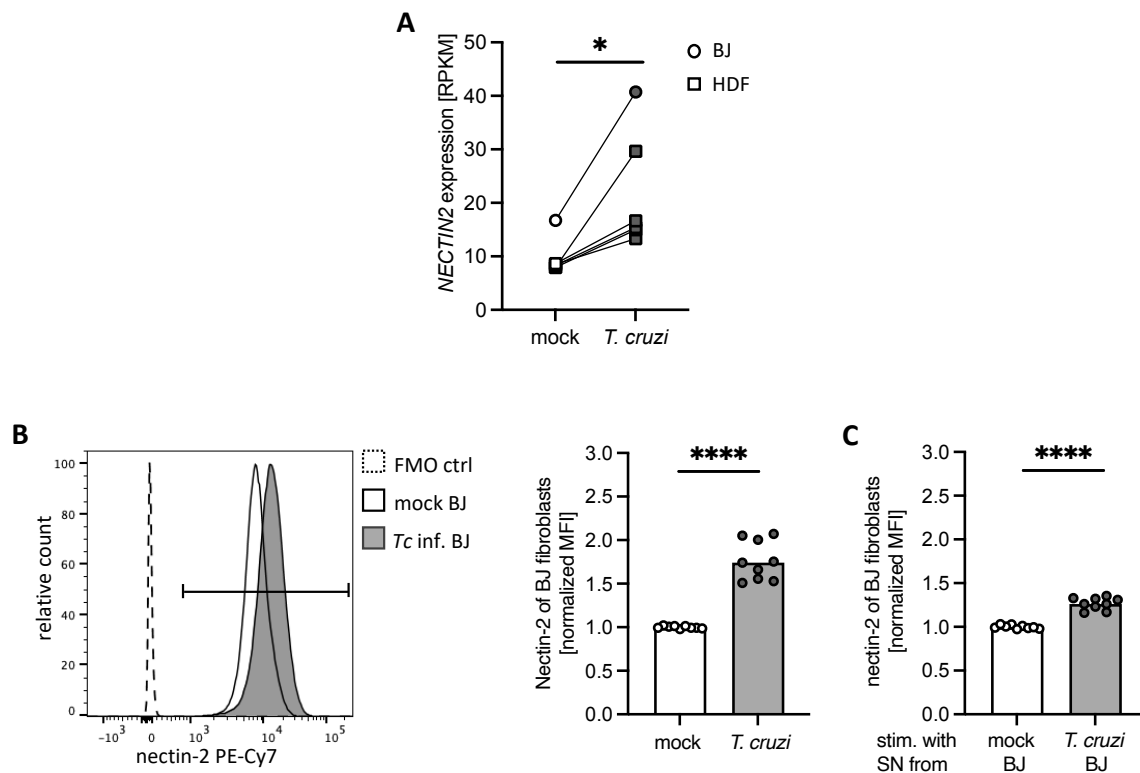


Figure 4.27: Dermal fibroblasts exhibit increased nectin-2 expression in response to *T. cruzi* infection. (A) Transcriptome analysis reveals an upregulated expression of the *NECTIN2* gene in HDF and BJ fibroblasts after *T. cruzi* infection. RNA sequencing was performed using mock and *T. cruzi*-infected HDFs and BJ fibroblasts 48 hpi (MOI=3). RPKM values display *NECTIN2* gene expression of BJ fibroblasts and 5 HDF donors. After negative test for normal distribution, statistical significance was analyzed by Wilcoxon test: * $p \leq 0.05$. (B) Flow cytometric analysis of nectin-2 expression on mock and *T. cruzi*-infected BJ fibroblast 48 hpi (MOI=3) Left: representative histogram of mock and *T. cruzi*-infected BJ fibroblasts. Right: normalized nectin-2 MFI of mock and *T. cruzi*-infected BJ fibroblasts. (C) Normalized nectin-2 MFI of BJ fibroblasts treated for 24 h with supernatants from mock and *T. cruzi*-infected BJ fibroblasts. Supernatants were previously obtained from indicated BJ fibroblasts cultured for 24 h in fresh culture medium between 24 and 48 hpi. MFI values were normalized to the average MFI of all respective mock controls. Bars display respective medians ($n=9$). After positive test for normal distribution, statistical differences were calculated by unpaired t-test with Welch's correction: **** $p \leq 0.0001$.

Besides nectin-2, HLA-E was investigated as a second potential modulator of the NK cell response against *T. cruzi*-infected dermal fibroblasts. Transcriptome analyses revealed a significantly ($p \leq 0.001$) higher expression of the *HLA-E* gene in HDF and BJ fibroblasts in response to *T. cruzi* infection 48 hpi (figure 4.28 A). In the individual HDF donors, the infection-mediated *HLA-E* gene expression increase ranged from about 75 – 450%, whereas BJ fibroblasts exhibited an increase of approximately 190%.

Afterwards, HLA-E protein expression of mock and *T. cruzi*-infected BJ fibroblasts was evaluated by flow cytometric analyses 48 hpi (figure 4.28 B). As depicted in the representative histogram, nearly all fibroblasts were positively stained for HLA-E. Therefore, normalized MFI values were assessed to evaluate the density of expressed HLA-E molecules. *T. cruzi* infection resulted in a significant ($p \leq 0.001$) increase in normalized HLA-E MFI of around 100% compared to the mock controls. In addition, it was investigated whether the increase in HLA-E expression is induced by cell-intrinsic processes of infected fibroblasts or by soluble factors secreted by infected fibroblasts. To this end, pre-seeded BJ fibroblasts were treated with supernatants from mock and *T. cruzi*-infected fibroblasts for 24 h (figure 4.28 C). Here, a significant ($p \leq 0.0001$) increase in normalized HLA-E MFI was likewise evident after treatment with supernatant from *T. cruzi*-infected fibroblasts compared to the mock controls. With an increase of about 80%, this effect was comparable to the increased HLA-E expression in response to direct *T. cruzi* infection.

Thus, the results demonstrated a *T. cruzi* infection-related increase in HLA-E expression on fibroblasts, which appears to be mediated by soluble factors released by infected fibroblasts. This increased HLA-E expression has the potential to modulate the NK cell response by interacting with corresponding with the inhibitory receptor NKG2A and the activating receptor NKG2C on NK cells [66].

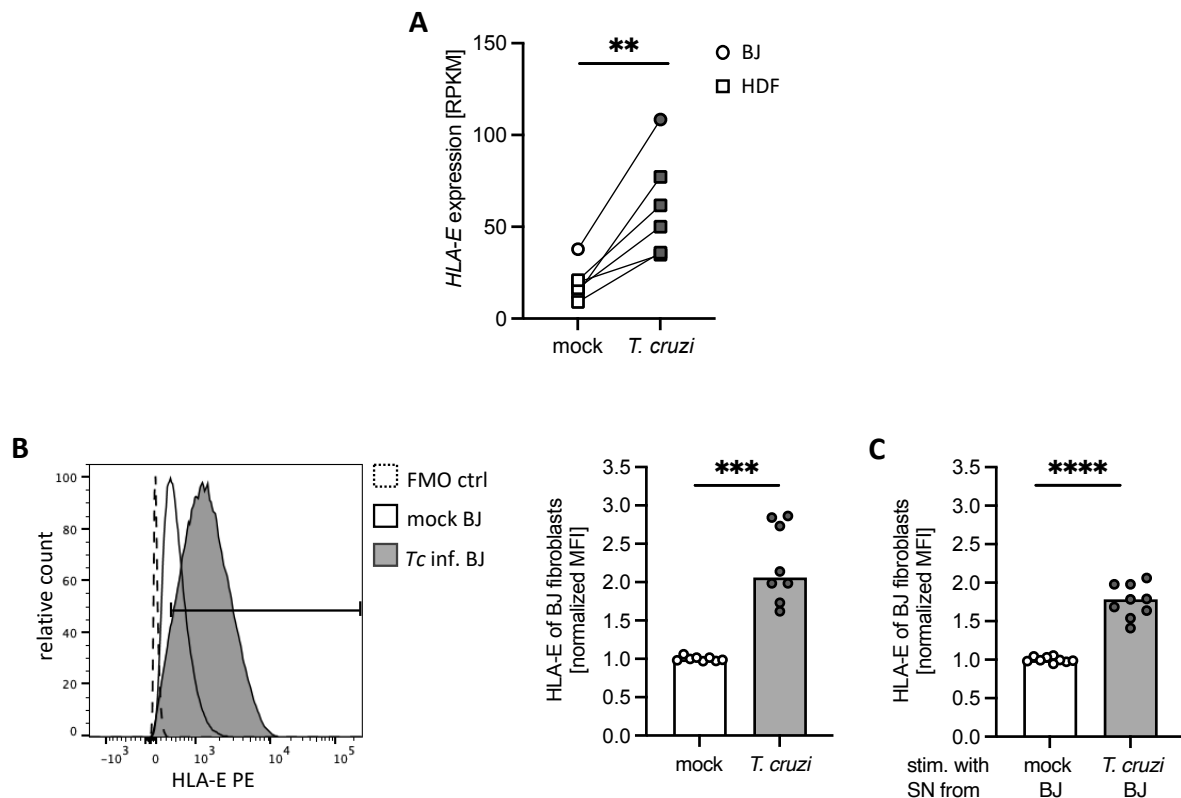


Figure 4.28: Dermal fibroblasts show increased HLA-E expression in response to *T. cruzi* infection. (A) Transcriptome analysis reveals an upregulated expression of the *HLA-E* gene in HDF and BJ fibroblasts after *T. cruzi* infection. RNA sequencing was performed using mock and *T. cruzi*-infected HDFs and BJ fibroblasts 48 hpi (MOI=3). RPKM values display *HLA-E* gene expression of BJ fibroblasts and 5 HDF donors. After positive test for normal distribution, statistical significance was analyzed by paired t-test: ** $p \leq 0.01$. (B) Flow cytometric analysis of HLA-E expression on mock and *T. cruzi*-infected BJ fibroblasts 48 hpi (MOI=3) Left: representative histogram of mock and *T. cruzi*-infected BJ fibroblasts. Right: normalized HLA-E MFI of mock and *T. cruzi*-infected BJ fibroblasts. (C) Normalized HLA-E MFI of BJ fibroblasts treated for 24 h with supernatant of mock and *T. cruzi*-infected BJ fibroblasts. Supernatants were previously obtained from indicated BJ fibroblasts cultured for 24 h in fresh culture medium between 24 and 48 hpi. MFI values were normalized to the mean of the mock controls. Bars display respective medians ($n=9$). After positive test for normal distribution, statistical differences were calculated by unpaired t-test with Welch's correction: *** $p \leq 0.001$; **** $p \leq 0.0001$.

5 Discussion

The protozoan parasite *T. cruzi* is the causative agent of the potentially life-threatening Chagas disease, which is divided into an acute and a chronic stage. Particularly during the chronic stage, the infection can lead to severe symptoms such as cardiomyopathy [135]. The present study focuses on the acute stage and the early immune response against infection. Since *T. cruzi* parasites are mainly transmitted by triatomine bugs during their blood meal, the skin is the primary site of infection [218]. Thus, the early immune response at the inoculation site is important to contain the parasite spread to surrounding cells as well as other tissues and organs before the adaptive immune response is initiated. In addition to the high relevance of the skin during the acute stage, the persistence of *T. cruzi* parasites in the skin during the chronic stage has also been demonstrated [157]. However, possible effects of *T. cruzi* persistence in the skin on the course of the disease are insufficiently understood.

Since *T. cruzi* is an obligatory intracellular parasite, we assume NK cells play an indispensable role for the defense against *T. cruzi*-infected cells in the skin. NK cells can recognize infected cells via different mechanisms and respond through direct cytotoxicity and the secretion of cytokines such as IFN- γ [31]. NK cells are present in healthy skin and can accumulate there in response to an inflammatory stimulus, as shown in the example of psoriasis [219], [220]. A study by Chessler and colleagues in 2009 indirectly demonstrated the recruitment of NK cells to the *T. cruzi* infection site in the skin in a murine model. Here, microarray analyses showed an increase of *grza* and *grzb* transcripts at the site of inoculation, which were not detectable when NK cells were depleted [221].

So far, little is known about NK cells during *T. cruzi* infection. However, depletion of NK cells in *T. cruzi*-infected mice resulted in an increase in parasitemia, demonstrating their relevance to parasite defense [182], [222]. Moreover, NK cells are the main producers of IFN- γ during the early stage of *T. cruzi* infection [175], [176]. The secreted IFN- γ is shown to be crucial for the parasite defense [175], [177]. For example, it induces macrophage activation and enhanced production of reactive oxygen species in infected L929 cells [175], [178], [181]. The relevance of cytotoxic NK cell activity in the acute stage has not yet been investigated. However, an increased amount of cytotoxic circulating NK cells was observed in asymptomatic compared with cardiac Chagas patients during the chronic phase [184]. In addition, increased expression of NK cell cytotoxicity-related genes was also determined [185]. Therefore, it can

be assumed that cytotoxic NK cell effector functions also protect against the progression of Chagas disease.

With increasing knowledge of the role of NK cells during *T. cruzi* infection, their relevance is becoming more apparent. Nevertheless, the mechanisms of NK cell activation by *T. cruzi*-infected cells are still unknown.

Hence, the NK cell response in the skin and the underlying stimulatory and inhibitory mechanisms were characterized using *in vitro* *T. cruzi*-infected dermal fibroblasts. Since the activity of NK cells is controlled by the interplay of activating and inhibitory signals from different receptors [30] and murine NK cells differ greatly from human ones in their receptor composition [13], only human NK cells were examined.

5.1 NK cell stimulation by *in vitro* coculture with *T. cruzi*-infected dermal fibroblasts

Dermal fibroblasts are the main cell type in the skin [223]. Since fibroblasts are one of the most susceptible cell types for *T. cruzi* infection [139], [218], the present study assumes, that dermal fibroblasts are highly parasitized during initial infection and thus play an essential role for the induction of the immune response.

Hence, it was investigated whether *T. cruzi*-infected primary human dermal fibroblasts (referred to as HDF) can directly activate NK cells. In order to study this, a heterologous coculture protocol for human NK cells and *in vitro* *T. cruzi*-infected HDF was established to mimic the NK cell response in the skin against parasitized fibroblasts in the dermis (figure 4.1).

Before coculture setup, NK cells were purified from isolated PBMCs by negative selection. Here, purities between 85 and 95% of NK cells were achieved. The other 5 – 15% could theoretically be composed of monocytes, DCs, NKT cells, T cells, and B cells. Since a dump channel was used to exclude non-NK cells, the precise composition could not be determined. The exact fraction of each cell type would have to be investigated by individual staining with different fluorochromes. However, since the utilized blood was obtained from healthy individuals, the lymphocyte populations were not primed for *T. cruzi*, which makes their activation during coculture unlikely. Although multiple washes of infected fibroblasts before coculture removed as many extracellular parasites as possible, a few remaining parasites cannot be excluded. Therefore, monocytes and DCs could theoretically be infected by

remaining extracellular parasites and subsequently contribute to NK cell activation by producing NK cell stimulating cytokines. For instance, *T. cruzi*-infected monocytes have been described to produce IL-12, which promotes NK cell activation in terms of cytokine production [224]. Stimulation of NK cell cytotoxicity by *T. cruzi*-infected monocytes has not been observed to date. Furthermore, *in vitro* *T. cruzi* infection of human DCs has been shown to induce the secretion of anti-inflammatory molecules [225], so DC-mediated NK cell activation seems to be unlikely. Thus, although indirect NK cell stimulation by remaining accessory cells cannot be completely excluded, it is highly unlikely in this experimental setting.

Before the NK cell response to *T. cruzi*-infected fibroblasts was investigated, the general responsiveness of the purified and rested NK cells to adherent cells was verified. To this end, NK cell coculture with HEK293 cells was performed. The cell line has been shown to express high levels of MICA and ULBP1 [205], which are both ligands for the activating NK cell receptor NKG2D [77], [78]. Indeed, strong degranulation of NK cells was observed after only 5 h of coculture, as indicated by the presence of CD107a on the NK cell surface. The depiction of NK cell cytotoxicity is based on the fact that CD107a molecules are contained in the lipid bilayer of cytotoxic granules and translocate to the plasma membrane during the degranulation process [204]. The coculture results confirmed that all prepared NK cells were responsive to adherent cells and thus utilizable to study the NK cell response to *T. cruzi*-infected fibroblasts.

A 24 h coculture was required to optimally visualize differences in NK cell degranulation in response to mock and *T. cruzi*-infected HDF. This suggests that the stimulatory signals transmitted here were weaker compared to those derived from HEK293 cells, or that additional inhibitory signals were present. However, statistically significantly higher NK cell degranulation was observed after coculture with *T. cruzi*-infected HDF compared to the mock controls, indicating that *T. cruzi*-infected HDF directly activate NK cells without the contribution of accessory cells. These results are in agreement with the increase of NK cell cytotoxicity mediators in *T. cruzi*-parasitized murine skin shown by Chessler and colleagues [221] and confirm the induction of cytotoxic effector functions in response to *T. cruzi*-infected cells for human NK cells.

For the following investigation of underlying mechanisms of NK cell activity modulation by *T. cruzi*-infected fibroblasts, the usage of primary fibroblasts was not practical due to their restricted proliferation and thus limited cell number. Therefore, the foreskin fibroblast cell line BJ was examined for the similarity of its response to *T. cruzi* infection compared to HDF. BJ fibroblasts have already been used in previous publications for *in vitro* infections with different *T. cruzi* strains [226]–[228]. However, a comparable response of the BJ fibroblasts and HDF to *T. cruzi* infection has never been demonstrated.

To investigate the similarity of the response, a comparative transcriptome analysis of mock and *T. cruzi*-infected HDF and BJ fibroblasts was conducted. A previous publication showed that immortalized pterygium fibroblasts differ from respective primary fibroblasts by a strongly increased expression of cell cycle related genes [229]. Since this was also the case for the dermal fibroblasts studied here, only those genes that were differentially expressed after *T. cruzi* infection compared to mock controls were considered for the comparative analysis (figure 4.2). The principal component analysis of DEGs revealed a similar response of all examined fibroblasts to the infection, as indicated by the clustering of all mock fibroblasts on the one hand and all *T. cruzi*-infected fibroblasts on the other. A heatmap additionally displayed comparable overall expression pattern of individual DEGs, confirming the similar responses of BJ fibroblasts and HDF to *T. cruzi* infection. Nevertheless, it cannot be excluded that the expression of individual genes relevant for the modulation of NK cell activity may differ in response to *T. cruzi* infection. This requires an individual assessment of the respective genes of interest.

In addition to the studied gene expression, a comparison of altered protein expression of HDF and BJ fibroblasts in response to *T. cruzi* infection by mass spectrometric analysis would be beneficial for further verification. Unfortunately, this was not feasible due to the limited cell number of the provided HDF.

Finally, examination of NK cell degranulation in response to mock and *T. cruzi*-infected BJ fibroblasts revealed significantly enhanced NK cell degranulation in response to infected BJ fibroblasts compared with mock controls. Here, the frequencies of CD107a⁺ NK cells were similar to those obtained after coculture with appropriately treated HDF.

Based on the results of comparative transcriptome analysis and the comparable NK cell activation by infected HDF and BJ fibroblasts, BJ fibroblasts were assumed to be a suitable

model for further characterization of the NK cell response to *T. cruzi*-infected dermal fibroblasts.

5.2 Cell-cell contact-dependent NK cell activation by *T. cruzi*-infected fibroblasts

In the following, BJ fibroblasts were used to study the underlying mechanisms of NK cell activity modulation by *T. cruzi*-infected dermal fibroblasts. As described in detail in section 1.1.3, NK cell activation is controlled by an equilibrium of signals recognized by various inhibitory and stimulatory NK cell receptors, with inhibitory signals predominating in the steady state [30].

5.2.1 NK cell activation by *T. cruzi*-infected fibroblasts is not mediated by reduction of inhibitory signals

The oldest-known mechanism of NK cell activation was described in a review by Ljunggren and Kärre in 1990 as the recognition of "*missing self*" on target cells [27]. The review was primarily based on work by Harel-Bellan and colleagues in 1986 and Storkus and colleagues in 1987. The authors previously demonstrated an inverse relationship between the expression level of MHC-I molecules on the target cell surface and lysis of target cells by NK cells [230], [231]. MHC-I molecules provide inhibitory signals to NK cells via the binding of the conserved NKG2A receptor and the variable inhibitory KIR molecules [62], [71], [232]. Downregulation of MHC-I molecules results in a shift in the equilibrium of stimulatory and inhibitory signals, and finally in NK cell activation. This mechanism of NK cell activation has been demonstrated for various viral infections such as Influenza virus or murine cytomegalovirus (MCMV) [233], [234].

To investigate the relevance of this mechanism, the expression of MHC-I molecules on the surface of *T. cruzi*-infected BJ fibroblasts was examined during the course of infection. Instead of a reduction of MHC-I expression, as was previously observed for *T. cruzi*-infected HeLa cells [235], an increase in MHC-I expression was detected on the BJ fibroblast surface in response to *T. cruzi* infection by flow cytometry (figure 4.4). These results were additionally supported by transcriptomic and proteomic data revealing an increased expression of MHC-I related genes (figure 4.14 and 4.15). Moreover, the present study shows that the increased expression of MHC-I molecules is largely dependent on IFN- β secreted by *T. cruzi*-infected

fibroblasts (figure 4.21). Whereas there is no evidence that HeLa cells are able to produce IFN- β , secretion of IFN- β by fibroblasts has already been demonstrated in response to various infections such as Dengue virus and *Chlamydia trachomatis* infections [127], [236]. Therefore, it is conceivable that the differential change in MHC-I expressions of HeLa cells and fibroblasts is based on their ability to secrete IFN- β in response to *T. cruzi* infection.

Overall, it can be concluded that NK cell activation by *T. cruzi*-infected dermal fibroblasts is not mediated via the "missing self" pathway.

5.2.2 NK cell activation by *T. cruzi*-infected fibroblasts is facilitated by the engagement of NKp46

In addition to the reduction of inhibitory signals, NK cell activation can also be mediated by an enhanced engagement of activating receptors [30]. One of these activating receptors is the NCR NKp46, which is constitutively expressed on around 80% of peripheral NK cells [237]. Besides viral pathogen-encoded ligands, HSPGs and vimentin exposed on the cell surface were identified as cellular ligands for NKp46 [92], [238].

The presence of vimentin on the surface of *T. cruzi*-infected fibroblasts was of particular interest. On the one hand, vimentin is the major intermediate filament in fibroblasts and is therefore constitutively present in the cytosol. Although it was found in most mesenchymal cells, particularly strong expression was detected in dermal fibroblasts [239], [240]. On the other hand, autoantibodies against vimentin were detected in acute and symptomatic chronic Chagas patients [241], suggesting the presence of extracellular or csVimentin.

In the present study, the amount of csVimentin detected on BJ fibroblasts in response to *T. cruzi* infection was significantly increased. The frequency of csVimentin⁺ BJ fibroblasts was increased 48 hpi from circa 10% to about 42% compared to the mock controls. As evident from the transcriptome data, this effect was not associated with an overall increase in vimentin expression. Therefore, it seems likely that the non-conventional localization of vimentin to the fibroblast surface occurs by secretion into the extracellular space via the classical endoplasmic reticulum/Golgi pathway, as has been shown for activated human macrophages [242]. Furthermore, vimentin released by dead cells could preferentially bind to the surface of infected fibroblasts. The exact mechanism remains to be investigated. Based on previous studies, it can be assumed in both cases that the binding of vimentin to the cell surface is at least partially mediated by the interaction of the amino terminal vimentin and negatively

charged phospholipids in the plasma membrane [243]. Moreover, Bhattacharya and colleagues demonstrated that extracellular vimentin can be bound to the cell surface by $\beta 3$ integrin and plectin [244]. A tendentially increased expression of the $\beta 3$ integrin encoding gene was found in a transcriptome analysis of HDF and BJ fibroblasts in response to *T. cruzi* infection (data not shown). Therefore, further investigation of the $\beta 3$ integrin protein expression and the associated binding of vimentin to the cell surface would be of great interest.

In the following step, the binding of NKp46 to *T. cruzi*-infected BJ fibroblasts was investigated (figure 4.6). Using an NKp46-Fc binding assay, a significantly increased frequency of NKp46-Fc bound BJ fibroblasts was detected after infection (~10%) compared to the mock controls (~1.6%). Although the results confirmed an increased binding of NKp46 to dermal fibroblasts in response to *T. cruzi* infection, the frequencies of fibroblasts bound to NKp46-Fc were lower than those of previously detected csVimentin⁺ fibroblasts. A possible explanation could be the higher number of washing steps while performing the binding assay compared with flow cytometric staining of csVimentin. This could lead to an increased detachment of the non-covalently cell surface-bound vimentin [243], [244] and potentially bound NKp46-Fc molecules, resulting in lower frequency of detected cells. However, using NKp46 ζ -transfected Jurkat reporter cells [203], increased and functional binding of NKp46 to BJ fibroblasts in response to *T. cruzi* infection could be substantiated.

Furthermore, NKp46 ζ -transfected Jurkat reporter cells were utilized to investigate cell-cell contact dependency of NKp46 engagement (figure 4.7). Here, enhanced activation of reporter cells was detectable exclusively after stimulation with *T. cruzi*-infected BJ fibroblasts compared to mock controls, but not after stimulation with just the appropriate culture supernatants. In fact, a significantly decreased frequency of activated reporter cells was detected after stimulation with culture supernatants of *T. cruzi*-infected BJ fibroblasts compared to supernatants of mock controls. These results were supported by the trend of lower soluble vimentin concentration in the culture supernatant of *T. cruzi*-infected BJ fibroblasts compared to mock controls. Together, these results indicate both a cell-cell contact-dependent engagement of NKp46 and enhanced binding of soluble vimentin by *T. cruzi*-infected cells. The increased binding of soluble vimentin, which may be released from

the cytosol of dead cells, could be mediated by enhanced expression of β 3 integrin, which has been shown to interact with vimentin as previously discussed [244].

Finally, the impact of NKp46 engagement on the NK cell response against *T. cruzi*-infected BJ fibroblasts was investigated via antibody-mediated blockade of NKp46 on NK cells prior to coculture (figure 4.8). The blockade caused decreased NK cell degranulation as well as secretion of cytotoxicity-mediating effector molecules and the cytokine IFN- γ in response to coculture with both *T. cruzi*-infected BJ fibroblasts and mock controls. The NKp46 blockade effect on the NK cell response against mock-treated BJ fibroblasts was presumably due to the basal presence of csVimentin and thus binding of NKp46, as shown previously in this study. However, due to the higher amount of activated NK cells after coculture with infected fibroblasts, the NKp46 blockade effect was more pronounced here. These results indicated an infection-mediated enhancement of NKp46 engagement.

Besides csVimentin, HSPGs could potentially also promote NKp46-induced NK cell activation by *T. cruzi*-infected dermal fibroblasts. Increased HSPG expression has previously been shown to occur on the surface of tumor cells and MCMV-infected B cells [45], [245]. In contrast, *T. cruzi*-infected endothelial cells are described to exhibit no altered levels, but an enhanced sulfation of HSPGs, which was associated with decreased binding ability of NKp46 [238], [246]. Consistent with this, transcriptome analyses of HDF and BJ fibroblasts performed in this study detected decreased expression of the HSPG-encoding gene in response to *T. cruzi* infection (data not shown). Although HSPG protein expression on the surface of fibroblasts infected with *T. cruzi* remains to be investigated, the present data strongly suggest that the increased presence of csVimentin triggers NKp46-mediated NK cell activation.

Taken together, it was demonstrated that the NK cell response to *T. cruzi*-infected dermal fibroblasts is promoted by the cell-cell contact-dependent engagement of NKp46, which is presumably mediated by the infection-related increased presence of csVimentin. This mechanism of NK cell activation was first described in a study by Garg and colleagues in 2006. The authors found an increased presence of vimentin on the surface of *Mycobacterium tuberculosis*-infected monocytes, which promoted NKp46-mediated lysis of infected monocytes by NK cells [92]. Since this 16-year-old study, NK cell activation mediated

by csVimentin has not been described in any other infection context, underscoring the importance of the present study.

5.2.3 NK cell activation by *T. cruzi*-infected fibroblasts is facilitated by the engagement of CD160

The activation of NK cells by *T. cruzi*-infected dermal fibroblasts in dependence of the CD160-HVEM interaction was investigated. CD160 is expressed on T cells and NK cells, among others [95], mediating inhibitory or activating signals depending on the expressing cell type. A co-inhibitory function has been indicated for CD4⁺ T cells [97] as well as for CD8⁺ T cells in the context of cerebral malaria [100]. However, there are also studies showing a co-stimulatory effect of CD160 on CD8⁺ T cells [98], [99]. Regarding NK cells, all published studies demonstrate a stimulatory effect of CD160 engagement [41], [102]–[104]. Since CD160 is expressed on about 70 – 90% of NK cells [110], the effect of CD160 engagement is expected to be widespread.

In 2013, Šedý and colleagues described HVEM as an activating ligand for CD160 on NK cells in the context of HCMV infections [32]. Therefore, transcriptome data from mock and *T. cruzi*-infected HDF and BJ fibroblasts were reviewed regarding the expression of the HVEM-encoding gene *TNFRSF14* (figure 4.9). This revealed increased expression of the *TNFRSF14* gene in both HDF and BJ fibroblasts in response to *T. cruzi* infection. Based on this, BJ fibroblasts were considered a suitable model to study the effects of increased HVEM expression. Flow cytometric analysis of HVEM protein expression on the surface of mock and *T. cruzi*-infected BJ fibroblasts showed a tripling of the frequency of HVEM⁺ fibroblasts from about 3% to around 9% at 48 hpi (figure 4.10). Increased expression of HVEM in response to an intracellular infection was also observed in murine corneal fibroblasts after Herpes simplex virus (HSV) infection [247], [248]. Due to the widely differing models, frequencies of HVEM⁺ cells are difficult to compare. However, increased HVEM expression in response to intracellular fibroblast infection with protozoan parasites such as *Leishmania* spp., *Toxoplasma* spp., or *Trypanosoma* spp. has not been described to date.

In the following, the binding of CD160 to mock and *T. cruzi*-infected BJ fibroblasts was investigated 48 hpi by a modified binding assay using His-tag expressing hrCD160 molecules (figure 4.11). Using this assay, a significant increase in the frequency of CD160 binding to

T. cruzi-infected fibroblasts was detected compared to mock controls. The frequencies of CD160-bound mock (~20%) and *T. cruzi*-infected (~40%) BJ fibroblasts were clearly higher than the determined frequencies of HVEM⁺ cells. On the one hand, this could be for technical reasons. As depicted in figure 4.10, the flow cytometric HVEM staining only showed a shift in response to the infection and no distinct population, as was the case for the CD160 binding (figure 4.11). Therefore, it is possible that HVEM was too weakly expressed on some fibroblasts to be detected by the utilized anti-HVEM antibody. On the other hand, later in the present study, an increased expression of HLA-C was also detected in response to *T. cruzi* infection (figure 4.19). Previous publications show that in addition to HVEM, HLA-C can also interact with CD160, resulting in increased NK cell activity [41], [103]. Therefore, the binding of hrCD160 to BJ fibroblasts could also be mediated by HLA-C in addition to HVEM. However, the results of the present study show that the KO of HLA-C results in an increase in NK cell activity in most cases (figure 4.25). This suggests that HLA-C primarily interacts with corresponding inhibitory KIRs and that the interaction with CD160 appears to be less relevant. Therefore, HVEM is assumed here to be primarily responsible for CD160 engagement in the physiological context. In addition to CD160, the inhibitory receptor BTLA has also been described as an interaction partner for HVEM [109]. However, BTLA was shown to be expressed on a much lower proportion of NK cells than CD160 [110]. Moreover, in a study by Šedý and colleagues, treatment of NK cells with HVEM-Fc molecules resulted in enhanced NK-cell activity [32]. Therefore, it can be suggested that the interaction of HVEM with CD160 is predominant on NK cells.

Finally, the impact of CD160 engagement by *T. cruzi*-infected BJ fibroblasts was investigated through antibody-mediated blockade of CD160 on NK cells prior to coculture. The blockade resulted in a significantly decreased NK cell degranulation and secretion of effector molecules after coculture with mock as well as *T. cruzi*-infected fibroblasts. Similar to NKp46 blockade, the effect of CD160 blockade in coculture with mock-treated fibroblasts can be explained by basal expression of the ligand, in this case HVEM. However, the infection-mediated increase in HVEM expression presumably mediated a higher frequency of activated NK cells and thus also a higher number of NK cells whose activity was reduced by the CD160 blockade. Nevertheless, regarding the calculated significances of the respective blockade-mediated effects, CD160 blockade appeared to have a less specific effect on the NK cell response against

T. cruzi-infected fibroblasts than NKp46 blockade. This may be due to the overall lower presence of the CD160 ligand HVEM compared to the NKp46 ligand csVimentin.

Overall, engagement of both NKp46 and CD160 appears to contribute to NK cell activation by *T. cruzi*-infected fibroblasts. The strong reduction of NK cell responses after blockade of both receptors indicates that NK cell activity is mediated by a precisely tuned balance of inhibitory and stimulatory signals. Whenever one of the stimulatory signals is removed, the balance appears to shift to the inhibitory side, preventing the activation of NK cells. Nevertheless, it cannot be excluded that further stimulatory or inhibitory signals are involved *in vivo*, which may influence the equilibrium.

5.3 Dual effect of IFN- β released by *T. cruzi*-infected fibroblasts on NK cell activity

5.3.1 NK cells are stimulated directly by IFN- β

In addition to direct interaction between NK and target cells, soluble factors may also contribute to NK cell activation. On the one hand, various cytokines have been described to promote NK cell responses. The most notable are IL-2, IL-12, IL-15, IL-18 as well as type I and type III IFNs [43], [47], [48]. On the other hand, in 2004 Lieke and colleagues showed that extracellular *T. cruzi* trypomastigotes promote NK cell cytotoxicity, resulting in lysis of the extracellular parasites [182]. The specific interacting molecules are not known. Based on this, it is also conceivable that parasitic factors released by infected cells could enhance NK cell activity.

Therefore, whether NK cell degranulation can be enhanced by soluble factors released by *T. cruzi*-infected cells was investigated (figure 4.13). Here, increased NK cell degranulation was observed in response to *T. cruzi*-infected BJ fibroblasts compared to mock controls. However, the median frequency of CD107a⁺ NK cells after stimulation with supernatants was about 10 – 20% lower than after direct coculture with the respective fibroblasts (figure 4.3, 4.8 B, 4.12B, 4.25 B and 4.26 B). This suggests that although soluble factors contribute to NK cell activation, it is further enhanced by additional cell-cell interactions.

NK cell activation by supernatants of *T. cruzi*-infected BJ fibroblasts could theoretically have been caused by both cellular and parasitic soluble factors. To determine the origin of soluble

NK cell activating factors, NK cells were also stimulated with supernatants from mock and *T. cruzi*-infected cells which were not of human origin. Although cross-reactivity of potentially secreted cytokines could not be completely excluded, it was assumed that, due to the different species, the released cellular factors could not be recognized by human NK cell receptors. Thus, potential NK cell activation was assumed to be mediated exclusively by parasitic factors. Vero81 cells were used to facilitate this. This kidney epithelial cell line is derived from the African green monkey and has already been described to be efficiently infected with different *T. cruzi* strains [249]. Light microscopic observation also confirmed comparable infection rates and kinetics between *T. cruzi*-infected BJ fibroblasts and Vero81 cells (data not shown). In contrast to the supernatants from *T. cruzi*-infected BJ fibroblasts, stimulation of NK cells with the supernatants from infected Vero81 cells did not result in increased NK cell degranulation compared to the control. Therefore, it was concluded that the NK cell stimulating factors in the supernatants of *T. cruzi*-infected BJ fibroblasts must be of cellular origin. These results were consistent with those of a study by Lieke and colleagues in 2006, which found no activation of murine NK cells after transwell coculture with *T. cruzi*-infected human 86-HG-39 cells [181].

As an alternative to Vero81 cells, which are derived from kidney epithelial cells, a dermal fibroblast cell line derived from a non-human species could be used for better comparability between cell types. However, the murine fibroblast cell line NIH-3T3, which was available for the present study, showed a clearly higher infection rate and faster intracellular parasite replication compared to the human BJ fibroblasts in pre-trials. For this reason, Vero81 cells were chosen to address the question here.

Following this, the next aim was to identify secreted cellular factors mediating NK cell activation. To this end, transcriptome data of mock and *T. cruzi*-infected HDF and BJ fibroblasts were evaluated for individual upregulated genes and signaling pathways (figure 4.14). The data visualization via a volcano plot revealed a significant upregulation of genes related to IFN signaling. In addition, over-representation analysis confirmed a significant enrichment of genes included in the pathways "IFN- α / β signaling" and "IFN signaling". The proteomic analysis of mock and *T. cruzi*-infected BJ fibroblasts also verified these results at protein level (figure 4.15). These data were in agreement with results of previously published gene expression studies of BJ fibroblasts infected with different *T. cruzi* strains, which

demonstrated an upregulation of genes associated with IFN and in particular type I IFN responses [227], [250], [251]. Moreover, Chessler and colleagues demonstrated that a type I IFN response is induced *in vivo* at the site of intradermal infection in the murine *T. cruzi* infection model [221].

Based on these results, supernatants from mock and *T. cruzi*-infected BJ fibroblasts were tested for secreted type I, II, and III IFNs (figure 4.16). Whereas no secretion of the type I IFN IFN- α and the type II IFN IFN- γ was detected, the type I IFN IFN- β as well as the type III IFNs IFN- λ 1 and IFN- λ 2/3 were found in statistically significantly increased concentrations in supernatants from BJ fibroblasts infected for at least 48 h.

More than 30 years ago, Kornbluth and Hoover demonstrated the ability of hrIFN- β to induce NK cell cytotoxicity *in vitro* [252]. Furthermore, Une and colleagues have shown that type I IFNs are crucial for the induction of NK cell cytotoxicity in experimental *T. cruzi* infection using IFNAR-deficient mice [253]. Based on these data, the present study examined the role of IFN- β secreted by *T. cruzi*-infected BJ fibroblasts for NK cell degranulation (figure 4.17). IFN- β neutralization had no effect on NK cell stimulation with supernatants of mock-treated fibroblasts. The absence of the IFN- β neutralization effect was consistent with the undetectable IFN- β levels in the supernatant of mock-treated fibroblasts (figure 4.16). In contrast, a significant reduction in NK cell degranulation was detectable after stimulation with supernatants from *T. cruzi*-infected fibroblasts when IFN- β was neutralized. These findings confirmed the importance of secreted IFN- β in stimulating NK cell cytotoxicity. However, IFN- β neutralization did not completely reduce the frequency of degranulating NK cells in response to the supernatants of infected fibroblasts to the level of mock controls. Since the neutralizing antibody was used in nearly 20-fold excess to the measured amount of IFN- β , an incomplete neutralization is unlikely. Hence, it seems probable that other soluble factors contribute to NK cell activation. A possible candidate might be IFN- λ , which has also been shown to be secreted by *T. cruzi*-infected BJ fibroblasts, since IFN- λ has been shown to induce similar signaling pathways as IFN- α/β [254]. Nonetheless, previous studies have only found an effect of IFN- λ on NK cell IFN- γ production and not on their cytotoxic effector function [48], [134]. As previously described, IFN- γ produced by NK cells has been shown to be crucial for parasite control in the early, acute phase of *T. cruzi* infection [175], [177]. Therefore, a more detailed consideration of the impact of IFN- λ secreted by *T. cruzi*-infected fibroblasts would be of great interest. However, as previous studies have failed to demonstrate an effect of IFN- λ on NK cell

cytotoxicity [48], [134], this cytokine seems to play a minor role for the observed increase in NK cell degranulation through treatment with supernatants from *T. cruzi*-infected fibroblasts. Accordingly, other undefined soluble factors appear to promote the cytotoxic function of NK cells in addition to IFN- β .

5.3.2 IFN- β dampens the NK cell response by promoting MHC-I expression on target cells

In addition to direct stimulation of NK cells via IFNAR engagement, IFN- β can also indirectly affect NK cell activity. IFN- β has been described to enhance the expression of MHC-I molecules [127]. This is in line with results of the present study, showing that the increase in HLA-A,B,C expression on fibroblasts in response to *T. cruzi* infection was inhibited by neutralization of IFN- β (figure 4.21). Furthermore, a slight but significant reduction in HLA-A,B,C expression levels was also evident after stimulation with supernatants from mock controls. Although IFN- β was not measurable in supernatants from mock-treated fibroblasts by LEGENDplex, these data suggest IFN- β secretion at very low level and autocrine or paracrine utilization by fibroblasts.

MHC-I molecules can interact with different activating and inhibitory KIRs, with higher binding affinity to receptors mediating inhibitory signals [62], [64]. Therefore, it is assumed that a IFN- β -mediated increase in MHC-I expression on the target cell surface inhibits NK cell activity.

To investigate the contribution of IFN- β -mediated stimulatory and inhibitory signals on the NK cell response, coculture experiments were performed with mock and *T. cruzi*-infected BJ fibroblasts without and with IFN- β neutralization (figure 4.26). The IFN- β neutralization should suppress both direct NK cell stimulation via engagement of IFNAR on NK cells and indirect NK cell inhibition via increased engagement of inhibitory KIRs through enhanced expression of HLA-A,B,C.

Evaluation of NK cell degranulation after 24 h of coculture showed no differences in the NK cell response to mock or *T. cruzi*-infected fibroblasts when IFN β was neutralized. This suggests that after 24 h, stimulatory signals transmitted by IFNARs were compensated by inhibitory signals mediated by increased expression of MHC-I molecules on the target cells. This assumption is in accordance with a study by Kornbluth and Hoover, showing that

IFN- β -mediated NK cell cytotoxicity peaks 6 h after the onset of stimulation and subsequently declines [252]. In addition, the present study demonstrated that MHC-I expression increased with progressing intracellular parasite amplification (figure 4.4).

Following this, the IFN- β -mediated effect on the NK cell response to mock and *T. cruzi*-infected fibroblasts was to be monitored over the entire coculture period to also visualize earlier effects. To this end, supernatants were assayed for released cytotoxic mediators (granzyme A, granzyme B, perforin, granulysin and sFasL) as well as secreted IFN- γ during coculture.

IFN- β neutralization during coculture with mock-treated fibroblasts led to an increased secretion of all studied mediators. These results were in line with the previously observed IFN- β neutralization-dependent reduction of HLA-A,B,C expression on mock-treated fibroblasts (figure 4.21), indicating NK cell activation via the “missing self” pathway [27]. The data support the hypothesis that a small amount of IFN- β is secreted by mock-treated fibroblasts and directly utilized in an autocrine or paracrine manner. Thus, IFN- β would be removed from the supernatant under this condition and could not contribute to NK cell activation through engagement of IFNAR on NK cells.

IFN- β neutralization during NK cell coculture with *T. cruzi*-infected fibroblasts had an opposite effect compared to the coculture with the corresponding mock controls. Here, IFN- β neutralization caused at least a trend toward reduced secretion of NK cell effector molecules, with granzyme B and IFN- γ detected at significantly lower levels. These results suggest that due to the increased secretion of IFN- β by infected fibroblasts, there is additional engagement of IFNAR on NK cells, promoting their activation. Thus, at least in the early phase of coculture with *T. cruzi*-infected fibroblasts, IFN- β -mediated stimulatory signals appear to predominate. However, in the later course of coculture, the signals of inhibitory KIRs might compensate IFNAR-mediated stimulatory signals due to the increasing expression of MHC-I ligands on fibroblasts, as suggested by the results of the degranulation assay described above.

Therefore, a consideration of the long-term effects of IFN- β secreted by *T. cruzi*-infected fibroblasts would be very interesting. Previous studies even indicate a detrimental effect of IFN- β during the later course of *T. cruzi* infections. Using IFNAR-deficient mice, Chessler and colleagues showed that type I IFNs increase parasitemia and decrease survival from day 25 – 30 of experimental *T. cruzi* infection [255]. Splenocytes derived from IFNAR-deficient mice exhibited higher IFN- γ secretion in response to *T. cruzi* antigen stimulation. This indicated

a type I IFN-dependent impairment of IFN- γ production by T cells, resulting in a diminished parasite defense. Type I IFN-mediated suppression of the T cell IFN- γ response has also been described for infections with other pathogens, such as *Mycobacterium leprae* [256]. Besides T cells, IFN- γ production by NK cells has also been described to be suppressed by IFN- β , here in the context of HSV infections [257]. However, whether IFN- β also negatively regulates IFN- γ production by NK cells during acute and chronic *T. cruzi* infection, particularly in humans, requires further investigation.

5.4 Cell-cell contact-dependent dampening of the NK cell response against *T. cruzi*-infected fibroblasts by HLA-C corresponding inhibitory KIRs

As previously described, *T. cruzi* infection of dermal fibroblasts did not exclusively induce an increase in the expression of molecules transmitting stimulatory signals to NK cells. Transcriptome, proteome, and flow cytometric analysis revealed an increased MHC-I expression in response to the infection (figure 4.4, 4.14 and 4.15). MHC-I molecules mediate inhibitory signals to NK cells through interaction with various inhibitory KIRs, thus preventing an unwanted NK cell response under steady-state conditions [26], [27], [232]. Furthermore, MHC-I molecules can also be bound by various stimulatory KIRs. However, these exhibit lower affinities and partly higher peptide selectivities for the respective MHC-I ligands compared to their inhibitory counterparts [64], [65]. In addition, the non-classical MHC-I molecule HLA-E also interacts with two members of the NKG2 receptor family [71] and will be discussed in section 5.5.

Based on a study by Ayo and colleagues, which found an association between the combination of HLA-C corresponding KIRs and the progression of Chagas disease [217], the present work focussed on the classical MHC-I molecule HLA-C. HLA-C is of particular importance for immune regulation. Unlike HLA-A and -B, it only makes a minor contribution to antigen presentation to T cells, but inhibits NK cell function via interaction with inhibitory KIRs [258].

5.4.1 *T. cruzi* infection enhances HLA-C expression on dermal fibroblasts and the binding of corresponding KIRs

Transcriptome analysis of mock and *T. cruzi*-infected HDF and BJ fibroblasts showed a trend towards increased expression of the gene encoding the HLA-C α -chain (figure 4.18). HDFs from

the different donors exhibited large differences in basal *HLA-C* gene expression, whereas all fibroblasts showed comparable infection-related increases in *HLA-C* gene expression. The differences in basal expression were probably caused by different HLA-C allotypes in the individual donors, which were not determined more precisely in the present study. Previous publications have shown that HLA-C expression intensity is determined by HLA-C allotypes and may influence the course of infections with pathogens such as HIV-1 [259], [260]. A first indication of a relationship between the HLA-C allotype, and thus the intensity of expression over the course of Chagas disease, was given in a study by Layrisse and colleagues. The authors demonstrated an association between the presence of the weakly expressed HLA-C allele HLA-C*03 and the development of Chagas cardiomyopathy [261]. The significance of this association will be discussed later on.

Compared to mock and *T. cruzi*-infected HDF, BJ fibroblasts exhibited a comparable infection-related increase in *HLA-C* gene expression, with relatively high expression rates overall. Therefore, it was concluded that BJ fibroblasts were a suitable model to study the effects of increased HLA-C expression on the NK cell response against *T. cruzi*-infected fibroblasts. Subsequent flow cytometric analysis of HLA-C expression on the surface of mock and *T. cruzi*-infected BJ fibroblasts confirmed the infection-related expression increase (figure 4.19). Previous publications had already shown an increase in general MHC-I expression as a consequence of infections such as dengue virus [262]. However, in these cases no individual measurement of HLA-A, -B and -C expression was performed. Studies specifically examining HLA-C expression in other contexts of infection exclusively found a downregulation of HLA-C expression in response to infection with pathogens such as HIV-1 and HCMV [259], [263], [264].

The present study demonstrated that the increase in HLA-C expression on the fibroblast surface after *T. cruzi* infection was not directly caused by the intracellular infection. This was concluded from an experiment in which treatment of BJ fibroblasts with filtered supernatants from mock and *T. cruzi*-infected fibroblasts resulted in a similar HLA-C expression increase compared to a direct infection (figure 4.20). IFN- β secreted by *T. cruzi*-infected fibroblasts appeared to be only partially responsible for the increase in HLA-C expression (figure 4.21). Indeed, neutralization of IFN- β led to a significant reduction in the frequency of

HLA-C⁺ fibroblasts treated with supernatants from *T. cruzi*-infected fibroblasts. However, frequency of HLA-C⁺ fibroblasts was still increased by approximately 70% compared to mock control supernatant-treated fibroblasts. In addition to IFN- β , IFN- λ , which is also secreted by infected fibroblasts (figure 4.16), could potentially contribute to the increase in HLA-C expression. To date, no studies investigating the effect of IFN- λ on HLA-C expression or the general expression of human MHC-I molecules have been published. Nevertheless, IFN- λ has been shown to increase the expression of MHC-I molecules on murine thymic epithelial cells [265]. Therefore, investigation of the role of secreted IFN- λ on MHC-I and especially HLA-C expression of mock and *T. cruzi*-infected fibroblasts would be immensely worthwhile.

In contrast to HLA-C, the increase in total HLA-A,B,C expression in response to treatment with supernatants of *T. cruzi*-infected fibroblasts appeared to be almost completely abolished by IFN- β neutralization. Since HLA-C has been shown to exhibit the weakest expression of all classical human MHC-I molecules [266], it can be assumed that its expression has the weakest impact on the overall expression of HLA-A,B,C. However, to estimate the precise effects of IFN- β on HLA-A and -B expression, additional individual stainings would have been required. Conceivably, HLA-C surface expression may be regulated differently by individual IFNs than HLA-A and -B expression. Related to this, it has been shown that type I IFNs can increase the expression of different MHC-I alleles to varying extents [267]. Since IFN- λ induces similar signaling pathways as type I IFNs [254], it could likewise differentially affect the expression of different MHC-I alleles.

Based on polymorphisms at positions 77 and 80 of the HLA-I heavy chain, HLA-C alleles are divided into two groups, each bound by different KIRs. HLA-C1 molecules are preferentially bound by the inhibitory KIR2DL2 and KIR2DL3, as well as their activating counterpart KIR2DS2. In contrast, HLA-C2 molecules are primarily bound by the inhibitory KIR2DL1 and the activating KIR2DS1 [62]. To optimally assess the consequences of a *T. cruzi* infection-induced increase of fibroblast HLA-C expression on activity of NK cells, both groups of HLA-C molecules were considered. Since HLA-C typing of BJ fibroblasts revealed heterozygosity for HLA-C1 and HLA-C2, they could be used as a good model to answer this question. The investigation into the binding of the HLA-C1 corresponding KIR2DL2 and the HLA-C2 corresponding KIR2DL1 revealed a significantly increased binding of both KIRs to infected fibroblasts compared to the mock controls (figure 4.22). These results confirmed, on the one hand, the increase in HLA-C

expression in response to *T. cruzi* infection and, on the other hand, the heterozygosity of BJ fibroblasts for HLA-C1 and HLA-C2.

5.4.2 Infection-induced HLA-C dampens the NK cell response in most individuals

As previously mentioned, HLA-C has been described to be bound by a variety of receptors, such as the inhibitory KIRs KIR2DL1, KIR2DL2, and KIR2DL3, their activating counterparts KIR2DS1 and KIR2DS2 [62], as well as the activating CD160 [41], [103]. To determine whether stimulatory or inhibitory signals mediated by upregulated HLA-C predominate, the impact of the increased HLA-C expression was investigated using a KO of HLA-C in BJ fibroblasts instead of blocking individual receptors on NK cells. To this end, CRISPR/Cas9 technology was used to create a double-strand break in the HLA-C gene, where an RFP and puromycin resistance gene were inserted for subsequent selection of successfully transduced clones. Following the generation of BJ HLA-C KO single-cell clones, the cells were mock-treated or infected with *T. cruzi* and analyzed for their HLA-C and general MHC-I expression (figure 4.23). For the analyses, a clone was selected that showed no impairment of overall MHC-I expression due to possible off-target effects compared with the WT control. Simultaneously, HLA-C appeared to be successfully knocked out in the selected clone, as it was detectable on less than 1% of transfected BJ fibroblasts by flow cytometric analysis. The staining of occasional cells was likely due to nonspecific binding of the anti-HLA-C antibody clone DT-9 to other MHC-I molecules, as indicated by a study from Corrah and colleagues [268].

Moreover, binding assays for KIR2DL1 and KIR2DL2 ensured that not only the binding site for the used anti-HLA-C antibody clone was disturbed, but also functional binding of corresponding receptors was prevented (figure 4.24). Regarding HLA-C2, a complete functional KO was clearly confirmed since, in contrast to WT BJ fibroblasts, no KIR2DL1-Fc molecules were bound even after *T. cruzi* infection. KIR2DL2-Fc molecules corresponding to HLA-C1 were not bound by mock-treated HLA-C KO BJ fibroblasts. Although the frequency of KIR2DL2-bound *T. cruzi*-infected HLA-C KO BJ fibroblasts was reduced 20-fold compared to WT BJ fibroblast controls, minimal binding of KIR2DL2 was still detectable. The remaining binding of KIR2DL2 could be explained by the interaction with certain HLA-B allotypes, for which binding to KIR2DL2 has been demonstrated with low affinity [63]. Overall, the binding assays

of the HLA-C1 and -C2 corresponding KIRs confirmed a successful, functional KO of HLA-C in the selected clone.

Finally, the influence of the HLA-C KO on the NK cell response to mock and *T. cruzi*-infected fibroblasts was investigated by coculture (figure 4.25). Compared to coculture with WT BJ fibroblasts, coculture with HLA-C KO BJ fibroblasts resulted in higher NK cell activity in all except one NK cell donor. This effect was observed for coculture with mock as well as with *T. cruzi*-infected HLA-C KO fibroblasts. These results demonstrate the contribution of HLA-C in preventing an unwanted NK cell response in steady-state. The elimination of HLA-C-mediated signals leads to NK cell recognition of "missing self" on target cells [27] and thus to enhanced NK cell activity in response to mock-treated HLA-C KO BJ fibroblasts. In the case of *T. cruzi*-infected fibroblasts, increased HLA-C expression appears primarily to dampen NK cell activity, possibly to prevent an exaggerated, adverse reaction. Since HLA-C is not specifically upregulated on infected but also on surrounding fibroblasts by secreted cytokines such as IFN- β , it is conceivable that HLA-C-mediated inhibitory signals should prevent lysis of uninfected fibroblasts and thus unnecessary tissue damage. Such an exaggerated NK cell reaction leading to tissue injury has been observed, for example, during *Ehrlichia chaffeensis* infection in the liver [269].

In contrast to all other tested NK cells, NK cells from donor A showed a reduced NK cell response to *T. cruzi*-infected HLA-C KO fibroblasts compared to WT controls. Thus, in this case, the infection-induced increase in HLA-C expression appeared to mediate stimulatory rather than inhibitory signals towards NK cells. This could be related to the genotype of HLA-C corresponding KIRs (KIR2DL1⁺/2DL2⁻/2DL3⁺/2DS1⁺/2DS2⁻), which was unique among all tested donors. In this case, HLA-C1 molecules on fibroblasts can mediate inhibitory signals exclusively via engagement of KIR2DL3 on NK cells. Work by Moesta and colleagues has shown that KIR2DL3 is a much weaker receptor for HLA-C1 than KIR2DL2. Due to two polymorphisms distal to the ligand-binding site, the angle between the two binding-relevant domains is altered, making HLA-C1 binding more difficult and resulting in fewer transduced inhibitory signals [63]. Therefore, it is possible that, in this case, HLA-C1 molecules on fibroblasts are additionally bound by the stimulatory CD160 on NK cells [41], [103] and thus transmit more stimulatory than inhibitory signals. Regarding HLA-C2 molecules, two corresponding KIRs are present on NK cells from donor A: KIR2DL1 and KIR2DS1. Both KIRs are externally almost identical, but

intracellularly transmit inhibitory and stimulatory signals, respectively [270]. As mentioned above, the interaction of activating KIRs with MHC-I ligands is generally weaker than that of their inhibitory counterparts [271]. However, in a study by Chapel and colleagues, peptide selectivity of KIR2DS1 was demonstrated [65], implying that binding of KIR2DS1 to HLA-C2 molecules of infected cells may be increased due to the altered repertoire of presented peptides. Such an infection-mediated induction of KIR2DS1 binding has been demonstrated, for example, for HCMV-infected fibroblasts [272]. To clarify whether *T. cruzi* infection of dermal fibroblasts also leads to induction of KIR2DS1 binding requires further investigation. Taken together, the data suggest that the combination of HLA-C corresponding KIRs present in NK cells derived from donor A mediates stimulatory instead of inhibitory signals in response to HLA-C exposed on *T. cruzi*-infected fibroblasts. To validate this, the experiments would need to be conducted with a larger sample size.

Overall, it was concluded that, on the one hand, the *T. cruzi* infection-induced increase in HLA-C on fibroblasts in most individuals presumably contributes to the containment of the NK cell response, thus preventing a possible exaggerated detrimental response. On the other hand, the results also provided first indications that this effect depends on the genotype of the HLA-C corresponding KIRs. This assumption is supported by the previously quoted study by Ayo and colleagues in 2015. Their data showed significantly more frequent presence of the activating KIR2DS2 in the simultaneous absence of its inhibitory counterpart KIR2DL2 in chronic Chagas patients (12.2%) compared to healthy controls (4.2%). Furthermore, this combination of HLA-C1 corresponding KIRs occurred significantly more frequently in symptomatic (22.7%) compared to asymptomatic chronic Chagas patients (6.9%) [217]. These data endorse the hypothesis of an exacerbated course of Chagas disease due to an exaggerated NK cell response mediated by insufficient inhibitory signals. This assumption is also supported by the study by Layrisse and colleagues. As mentioned above, the authors revealed a correlation between the presence of the HLA-C*03 allele and a symptomatic course of Chagas disease in the chronic stage [261]. Since HLA-C*03 is the weakest expressed HLA-C1 allele [259], it can be assumed to mediate the weakest inhibitory signals to NK cells. Based on this, an investigation of *T. cruzi* infection-mediated HLA-C expression in parasitized tissues during the chronic stage of Chagas disease would also be of great interest.

5.5 Further potential modulators of NK cell responses against *T. cruzi*-infected fibroblasts

Besides the discussed mechanisms regulating the NK cell response to *T. cruzi*-infected fibroblasts, two additional potential modulators of NK cell activity were identified by transcriptome analysis of mock and *T. cruzi*-infected HDF and BJ fibroblasts. Here, a significantly increased expression of the genes encoding for nectin-2 and the α -chain of HLA-E were observed in response to *T. cruzi* infection (figure 4.27 A and 4.28 A). The increased nectin-2 and HLA-E protein expression on the fibroblast surface in response to infection was subsequently confirmed by flow cytometric analysis (figure 4.27 B and 4.28 B). Both molecules have been described to interact with stimulatory as well as with inhibitory receptors on NK cells, resulting in an altered NK cell response.

Nectin-2 has been shown to be bound by the stimulatory DNAM-1 [111] as well as inhibitory acting TIGIT [112] and PVRIG [113] on NK cells. However, binding affinities of the different receptors for nectin-2 differ widely, with TIGIT having the lowest and PVRIG the highest binding affinity [50], [113]. Besides the binding affinities, the expression levels of the different receptors on NK cells also need to be considered. Whereas DNAM-1 is expressed on around 90% of NK cells [273], flow cytometric analysis of PVRIG expression showed that it was only present on about a quarter of total NK cells, with low expression overall per cell [113]. Therefore, regarding the total NK cell population, it is likely that the stimulatory effect of nectin-2 through engagement of DNAM-1 is predominant on most NK cells. This assumption is also supported by a study by Molfetta and colleagues. Here, the nectin-2 surface expression was increased on various cell lines and primary cells by blocking the ubiquitin pathway, which resulted in increased cytotoxic effector functions in cocultured NK cells. Moreover, the increased NK cell cytotoxicity was proven to be mediated by DNAM-1, as treatment with a blocking anti-DNAM-1 antibody abolished the effect [274].

Whether the increased nectin-2 expression on fibroblasts in response to *T. cruzi* infection also contributes to the increase in NK cell activity remains to be investigated.

The non-classical MHC-I molecule HLA-E has also been shown to mediate both inhibitory and stimulatory signals to NK cells by interacting with two different members of the NKG2 family [71]. Usually, HLA-E presents peptides derived from signal sequences of other MHC-I

molecules, thereby reflecting the general MHC-I expression [69], [275]. Since an increase in HLA-A,B,C expression in response to *T. cruzi* infection was previously observed in the present study (figure 4.4), an increased presence of HLA-E on the fibroblast surface was anticipated. The described HLA-E peptide complexes primarily interact with NKG2A, sending inhibitory signals to NK cells [69]. In contrast, the stimulatory NKG2C has been shown to bind to these complexes with a six-fold lower binding affinity [276]. However, besides peptides derived from signal sequences of other MHC-I molecules, HLA-E has also been shown to present the signal peptide of the HCMV glycoprotein UL40 on the surface of infected cells, leading to specific interaction with the stimulatory NKG2C on NK cells [73], [277]. In this context, an increased IFN- γ production by NKG2C⁺ NK cells during HCMV infection [278] and an enhanced proliferation of NKG2C⁺ NK cells have been observed [279]. Nevertheless, this does not seem to apply to NK cells during *T. cruzi* infection. Here, no change in the frequency of NKG2C⁺ NK cells was observed after coculture with *T. cruzi*-infected fibroblasts compared with mock controls (data not shown). In contrast, the frequency of NKG2A⁺ NK cells significantly increased by around 30% in response to coculture with *T. cruzi*-infected compared to mock-treated HDF (data not shown). Therefore, it seems likely that HLA-E, which is upregulated on dermal fibroblasts in response to *T. cruzi* infection, transmits inhibitory rather than stimulatory signals to NK cells. However, further investigations are required for a reliable statement.

Furthermore, in the present study it was observed that the increase of nectin-2 and HLA-E expression on BJ fibroblasts in response to *T. cruzi* infection was at least partially mediated by soluble factors released by infected fibroblasts (figure 4.27 C and 4.28 C). Again, IFN- β secreted by *T. cruzi*-infected fibroblasts could play a pivotal role, since a study by Wolpert and colleagues revealed an IFN- β -dependent increase in surface expression of nectin-2 as well as HLA-E on glioblastoma-initiating cells [280]. Whether this also applies to the increased nectin-2 and HLA-E expression on dermal fibroblasts needs to be verified. Furthermore, increased expression of HLA-E on the cell surface could be indirectly mediated by increased expression of other MHC-I molecules. Nevertheless, this once again illustrates the complexity of the effects of IFN- β secreted by *T. cruzi*-infected fibroblasts on the NK cell response.

6 Future Perspectives

The results of the present study first revealed a direct activation of NK cells by *T. cruzi*-infected dermal fibroblasts, and subsequently characterized diverse underlying mechanisms controlling the intensity of the NK cell response.

Nevertheless, it has not yet been clarified whether the activated NK cells specifically lyse *T. cruzi*-infected fibroblasts or whether surrounding healthy cells are also compromised by released cytotoxic mediators. To investigate this, the duration and E:T ratio of NK cell fibroblast cocultures would need to be adjusted to optimally visualize target cell lysis by flow cytometric analysis. Here, NK cell-mediated permeabilization of fibroblasts could be visualized using a fixable viability dye, while infected fibroblasts could be distinguished by subsequent intracellular parasite staining. Besides target cell lysis, whether the activity of human NK cells induces trypanocidal mechanisms in *T. cruzi*-infected fibroblasts, as has been demonstrated for murine cells [181], could be studied. For this purpose, the average number of parasites per fibroblast without and with cocultured NK cells could be determined by fluorescence microscopy using the Opera Phenix high content screening system.

In addition to this further characterization of NK cell effector functions against *T. cruzi*-infected fibroblasts, several potential regulators of the NK cell response could be analyzed in more detail. This study demonstrated, for example, an increased presence of vimentin, HVEM, and MHC-I molecules such as HLA-C on the fibroblast surface in response to *T. cruzi* infection, leading to enhancement or inhibition of the NK cell response, respectively. However, the equilibrium regulating the NK cell response could be influenced by additional differentially expressed ligands such as nectin-2 and HLA-E, which were also found to be upregulated in response to the infection and which are known to interact with various NK cell receptors. To determine how their altered expression affects the NK cell response against *T. cruzi*-infected fibroblasts, the interaction of these ligands with the corresponding NK cell receptors could be prevented by, for example, a CRISPR/Cas9-mediated nectin-2 or HLA-E KO in BJ fibroblasts analogous to the HLA-C KO described in this study.

Moreover, a more detailed investigation of the effect of IFN- β and IFN- λ secreted by infected fibroblasts would be of great interest. In this study, IFN- β was shown to both positively and negatively influence NK cell responses induced by *T. cruzi*-infected fibroblasts through multiple pathways. The impact of secreted IFN- λ could not be clarified yet. The effect could be investigated analogously to IFN- β through antibody-mediated neutralization of the

cytokine in the supernatants from mock and *T. cruzi*-infected fibroblasts, as well as during direct fibroblast cocultures with NK cells.

By studying the NK cell interaction with *T. cruzi*-infected dermal fibroblasts, the early acute NK cell response in *T. cruzi*-parasitized skin was reflected. In the future, the NK cell response during the later acute phase as well as the chronic phase of Chagas disease should be characterized, whereby the interaction of NK cells with parasitized skeletal and cardiac muscle cells is particularly interesting. First, a comparative transcriptome analysis of the different mock and *T. cruzi*-infected muscle cells could be performed to identify similarities and differences to skin fibroblasts. Based on the collected transcriptome data, further mechanistic analyses could be performed analogous to the protocols established in the present study.

In the long term, elucidation of the contribution of NK cells to parasite control at different stages of infection and knowledge of the underlying mechanisms affecting NK cell function could contribute to the development of new therapeutic options.

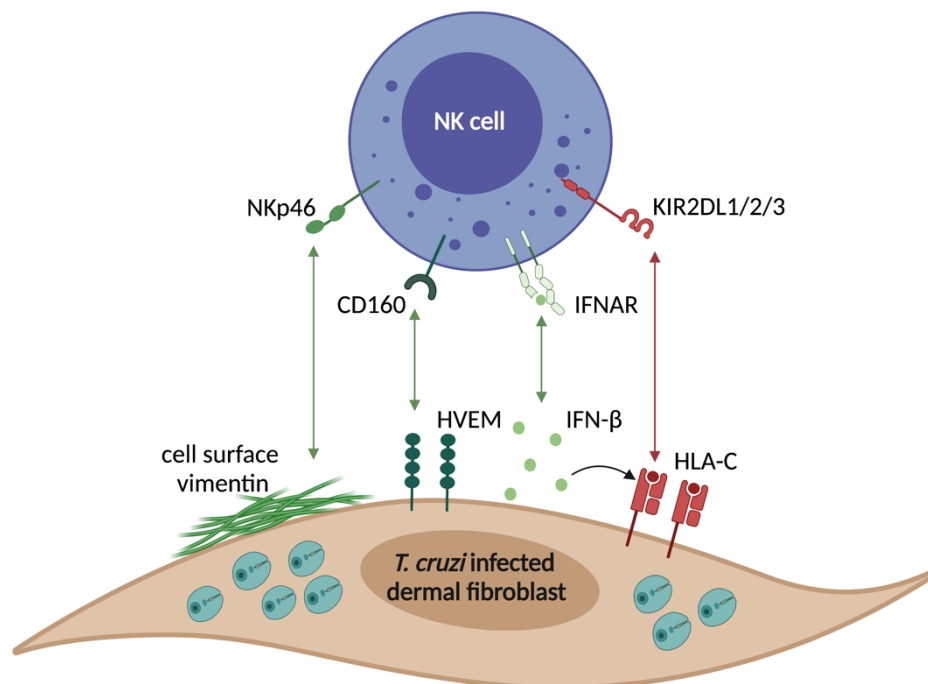
7 Abstract

The potentially life-threatening Chagas disease is caused by the protozoan parasite *Trypanosoma cruzi* (*T. cruzi*). It is mainly prevalent in rural areas in Latin America and is classified as one of the 20 neglected tropical diseases by the WHO. Whereas the acute stage of infection is usually mild or asymptomatic, about 30% of infected individuals develop cardiac or gastrointestinal symptoms during the chronic stage. The approved drugs can entirely eliminate the parasites exclusively during the acute stage, with treatment often accompanied by severe side effects. Since *T. cruzi* parasites are mainly transmitted to humans by triatomine bugs, the skin is the main entry route for the parasites. Thus, it is likely that the early immune response against parasitized skin fibroblasts influences the parasite's spread to other tissues and organs. Considering the obligatory intracellular life cycle of *T. cruzi*, natural killer (NK) cells are expected to substantially contribute to the innate immune response. They can sense their target cells through a variety of different mechanisms, resulting in direct cytotoxic effector functions and secretion of cytokines such as IFN- γ .

The present study aimed to investigate the response of human NK cells to *T. cruzi*-infected dermal fibroblasts as well as the underlying mechanisms. Initially, *in vitro* cocultures were established for this purpose, demonstrating that *T. cruzi*-infected primary human dermal fibroblasts as well as infected cells of the foreskin fibroblast cell line BJ promote NK cell degranulation. Since transcriptome analysis demonstrated a comparable response of primary and BJ fibroblasts to *T. cruzi* infection, BJ fibroblasts were used for subsequent mechanistic analyses. Here, NK cell activation by *T. cruzi*-infected BJ fibroblasts was shown to be strongly dependent on the engagement of the stimulatory NK cell receptors NKp46 and CD160. *T. cruzi* infection of BJ fibroblasts resulted in the increased presence of the respective ligands vimentin and HVEM on the fibroblast surface as well as an increased binding of NKp46 and CD160. Finally, NKp46 and CD160 receptor blockade on NK cells led to significantly reduced NK cell effector functions. In addition to these cell-cell contact-dependent mechanisms, contact-independent activation of NK cells by supernatants of *T. cruzi*-infected fibroblasts was observed. IFN- β neutralization experiments demonstrated that IFN- β secreted by *T. cruzi*-infected BJ fibroblasts directly promoted NK cell activity. However, secreted IFN- β also increased MHC-I expression on fibroblasts, leading to the reduction of the NK cell response through interaction with inhibitory NK cell receptors. Results of coculture experiments indicate that activating stimuli predominate in the first few hours, but these could be

compensated by inhibitory signals in the later course of infection. Finally, the role of the MHC-I molecule HLA-C was investigated, which showed increased expression on fibroblasts in response to *T. cruzi* infection and which has been described to interact with both the activating CD160 as well as activating and inhibitory KIRs on NK cells. NK cell cocultures with HLA-C KO BJ fibroblasts generated in this study showed that HLA-C inhibited NK cell activity of most individuals, probably to avoid an exaggerated response.

In conclusion, the *in vitro* model established in this study enables the investigation of regulatory mechanisms of the NK cell response in *T. cruzi*-parasitized dermis. Characterization of these mechanisms revealed that the NK cell response here is controlled by a precisely tuned balance of diverse stimulatory and inhibitory signals. In the future, the better understanding of these mechanisms may help to develop efficient and tolerable therapy options.



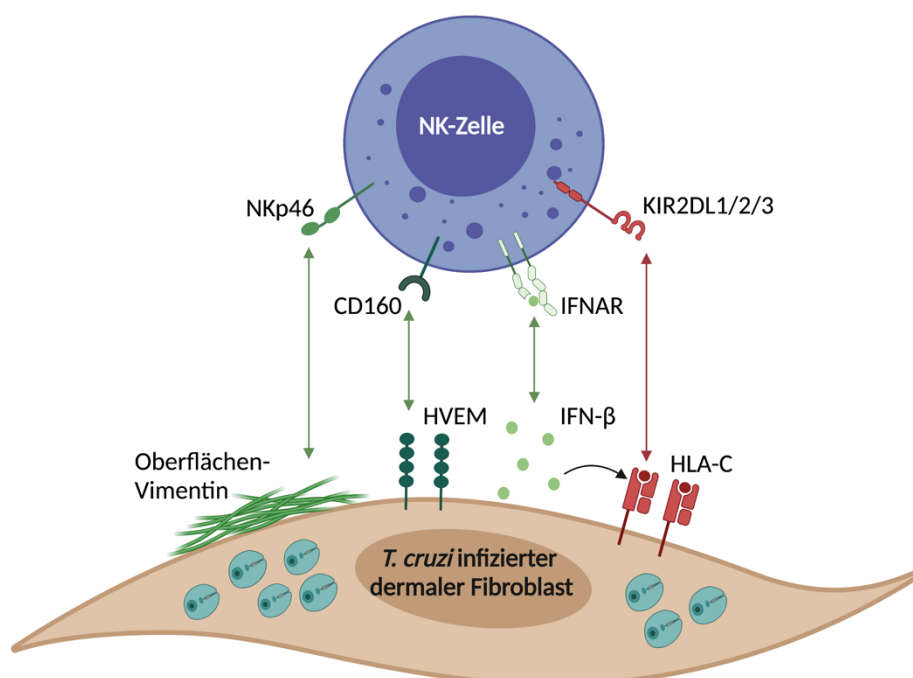
8 Zusammenfassung

Die potenziell lebensbedrohliche Chagas-Krankheit wird durch den Protozoen-Parasiten *Trypanosoma cruzi* (*T. cruzi*) verursacht. Sie ist hauptsächlich in ländlichen Gebieten Lateinamerikas verbreitet und wird von der WHO als eine der 20 vernachlässigten Tropenkrankheiten eingestuft. Während das akute Stadium der Infektion in der Regel mild oder asymptomatisch verläuft, entwickeln etwa 30 % der Infizierten im chronischen Stadium kardiale oder gastrointestinale Symptome. Die zugelassenen Arzneimittel können die Parasiten ausschließlich während der akuten Phase vollständig eliminieren, wobei die Behandlung häufig mit schweren Nebenwirkungen einhergeht. Da die Übertragung von *T. cruzi* Parasiten auf den Menschen hauptsächlich durch Raubwanzen erfolgt, stellt die Haut den wichtigsten Eintrittsweg dar. Somit ist anzunehmen, dass die frühe Immunreaktion gegen parasitierte dermale Fibroblasten die Ausbreitung der Parasiten in andere Gewebe und Organe beeinflusst. In Anbetracht des obligatorisch intrazellulären Lebenszyklus von *T. cruzi* ist davon auszugehen, dass Natürliche Killerzellen (NK-Zellen) einen beträchtlichen Beitrag zur angeborenen Immunantwort leisten. Sie können ihre Zielzellen durch eine Vielzahl unterschiedlicher Mechanismen erkennen, was zu einer direkten zytotoxischen Effektor-Funktion und zur Sekretion von Zytokinen wie IFN- γ führt.

In der vorliegenden Arbeit sollten die Reaktion menschlicher NK-Zellen auf *T. cruzi* infizierte dermale Fibroblasten sowie die zugrunde liegenden Mechanismen untersucht werden. Zunächst wurden zu diesem Zweck *in vitro*-Kokulturen etabliert, die eine Verstärkung der NK-Zell-Degranulation durch *T. cruzi*-infizierte primäre humane dermale Fibroblasten sowie infizierte Zellen der Vorhautfibroblasten-Zelllinie BJ nachwies. Da eine Transkriptomanalyse eine vergleichbare Reaktion von primären und BJ-Fibroblasten auf eine *T. cruzi*-Infektion nachwies, wurden BJ-Fibroblasten für die nachfolgenden mechanistischen Analysen verwendet. Hier zeigte sich, dass die Aktivierung von NK-Zellen durch *T. cruzi* infizierte BJ-Fibroblasten stark von der Aktivierung der stimulierenden NK-Zell-Rezeptoren NKp46 und CD160 abhängt. Eine *T. cruzi*-Infektion von BJ-Fibroblasten führte zu einem erhöhten Vorkommen der jeweiligen Liganden Vimentin und HVEM auf der Fibroblasten-Oberfläche sowie zu einer erhöhten Bindung von NKp46 und CD160. Schließlich führte die Blockade von NKp46 und CD160 auf NK-Zellen zu einer signifikanten Verringerung verschiedener NK-Zell-Effektorfunktionen. Zusätzlich zu diesen Zell-Zell-Kontakt-abhängigen Mechanismen wurde eine Kontakt-unabhängige Aktivierung von NK-Zellen durch Überstände *T. cruzi*

infizierter Fibroblasten beobachtet. IFN- β -Neutralisationsexperimente wiesen nach, dass durch *T. cruzi* infizierte BJ-Fibroblasten sekretiertes IFN- β die NK-Zell-Aktivität direkt fördert. Das sekretierte IFN- β steigerte jedoch auch die MHC-I-Expression auf BJ-Fibroblasten, was durch die Interaktion mit inhibitorischen NK-Zell-Rezeptoren zur Verringerung der NK-Zell-Antwort führte. Die Ergebnisse der Kokultur-Experimente deuten darauf hin, dass in den ersten Stunden aktivierende Stimuli überwiegen, die jedoch im späteren Verlauf der Infektion durch hemmende Signale kompensiert werden könnten. Schließlich wurde die Rolle des MHC-I Moleküls HLA-C untersucht, das hier als Reaktion auf die *T. cruzi*-Infektion verstärkt auf Fibroblasten exprimiert wurde und beschrieben ist sowohl mit dem stimulierenden CD160 als auch mit aktivierenden und inhibitorischen KIRs auf NK-Zellen zu interagieren. NK-Zell-Kokulturen mit in dieser Arbeit generierten HLA-C KO BJ-Fibroblasten zeigten, dass HLA-C die NK-Zell-Aktivität der meisten Individuen inhibierte, möglicherweise um eine übermäßige Reaktion zu vermeiden.

Zusammenfassend wurde in dieser Studie ein *in-vitro*-Modell etabliert, welches die Untersuchung der Mechanismen zur Regulation der NK-Zell-Antwort in *T. cruzi*-parasitierter Dermis ermöglicht. Die Charakterisierung dieser Mechanismen zeigte, dass die NK-Zell-Antwort hier durch ein fein abgestimmtes Gleichgewicht verschiedener stimulatorischer und inhibitorischer Signale gesteuert wird. In Zukunft könnte das bessere Verständnis dieser Mechanismen dazu beitragen, effiziente und verträgliche Therapiemöglichkeiten zu entwickeln.



9 Literature

- [1] R. Kiessling, E. Klein, H. Pross, and H. Wigzell, “„Natural” killer cells in the mouse. II. Cytotoxic cells with specificity for mouse Moloney leukemia cells. Characteristics of the killer cell”, *Eur. J. Immunol.*, vol. 5, no. 2, pp. 117–121, 1975.
- [2] G. Trinchieri, “Biology of Natural Killer Cells”, *Adv. Immunol.*, vol. 47, pp. 187–376, 1989.
- [3] R. Vankayalapati, A. Garg, A. Porgador, D. E. Griffith, P. Klucar, *et al.*, “Role of NK Cell-Activating Receptors and Their Ligands in the Lysis of Mononuclear Phagocytes Infected with an Intracellular Bacterium”, *J. Immunol.*, vol. 175, no. 7, pp. 4611–4617, 2005.
- [4] T. M. Scharton and P. Scott, “Natural killer cells are a source of interferon γ that drives differentiation of CD4+ T cell subsets and induces early resistance to leishmania major in mice”, *J. Exp. Med.*, vol. 178, no. 2, pp. 567–578, 1993.
- [5] A. G. Freud, B. L. Mundy-Bosse, J. Yu, and M. A. Caligiuri, “The Broad Spectrum of Human Natural Killer Cell Diversity”, *Immunity*, vol. 47, no. 5. NIH Public Access, pp. 820–833, 2017.
- [6] J. C. Sun and L. L. Lanier, “NK cell development, homeostasis and function: Parallels with CD8 + T cells”, *Nature Reviews Immunology*, vol. 11, no. 10. NIH Public Access, pp. 645–657, 2011.
- [7] L. L. Lanier, C. Chang, M. Azuma, J. J. Ruitenber, J. J. Hemperly, *et al.*, “Molecular and functional analysis of human natural killer cell-associated neural cell adhesion molecule (N-CAM/CD56).”, *J. Immunol.*, vol. 146, no. 12, pp. 4421–6, 1991.
- [8] M. A. Cooper, T. A. Fehniger, and M. A. Caligiuri, “The biology of human natural killer-cell subsets”, *Trends Immunol.*, vol. 22, no. 11, pp. 633–640, 2001.
- [9] Y. Cao, X. Wang, T. Jin, Y. Tian, C. Dai, *et al.*, “Immune checkpoint molecules in natural killer cells as potential targets for cancer immunotherapy”, *Signal Transduct. Target. Ther.*, vol. 5, no. 1, p. 250, 2020.
- [10] A. Chan, D.-L. Hong, A. Atzberger, S. Kollnberger, A. D. Filer, *et al.*, “CD56bright Human NK Cells Differentiate into CD56dim Cells: Role of Contact with Peripheral Fibroblasts”, *J. Immunol.*, vol. 179, no. 1, pp. 89–94, 2007.
- [11] C. I. Domaica, M. B. Fuertes, I. Uriarte, M. V Girart, and J. Sardañ Ons, “Human Natural Killer Cell Maturation Defect Supports In Vivo CD56 bright to CD56 dim Lineage Development”, *PLoS One*, vol. 7, no. 12, p. 51677, 2012.
- [12] C. Fauriat, E. O. Long, H.-G. Ljunggren, and Y. T. Bryceson, “Regulation of human NK-cell cytokine and chemokine production by target cell recognition”, *Blood*, vol. 115, no. 11, pp. 2167–2176, 2010.
- [13] A. Goyos, M. Fort, A. Sharma, and H. Lebec, “Current Concepts in Natural Killer Cell Biology and Application to Drug Safety Assessments”, *Toxicol. Sci.*, vol. 170, no. 1, pp. 10–19, 2019.
- [14] T. Bald, M. F. Krummel, M. J. Smyth, and K. C. Barry, “The NK cell–cancer cycle: advances and new challenges in NK cell–based immunotherapies”, *Nat. Immunol.*, vol. 21, no. 8, pp. 835–847, 2020.
- [15] R. M. Srivastava, B. Savithri, and A. Khar, “Activating and inhibitory receptors and their role in Natural Killer cell function”, *Indian J. Biochem. Biophys.*, vol. 40, no. 5, pp. 291–299, 2003.
- [16] S. P. Cullen and S. J. Martin, “Mechanisms of granule-dependent killing”, *Cell Death Differ.*, vol. 15, no. 2, pp. 251–262, 2008.

- [17] Y. T. Bryceson, M. E. March, D. F. Barber, H.-G. Ljunggren, and E. O. Long, "Cytolytic granule polarization and degranulation controlled by different receptors in resting NK cells", *J. Exp. Med.*, vol. 202, no. 7, pp. 1001–1012, 2005.
- [18] F. Dotiwala and J. Lieberman, "Granulysin: killer lymphocyte safeguard against microbes", *Curr. Opin. Immunol.*, vol. 60, pp. 19–29, 2019.
- [19] H. Barman, M. Walch, S. Latinovic-Golic, C. Dumrese, M. Dolder, *et al.*, "Cholesterol in Negatively Charged Lipid Bilayers Modulates the Effect of the Antimicrobial Protein Granulysin", *J. Membr. Biol.*, vol. 212, no. 1, pp. 29–39, 2006.
- [20] F. Dotiwala, S. Mulik, R. B. Polidoro, J. A. Ansara, B. A. Burleigh, *et al.*, "Killer lymphocytes use granulysin, perforin and granzymes to kill intracellular parasites", *Nat. Med.*, vol. 22, no. 2, pp. 210–216, 2016.
- [21] M. J. Smyth, E. Cretney, J. M. Kelly, J. A. Westwood, S. E. A. Street, *et al.*, "Activation of NK cell cytotoxicity", *Mol. Immunol.*, vol. 42, no. 4, pp. 501–510, 2005.
- [22] R. P. A. Wallin, V. Screpanti, J. Michaëlsson, A. Grandien, and H.-G. Ljunggren, "Regulation of perforin-independent NK cell-mediated cytotoxicity.", *Eur. J. Immunol.*, vol. 33, no. 10, pp. 2727–35, 2003.
- [23] E. Vivier, D. H. Raulet, A. Moretta, M. A. Caligiuri, L. Zitvogel, *et al.*, "Innate or Adaptive Immunity? The Example of Natural Killer Cells", *Science (80-)*, vol. 331, no. 6013, pp. 44–49, 2011.
- [24] K. Schroder, P. J. Hertzog, T. Ravasi, and D. A. Hume, "Interferon- γ : an overview of signals, mechanisms and functions", *J. Leukoc. Biol.*, vol. 75, no. 2, pp. 163–189, 2004.
- [25] R. Wang, J. J. Jaw, N. C. Stutzman, Z. Zou, and P. D. Sun, "Natural killer cell-produced IFN- γ and TNF- α induce target cell cytotoxicity through up-regulation of ICAM-1.", *J. Leukoc. Biol.*, vol. 91, no. 2, pp. 299–309, 2012.
- [26] L. L. Lanier, "NK cell recognition", *Annual Review of Immunology*, vol. 23, no. 1, pp. 225–274, 2005.
- [27] H.-G. Ljunggren and K. Kärre, "In search of the 'missing self': MHC molecules and NK cell recognition", *Immunol. Today*, vol. 11, pp. 237–244, 1990.
- [28] E. O. Long and S. Rajagopalan, "Stress Signals Activate Natural Killer Cells", *J. Exp. Med.*, vol. 196, no. 11, p. 1399, 2002.
- [29] N. W. Zwirner and C. I. Domaica, "Cytokine regulation of natural killer cell effector functions", *BioFactors*, vol. 36, no. 4, pp. 274–288, 2010.
- [30] E. Vivier, S. Ugolini, D. Blaise, C. Chabannon, and L. Brossay, "Targeting natural killer cells and natural killer T cells in cancer", *Nat. Rev. Immunol.*, vol. 12, no. 4, pp. 239–252, 2012.
- [31] E. O. Long, H. S. Kim, D. Liu, M. E. Peterson, and S. Rajagopalan, "Controlling natural killer cell responses: integration of signals for activation and inhibition", *Annu. Rev. Immunol.*, vol. 31, pp. 227–58, 2013.
- [32] J. R. Šedý, R. L. Bjordahl, V. Bekiaris, M. G. Macauley, B. C. Ware, *et al.*, "CD160 Activation by Herpesvirus Entry Mediator Augments Inflammatory Cytokine Production and Cytolytic Function by NK Cells", *J. Immunol.*, vol. 191, no. 2, pp. 828–836, 2013.
- [33] C. Sordo-Bahamonde, S. Lorenzo-Herrero, A. P. Gonzalez-Rodriguez, Á. R. Payer, E. González-García, *et al.*, "BTLA/HVEM Axis Induces NK Cell Immunosuppression and Poor Outcome in Chronic Lymphocytic Leukemia.", *Cancers (Basel)*, vol. 13, no. 8, 2021.

- [34] N. Stanietzky and O. Mandelboim, "Paired NK cell receptors controlling NK cytotoxicity", *FEBS Lett.*, vol. 584, no. 24, pp. 4895–4900, 2010.
- [35] M. Valés-Gómez, H. T. Reyburn, R. A. Erskine, M. López-Botet, and J. L. Strominger, "Kinetics and peptide dependency of the binding of the inhibitory NK receptor CD94/NKG2-A and the activating receptor CD94/NKG2-C to HLA-E", *EMBO J.*, vol. 18, no. 15, pp. 4250–60, 1999.
- [36] X. Yu, K. Harden, L. C. Gonzalez, M. Francesco, E. Chiang, *et al.*, "The surface protein TIGIT suppresses T cell activation by promoting the generation of mature immunoregulatory dendritic cells", *Nat. Immunol.*, vol. 10, no. 1, pp. 48–57, 2009.
- [37] L. L. Lanier, "Natural killer cell receptor signaling", *Curr. Opin. Immunol.*, vol. 15, no. 3, pp. 308–314, 2003.
- [38] C. Bottino, R. Castriconi, L. Moretta, and A. Moretta, "Cellular ligands of activating NK receptors", *Trends Immunol.*, vol. 26, no. 4, pp. 221–6, 2005.
- [39] A. D. Barrow, C. J. Martin, and M. Colonna, "The Natural Cytotoxicity Receptors in Health and Disease", *Front. Immunol.*, vol. 10, p. 909, 2019.
- [40] O. Mandelboim, P. Malik, D. M. Davis, C. H. Jo, J. E. Boyson, *et al.*, "Human CD16 as a lysis receptor mediating direct natural killer cell cytotoxicity", *Proc. Natl. Acad. Sci. U. S. A.*, vol. 96, no. 10, pp. 5640–4, 1999.
- [41] P. Le Bouteiller, A. Barakonyi, J. Giustiniani, F. Lenfant, A. Marie-Cardine, *et al.*, "Engagement of CD160 receptor by HLA-C is a triggering mechanism used by circulating natural killer (NK) cells to mediate cytotoxicity", *Proc. Natl. Acad. Sci. U. S. A.*, vol. 99, no. 26, pp. 16963–16968, 2002.
- [42] Y. T. Bryceson, M. E. March, H. G. Ljunggren, and E. O. Long, "Activation, coactivation, and costimulation of resting human natural killer cells", *Immunol. Rev.*, vol. 214, no. 1, pp. 73–91, 2006.
- [43] J. B. Swann, Y. Hayakawa, N. Zerafa, K. C. F. Sheehan, B. Scott, *et al.*, "Type I IFN Contributes to NK Cell Homeostasis, Activation, and Antitumor Function", *J. Immunol.*, vol. 178, no. 12, pp. 7540–7549, 2007.
- [44] J. W. Ho, O. Herschkovitz, M. Peiris, A. Zilka, A. Bar-Ilan, *et al.*, "H5-type influenza virus hemagglutinin is functionally recognized by the natural killer-activating receptor NKp44.", *J. Virol.*, vol. 82, no. 4, pp. 2028–32, 2008.
- [45] M.-L. Hecht, B. Rosental, T. Horlacher, O. Herschkovitz, J. L. De Paz, *et al.*, "Natural cytotoxicity receptors NKp30, NKp44 and NKp46 bind to different heparan sulfate/heparin sequences", *J. Proteome Res.*, vol. 8, no. 2, pp. 712–20, 2009.
- [46] C. J. Chan, M. J. Smyth, and L. Martinet, "Molecular mechanisms of natural killer cell activation in response to cellular stress", *Cell Death Differ.*, vol. 21, no. 1, pp. 5–14, 2014.
- [47] R. Romee, J. W. Leong, and T. A. Fehniger, "Utilizing cytokines to function-enable human NK cells for the immunotherapy of cancer", *Scientifica (Cairo)*, vol. 2014, p. 205796, 2014.
- [48] F. Souza-Fonseca-Guimaraes, A. Young, D. Mittal, L. Martinet, C. Bruedigam, *et al.*, "NK cells require IL-28R for optimal in vivo activity", *Proc. Natl. Acad. Sci. U. S. A.*, vol. 112, no. 18, pp. E2376–E2384, 2015.
- [49] T. Pazina, A. Shemesh, M. Brusilovsky, A. Porgador, and K. S. Campbell, "Regulation of the Functions of Natural Cytotoxicity Receptors by Interactions with Diverse Ligands and Alterations in Splice Variant Expression", *Front. Immunol.*, vol. 8, p. 369, 2017.
- [50] N. Stein, P. Tsukerman, and O. Mandelboim, "The paired receptors TIGIT and DNAM-1 as targets for

- therapeutic antibodies”, *Hum. Antibodies*, vol. 25, no. 3–4, pp. 111–119, 2017.
- [51] A. P. Gonzalez-Rodriguez, M. Villa-Álvarez, C. Sordo-Bahamonde, S. Lorenzo-Herrero, and S. Gonzalez, “NK Cells in the Treatment of Hematological Malignancies”, *J. Clin. Med.*, vol. 8, no. 10, 2019.
- [52] K. A. Holder and M. D. Grant, “TIGIT Blockade: A Multipronged Approach to Target the HIV Reservoir”, *Front. Cell. Infect. Microbiol.*, vol. 10, no. May, pp. 1–9, 2020.
- [53] M. Carrington and P. Norman, “The KIR Gene Cluster”, *Annu. Rev. Genomics Hum. Genet.*, vol. 7, no. 1, pp. 277–300, 2003.
- [54] M. M. A. Rahim and A. P. Makrigiannis, “Ly49 receptors: evolution, genetic diversity, and impact on immunity”, *Immunol. Rev.*, vol. 267, no. 1, pp. 137–47, 2015.
- [55] L. A. Guethlein, P. J. Norman, H. G. Hilton, and P. Parham, “Co-evolution of MHC class I and variable NK cell receptors in placental mammals”, *Immunol. Rev.*, vol. 267, no. 1, pp. 259–82, 2015.
- [56] A. B. H. Bakker, J. H. Phillips, C. G. Figdor, and L. L. Lanier, “Killer cell inhibitory receptors for MHC class I molecules regulate lysis of melanoma cells mediated by NK cells, $\gamma\delta$ T cells, and antigen-specific CTL”, *J. Immunol.*, vol. 160, no. 11, pp. 5239–5245, 1998.
- [57] N. K. Björkström, V. Béziat, F. Cichocki, L. L. Liu, J. Levine, *et al.*, “CD8 T cells express randomly selected KIRs with distinct specificities compared with NK cells”, *Blood*, vol. 120, no. 17, pp. 3455–65, 2012.
- [58] M. Uhrberg, “The KIR gene family: life in the fast lane of evolution”, *Eur. J. Immunol.*, vol. 35, no. 1, pp. 10–15, 2005.
- [59] K. C. Hsu, S. Chida, D. E. Geraghty, and B. Dupont, “The killer cell immunoglobulin-like receptor (KIR) genomic region: gene-order, haplotypes and allelic polymorphism”, *Immunol. Rev.*, vol. 190, no. 1, pp. 40–52, 2002.
- [60] G. M. O’Connor, K. J. Guinan, R. T. Cunningham, D. Middleton, P. Parham, *et al.*, “Functional polymorphism of the KIR3DL1/S1 receptor on human NK cells”, *J. Immunol.*, vol. 178, no. 1, pp. 235–41, 2007.
- [61] A. R. Manser, S. Weinhold, and M. Uhrberg, “Human KIR repertoires: Shaped by genetic diversity and evolution”, *Immunol. Rev.*, vol. 267, no. 1, pp. 178–196, 2015.
- [62] I. Nowak, K. Wilczyńska, J. R. Wilczyński, A. Malinowski, P. Radwan, *et al.*, “KIR, LILRB and their Ligands’ Genes as Potential Biomarkers in Recurrent Implantation Failure”, *Arch. Immunol. Ther. Exp. (Warsz.)*, vol. 65, no. 5, pp. 391–399, 2017.
- [63] A. K. Moesta, P. J. Norman, M. Yawata, N. Yawata, M. Gleimer, *et al.*, “Synergistic polymorphism at two positions distal to the ligand-binding site makes KIR2DL2 a stronger receptor for HLA-C than KIR2DL3”, *J. Immunol.*, vol. 180, no. 6, pp. 3969–79, 2008.
- [64] M. D. Blunt and S. I. Khakoo, “Activating killer cell immunoglobulin-like receptors: Detection, function and therapeutic use”, *International Journal of Immunogenetics*, vol. 47, no. 1. Int J Immunogenet, pp. 1–12, 2020.
- [65] A. Chapel, W. F. Garcia-Beltran, A. Hölzemer, M. Ziegler, S. Lunemann, *et al.*, “Peptide-specific engagement of the activating NK cell receptor KIR2DS1”, *Sci. Rep.*, vol. 7, no. 1, p. 2414, 2017.
- [66] F. Borrego, M. Masilamani, A. I. Marusina, X. Tang, and J. E. Coligan, “The CD94/NKG2 family of receptors: From molecules and cells to clinical relevance”, *Immunol. Res.*, vol. 35, no. 3, pp. 263–277, 2006.

- [67] S. Lazetic, C. Chang, J. P. Houchins, L. L. Lanier, and J. H. Phillips, "Human natural killer cell receptors involved in MHC class I recognition are disulfide-linked heterodimers of CD94 and NKG2 subunits", *J. Immunol.*, vol. 157, no. 11, pp. 4741–5, 1996.
- [68] M. Carretero, G. Palmieri, M. Llano, V. Tullio, A. Santoni, *et al.*, "Specific engagement of the CD94/NKG2-A killer inhibitory receptor by the HLA-E class Ib molecule induces SHP-1 phosphatase recruitment to tyrosine-phosphorylated NKG2-A: Evidence for receptor function in heterologous transfectants", *Eur. J. Immunol.*, vol. 28, no. 4, pp. 1280–1291, 1998.
- [69] N. Lee, D. R. Goodlett, A. Ishitani, H. Marquardt, and D. E. Geraghty, "HLA-E surface expression depends on binding of TAP-dependent peptides derived from certain HLA class I signal sequences", *J. Immunol.*, vol. 160, no. 10, pp. 4951–60, 1998.
- [70] L. L. Lanier, "DAP10- and DAP12-associated receptors in innate immunity", *Immunol. Rev.*, vol. 227, no. 1, pp. 150–60, 2009.
- [71] V. M. Braud, D. S. J. Allan, C. A. O'Callaghan, K. Söderström, A. D'Andrea, *et al.*, "HLA-E binds to natural killer cell receptors CD94/NKG2A, B and C", *Nature*, vol. 391, no. 6669, pp. 795–799, 1998.
- [72] R. E. Vance, A. M. Jamieson, and D. H. Raulet, "Recognition of the class Ib molecule Qa-1(b) by putative activating receptors CD94/NKG2C and CD94/NKG2E on mouse natural killer cells", *J. Exp. Med.*, vol. 190, no. 12, pp. 1801–12, 1999.
- [73] Q. Hammer, T. Rückert, E. M. Borst, J. Dunst, A. Haubner, *et al.*, "Peptide-specific recognition of human cytomegalovirus strains controls adaptive natural killer cells", *Nat. Immunol.*, vol. 19, no. 5, pp. 453–463, 2018.
- [74] S. Lopez-Vergès, J. M. Milush, B. S. Schwartz, M. J. Pando, J. Jarjoura, *et al.*, "Expansion of a unique CD57⁺NKG2Chi natural killer cell subset during acute human cytomegalovirus infection", *Proc. Natl. Acad. Sci. U. S. A.*, vol. 108, no. 36, pp. 14725–32, 2011.
- [75] J. Wu, Y. Song, A. B. Bakker, S. Bauer, T. Spies, *et al.*, "An activating immunoreceptor complex formed by NKG2D and DAP10", *Science*, vol. 285, no. 5428, pp. 730–2, 1999.
- [76] D. H. Raulet, S. Gasser, B. G. Gowen, W. Deng, and H. Jung, "Regulation of Ligands for the NKG2D Activating Receptor", *Annu. Rev. Immunol.*, vol. 31, no. 1, pp. 413–441, 2013.
- [77] S. Bauer, V. Groh, J. Wu, A. Steinle, J. H. Phillips, *et al.*, "Activation of NK cells and T cells by NKG2D, a receptor for stress-inducible MICA", *Science*, vol. 285, no. 5428, pp. 727–9, 1999.
- [78] D. Cosman, J. Müllberg, C. L. Sutherland, W. Chin, R. Armitage, *et al.*, "ULBPs, novel MHC class I-related molecules, bind to CMV glycoprotein UL16 and stimulate NK cytotoxicity through the NKG2D receptor", *Immunity*, vol. 14, no. 2, pp. 123–133, 2001.
- [79] M. P. Correia, A. Stojanovic, K. Bauer, D. Juraeva, L.-O. Tykocinski, *et al.*, "Distinct human circulating NKp30+FcεRIγ+CD8+ T cell population exhibiting high natural killer-like antitumor potential", *Proc. Natl. Acad. Sci. U. S. A.*, vol. 115, no. 26, pp. E5980–E5989, 2018.
- [80] B. Meresse, S. A. Curran, C. Ciszewski, G. Orbelyan, M. Setty, *et al.*, "Reprogramming of CTLs into natural killer-like cells in celiac disease", *J. Exp. Med.*, vol. 203, no. 5, pp. 1343–55, 2006.

- [81] D. V Correia, M. Fogli, K. Hudspeth, M. G. da Silva, D. Mavilio, *et al.*, “Differentiation of human peripheral blood V δ 1+ T cells expressing the natural cytotoxicity receptor NKp30 for recognition of lymphoid leukemia cells”, *Blood*, vol. 118, no. 4, pp. 992–1001, 2011.
- [82] M. von Lilienfeld-Toal, J. Nattermann, G. Feldmann, E. Sievers, S. Frank, *et al.*, “Activated gammadelta T cells express the natural cytotoxicity receptor natural killer p 44 and show cytotoxic activity against myeloma cells”, *Clin. Exp. Immunol.*, vol. 144, no. 3, pp. 528–33, 2006.
- [83] C. A. Stewart, T. Walzer, S. H. Robbins, B. Malissen, E. Vivier, *et al.*, “Germ-line and rearranged Tcrd transcription distinguish bona fide NK cells and NK-like $\gamma\delta$ T cells”, *Eur. J. Immunol.*, vol. 37, no. 6, pp. 1442–1452, 2007.
- [84] A. Diefenbach, M. Colonna, and S. Koyasu, “Development, differentiation, and diversity of innate lymphoid cells”, *Immunity*, vol. 41, no. 3, pp. 354–365, 2014.
- [85] T. Verrier, N. Satoh-Takayama, N. Serafini, S. Marie, J. P. Di Santo, *et al.*, “Phenotypic and Functional Plasticity of Murine Intestinal NKp46+ Group 3 Innate Lymphoid Cells”, *J. Immunol.*, vol. 196, no. 11, pp. 4731–8, 2016.
- [86] D. Pende, S. Parolini, A. Pessino, S. Sivori, R. Augugliaro, *et al.*, “Identification and molecular characterization of NKp30, a novel triggering receptor involved in natural cytotoxicity mediated by human natural killer cells”, *J. Exp. Med.*, vol. 190, no. 10, pp. 1505–16, 1999.
- [87] J. Kleeff, T. Ishiwata, A. Kumbasar, H. Friess, M. W. Büchler, *et al.*, “The cell-surface heparan sulfate proteoglycan glypican-1 regulates growth factor action in pancreatic carcinoma cells and is overexpressed in human pancreatic cancer”, *J. Clin. Invest.*, vol. 102, no. 9, pp. 1662–73, 1998.
- [88] M. Jarahian, M. Fiedler, A. Cohnen, D. Djandji, G. J. Hämmerling, *et al.*, “Modulation of NKp30- and NKp46-Mediated Natural Killer Cell Responses by Poxviral Hemagglutinin”, *PLoS Pathog.*, vol. 7, no. 8, p. e1002195, 2011.
- [89] E. Mavoungou, J. Held, L. Mewono, and P. G. Kremsner, “A Duffy binding-like domain is involved in the NKp30-mediated recognition of *Plasmodium falciparum*-parasitized erythrocytes by natural killer cells”, *J. Infect. Dis.*, vol. 195, no. 10, pp. 1521–31, 2007.
- [90] M. Vitale, C. Bottino, S. Sivori, L. Sanseverino, R. Castriconi, *et al.*, “NKp44, a novel triggering surface molecule specifically expressed by activated natural killer cells, is involved in non-major histocompatibility complex-restricted tumor cell lysis”, *J. Exp. Med.*, vol. 187, no. 12, pp. 2065–72, 1998.
- [91] S. Sivori, M. Vitale, L. Morelli, L. Sanseverino, R. Augugliaro, *et al.*, “p46, a novel natural killer cell-specific surface molecule that mediates cell activation”, *J. Exp. Med.*, vol. 186, no. 7, pp. 1129–36, 1997.
- [92] A. Garg, P. F. Barnes, A. Porgador, S. Roy, S. Wu, *et al.*, “Vimentin Expressed on Mycobacterium tuberculosis-Infected Human Monocytes Is Involved in Binding to the NKp46 Receptor”, *J. Immunol.*, vol. 177, no. 9, pp. 6192–6198, 2006.
- [93] O. Mandelboim, N. Lieberman, M. Lev, L. Paul, T. I. Arnon, *et al.*, “Recognition of haemagglutinins on virus-infected cells by NKp46 activates lysis by human NK cells”, *Nature*, vol. 409, no. 6823, pp. 1055–1060, 2001.

- [94] H. Maïza, G. Leca, I. G. Mansur, V. Schiavon, L. Boumsell, *et al.*, “A novel 80-kD cell surface structure identifies human circulating lymphocytes with natural killer activity”, *J. Exp. Med.*, vol. 178, no. 3, pp. 1121–6, 1993.
- [95] A. Anumanthan, A. Bensussan, L. Boumsell, A. D. Christ, R. S. Blumberg, *et al.*, “Cloning of BY55, a novel Ig superfamily member expressed on NK cells, CTL, and intestinal intraepithelial lymphocytes”, *J. Immunol.*, vol. 161, no. 6, pp. 2780–90, 1998.
- [96] P. Fons, S. Chabot, J. E. Cartwright, F. Lenfant, F. L’Faqihi, *et al.*, “Soluble HLA-G1 inhibits angiogenesis through an apoptotic pathway and by direct binding to CD160 receptor expressed by endothelial cells”, *Blood*, vol. 108, no. 8, pp. 2608–15, 2006.
- [97] G. Cai, A. Anumanthan, J. A. Brown, E. A. Greenfield, B. Zhu, *et al.*, “CD160 inhibits activation of human CD4+ T cells through interaction with herpesvirus entry mediator”, *Nat. Immunol.*, vol. 9, no. 2, pp. 176–85, 2008.
- [98] C. L. Tan, M. J. Peluso, J. M. Drijvers, C. M. Mera, S. M. Grande, *et al.*, “CD160 Stimulates CD8+ T Cell Responses and Is Required for Optimal Protective Immunity to *Listeria monocytogenes*”, *ImmunoHorizons*, vol. 2, no. 7, pp. 238–250, 2018.
- [99] M. H. Nikolova, M. N. Muhtarova, H. B. Taskov, K. Kostov, L. Vezenkov, *et al.*, “The CD160+ CD8high cytotoxic T cell subset correlates with response to HAART in HIV-1+ patients”, *Cell. Immunol.*, vol. 237, no. 2, pp. 96–105, 2005.
- [100] F. Muscate, N. Stetter, C. Schramm, J. Schulze zur Wiesch, L. Bosurgi, *et al.*, “HVEM and CD160: Regulators of Immunopathology During Malaria Blood-Stage”, *Front. Immunol.*, vol. 9, p. 2611, 2018.
- [101] M. Maeda, C. Carpenito, R. C. Russell, J. Dasanjh, L. L. Veinotte, *et al.*, “Murine CD160, Ig-Like Receptor on NK Cells and NKT Cells, Recognizes Classical and Nonclassical MHC Class I and Regulates NK Cell Activation”, *J. Immunol.*, vol. 175, no. 7, pp. 4426–4432, 2005.
- [102] T. C. Tu, N. K. Brown, T. J. Kim, J. Wroblewska, X. Yang, *et al.*, “CD160 is essential for NK-mediated IFN- γ Production”, *J. Exp. Med.*, vol. 212, no. 3, pp. 415–429, 2015.
- [103] A. Barakonyi, M. Rabot, A. Marie-Cardine, M. Aguerre-Girr, B. Polgar, *et al.*, “Cutting Edge: Engagement of CD160 by its HLA-C Physiological Ligand Triggers a Unique Cytokine Profile Secretion in the Cytotoxic Peripheral Blood NK Cell Subset”, *J. Immunol.*, vol. 173, no. 9, pp. 5349–5354, 2004.
- [104] P. Le Bouteiller, J. Tabiasco, B. Polgar, N. Kozma, J. Giustiniani, *et al.*, “CD160: A unique activating NK cell receptor”, *Immunol. Lett.*, vol. 138, no. 2, pp. 93–96, 2011.
- [105] J. Giustiniani, A. Marie-Cardine, and A. Bensussan, “A soluble form of the MHC class I-specific CD160 receptor is released from human activated NK lymphocytes and inhibits cell-mediated cytotoxicity”, *J. Immunol.*, vol. 178, no. 3, pp. 1293–300, 2007.
- [106] J. Giustiniani, A. Bensussan, and A. Marie-Cardine, “Identification and characterization of a transmembrane isoform of CD160 (CD160-TM), a unique activating receptor selectively expressed upon human NK cell activation”, *J. Immunol.*, vol. 182, no. 1, pp. 63–71, 2009.
- [107] A. W. MacFarlane and K. S. Campbell, “Signal transduction in natural killer cells”, *Curr. Top. Microbiol. Immunol.*, vol. 298, pp. 23–57, 2006.

- [108] M. Rabot, A. Bensussan, and P. Le Bouteiller, "Engagement of the CD160 activating NK cell receptor leads to its association with CD2 in circulating human NK cells", *Transpl. Immunol.*, vol. 17, no. 1, pp. 36–8, 2006.
- [109] J. R. Sedy, M. Gavrieli, K. G. Potter, M. A. Hurchla, R. C. Lindsley, *et al.*, "B and T lymphocyte attenuator regulates T cell activation through interaction with herpesvirus entry mediator", *Nat. Immunol.*, vol. 6, no. 1, pp. 90–98, 2005.
- [110] Q. Meng, A. K. Zaidi, J. Sedy, A. Bensussan, and D. L. Popkin, "Soluble Fc-Disabled Herpes Virus Entry Mediator Augments Activation and Cytotoxicity of NK Cells by Promoting Cross-Talk between NK Cells and Monocytes", *J. Immunol.*, vol. 202, no. 7, pp. 2057–2068, 2019.
- [111] C. Bottino, R. Castriconi, D. Pende, P. Rivera, M. Nanni, *et al.*, "Identification of PVR (CD155) and Nectin-2 (CD112) as Cell Surface Ligands for the Human DNAM-1 (CD226) Activating Molecule", *J. Exp. Med.*, vol. 198, no. 4, pp. 557–567, 2003.
- [112] F. A. Deuss, B. S. Gully, J. Rossjohn, and R. Berry, "Recognition of nectin-2 by the natural killer cell receptor T cell immunoglobulin and ITIM domain (TIGIT)", *J. Biol. Chem.*, vol. 292, no. 27, pp. 11413–11422, 2017.
- [113] Y. Zhu, A. Paniccia, A. C. Schulick, W. Chen, M. R. Koenig, *et al.*, "Identification of CD112R as a novel checkpoint for human T cells", *J. Exp. Med.*, vol. 213, no. 2, pp. 167–76, 2016.
- [114] N. Stanietzky, H. Simic, J. Arapovic, A. Toporik, O. Levy, *et al.*, "The interaction of TIGIT with PVR and PVRL2 inhibits human NK cell cytotoxicity", *PNAS*, vol. 105, p. 17858-17863, 2009.
- [115] J. Li, S. Whelan, M. F. Kotturi, D. Meyran, C. D'Souza, *et al.*, "PVRIG is a novel natural killer cell immune checkpoint receptor in acute myeloid leukemia", *Haematologica*, vol. 106, no. 12, pp. 3115–3124, 2021.
- [116] A. Shibuya, D. Campbell, C. Hannum, H. Yssel, K. Franz-Bacon, *et al.*, "DNAM-1, a novel adhesion molecule involved in the cytolytic function of T lymphocytes", *Immunity*, vol. 4, no. 6, pp. 573–81, 1996.
- [117] N. Reymond, A.-M. Imbert, E. Devilard, S. Fabre, C. Chabannon, *et al.*, "DNAM-1 and PVR regulate monocyte migration through endothelial junctions", *J. Exp. Med.*, vol. 199, no. 10, pp. 1331–41, 2004.
- [118] Y. Wu, Z. Tian, and H. Wei, "Developmental and Functional Control of Natural Killer Cells by Cytokines", *Front. Immunol.*, vol. 8, p. 930, 2017.
- [119] M. L. Stackaruk, A. J. Lee, and A. A. Ashkar, "Type I interferon regulation of natural killer cell function in primary and secondary infections", *Expert Rev. Vaccines*, vol. 12, no. 8, pp. 875–884, 2013.
- [120] S. Ali, R. Mann-Nüttel, A. Schulze, L. Richter, J. Alferink, *et al.*, "Sources of Type I Interferons in Infectious Immunity: Plasmacytoid Dendritic Cells Not Always in the Driver's Seat", *Front. Immunol.*, vol. 10, p. 778, 2019.
- [121] F. J. Culley, "Natural killer cells in infection and inflammation of the lung", *Immunology*, vol. 128, no. 2, pp. 151–63, 2009.
- [122] S. L. Pogue, B. T. Preston, J. Stalder, C. R. Bebbington, and P. M. Cardarelli, "The Receptor for Type I IFNs Is Highly Expressed on Peripheral Blood B Cells and Monocytes and Mediates a Distinct Profile of Differentiation and Activation of These Cells", *J. Interf. Cytokine Res.*, vol. 24, no. 2, pp. 131–139, 2004.
- [123] G. Schreiber and J. Piehler, "The molecular basis for functional plasticity in type I interferon signaling", *Trends Immunol.*, vol. 36, no. 3, pp. 139–49, 2015.

- [124] Y. Nan, C. Wu, and Y.-J. Zhang, "Interplay between Janus Kinase/Signal Transducer and Activator of Transcription Signaling Activated by Type I Interferons and Viral Antagonism", *Front. Immunol.*, vol. 8, p. 1758, 2017.
- [125] L. B. Ivashkiv and L. T. Donlin, "Regulation of type I interferon responses", *Nat. Rev. Immunol.*, vol. 14, no. 1, p. 36, 2014.
- [126] W. M. Schneider, M. D. Chevillotte, and C. M. Rice, "Interferon-stimulated genes: A complex web of host defenses", *Annual Review of Immunology*, vol. 32. Annu Rev Immunol, pp. 513–545, 2014.
- [127] J. Rödel, H. Vogelsang, K. Prager, M. Hartmann, K. H. Schmidt, *et al.*, "Role of interferon-stimulated gene factor 3 γ and beta interferon in HLA class I enhancement in synovial fibroblasts upon infection with *Chlamydia trachomatis*", *Infect. Immun.*, vol. 70, no. 11, pp. 6140–6146, 2002.
- [128] J. S. Orange and C. A. Biron, "Characterization of early IL-12, IFN- $\alpha\beta$, and TNF effects on antiviral state and NK cell responses during murine cytomegalovirus infection", *J. Immunol.*, vol. 156, no. 12, pp. 4746–56, 1996.
- [129] K. B. Nguyen, T. P. Salazar-Mather, M. Y. Dalod, J. B. Van Deusen, X. Wei, *et al.*, "Coordinated and Distinct Roles for IFN- $\alpha\beta$, IL-12, and IL-15 Regulation of NK Cell Responses to Viral Infection", *J. Immunol.*, vol. 169, no. 8, pp. 4279–4287, 2002.
- [130] A. Wack, E. Terczyńska-Dyla, and R. Hartmann, "Guarding the frontiers: the biology of type III interferons", *Nat. Immunol.*, vol. 16, no. 8, pp. 802–809, 2015.
- [131] F. J. D. Mennechet and G. Uzé, "Interferon- λ -treated dendritic cells specifically induce proliferation of FOXP3-expressing suppressor T cells", *Blood*, vol. 107, no. 11, pp. 4417–4423, 2006.
- [132] P. Sheppard, W. Kindsvogel, W. Xu, K. Henderson, S. Schlutsmeyer, *et al.*, "IL-28, IL-29 and their class II cytokine receptor IL-28R", *Nat. Immunol.*, vol. 4, no. 1, pp. 63–8, 2003.
- [133] E. Andreakos, I. Zanoni, and I. E. Galani, "Lambda interferons come to light: dual function cytokines mediating antiviral immunity and damage control", *Curr. Opin. Immunol.*, vol. 56, pp. 67–75, 2019.
- [134] S. Gimeno Brias, M. Marsden, J. Forbester, M. Clement, C. Brandt, *et al.*, "Interferon lambda is required for interferon gamma-expressing NK cell responses but does not afford antiviral protection during acute and persistent murine cytomegalovirus infection", *PLoS One*, vol. 13, no. 5, p. e0197596, 2018.
- [135] World Health Organization (WHO), "Integrating neglected tropical diseases into global health and development: fourth WHO report on neglected tropical diseases", *World Heal. Organ.*, p. 270, 2017.
- [136] I. B. Zecca, C. L. Hodo, S. Slack, L. Auckland, and S. A. Hamer, "Trypanosoma cruzi infections and associated pathology in urban-dwelling Virginia opossums (*Didelphis virginiana*)", *Int. J. Parasitol. Parasites Wildl.*, vol. 11, pp. 287–293, 2020.
- [137] G. G. Rosal, B. Noguera-Torres, M. E. Villagrán, J. A. de Diego-Cabrera, O. D. Montañez-Valdez, *et al.*, "Chagas disease: Importance of rats as reservoir hosts of *Trypanosoma cruzi* (Chagas, 1909) in western Mexico", *J. Infect. Public Health*, vol. 11, no. 2, pp. 230–233, 2018.
- [138] V. Hemmige, H. Tanowitz, and A. Sethi, "Trypanosoma cruzi infection: a review with emphasis on cutaneous manifestations", *Int. J. Dermatol.*, vol. 51, no. 5, pp. 501–508, 2012.
- [139] L. O. Andrade and N. W. Andrews, "Opinion: The *Trypanosoma cruzi* - Host-cell interplay: Location, invasion, retention", *Nat. Rev. Microbiol.*, vol. 3, no. 10, pp. 819–823, 2005.

- [140] R. de C. Ruiz, V. L. Rigoni, J. Gonzalez, and N. Yoshida, "The 35/50 kDa surface antigen of *Trypanosoma cruzi* metacyclic trypomastigotes, an adhesion molecule involved in host cell invasion", *Parasite Immunol.*, vol. 15, no. 2, pp. 121–125, 1993.
- [141] S. Schenkman and D. Eichinger, "Trypanosoma cruzi trans-sialidase and cell invasion", *Parasitol. Today*, vol. 9, no. 6, pp. 218–222, 1993.
- [142] I. Tardieux, P. Webster, J. Ravesloot, W. Boron, J. A. Lunn, *et al.*, "Lysosome recruitment and fusion are early events required for trypanosome invasion of mammalian cells", *Cell*, vol. 71, no. 7, pp. 1117–1130, 1992.
- [143] N. W. Andrews and M. B. Whitlow, "Secretion by *Trypanosoma cruzi* of a hemolysin active at low pH", *Mol. Biochem. Parasitol.*, vol. 33, no. 3, pp. 249–256, 1989.
- [144] J. A. Dvorak and T. P. Hyde, "Trypanosoma cruzi: Interaction with vertebrate cells in vitro: I. Individual interactions at the cellular and subcellular levels", *Exp. Parasitol.*, vol. 34, no. 2, pp. 268–283, 1973.
- [145] B. A. Burleigh and A. M. Woolsey, "Cell signalling and *Trypanosoma cruzi* invasion", *Cell. Microbiol.*, vol. 4, no. 11, pp. 701–11, 2002.
- [146] K. M. Tyler and D. M. Engman, "The life cycle of *Trypanosoma cruzi* revisited", *Int. J. Parasitol.*, vol. 31, no. 5–6, pp. 472–481, 2001.
- [147] P. F. Araujo, A. B. Almeida, C. F. Pimentel, A. R. Silva, A. Sousa, *et al.*, "Sexual transmission of American trypanosomiasis in humans: a new potential pandemic route for Chagas parasites", *Mem. Inst. Oswaldo Cruz*, vol. 112, no. 6, pp. 437–446, 2017.
- [148] F. Guhl and J. D. Ramírez, "Poverty, Migration, and Chagas Disease", *Curr. Trop. Med. Reports*, vol. 8, no. 1, pp. 52–58, 2021.
- [149] C. Monroyi, M. Mejtai, A. Rodasi, R. Rosalesi, M. Horio, *et al.*, "Comparision of indoor searches with whole house demolition collections of vectors of Chagas disease and their indoor distribution", *Med. Entomol. Zool.*, vol. 49, no. 3, pp. 195–200, 1998.
- [150] M. S. Gaspé, M. del P. Fernández, M. V. Cardinal, G. F. Enriquez, L. I. Rodríguez-Planes, *et al.*, "Urbanisation, risk stratification and house infestation with a major vector of Chagas disease in an endemic municipality of the Argentine Chaco", *Parasit. Vectors*, vol. 13, no. 1, p. 316, 2020.
- [151] G. A. Schmunis, "Epidemiology of Chagas disease in non-endemic countries: The role of international migration", in *Memorias do Instituto Oswaldo Cruz*, 2007, vol. 102, pp. 75–85.
- [152] F. Guhl, C. Jaramillo, G. A. Vallejo, F. C. A-Arroyo, and A. Aufderheide, "Chagas disease and human migration", *Mem. Inst. Oswaldo Cruz*, vol. 95, no. 4, pp. 553–555, 2000.
- [153] A. Requena-Méndez, E. Aldasoro, E. de Lazzari, E. Sicuri, M. Brown, *et al.*, "Prevalence of Chagas Disease in Latin-American Migrants Living in Europe: A Systematic Review and Meta-analysis", *PLoS Negl. Trop. Dis.*, vol. 9, no. 2, p. e0003540, 2015.
- [154] J. A. Pérez-Molina and I. Molina, "Chagas disease", *Lancet (London, England)*, vol. 391, no. 10115, pp. 82–94, 2018.
- [155] R. L. Tarleton, "Parasite persistence in the aetiology of Chagas disease", *Int. J. Parasitol.*, vol. 31, no. 5–6, pp. 550–4, 2001.

- [156] L. Zhang and R. L. Tarleton, "Parasite Persistence Correlates with Disease Severity and Localization in Chronic Chagas' Disease", *J. Infect. Dis.*, vol. 180, no. 2, pp. 480–486, 1999.
- [157] A. I. Ward, M. D. Lewis, A. A. Khan, C. J. McCann, A. F. Francisco, *et al.*, "In Vivo Analysis of *Trypanosoma cruzi* Persistence Foci at Single-Cell Resolution", *MBio*, 2020.
- [158] A. V. Matos Ferreira, M. Segatto, Z. Menezes, A. M. Macedo, C. Gelape, *et al.*, "Evidence for *Trypanosoma cruzi* in adipose tissue in human chronic Chagas disease", *Microbes Infect.*, vol. 13, no. 12–13, pp. 1002–1005, 2011.
- [159] C. Bern, "Chagas' Disease", *N. Engl. J. Med.*, vol. 373, no. 5, pp. 456–466, 2015.
- [160] J. H. Maguire, R. Hoff, I. Sherlock, A. C. Guimarães, A. C. Sleight, *et al.*, "Cardiac morbidity and mortality due to Chagas' disease: prospective electrocardiographic study of a Brazilian community", *Circulation*, vol. 75, no. 6, pp. 1140–5, 1987.
- [161] N. M. Matsuda, S. M. Miller, and P. R. B. Evora, "The chronic gastrointestinal manifestations of Chagas disease", *Clinics (Sao Paulo)*, vol. 64, no. 12, pp. 1219–24, 2009.
- [162] A. Morrot, S. R. Villar, F. B. González, and A. R. Pérez, "Evasion and Immuno-Endocrine Regulation in Parasite Infection: Two Sides of the Same Coin in Chagas Disease?", *Front. Microbiol.*, vol. 7, p. 704, 2016.
- [163] F. Kierszenbaum, "Mechanisms of pathogenesis in Chagas disease", *Acta Parasitol.*, vol. 52, no. 1, pp. 1–12, 2007.
- [164] K. M. Bonney and D. M. Engman, "Autoimmune pathogenesis of Chagas heart disease: looking back, looking ahead", *Am. J. Pathol.*, vol. 185, no. 6, pp. 1537–47, 2015.
- [165] S. Meymandi, S. Hernandez, S. Park, D. R. Sanchez, and C. Forsyth, "Treatment of Chagas Disease in the United States", *Curr. Treat. options Infect. Dis.*, vol. 10, no. 3, pp. 373–388, 2018.
- [166] J. A. Castro and E. G. Diaz de Toranzo, "Toxic effects of nifurtimox and benznidazole, two drugs used against American trypanosomiasis (Chagas' disease)", *Biomed. Environ. Sci.*, vol. 1, no. 1, pp. 19–33, 1988.
- [167] A. E. Bivona, A. S. Alberti, N. Cerny, S. N. Trinitario, and E. L. Malchiodi, "Chagas disease vaccine design: the search for an efficient *Trypanosoma cruzi* immune-mediated control", *Biochim Biophys Acta Mol Basis Dis*, vol. 1866, no. 5, p. 165658, 2020.
- [168] C. Y. Han, H. Issa, J. Rychtář, D. Taylor, and N. Umana, "A voluntary use of insecticide treated nets can stop the vector transmission of Chagas disease", *PLoS Negl. Trop. Dis.*, vol. 14, no. 11, p. e0008833, 2020.
- [169] F. Espinoza-Gómez, A. Maldonado-Rodríguez, R. Coll-Cárdenas, C. M. Hernández-Suárez, and I. Fernández-Salas, "Presence of Triatominae (Hemiptera, Reduviidae) and Risk of Transmission of Chagas Disease in Colima, México", *Mem. Inst. Oswaldo Cruz*, vol. 97, no. 1, pp. 25–30, 2002.
- [170] E. Dumonteil and S. Gourbière, "Predicting *Triatoma dimidiata* abundance and infection rate: A risk map for natural transmission of Chagas disease in the Yucatán Peninsula of Mexico", *Am. J. Trop. Med. Hyg.*, vol. 70, no. 5, pp. 514–519, 2004.
- [171] G. R. Acevedo, M. C. Girard, and K. A. Gómez, "The Unsolved Jigsaw Puzzle of the Immune Response in Chagas Disease", *Front. Immunol.*, vol. 9, p. 1929, 2018.
- [172] F. Cardillo, R. T. Pinho, P. R. Z. Antas, and J. Mengel, "Immunity and immune modulation in *Trypanosoma cruzi* infection", *Pathog. Dis.*, vol. 73, no. 9, p. ftv082, 2015.

- [173] H. Hasegawa, I. Mizoguchi, Y. Chiba, M. Ohashi, M. Xu, *et al.*, “Expanding Diversity in Molecular Structures and Functions of the IL-6/IL-12 Heterodimeric Cytokine Family”, *Front. Immunol.*, vol. 7, p. 479, 2016.
- [174] T. Scharton-Kersten, L. C. Afonso, M. Wysocka, G. Trinchieri, and P. Scott, “IL-12 is required for natural killer cell activation and subsequent T helper 1 cell development in experimental leishmaniasis”, *J. Immunol.*, vol. 154, no. 10, pp. 5320–30, 1995.
- [175] F. Cardillo, J. C. Voltarelli, S. G. Reed, and J. S. Silva, “Regulation of *Trypanosoma cruzi* infection in mice by gamma interferon and interleukin 10: role of NK cells”, *Infect. Immun.*, vol. 64, no. 1, pp. 128–34, 1996.
- [176] A. Guilmot, Y. Carlier, and C. Truyens, “Differential IFN- γ production by adult and neonatal blood CD56+ natural killer (NK) and NK-like-T cells in response to *Trypanosoma cruzi* and IL-15”, *Parasite Immunol.*, vol. 36, no. 1, pp. 43–52, 2014.
- [177] T. Williams, I. Guerrero-Ros, Y. Ma, F. Matos, D. Santos, *et al.*, “Induction of Effective Immunity against *Trypanosoma cruzi*”, 2020.
- [178] R. E. McCabe, S. G. Meagher, and B. T. Mullins, “Endogenous interferon- γ , macrophage activation, and murine host defense against acute infection with *Trypanosoma cruzi*”, *J. Infect. Dis.*, vol. 163, no. 4, pp. 912–915, 1991.
- [179] R. T. Gazzinelli, I. P. Oswald, S. Hieny, S. L. James, and A. Sher, “The microbicidal activity of interferon- γ -treated macrophages against *Trypanosoma cruzi* involves an L-arginine-dependent, nitrogen oxide-mediated mechanism inhibitable by interleukin-10 and transforming growth factor- β ”, *Eur. J. Immunol.*, vol. 22, no. 10, pp. 2501–2506, 1992.
- [180] R. L. Coffman, H. F. Savelkoul, and D. A. Leberman, “Cytokine regulation of immunoglobulin isotype switching and expression”, *Semin. Immunol.*, vol. 1, no. 1, pp. 55–63, 1989.
- [181] T. Lieke, C. Steeg, S. E. B. Graefe, B. Fleischer, and T. Jacobs, “Interaction of natural killer cells with *Trypanosoma cruzi*-infected fibroblasts”, *Clin. Exp. Immunol.*, vol. 145, no. 2, pp. 357–364, 2006.
- [182] T. Lieke, S. E. B. Graefe, U. Klauenberg, B. Fleischer, and T. Jacobs, “NK Cells Contribute to the Control of *Trypanosoma cruzi* Infection by Killing Free Parasites by Perforin-Independent Mechanisms”, *Infect. Immun.*, vol. 72, no. 12, pp. 6817–6825, 2004.
- [183] D. M. Vitelli-Avelar, R. Sathler-Avelar, R. L. Massara, J. D. Borges, P. S. Lage, *et al.*, “Are increased frequency of macrophage-like and natural killer (NK) cells, together with high levels of NKT and CD4+CD25^{high} T cells balancing activated CD8+ T cells, the key to control Chagas’ disease morbidity?”, *Clin. Exp. Immunol.*, vol. 145, no. 1, pp. 81–92, 2006.
- [184] D. M. Vitelli-Avelar, R. Sathler-Avelar, J. C. P. Dias, V. P. M. Pascoal, A. Teixeira-Carvalho, *et al.*, “Chagasic Patients with Indeterminate Clinical Form of the Disease have High Frequencies of Circulating CD3+CD16-CD56+ Natural Killer T Cells and CD4+CD25^{High} Regulatory T Lymphocytes”, *Scand. J. Immunol.*, vol. 62, no. 3, pp. 297–308, 2005.
- [185] L. R. P. Ferreira, F. M. Ferreira, H. I. Nakaya, X. Deng, D. da S. Cândido, *et al.*, “Blood Gene Signatures of Chagas Cardiomyopathy With or Without Ventricular Dysfunction”, *J. Infect. Dis.*, vol. 215, no. 3, pp. 387–395, 2017.

- [186] K. Murphy, C. Weaver, and C. Janeway, "Janeway's Immunobiology, 9th edition", 2017.
- [187] S. Kumar and R. L. Tarleton, "The relative contribution of antibody production and CD8+ T cell function to immune control of *Trypanosoma cruzi*", *Parasite Immunol.*, vol. 20, no. 5, pp. 207–216, 1998.
- [188] A. M. Rodriguez, F. Santoro, D. Afchain, H. Bazin, and A. Capron, "Trypanosoma cruzi infection in B cell-deficient rats", *Infect. Immun.*, vol. 31, no. 2, pp. 524–529, 1981.
- [189] L. F. Umekita, H. A. Takehara, and I. Mota, "Role of the antibody Fc in the immune clearance of *Trypanosoma cruzi*", *Immunol. Lett.*, vol. 17, no. 1, pp. 85–89, 1988.
- [190] I. Mota and L. F. Umekita, "The effect of C3 depletion on the clearance of *Trypanosoma cruzi* induced by IgG antibodies", *Immunol. Lett.*, vol. 21, no. 3, pp. 223–225, 1989.
- [191] S. Kumar and R. L. Tarleton, "Antigen-specific Th1 but not Th2 cells provide protection from lethal *Trypanosoma cruzi* infection in mice", *J. Immunol.*, vol. 166, no. 7, pp. 4596–603, 2001.
- [192] D. F. Hoft, A. R. Schnapp, C. S. Eickhoff, and S. T. Roodman, "Involvement of CD4(+) Th1 cells in systemic immunity protective against primary and secondary challenges with *Trypanosoma cruzi*", *Infect. Immun.*, vol. 68, no. 1, pp. 197–204, 2000.
- [193] R. L. Tarleton, "Depletion of CD8+ T cells increases susceptibility and reverses vaccine-induced immunity in mice infected with *Trypanosoma cruzi*", *J. Immunol.*, vol. 144, no. 2, pp. 717–24, 1990.
- [194] R. L. Tarleton, B. H. Koller, A. Latour, and M. Postan, "Susceptibility of β 2-microglobulin-deficient mice to *Trypanosoma cruzi* infection", *Nature*, vol. 356, no. 6367, pp. 338–340, 1992.
- [195] A. D. Pack, M. H. Collins, C. S. Rosenberg, and R. L. Tarleton, "Highly competent, non-exhausted CD8+ T cells continue to tightly control pathogen load throughout chronic *Trypanosoma cruzi* infection", *PLoS Pathog.*, vol. 14, no. 11, p. e1007410, 2018.
- [196] T. Hoi Pang Low, M. A. M Santos, B. Wizel, H. Pang Low, and R. L. Tarleton, "Amastigote Surface Proteins of *Trypanosoma cruzi* Are Targets for CD8 CTL", *J Immunol Ref.*, vol. 160, pp. 1817–1823, 1998.
- [197] R. L. Tarleton, "CD8+ T cells in *Trypanosoma cruzi* infection", *Semin. Immunopathol.*, vol. 37, no. 3, pp. 233–238, 2015.
- [198] D. Martin and R. Tarleton, "Generation, specificity, and function of CD8+ T cells in *Trypanosoma cruzi* infection", *Immunol. Rev.*, vol. 201, pp. 304–317, 2004.
- [199] V. Ferreira, C. Valck, G. Sánchez, A. Gingras, S. Tzima, *et al.*, "The classical activation pathway of the human complement system is specifically inhibited by calreticulin from *Trypanosoma cruzi*", *J. Immunol.*, vol. 172, no. 5, pp. 3042–50, 2004.
- [200] L. M. De Pablos and A. Osuna, "Multigene families in *Trypanosoma cruzi* and their role in infectivity", *Infect. Immun.*, vol. 80, no. 7, pp. 2258–64, 2012.
- [201] D. A. Bermejo, M. C. Amezcua Vesely, M. Khan, E. V. Acosta Rodríguez, C. L. Montes, *et al.*, "*Trypanosoma cruzi* infection induces a massive extrafollicular and follicular splenic B-cell response which is a high source of non-parasite-specific antibodies", *Immunology*, vol. 132, no. 1, pp. 123–133, 2011.
- [202] W. F. Garcia-Beltran, A. Hölzemer, G. Martus, A. W. Chung, Y. Pacheco, *et al.*, "Open conformers of HLA-F are high-affinity ligands of the activating NK-cell receptor KIR3DS1", *Nat. Immunol.*, vol. 17, no. 9, pp. 1067–1074, 2016.

- [203] A. Niehrs, W. F. Garcia-Beltran, P. J. Norman, G. M. Watson, A. Hölzemer, *et al.*, “A subset of HLA-DP molecules serve as ligands for the natural cytotoxicity receptor NKp44”, *Nat. Immunol.*, vol. 20, no. 9, pp. 1129–1137, 2019.
- [204] G. Alter, J. M. Malenfant, and M. Altfeld, “CD107a as a functional marker for the identification of natural killer cell activity”, *J. Immunol. Methods*, vol. 294, no. 1–2, pp. 15–22, 2004.
- [205] A. López-Soto, A. Quiñones-Lombraña, R. López-Arbesú, C. López-Larrea, and S. González, “Transcriptional regulation of ULBP1, a human ligand of the NKG2D receptor”, *J. Biol. Chem.*, vol. 281, no. 41, pp. 30419–30430, 2006.
- [206] Y. Cui, J. Xu, M. Cheng, X. Liao, and S. Peng, “Review of CRISPR/Cas9 sgRNA Design Tools”, *Interdiscip. Sci. Comput. Life Sci.*, vol. 10, no. 2, pp. 455–465, 2018.
- [207] X.-D. Tang, F. Gao, M.-J. Liu, Q.-L. Fan, D.-K. Chen, *et al.*, “Methods for Enhancing Clustered Regularly Interspaced Short Palindromic Repeats/Cas9-Mediated Homology-Directed Repair Efficiency”, *Front. Genet.*, vol. 10, p. 551, 2019.
- [208] Y. Tsuyuki, H. Fujimaki, N. Hikawa, K. Fujita, T. Nagata, *et al.*, “IFN-gamma induces coordinate expression of MHC class I-mediated antigen presentation machinery molecules in adult mouse Schwann cells”, *Neuroreport*, vol. 9, no. 9, pp. 2071–5, 1998.
- [209] K. Früh and Y. Yang, “Antigen presentation by MHC class I and its regulation by interferon gamma”, *Curr. Opin. Immunol.*, vol. 11, no. 1, pp. 76–81, 1999.
- [210] F. Zhou, “Molecular Mechanisms of IFN- γ to Up-Regulate MHC Class I Antigen Processing and Presentation”, *Int. Rev. Immunol.*, vol. 28, no. 3–4, pp. 239–260, 2009.
- [211] M. Gamliel, K. L. Anderson, R. P. Ebstein, N. Yirmiya, and D. Mankuta, “Paternal HLA-C and maternal killer-cell immunoglobulin-like receptor genotypes in the development of autism”, *Front. Pediatr.*, vol. 4, no. JUL, pp. 1–8, 2016.
- [212] B. P. McSharry, H.-G. Burgert, D. P. Owen, R. J. Stanton, V. Prod’homme, *et al.*, “Adenovirus E3/19K Promotes Evasion of NK Cell Recognition by Intracellular Sequestration of the NKG2D Ligands Major Histocompatibility Complex Class I Chain-Related Proteins A and B”, *J. Virol.*, vol. 82, no. 9, pp. 4585–4594, 2008.
- [213] H. Achdout, T. Meninger, S. Hirsh, A. Glasner, Y. Bar-On, *et al.*, “Killing of avian and Swine influenza virus by natural killer cells”, *J. Virol.*, vol. 84, no. 8, pp. 3993–4001, 2010.
- [214] J. Wang, S. Vasaikar, Z. Shi, M. Greer, and B. Zhang, “WebGestalt 2017: a more comprehensive, powerful, flexible and interactive gene set enrichment analysis toolkit”, *Nucleic Acids Res.*, vol. 45, no. W1, pp. W130–W137, 2017.
- [215] P. N. Redlich and S. E. Grossberg, “Analysis of antigenic domains on natural and recombinant human IFN-beta by the inhibition of biologic activities with monoclonal antibodies”, *J. Immunol.*, vol. 143, no. 6, pp. 1887–93, 1989.
- [216] P. Cresswell, N. Bangia, T. Dick, and G. Diedrich, “The nature of the MHC class I peptide loading complex”, *Immunol. Rev.*, vol. 172, no. 1, pp. 21–28, 1999.

- [217] C. M. Ayo, P. G. Reis, M. M. de O. Dalalio, J. E. L. Visentainer, C. de F. Oliveira, *et al.*, “Killer Cell Immunoglobulin-like Receptors and Their HLA Ligands are Related with the Immunopathology of Chagas Disease”, *PLoS Negl. Trop. Dis.*, vol. 9, no. 5, pp. 1–13, 2015.
- [218] V. Monteon, “Trypanosoma cruzi: the early contact between insect-derived metacyclic trypomastigotes and the mammalian cells”, *Ann. Parasitol.*, vol. 65, no. 3, pp. 193–204, 2019.
- [219] L. M. Ebert, S. Meuter, and B. Moser, “Homing and function of human skin gammadelta T cells and NK cells: relevance for tumor surveillance”, *J. Immunol.*, vol. 176, no. 7, pp. 4331–6, 2006.
- [220] C. Ottaviani, F. Nasorri, C. Bedini, O. de Pità, G. Girolomoni, *et al.*, “CD56brightCD16(-) NK cells accumulate in psoriatic skin in response to CXCL10 and CCL5 and exacerbate skin inflammation”, *Eur. J. Immunol.*, vol. 36, no. 1, pp. 118–28, 2006.
- [221] A.-D. C. Chessler, M. Unnikrishnan, A. K. Bei, J. P. Daily, B. A. Burleigh, *et al.*, “Trypanosoma cruzi triggers an early type I IFN response in vivo at the site of intradermal infection”, *J. Immunol.*, vol. 182, no. 4, pp. 2288–96, 2009.
- [222] F. Cardillo, F. Q. Cunha, W. M. S. C. Tamashiro, M. Russo, S. B. Garcia, *et al.*, “NK1.1+ cells and T-cell activation in euthymic and thymectomized C57Bl/6 mice during acute Trypanosoma cruzi infection”, *Scand. J. Immunol.*, vol. 55, no. 1, pp. 96–104, 2002.
- [223] M. A. Kisiel and A. S. Klar, “Isolation and culture of human dermal fibroblasts”, *Methods Mol. Biol.*, vol. 1993, pp. 71–78, 2019.
- [224] A. Guilmot, J. Bosse, Y. Carlier, and C. Truyens, “Monocytes Play an IL-12-Dependent Crucial Role in Driving Cord Blood NK Cells to Produce IFN- γ in Response to Trypanosoma cruzi”, *PLoS Negl. Trop. Dis.*, vol. 7, no. 6, p. e2291, 2013.
- [225] C. V. Poncini, C. D. Alba Soto, E. Batalla, M. E. Solana, and S. M. González Cappa, “Trypanosoma cruzi induces regulatory dendritic cells in vitro”, *Infect. Immun.*, vol. 76, no. 6, pp. 2633–41, 2008.
- [226] G. A. Mott, J. A. Costales, and B. A. Burleigh, “A Soluble Factor from Trypanosoma cruzi Inhibits Transforming Growth Factor- β -Induced MAP Kinase Activation and Gene Expression in Dermal Fibroblasts”, *PLoS One*, vol. 6, no. 9, p. e23482, 2011.
- [227] G. A. Houston-Ludlam, A. T. Belew, and N. M. El-Sayed, “Comparative Transcriptome Profiling of Human Foreskin Fibroblasts Infected with the Sylvio and Y Strains of Trypanosoma cruzi”, *PLoS One*, vol. 11, no. 8, p. e0159197, 2016.
- [228] H. Jung, S. Han, and Y. Lee, “Transcriptome analysis of alternative splicing in the pathogen life cycle in human foreskin fibroblasts infected with Trypanosoma cruzi”, *Sci. Rep.*, vol. 10, no. 1, p. 17481, 2020.
- [229] A. Hou, P. M. Voorhoeve, W. Lan, M. Tin, and L. Tong, “Comparison of gene expression profiles in primary and immortalized human pterygium fibroblast cells”, *Exp. Cell Res.*, vol. 319, no. 18, pp. 2781–9, 2013.
- [230] A. Harel-Bellan, A. Quillet, C. Marchiol, R. Demarst, T. Tursz, *et al.*, “Natural killer susceptibility of human cells may be regulated by genes in the HLA region on chromosome 6 (natural killer cells/natural killer targets/mutant cell lines)”, 1986.
- [231] W. J. Storkus, D. N. Howell, R. D. Salter, J. R. Dawson, and P. Cresswell, “NK susceptibility varies inversely with target cell class I HLA antigen expression”, *J. Immunol.*, vol. 138, no. 6, pp. 1657–9, 1987.

- [232] V. Litwin, J. Gumperz, P. Parham, J. H. Phillips, and L. L. Lanier, "NKB1: a natural killer cell receptor involved in the recognition of polymorphic HLA-B molecules", *J. Exp. Med.*, vol. 180, no. 2, pp. 537–43, 1994.
- [233] M. Koutsakos, H. E. G. McWilliam, T. E. Aktepe, S. Fritzlar, P. T. Illing, *et al.*, "Downregulation of MHC Class I Expression by Influenza A and B Viruses", *Front. Immunol.*, vol. 10, p. 1158, 2019.
- [234] M. Babić, M. Pyzik, B. Zafirova, M. Mitrović, V. Butorac, *et al.*, "Cytomegalovirus immunoevasin reveals the physiological role of "missing self" recognition in natural killer cell dependent virus control in vivo", *J. Exp. Med.*, vol. 207, no. 12, pp. 2663–73, 2010.
- [235] R. Camargo, L. O. Faria, A. Kloss, C. B. F. Favali, U. Kuckelkorn, *et al.*, "Trypanosoma cruzi Infection Down-Modulates the Immunoproteasome Biosynthesis and the MHC Class I Cell Surface Expression in HeLa Cells", *PLoS One*, vol. 9, no. 4, p. e95977, 2014.
- [236] I. Kurane, J. Janus, and F. A. Ennis, "Dengue virus infection of human skin fibroblasts in vitro production of IFN- α , IL-6 and GM-CSF", *Arch. Virol.*, vol. 124, p. 21-30, 1992.
- [237] A. Podhorzer, A. Machicote, S. Belén, L. Lauferman, O. Imventarza, *et al.*, "Intrahepatic and peripheral blood phenotypes of natural killer and T cells: differential surface expression of killer cell immunoglobulin-like receptors", *Immunology*, vol. 154, no. 2, pp. 261–273, 2018.
- [238] N. Bloushtain, U. Qimron, A. Bar-Ilan, O. Hershkovitz, R. Gazit, *et al.*, "Membrane-Associated Heparan Sulfate Proteoglycans Are Involved in the Recognition of Cellular Targets by NKp30 and NKp46", *J. Immunol.*, vol. 173, no. 4, pp. 2392–2401, 2004.
- [239] B. L. Granger and E. Lazarides, "Desmin and vimentin coexist at the periphery of the myofibril Z disc", *Cell*, vol. 18, no. 4, pp. 1053–1063, 1979.
- [240] C. S. Giometti, K. E. Willard, and N. L. Anderson, "Cytoskeletal proteins from human skin fibroblasts, peripheral blood leukocytes, and a lymphoblastoid cell line compared by two-dimensional gel electrophoresis", *Clin. Chem.*, vol. 28, no. 4 II, pp. 955–961, 1982.
- [241] M. S. Nascimento, A. M. S. Stolf, H. F. de Andrade Junior, R. P. Pandey, and E. S. Umezawa, "Vimentin and anti vimentin antibodies in Chagas' disease", *Arq. Bras. Cardiol.*, vol. 110, no. 4, pp. 348–353, 2018.
- [242] N. Mor-Vaknin, A. Punturieri, K. Sitwala, and D. M. Markovitz, "Vimentin is secreted by activated macrophages", *Nat. Cell Biol.*, vol. 5, no. 1, pp. 59–63, 2003.
- [243] S. Horkovics-Kovats and P. Traub, "Specific Interaction of the Intermediate Filament Protein Vimentin and Its Isolated N-Terminus with Negatively Charged Phospholipids As Determined by Vesicle Aggregation, Fusion, and Leakage Measurements", *Biochemistry*, vol. 29, no. 37, pp. 8652–8657, 1990.
- [244] R. Bhattacharya, A. M. Gonzalez, P. J. Debiase, H. E. Trejo, R. D. Goldman, *et al.*, "Recruitment of vimentin to the cell surface by beta3 integrin and plectin mediates adhesion strength", *J. Cell Sci.*, vol. 122, no. Pt 9, pp. 1390–400, 2009.
- [245] N. Jarousse, D. L. Trujillo, S. Wilcox-Adelman, and L. Coscoy, "Virally-Induced Upregulation of Heparan Sulfate on B Cells via the Action of Type I IFN", *J. Immunol.*, vol. 187, no. 11, pp. 5540–5547, 2011.
- [246] S. A. Morris, M. Wittner, L. Weiss, V. B. Hatcher, H. B. Tanowitz, *et al.*, "Extracellular matrix derived from Trypanosoma cruzi infected endothelial cells directs phenotypic expression", *J. Cell. Physiol.*, vol. 145, no. 2, pp. 340–346, 1990.

- [247] R. G. Edwards, S. J. Kopp, I. Ifergan, J.-W. Shui, M. Kronenberg, *et al.*, “Murine Corneal Inflammation and Nerve Damage After Infection With HSV-1 Are Promoted by HVEM and Ameliorated by Immune-Modifying Nanoparticle Therapy”, *Invest. Ophthalmol. Vis. Sci.*, vol. 58, no. 1, pp. 282–291, 2017.
- [248] S. K. Kovacs, V. Tiwari, E. Prandovszky, S. Dosa, S. Bacsa, *et al.*, “Expression of herpes virus entry mediator (HVEM) in the cornea and trigeminal Ganglia of normal and HSV-1 infected Mice”, *Curr. Eye Res.*, vol. 34, no. 10, pp. 896–904, 2009.
- [249] S. A. Kikuchi, C. L. Sodré, D. E. Kalume, C. G. R. Elias, A. L. S. Santos, *et al.*, “Proteomic analysis of two *Trypanosoma cruzi* zymodeme 3 strains”, *Exp. Parasitol.*, vol. 126, no. 4, pp. 540–551, 2010.
- [250] Y. Li, S. Shah-Simpson, K. Okrah, A. T. Belew, J. Choi, *et al.*, “Transcriptome Remodeling in *Trypanosoma cruzi* and Human Cells during Intracellular Infection”, *PLoS Pathog.*, vol. 12, no. 4, p. e1005511, 2016.
- [251] A. E. R. Oliveira, M. C. A. Pereira, A. T. Belew, L. R. P. Ferreira, L. M. N. Pereira, *et al.*, “Gene expression network analyses during infection with virulent and avirulent *Trypanosoma cruzi* strains unveil a role for fibroblasts in neutrophil recruitment and activation”, *PLoS Pathog.*, vol. 16, no. 8, pp. 1–27, 2020.
- [252] J. Kornbluth and R. G. Hoover, “Changes in gene expression associated with IFN-beta and IL-2-induced augmentation of human natural killer cell function”, *J. Immunol.*, vol. 141, no. 9, pp. 3234–40, 1988.
- [253] C. Une, J. Andersson, and A. Orn, “Role of IFN-alpha/beta and IL-12 in the activation of natural killer cells and interferon-gamma production during experimental infection with *Trypanosoma cruzi*”, *Clin. Exp. Immunol.*, vol. 134, no. 2, pp. 195–201, 2003.
- [254] Z. Zhou, O. J. Hamming, N. Ank, S. R. Paludan, A. L. Nielsen, *et al.*, “Type III interferon (IFN) induces a type I IFN-like response in a restricted subset of cells through signaling pathways involving both the Jak-STAT pathway and the mitogen-activated protein kinases”, *J. Virol.*, vol. 81, no. 14, pp. 7749–58, 2007.
- [255] A.-D. C. Chessler, K. L. Caradonna, A. Da’dara, and B. A. Burleigh, “Type I interferons increase host susceptibility to *Trypanosoma cruzi* infection”, *Infect. Immun.*, vol. 79, no. 5, pp. 2112–9, 2011.
- [256] R. M. B. Teles, T. G. Graeber, S. R. Krutzik, D. Montoya, M. Schenk, *et al.*, “Type I interferon suppresses type II interferon-triggered human anti-mycobacterial responses”, *Science*, vol. 339, no. 6126, pp. 1448–53, 2013.
- [257] A. J. Lee, F. Mian, S. M. Poznanski, M. Stackaruk, T. Chan, *et al.*, “Type I Interferon Receptor on NK Cells Negatively Regulates Interferon- γ Production”, *Front. Immunol.*, vol. 10, p. 1261, 2019.
- [258] H. Xu, B. Wang, M. Ono, A. Kagita, K. Fujii, *et al.*, “Targeted Disruption of HLA Genes via CRISPR-Cas9 Generates iPSCs with Enhanced Immune Compatibility”, *Cell Stem Cell*, vol. 24, no. 4, pp. 566-578.e7, 2019.
- [259] R. Apps, Y. Qi, J. M. Carlson, H. Chen, X. Gao, *et al.*, “Influence of HLA-C expression level on HIV control”, *Science*, vol. 340, no. 6128, pp. 87–91, 2013.
- [260] E. W. Petersdorf, T. A. Gooley, M. Malkki, A. P. Bacigalupo, A. Cesbron, *et al.*, “HLA-C expression levels define permissible mismatches in hematopoietic cell transplantation”, *Blood*, vol. 124, no. 26, pp. 3996–4003, 2014.
- [261] Z. Layrisse, M. T. Fernandez, S. Montagnani, M. Matos, O. Balbas, *et al.*, “HLA-C(*)03 is a risk factor for cardiomyopathy in Chagas disease”, *Hum. Immunol.*, vol. 61, no. 9, pp. 925–9, 2000.

- [262] J. L. McKechnie, D. Beltrán, A. Pitti, L. Saenz, A. B. Araúz, *et al.*, “HLA Upregulation During Dengue Virus Infection Suppresses the Natural Killer Cell Response”, *Front. Cell. Infect. Microbiol.*, vol. 9, p. 268, 2019.
- [263] K. Hopfensperger, J. Richard, C. M. Stürzel, F. Bibollet-Ruche, R. Apps, *et al.*, “Convergent Evolution of HLA-C Downmodulation in HIV-1 and HIV-2”, *MBio*, vol. 11, no. 4, 2020.
- [264] Y. Jun, E. Kim, M. Jin, H. C. Sung, H. Han, *et al.*, “Human cytomegalovirus gene products US3 and US6 down-regulate trophoblast class I MHC molecules”, *J. Immunol.*, vol. 164, no. 2, pp. 805–11, 2000.
- [265] M. Benhammedi, J. Mathé, M. Dumont-Lagacé, K. S. Kobayashi, L. Gaboury, *et al.*, “IFN- λ Enhances Constitutive Expression of MHC Class I Molecules on Thymic Epithelial Cells”, *J. Immunol.*, vol. 205, no. 5, pp. 1268–1280, 2020.
- [266] D. Snary, C. J. Barnstable, W. F. Bodmer, and M. J. Crumpton, “Molecular structure of human histocompatibility antigens: the HLA-C series”, *Eur. J. Immunol.*, vol. 7, no. 8, pp. 580–5, 1977.
- [267] H. Schmidt, V. Gekeler, H. Haas, G. Engler-Blum, I. Steiert, *et al.*, “Differential regulation of HLA class I genes by interferon”, *Immunogenetics*, vol. 31, no. 4, pp. 245–52, 1990.
- [268] T. W. Corrah, N. Goonetilleke, J. Kopycinski, S. G. Deeks, M. S. Cohen, *et al.*, “Reappraisal of the Relationship between the HIV-1-Protective Single-Nucleotide Polymorphism 35 Kilobases Upstream of the HLA-C Gene and Surface HLA-C Expression”, *J. Virol.*, vol. 85, no. 7, pp. 3367–3374, 2011.
- [269] H. L. Stevenson, M. D. Estes, N. R. Thirumalapura, D. H. Walker, and N. Ismail, “Natural killer cells promote tissue injury and systemic inflammatory responses during fatal Ehrlichia-induced toxic shock-like syndrome”, *Am. J. Pathol.*, vol. 177, no. 2, pp. 766–76, 2010.
- [270] M. Uhrberg, N. M. Valiante, B. P. Shum, H. G. Shilling, K. Lienert-Weidenbach, *et al.*, “Human Diversity in Killer Cell Inhibitory Receptor Genes”, *Immunity*, vol. 7, no. 6, pp. 753–763, 1997.
- [271] C. A. Stewart, F. Laugier-Anfossi, F. Vely, X. Saulquin, J. Riedmuller, *et al.*, “Recognition of peptide-MHC class I complexes by activating killer immunoglobulin-like receptors”, *Proc. Natl. Acad. Sci.*, vol. 102, no. 37, pp. 13224–13229, 2005.
- [272] K. van der Ploeg, C. Chang, M. A. Ivarsson, A. Moffett, M. R. Wills, *et al.*, “Modulation of Human Leukocyte Antigen-C by Human Cytomegalovirus Stimulates KIR2DS1 Recognition by Natural Killer Cells”, *Front. Immunol.*, vol. 8, p. 298, 2017.
- [273] K. A. Stannard, S. Lemoine, N. J. Waterhouse, F. Vari, L. Chatenoud, *et al.*, “Human peripheral blood DNAM-1neg NK cells are a terminally differentiated subset with limited effector functions”, *Blood Adv.*, vol. 3, no. 11, pp. 1681–1694, 2019.
- [274] R. Molfetta, N. D. Milito, B. Zitti, M. Lecce, C. Fionda, *et al.*, “The Ubiquitin-proteasome pathway regulates Nectin2/CD112 expression and impairs NK cell recognition and killing”, *Eur. J. Immunol.*, vol. 49, no. 6, pp. 873–883, 2019.
- [275] V. Braud, E. Yvonne Jones, and A. McMichael, “The human major histocompatibility complex class Ib molecule HLA-E binds signal sequence-derived peptides with primary anchor residues at positions 2 and 9”, *Eur. J. Immunol.*, vol. 27, no. 5, pp. 1164–1169, 1997.
- [276] B. K. Kaiser, J. C. Pizarro, J. Kerns, and R. K. Strong, “Structural basis for NKG2A/CD94 recognition of HLA-E”, *Proc. Natl. Acad. Sci. U. S. A.*, vol. 105, no. 18, pp. 6696–701, 2008.

- [277] F. Gong, S. Song, G. Lv, Y. Pan, D. Zhang, *et al.*, “Human leukocyte antigen E in human cytomegalovirus infection: friend or foe?”, *Acta Biochim. Biophys. Sin. (Shanghai)*, vol. 44, no. 7, pp. 551–554, 2012.
- [278] B. Foley, S. Cooley, M. R. Verneris, J. Curtsinger, X. Luo, *et al.*, “Human cytomegalovirus (CMV)-induced memory-like NKG2C(+) NK cells are transplantable and expand in vivo in response to recipient CMV antigen”, *J. Immunol.*, vol. 189, no. 10, pp. 5082–8, 2012.
- [279] M. Gumá, A. Angulo, C. Vilches, N. Gómez-Lozano, N. Malats, *et al.*, “Imprint of human cytomegalovirus infection on the NK cell receptor repertoire”, *Blood*, vol. 104, no. 12, pp. 3664–3671, 2004.
- [280] F. Wolpert, C. Happold, G. Reifenberger, A.-M. Florea, R. Deenen, *et al.*, “Interferon- β Modulates the Innate Immune Response against Glioblastoma Initiating Cells”, *PLoS One*, vol. 10, no. 10, p. e0139603, 2015.